THESE DE DOCTORAT

Pour l'obtention du grade de

DOCTEUR DE L'UNIVERSITÉ DE PAU ET DES PAYS DE L'ADOUR

Spécialité : Chimie des polymères

par

Célia BADJI

Vieillissement de matériaux composites renforcés de fibres naturelles : étude de l'impact sur les propriétés d'aspect et sur les émissions dans l'air intérieur

Soutenue le 06 Décembre 2017 devant la comission d'examen

Jean-Charles BÉNÉZET, Maître de recherche HDR, IMT Mines Alès	Co-directeur
Anne BERGERET, Professeur, IMT Mines Alès	Examinateur
Patrice BLONDEAU, Maître de conférences HDR, Université de La Rochelle	Rapporteur
Valérie DESAUZIERS, Professeur, IMT Mines Alès	Co-Directeur
Hélène GARAY, Enseignant-Chercheur, IMT Mines Alès	Examinateur
Jean-Luc GARDETTE, Professeur des universités, Université Clermont Auvergne	Rapporteur
Valérie NASSIET, Professeur des universités, Ecole Nationale d'Ingénieurs de Tarbes	Examinateur

REMERCIEMENTS

Cette thèse s'est déroulée au sein des pôles Matériaux Polymères Avancés (MPA) et Réactivité et Interactions entre les Matériaux et l'Environnement (RIME) du Centre des Matériaux des mines d'Alès (C2MA). Je souhaiterais premièrement remercier Valérie NASSIET de m'avoir fait l'honneur de présider mon jury de thèse. Je remercie également Patrice BLONDEAU et Jean-Luc GARDETTE d'avoir accepté de juger mon travail de thèse et d'en être les rapporteurs.

Je tiens à remercier tout particulièrement mes directeurs de thèse Valérie DESAUZIERS et Jean-Charles BÉNÉZET pour m'avoir fait confiance tout au long de ces trois années. Ils m'ont beaucoup appris et nos échanges ont toujours été fructueux. Je souhaite faire part de ma reconnaissance envers Anne BERGERET et Hélène GARAY pour avoir encadré ce projet dans la bonne humeur mais aussi pour leur grande disponibilité lorsque j'en avais besoin. Mes remerciements vont aussi à Joana BEIGBEDER dont la contribution a été indispensable mais aussi pour sa grande gentillesse et sa patience.

J'exprime ma profonde gratitude à Jean-Serge (autrement nommé Mac Gyver du labo) qui a toujours su trouver les solutions aux problèmes ainsi que Sylvie mais aussi Hervé et Olivier pour leur aide et leurs histoires plus qu'intéressantes aux pauses café. Un remerciement particulier à toute la famille SPICE RIME, premièrement Dr Jane (alias Britney) et Dr Mylène qui m'ont accueillie les bras ouverts et sans qui l'aventure n'aurait pas été aussi joyeuse qu'elle ne l'a été, PhD Alexandre qui a toujours su se rendre disponible pour les soucis informatiques et toujours partant pour les Escape Game.
Je remercie également Lata d'avoir partagé son expérience avec moi en tout début de thèse, Vanessa que j'ai retrouvé avec grande joie à Alès (et que j'espère retrouver encore !), Tamara pour sa gentillesse inégalable, sa volonté de toujours venir en aide aux gens et pour ses plats libanais, Sonia pour sa joie de vivre et son écoute (surtout ne change pas !) mais aussi Anne-Laure pour nos jours de plainte et nos midis Dell'Arte.

Je tiens à remercier Nicole et Gérard, mes anges-gardiens depuis 10 ans et qui ont toujours essayé de faciliter mes démarches.

Je m'adresse enfin à ma petite famille en particulier mes trois sœurs, celles qui ont le plus cru en moi et qui m'ont donné la force et le courage lorsque j'en avais besoin ainsi que mes parents qui m'ont soutenu jusqu'au dernier jour. Enfin, un dernier mot pour Bilhel qui a vécu patiemment cette aventure à mes côtés, qui m'apaise et me soulage et me rend heureuse de jour en jour. J'espère qu'il sait que je suis aussi fière de lui.

Table des abréviations

ACEA : European Automobile Manufacturers Association

ACP : Analyse en Composantes Principales

ADEME : Agence de l'Environnement et de la Maîtrise de l'Energie

AIAM : Association of International Automobile Manufacturers

ASEF : Association Santé Environnement de France

BMW : Bavarian Motors Works

BRDF : Bidirectional Reflectance Distribution Function

CAFE: Corporate Average Fuel Economy

CAGR : Taux de croissance annuel composé

CAR : Carboxen

CIE : Commission Internationale de l'Eclairage

CIRC : Centre International de Recherche sur le Cancer

CMR : Cancérogène, Mutagène, toxique pour la Reproduction

COSV : Composés Organiques Semi-Volatils

COV : Composés Organiques Volatils

COVT : Composés Organiques Volatils Totaux

DOSEC : Device for On Site Emission Control `

DSC : Differential Scanning Calorimetry

DVB : Divinylbenzène

FRD: Fibre Recherche et Développement

FTIR : Fourier Transform Infrared spectroscopy

FID : Détection par Ionisation de Flamme

GC : Chromatographie en phase gazeuse

HS : Headspace

ISO : International Organization for Standardization

JAMA : Japan Automobile Manufacturers Association

MA : Anhydride maléique

MS : Spectrométrie de masse

OEM : Original automotive Equipment Manufacturers

OMS : Organisation Mondiale de la Santé

PBS : Polybutylène succinate

PCA : Principal Component Analysis

PDMS : Polydiméthylsiloxane

PEBD : Polyéthylène basse densité

PEHD : Polyéthylène haute densité

PLA : Polyacide lactique

PP : Polypropylène

PSA : Peugeot Société Anonyme

PVC : Polychlorure de vinyle

RTM : Resin Transfer Molding

SCS: Sick Car Syndrome

SPME: Micro-Extraction sur Phase Solide

TVOCs : Total Volatile Organic Compounds

UV : Ultraviolet

VIAQ : Vehicle Indoor Air Quality

VOCs : Volatile Organic Compounds

WPC : Wood Plastic Composites

Table des symboles

a* : Coordonnée chromatique sur l'axe vert-rouge

b* : Coordonnée chromatique sur l'axe bleu-jaune

C : Concentration du composé dans l'air ($\mu g.cm^{-3}$)

C_a : Concentration du composé à la surface de sorption ($\mu g.cm^{-3}$)

C_s : Concentration en phase gazeuse à la surface du matériau ($\mu g.m^{-3}$)

D : Coefficient de diffusion ($m^2.s\text{-}^{1}$)

E : Module d'élasticité (MPa)

E_a : Energie d'activation ($J.mol^{-1}$)

EF : Taux d'émission ($\mu g.m^{-2}.h^{-1}$)

G_2 : Brillant de contraste

G_1 : Brillant de haze

I : Intensité ($W.m^{-2}$)

k : constante de vitesse réactionnelle

L* : Coordonnée de clarté sur l'axe foncé-clair

Q: Energie UV cumulée ($J.m^{-2}$)

R : Constante universelle des gaz parfaits (8,314 $J.mol^{-1}.K^{-1}$)

RH : Humidité relative (%)

Sa : Paramètre de rugosité (μm)

t : Temps (s)

T : température

ΔH_m : Enthalpie de fusion ($J.g^{-1}$)

θ : Angle de détection (°)

λ : Longueur d'onde (nm)

ν : Nombre d'onde (cm^{-1})

ρ : masse volumique ($g.cm^{-3}$)

σ : Contrainte à la flèche conventionnelle (MPa)

X_c : Taux de cristallinité (%)

SOMMAIRE

CHAPITRE II: VIEILLISSEMENTS NATURELS EXTÉRIEUR ET SOUS VITRE PARE-BRISE DE BIOCOMPOSITES PP/CHANVRE: IMPACT SUR LES PROPRIÉTÉS PHYSICO-CHIMIQUES ET LES RELATIONS ENTRE LES PROPRIÉTÉS

INTRODUCTION GÉNÉRALE

Depuis le protocole de Kyoto acté en 1997, la France, pays signataire de l'accord international sur la préservation de l'environnement, a pour objectif de réduire de 75% les émissions en CO_2 entre 1990 et 2050 pour limiter l'effet de serre [1,2]. De plus, une prise de conscience non négligeable sur l'impact environnemental des activités humaines, conduisant à l'épuisement de nos ressources, a fortement incité les chercheurs et industriels au développement de matériaux respectueux de l'environnement. Ainsi, afin de limiter le recours aux ressources fossiles, l'utilisation de matériaux issus de ressources renouvelables émerge depuis quelques années. Aussi, la contribution à la transition écologique se reflète de plus en plus dans les secteurs tels que l'automobile ou la construction où la performance mécanique des matériaux nécessite d'être améliorée par des renforts. En effet, les composites à fibres naturelles semblent être une alternative prometteuse aux composites traditionnels renforcés de fibres synthétiques. En plus de présenter des avantages environnementaux, les propriétés mécaniques spécifiques des fibres végétales (rapport entre la propriété mécanique considérée et la densité) sont comparables à celles des fibres de verre couramment utilisées pour le renfort des matériaux. Ces composites renforcés de fibres naturelles, que l'on appelle plus souvent biocomposites, sont par ailleurs très intéressants sur le plan économique puisque leur légèreté favorise notamment une baisse de la consommation en carburant et une émission réduite de gaz à effet de serre pour le secteur automobile. Cependant, la faible résistance thermique des fibres naturelles limite le choix des matrices dans lesquelles elles peuvent être incorporées et seules celles dont la température de mise en forme est inférieure à 200°C telles les polyoléfines (polyéthylène PE, polypropylène PP, polychlorure de vinyle PVC) sont envisageables.

Cependant, l'un des verrous souvent mis aussi en exergue demeure la sensibilité des biocomposites aux variations climatiques suite à leur exposition face aux agressions extérieures telles que les rayons ultraviolets (UV) provenant du soleil, la chaleur ou l'humidité élevée. Cette sensibilité peut se manifester par une perte de la tenue mécanique. De plus, les modifications de structure des biocomposites peuvent induire des changements d'aspect visuel. Ainsi, une étude quantitative des relations existant entre la structure et les propriétés macroscopiques des biocomposites permettrait d'apporter des éléments de

compréhension sur leurs mécanismes de dégradation et expliquer l'endommagement provoqué par les facteurs extérieurs.

Par ailleurs, les biocomposites sont reconnus comme responsables d'odeurs [3,4]. Puisque ces derniers sont actuellement intégrés dans les équipements intérieurs d'automobile tels que les tableaux de bord ou les panneaux de porte [5], ces odeurs peuvent donc nuire au bien-être des passagers du véhicule et potentiellement contribuer au « new car smell ». Ils sont donc des sources potentielles de polluants pouvant compromettre la qualité de l'air intérieur d'automobile. Des règlementations mises en place ces dernières années notamment en Asie visent à limiter la dégradation de la qualité de l'air intérieur d'habitacle. Ces dernières proposent des valeurs limites de concentration de certains composés retrouvés dans les véhicules dont l'impact sur notre santé est reconnu. Par ailleurs, des normes sont proposées aux constructeurs automobiles afin de mesurer les émissions de COV des véhicules et des pièces intérieures avant mise sur le marché du véhicule. Toutefois, l'impact des émissions de Composés Organiques Volatils (COV) par des biocomposites sur la qualité sanitaire de l'air intérieur de véhicule reste encore peu documenté. Ainsi, il est proposé dans cette étude de déterminer la contribution des fibres naturelles et l'impact des conditions d'usage sur le profil d'émission de COV des biocomposites. Pour cela, une méthodologie précédemment développée au laboratoire permettant une mesure simple et non destructive des émissions de surface des matériaux a été appliquée En effet, les indicateurs de dégradation habituellement suivis au cours du vieillissement consistent notamment en l'évaluation de la performance mécanique à travers des tests destructifs. Un suivi de traceurs tels que les émissions de COV et/ou l'aspect visuel permettrait donc de s'affranchir de cette démarche classique destructive.

Le vieillissement naturel reste le moyen le plus fiable pour évaluer la durabilité des matériaux. Cependant, il nécessite souvent une exposition de longue durée pour identifier une dégradation effective du matériau. Ainsi, des essais de vieillissement artificiel en enceinte dédiée permettent d'accélérer les processus de dégradation des matériaux. Toutefois, il apparaît primordial de vérifier la fiabilité de ce type d'approches quant à la représentativité des conditions extérieures en laboratoire. Aussi, un facteur d'accélération de la dégradation des matériaux entre l'exposition artificielle et l'exposition naturelle permet d'estimer le temps nécessaire de test en enceinte pour représenter une certaine

durée d'exposition du matériau en conditions réelles. Cependant, il n'existe pas de facteur d'accélération universel pouvant être appliqué à toute étude de cas puisque le degré de dégradation dépend fortement du matériau et des conditions de vieillissement De plus, lorsque le nombre de propriétés étudiées est conséquent, il semble nécessaire de proposer une analyse synthétique et fiable permettant d'estimer un facteur d'accélération par matériau et par propriété considérée. Au vu des applications en environnements extérieurs et intérieurs des biocomposites, l'intérêt sera d'étudier l'évolution de leur comportement en conditions réelles et artificielles et déterminer l'influence des conditions d'usage
(extérieure et intérieure) sur leurs caractéristiques initiales telles que la tenue mécanique, la microstructure, l'apparence visuelle et les émissions de COV pour l'application intérieure. Dans ce contexte, ce travail de thèse a été entrepris et le manuscrit qui en découle s'articule en 5 chapitres : L'état de l'art sur l'utilisation de biocomposites en industrie ainsi que les principaux verrous scientifiques limitant leur développement constituera le Chapitre I. Il en sera déduit la nature du biocomposite qui sera étudié (matrice polymère et renfort de fibres végétales). Ce chapitre présentera aussi les différents paramètres responsables de la dégradation des biocomposites et l'influence de chaque facteur sur l'évolution des propriétés physico-chimiques, mécaniques et d'aspect visuel dans leurs conditions d'usage. Aussi, les études quantitatives des polluants fréquemment identifiés dans les habitacles de véhicule seront présentées et les émissions de COV seront mises en relations avec les autres propriétés d'usage. La partie 1 du Chapitre II présentera l'impact de vieillissements naturels extérieur et sous vitre pare-brise des biocomposites étudiés sur leur durabilité au cours d'une année. Le vitrage pare-brise est choisi afin de simuler un environnement intérieur d'automobile. L'influence des conditions d'usage sera évaluée à travers le suivi des propriétés mécaniques, physiques et chimiques. La nature des relations existant entre les différentes propriétés suivies au cours des vieillissements sera établie dans une seconde partie à travers une approche statistique permettant de mettre en évidence l'évolution des corrélations au cours de l'exposition. Le Chapitre III sera consacré à l'étude de l'impact de l'exposition sous vitrage sur les émissions de COV des biocomposites. Premièrement, l'impact du vieillissement et de l'incorporation de fibres végétales dans le matériau sur les émissions sera évalué. Ensuite,

des mécanismes réactionnels de dégradation des matériaux seront proposés à partir des COV analysés. Enfin, une analyse statistique sera effectuée afin d'évaluer la possibilité d'utiliser les émissions de COV comme indicateur de vieillissement.

Enfin, le **Chapitre IV** traitera de la comparaison entre un vieillissement accéléré effectué en enceinte de laboratoire et le vieillissement extérieur naturel des matériaux biocomposites afin d'évaluer la simulation des conditions extérieures en enceinte.

Références

[1] Feature, construction, solutions, medical, biocomposites, n°111, JEC Compos. Mag. (2017) 1–122.

[2] COP21: les engagements nationaux de la France, (2015). gouvernement.fr.

[3] O. Faruk, A.K. Bledzki, H.-P. Fink, M. Sain, Biocomposites reinforced with natural fibers: 2000–2010, Prog. Polym. Sci. 37 (2012) 1552–1596. doi:10.1016/j.progpolymsci.2012.04.003.

[4] H.-S. Kim, B.-H. Lee, H.-J. Kim, H.-S. Yang, Mechanical–thermal properties and VOC emissions of natural-flour-filled biodegradable polymer hybrid bio-composites, J. Polym. Environ. 19 (2011) 628–636. doi:10.1007/s10924-011-0313-5.

[5] Z.L. Yan, H. Wang, K.T. Lau, S. Pather, J.C. Zhang, G. Lin, Y. Ding, Reinforcement of polypropylene with hemp fibres, Compos. Part B Eng. 46 (2013) 221–226. doi:10.1016/j.compositesb.2012.09.027.

CHAPITRE I

SYNTHESE BIBLIOGRAPHIQUE

L'étude bibliographique présente tout d'abord les secteurs d'application principaux des biocomposites ainsi que leurs caractéristiques générales. Ensuite, les principales causes des variations des propriétés des biocomposites ainsi que leur impact sur leurs propriétés sont décrites. Puis, l'état de l'art sur l'impact des émissions de Composés Organiques Volatils (COV) sur la qualité de l'air intérieur de véhicule (une des principales utilisations des biocomposites) est présenté. Enfin, les relations entre les propriétés des polymères dégagées dans la littérature sont détaillées.

I. Les secteurs d'application des biocomposites

I.1. Evolution du marché mondial

Le développement de matériaux biocomposites, définis comme partiellement ou totalement constitués de matériaux issus de la biomasse, résulte d'une prise de conscience des problèmes environnementaux et des règlementations de plus en plus contraignantes sur les émissions en CO_2.

Leur développement s'étend sur tous les continents. L'Amérique du Nord présente le plus grand marché de composites renforcés de fibres naturelles, notamment dû à leur prédominance dans les activités liées au bâtiment et la construction, dont les composites renforcés de fibres de bois sont les plus représentatifs. En Europe, la production en composites renforcés de fibres naturelles et farine de bois constitue 15% de la production totale en composites [1]. En 2012, l'Union européenne a produit 397 000 tonnes de biocomposites et cela devrait augmenter de 1,2% voire 3% en 2020 selon les incitations pour le développement des produits biosourcés et les scénarios de politique gouvernementale [2]. Cependant, une demande croissante émerge aussi de l'Asie. En effet, il est envisagé que, durant la décennie prochaine, l'Asie-Pacifique incluant le Japon, la Chine et la Corée du Sud devrait témoigner de la plus forte croissance globale en biocomposites puisque l'industrie automobile y est de plus en plus développée [3]. De plus, celle-ci dispose d'abondantes matières premières issues de la biomasse nécessaires pour produire des biocomposites [4].

Le graphe suivant (Figure 1) représente la répartition en volume du marché global des biocomposites en fonction de leur secteur d'application [5]. Cette figure démontre clairement que la construction présente la plus grande part de marché suivie par l'industrie

automobile. Ces deux secteurs d'applications seront donc détaillés dans la suite de cet état de l'art.

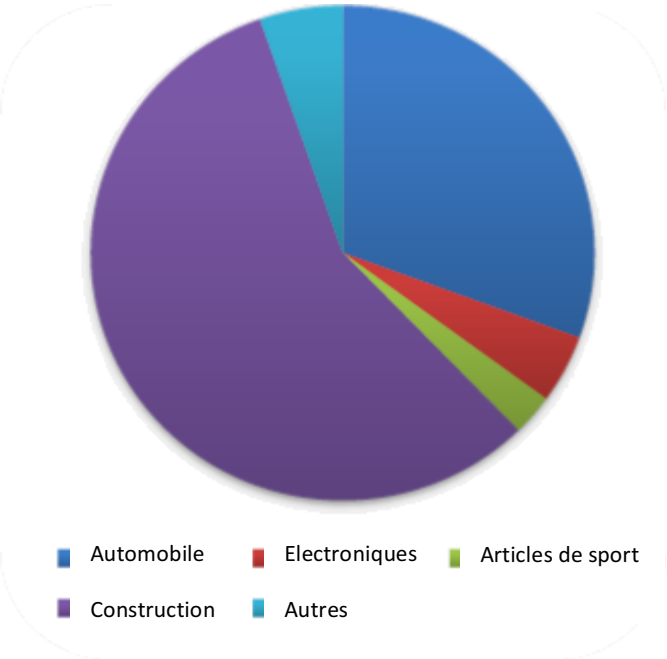

Figure 1 - Répartition des biocomposites par application

I.2. Secteur de la construction

Le secteur de la construction domine le marché global des biocomposites avec une part en volume de plus de 50% en 2015 [6]. Cela s'explique notamment par une volonté croissante de réduire l'empreinte environnementale des constructions mais aussi par le développement accru d'infrastructures. Les principaux produits commercialisés constitués de matériaux biocomposites sont les lames de terrasse (decking), parements et clôtures [7].

Par ailleurs, les composites à renforts de fibres ou de farines de bois (Wood Plastic Composites, autrement désignés WPC) sont les plus répandus, particulièrement dans le marché résidentiel en raison de leur légèreté, de leurs caractéristiques esthétiques et de leurs propriétés mécaniques. Ils représentent 60% du marché de la construction [6,8] mais aussi une alternative avantageuse, en termes de coût de maintenance et de poids, aux lames de terrasse classiques exclusivement constituées de bois [9]. Les Etats-Unis et la Chine sont les pays les plus grands producteurs de WPC. En Europe, il s'avère que le marché des WPC pour un usage en lames de terrasse est resté longtemps au stade de développement pour atteindre actuellement un stade de maturité [8].

Les WPC sont principalement extrudés sous forme de planches de terrasse creuses ou

pleines (Figure 2). Même si les profils creux restent moins coûteux, plus légers et représentent 56% en masse de la totalité des produits en WPC en 2015 [10], les profils pleins en WPC tendent à être plus développés [8] notamment pour raisons esthétiques et pour leur résistance aux intempéries plus élevée [11,12].

Figure 2 - Lames de terrasse en WPC pleines (gauche) et creuses (droite) Ecodeck® [12]

La fibre de bois joue un rôle majeur dans les performances des WPC au cours de leur cycle de vie. Elle est utilisée comme renfort pour réduire les coûts de production de matériaux destinés à la construction [13]. Dans ce secteur, les bois de résineux (épicéa, pin) sont principalement utilisés [8]. Cela peut s'expliquer par leur coût moins élevé que celui des bois de feuillus (érable, chêne) bien qu'ils se dégradent plus rapidement que ces derniers [14].

Le polyéthylène (PE) est la matrice la plus utilisée pour les WPC. Cependant, la structure et la résistance aux agents chimiques du polypropylène (PP) sont appréciées, notamment en Europe [8]. Par ailleurs, le faible degré d'expansion/contraction thermique (CTE) du PP et du PE est un point fort vis-à-vis des variations de température extérieures [15]. De plus, ces polymères présentent un CTE encore plus faible une fois renforcés de farines ou fibres de bois [16]. Cependant, la température de fusion du PP nécessitant des conditions thermiques de mise en œuvre plus élevées, sa plus grande fragilité et son prix supérieur à celui du PE représentent un frein à son développement, notamment en Amérique du Nord [17].

Le ratio fibres de bois/matrice thermoplastique conditionne fortement les caractéristiques des WPC. Le choix se porte généralement vers un ratio 50/50 en masse [18]. Cependant, de par leur instabilité et leur sensibilité en environnement extérieur, des adjuvants tels que des colorants, agents de couplage, stabilisants UV et thermiques ou lubrifiants sont ajoutés aux WPC afin d'améliorer les caractéristiques et la durabilité des produits finis.

Aujourd'hui, suite aux politiques de gouvernement tendant à préserver les forêts, les fabricants de WPC favorisent le renforcement partiel des plastiques par des composés biosourcés alternatifs aux fibres de bois permettant des performances de matériaux plus ciblées [18,19]. En effet, des renforts alternatifs tels que les fibres techniques et sous-produits végétaux (bambou, lin, chanvre et balles céréalières comme le riz et le blé) sont de plus en plus valorisés [17,18]. La fibre de chanvre constitue l'une des fibres alternatives les plus intéressantes [19]. Le chanvre est une plante qui permettrait de produire plus de matière première destinée à la construction pour une même superficie que la plupart des arbres [20]. En ce qui concerne les balles céréalières comme le riz, leur composition chimique présentant une forte teneur en silicates, composés hydrophobes, limite l'absorption d'eau et donc l'instabilité dimensionnelle [17]. Cependant, certains aspects contraignants, tels que la mauvaise coulabilité des fibres dans les doseurs d'alimentation des appareillages lors de la mise en œuvre [21], justifient le fait que ce type de biocomposites restent principalement dans les centres de recherche et développement notamment pour mieux maîtriser ces aspects.

Les biocomposites restent cependant moins développés pour des usages en intérieur de bâtiments. Ce type d'application intérieure est pour l'instant surtout réservé au domaine automobile décrit ci-après.

I.3. Secteur de l'automobile

La conception de pièces de véhicule partiellement obtenues à partir de matériaux biosourcés a été initiée par le fondateur de la compagnie Ford Motors dans les années 1930s [22]. Depuis, des recherches ont été entreprises conduisant à l'utilisation étendue de biocomposites durant le 20ème siècle dont la fin est caractérisée par une diminution évidente des ressources fossiles selon le pic de Hubbert (peak oil) [23,24]. Les biocomposites peuvent être retrouvés dans les pièces intérieures de véhicule sous forme de composants non structurels tels que les intérieurs de portes, dossiers ou tableaux de bord. Cependant, ceux-ci tendent à être de plus en plus utilisés pour des composants plus structurels tels que les planchers, motopropulseurs ou systèmes de direction [25–27]. Le PP chargé de fibres de lin ou de chanvre est la matrice la plus développée dans ce secteur. Cette volonté de développer l'utilisation de biocomposites peut être attribuée à un besoin croissant en

véhicules plus sûrs, plus légers et donc moins consommateurs en carburant puisque l'intégration de composites renforcés de fibres naturelles dans les véhicules peut permettre un gain de masse global de 10% pour des performances mécaniques équivalentes à celles des composites traditionnels [28]. Par ailleurs, une réduction d'environ 57 kg résulterait en un gain économique de 0,09 à 0,21 km par litre de carburant [29]. De plus, l'énergie pour fabriquer des composites renforcés de fibres naturelles nécessite seulement 60% de celle requise pour les composites à fibres synthétiques [30].Ainsi, les émissions de gaz à effet de serre sont limitées du fait d'une consommation en énergie moindre au cours de la production [31]. En effet, il a été démontré qu'en convertissant l'énergie en émission de CO_2, celle-ci pouvait être réduite de 3 tonnes CO_2 par tonne de composite en substituant les fibres de verre par des fibres de chanvre.

Les constructeurs allemands sont particulièrement actifs en ce qui concerne l'intégration de biocomposites dans leurs véhicules. Les premiers efforts commercialisés réalisés par Mercedes-Benz [8] sont des composites à base de polymères renforcés de fibres de jute, banane, lin, chanvre, sisal, laine, et coton pour les intérieurs de porte, housses, panneaux et dossier de siège des modèles classe E (1994), classe A (2004) et classe S (2006) [25,26,32,33]. Ainsi, une réduction de masse de 20% et jusqu'à 45% des panneaux de porte des modèles classe E et classe S [25] respectivement a été observée. La Figure 3 représente le modèle classe E plus récent dont l'intérieur est composé de 50 pièces différentes incluant des fibres naturelles [33]. Les compagnies Volkswagen et Bavarian Motor Works (BMW) s'engagent aussi dans cette démarche d'utilisation de matériaux verts [33–36]. Par exemple, Volkswagen utilise des biocomposites pour les composants structurels tel que le composite PP/fibres naturelles [35].

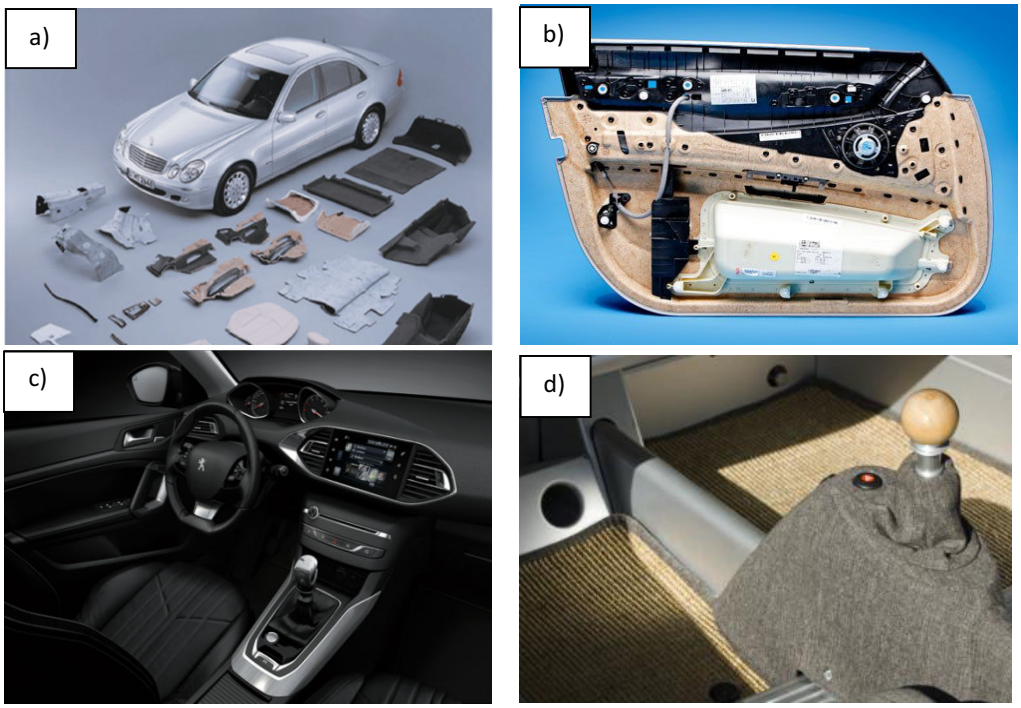

Figure 3 – Pièces intérieures de véhicules de constructeurs allemands (Mercedes E-class (a) [37], BMW (b) [38]) [40]) et de constructeurs français (Peugeot 308 (c) [39], Lotus Eco Elise (d) [40]) constituées de biocompositesconstituées de biocomposites

Les constructeurs français PSA et Renault sont aussi concernés par le développement de matériaux respectueux de l'environnement, notamment à travers des « bioconcept-cars » [41,42]. Cependant, certains véhicules sont aussi retrouvés sur le marché [43]. Aussi, l'approche holistique adoptée est illustrée pour le véhicule Lotus Eco Elise par l'utilisation de fibres végétales locales (chanvre) (Figure 4) [40,44]. Par ailleurs, comme observé dans le Tableau 1, les constructeurs automobiles japonais Mitsubishi Motors (MMC) et Toyota adoptent aussi une technologie verte pour leurs véhicules [25,32].

Les fabricants et fournisseurs d'équipements dont les équipementiers français Faurecia SA et Valéo SA classés aux 9ème et 10ème rangs parmi les équipementiers mondiaux selon l'indice Roland Berger en 2016 [45], tendent à développer des matériaux à partir de fibres végétales et participent donc au développement d'une économie « sobre » en carbone [46]. De plus, Faurecia favorise particulièrement le développement de matériaux destinés aux intérieurs d'automobile à base de chanvre [46].

Des technologies communes aux fabricants et constructeurs automobiles prennent de plus en plus d'essor. Le procédé de moulage par injection NAFIlean®, dont le projet réunit Peugeot SA (PSA) et l'équipementier Faurecia en 2013, en est un exemple concret [46]. Ce

procédé consiste à formuler des composites PP renforcé de 20% en masse de fibres de chanvre pour les 4 panneaux de porte de la Peugeot 308. Ce biocomposite correspond à la première pièce structurelle bio-sourcée moulée par injection sur le marché des intérieurs d'automobiles permettant de créer des formes et architectures complexes tout en apportant un gain de poids [47]. Par ailleurs, en 2016, ce matériau a été utilisé pour la première fois pour le tableau de bord complet de la Giulia (Alfa Roméo) [48,47,49].

PSA Peugeot-Citroën, Faurecia et Lineo ont aussi développé Flaxpreg^{TM}, un composite sandwich léger à matrice époxy renforcé de fibres de lin longues dont l'originalité réside dans la suppression des étapes de filature et de tissage, induisant des fibres planes non torsadées, pour réduire le coût de production du FlaxTape^{TM} non-tissé. Aussi, le chimiste japonais Mitsubishi Chemicals et Faurecia se sont associés afin de développer un bioplastique polybutylène succinate (PBS), entièrement fabriqué à partir de matières premières renouvelables, biodégradable et renforcé de fibres de chanvre à la résistance mécanique et à la tenue au feu élevées. Ce matériau pourrait être 100% recyclable en 2018 [47,50]. Ainsi, parmi les biocomposites les plus développés par les constructeurs et fabricants de véhicule cités précédemment, le renfort des matériaux par des fibres de chanvre semble être maîtrisé.

Des avancées communes aux secteurs académique et industriel ont permis de progresser rapidement dans cette démarche [51,52]. Par exemple, des études en universités et instituts de recherche en partenariat avec la compagnie brésilienne Ancel-Reinforced Plastics ont démontré par analyse de cycle de vie (ACV), qu'il était possible de fabriquer un capot frontal structurel d'un véhicule à base de fibres de jute en substitution aux fibres de verre présentant de meilleures caractéristiques et performances environnementales grâce à un poids plus faible [52].

L'utilisation sous forme de composants extérieurs d'automobile connaît aussi un intérêt croissant [32,33,53]. La première version des biocomposites est apparue en 2000 sur le modèle Mercedes-Benz Travego équipé d'un moteur renforcé de polyester/lin et d'enceintes pour isolation acoustique. Grâce à tous ces développements, le secteur automobile pourrait être le segment le plus prometteur dans l'adoption de biocomposites au sein de son marché entre 2016 et 2021 [54].

Tableau 1 - Pièces intérieures en biocomposites de différents modèles de véhicule

Constructeurs	Modèles	Pièces	Matrices	Fibres	Source
Daimler/ Mercedes-Benz	Classes A, C, E, S	Housses, revêtements, dossiers, tableaux de bord, panneaux de porte, panneaux de recouvrement	Epoxy, polyesters, PP, PE	jute, banane, lin, chanvre, sisal, laine, coton	[25,26,32,33,37]
Volkswagen	Golf A4, Passat, Audi A2	Dossiers de siège, revêtement de bavette arrière, panneaux de porte	PP, PU	lin, sisal	[25,33]
BMW	Séries 3, 5, 7	Revêtements, panneaux de porte, panneaux isolants acoustiques	PU, copolymère acrylique	chanvre, lin, sisal	[37,55]
Ford	Ford Mondeo, Ford Flex 2010 SUV	Panneaux de porte	PP	kénaf, paille de blé	[34] [56]
General Motors	Chevrolet Impala	Plage arrière	PP	lin	[33]
Toyota	ES3	Garniture et autres pièces intérieures	PLA	kénaf	[37]
Mitsubishi Motors		Panneaux de porte, plancher de coffre	PBS	bambou	[34,37]
Renault	Clio	Plage arrière	PP	lin	[37,56]
Peugeot	Peugeot 308, Peugeot 406	Panneaux de porte, plage arrière, faux-plancher de coffre	PP	chanvre	[46]
Citroën	C3, C5	Plage arrière, revêtement de coffre, intérieurs de porte		bois	[43][33]
Lotus	Eco Elise	Tapis intérieurs, sièges	polyester	chanvre, sisal, laine	[40,44,56]
Alfa Romeo	Giulia	Tableau de bord	PP	chanvre	[49]

II. Les matrices

Cette partie décrit les différents types de matrice développés en industrie ainsi que les caractéristiques thermo-mécaniques de l'une des polyoléfines les plus produites dans le monde.

II.1. Généralités

La matrice joue le rôle de liant entre les renforts et les protège. Les biocomposites utilisés dans le secteur de la construction sont principalement constitués d'une matrice polymère thermoplastique (polyoléfines), alors que le secteur de l'automobile favorise également le développement de polymères thermodurcissables (époxy, polyesters) pour certaines pièces

[25]. La différence entre ces deux matières plastiques réside en la structure des chaînes macromoléculaires, réticulées dans le cas des polymères thermodurcissables et libres pour les polymères thermoplastiques. Les composites à matrice thermoplastique tendent à remplacer de plus en plus les thermodurcissables pour les avantages qu'ils présentent tels que le recyclage et les possibilités plus diverses de design [31,30,34]. Leur tonnage évoluerait plus rapidement que celui des thermodurcissables. Par ailleurs, la grande ductilité de la matrice thermoplastique confère aux biocomposites une meilleure résistance aux chocs et une meilleure résistance à l'impact en comparaison à ceux à base de polymères thermodurcissables [57]. Leur structure peut être de nature amorphe ou semi-cristalline [58–61]. Cette spécificité s'avère importante car elle conditionne essentiellement la réponse mécanique du biocomposite auquel le polymère est intégré.

Le polymère peut provenir de ressources renouvelables (biosourcé) ou non renouvelables (pétrosourcé) et peut être biodégradable ou non biodégradable (Figure 4). Les matrices à polymère synthétique généralement utilisées dans les biocomposites retrouvés dans les véhicules ou dans les matériaux de construction sont le PP, le PE et le PVC [15,62,63]. Ceux-ci sont suivis par les polymères biosourcés tels que le PBS et le PLA [64,65].

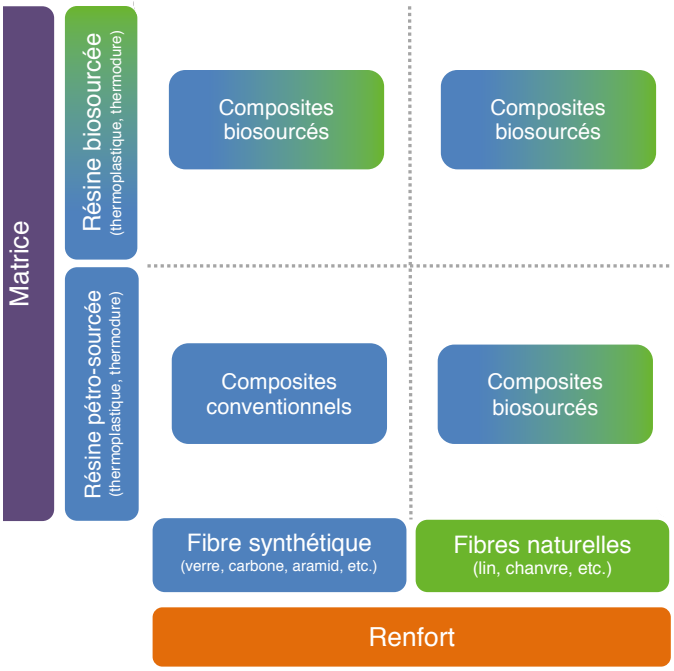

Figure 4 - Les différentes combinaisons entre matrice et renfort [66]

Aussi, le choix de la matrice est limité par la température de dégradation des fibres végétales, environ 200 °C, qui est la température de mise en œuvre des biocomposites [27]. De plus, les contraintes techniques et économiques des industriels liés aux matériaux 100% issus de la biomasse affectent la production en série. De manière ponctuelle, lorsque ces matériaux sont utilisés dans des véhicules de série, ils se limitent à des applications où le produit sera soumis à des contraintes thermiques et mécaniques restreintes [67]. Par ailleurs, les biocomposites dérivés de matrices synthétiques présentent une balance intéressante entre les intérêts environnementaux et économiques pour plusieurs applications [68]. Les polymères tels que le PE ou le PP seront privilégiés au détriment des PBS et PLA. De plus, leur moindre coût leur vaut leur succès dans les biocomposites utilisés dans les deux secteurs cités précédemment. Au vu des avantages liés à l'utilisation de thermoplastiques, le PP est donc sélectionné pour notre étude comme matrice des biocomposites.

II.2. Le polypropylène (PP) et son comportement thermomécanique

Le polypropylène, dont la formule chimique est C_nH_{2n} (Figure 5), est la deuxième matière plastique la plus largement produite après le PE [69]. Il trouve de nombreuses applications telles que les emballages alimentaires ou les pièces extérieures et intérieures d'automobile. En effet, il est retrouvé non renforcé dans les pièces moulées d'automobile tels que les pare-chocs [70], et renforcé sous forme de composites dans les panneaux de porte ou tableaux de bord [37].

Le PP est une polyoléfine saturée. Il est par ailleurs très résistant à la fatigue, la flexion et la déformation thermique. Il reste cependant très fragile et sensible au rayonnement UV et la température en raison de structure branchée [15]. C'est pourquoi des antioxydants sont souvent ajoutés pour une meilleure stabilité thermique du polymère [15,71,72].

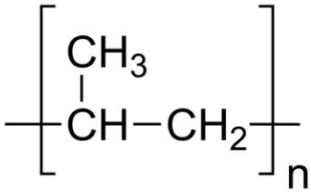

Figure 5 – Structure du PP

Le PP présente un comportement viscoélastique non linéaire. Plusieurs paramètres tels que la formulation, le procédé de mise en œuvre (organisation des chaînes macromoléculaires, consommation d'additifs), l'environnement d'utilisation ou la sollicitation influent sur la réponse mécanique du polymère [73,74]. Par exemple, les différents modes de déformation uniaxiaux tels que la traction, la flexion ou la compression peuvent influencer considérablement la valeur du module traduisant la rigidité du matériau lorsque le matériau est inhomogène et anisotrope dans le cas de polymères chargés [75]. Par ailleurs, la répartition des contraintes le long du matériau au cours de la sollicitation diffère en fonction du mode de déformation.

Le type de PP (homopolymère, copolymère séquencé, statistique) est choisi en fonction de la spécificité requise et du coût associé. Les homopolymères et copolymères sont les plus communément utilisés bien que la première famille soit plus rigide et plus résistante à la traction [76,77]. Par ailleurs, le profil mécanique sera aussi différent en fonction du type de PP. Le Tableau 2 répertorie les propriétés thermomécaniques d'un PP homopolymère [77].

Le comportement mécanique de ce polymère dépend aussi de sa morphologie microstructurale. En effet, les polymères semi-cristallins tels que le PP ont la particularité de pouvoir cristalliser entre leur température de transition vitreuse T_g et leur température de fusion T_f. Or, un taux de cristallinité élevé induit une rigidité relativement importante [78]. Par ailleurs, une cristallisation du PP isotactique a été mise en évidence dans la littérature une fois en contact avec des charges lors de son refroidissement au cours de la mise en œuvre [79]. Cela induit l'apparition d'autres structures cristallines et peut affecter le taux de cristallinité. Aussi, il a été démontré que le PP cristallisait sous les phases α et β en présence de cellulose agissant en tant qu'agents de nucléation alors que le PP non chargé cristallise seulement sous la phase α [80]. Donc, pour une analyse correcte de la microstructure du polymère, la contribution des charges ou renforts doit être maîtrisée.

Tableau 2 - Propriétés thermomécaniques d'un PP homopolymère [15][77]

Indice de fluidité (g/10min)	**Cristallinité (%)**	**Résistance à l'impact ($Kj.m^{-2}$)**	**ρ ($g.cm^{-3}$)**	**T_g (°C)**	**T_f (°C)**	**Résistance à la traction ($N.mm^{-2}$)**	**Module (GPa)**
2 à 5	30 à 50	3-30	0,9 à 0.91	-20 à -18	160 à 165	33	1,4

III. Les fibres naturelles

III.1. Production et développement des fibres naturelles

Les fibres naturelles sont principalement développées et valorisées pour le textile, le biocarburant et le renforcement de matériaux. La Figure 6 représente les parts de marché des fibres synthétiques et naturelles dans le monde. 37%, soit 36,6 MT, de fibres naturelles sur 99 millions de tonnes (MT) de fibres totales produites, ont été consommées en 2016 [81].

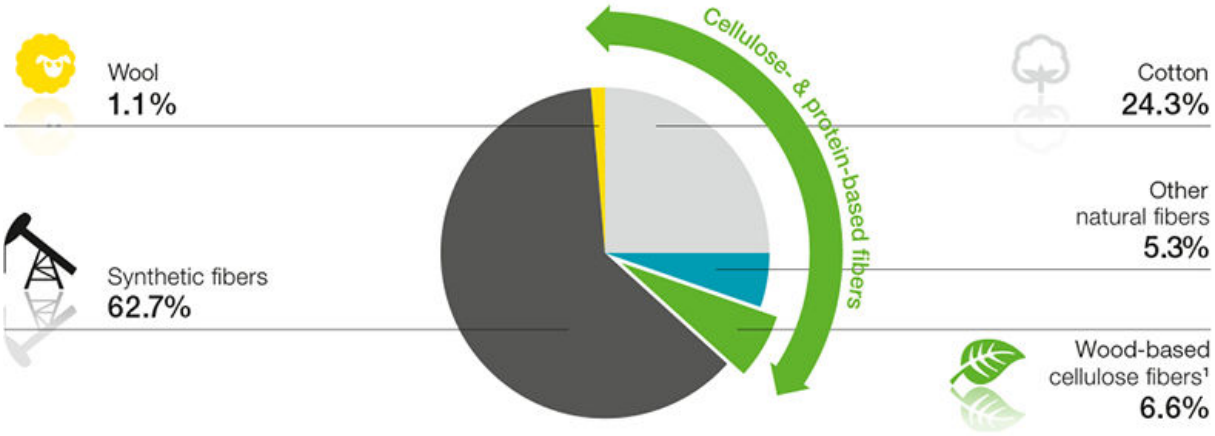

Figure 6 - Répartition du marché des fibres synthétiques et naturelles par type [81]

Les européens sont les premiers consommateurs de fibres naturelles, toute application confondue [30]. Le coton, représentant la plus grande part des fibres naturelles consommées en 2016, est principalement exploité par la Chine, avec 60% des réserves mondiales (Tableau 3) [82]. La Chine est par ailleurs le premier producteur de chanvre à l'échelle mondiale [48]. La France se place en tant que premier producteur européen de fibres végétales en termes de surface cultivée [83]. Elle produit ainsi 80% des fibres européennes soit 169 000 tonnes de lin et de chanvre chaque année [84]. Par ailleurs, la plupart des fibres industrielles dérivent des plantes libériennes (lin, chanvre, jute, kénaf) [34]. Les fibres de plantes exotiques telles que le jute, le kénaf ou la canne à sucre sont plutôt produites par les pays émergents et en voie de développement (Brésil, Inde, Bangladesh) [35]. Ainsi, les fibres naturelles offrent la possibilité aux pays en voie de développement et cultivateurs de plantes à fibre d'utiliser leurs propres ressources

naturelles dans l'industrie des composites.

Tableau 3 – Production annuelle mondiale et pays producteurs principaux de fibres naturelles [17,30,85,86]

Fibres naturelles	**Production mondiale (10^3 tonnes)**	**1er pays producteur mondial**
Canne à sucre	75 000	Brésil
Bambou	30 000	Chine
Lin	830	France, Belgique
Chanvre	214	Chine
Coton	26 000	Chine
Soie	202 000	Chine
Sisal	378	Mexique
Kénaf	970	Bangladesh, Inde
Jute	2 300	Inde, Bangladesh

Selon une étude menée en 2016 par l'Agence De l'Environnement et de la Maîtrise de l'Energie (ADEME) et la société Fibre Recherche et Développement (FRD), les fibres peuvent être réparties selon leur degré d'utilisation et de connaissance [49]. Selon la Figure 7, trois groupes de plantes à fibres se distinguent (disponibles, en développement, potentielles) selon leur taux de production, le développement des implantations et leur validation à l'échelle industrielle.

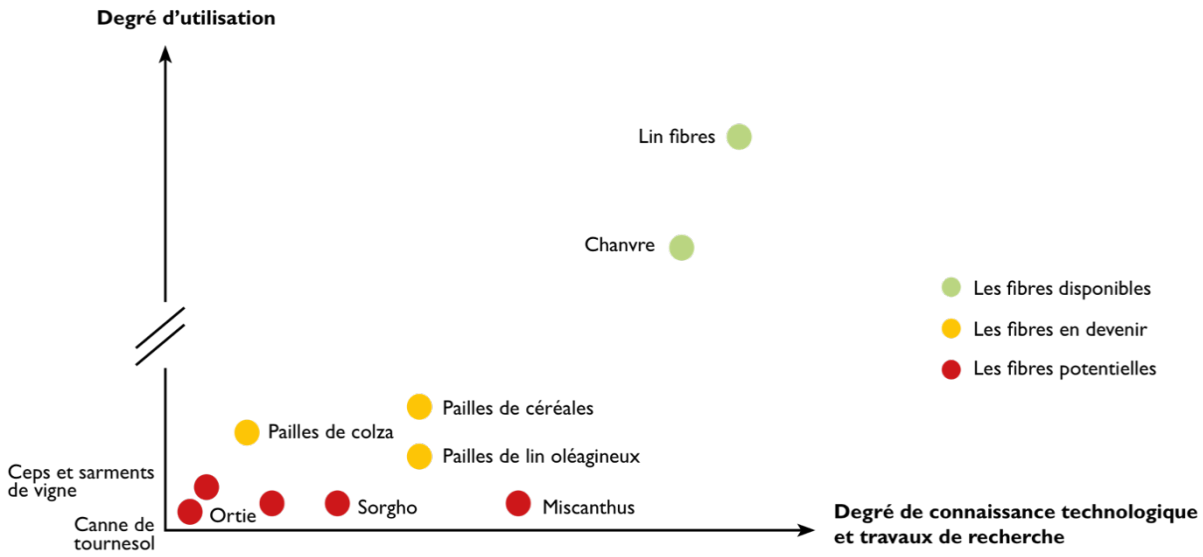

Figure 7 - Degré de maturité de l'utilisation des fibres végétales dans les matériaux en France [49]

A l'issue de leur première transformation, les fibres incluses dans les biocomposites peuvent être de taille centimétrique, millimétrique ou micrométrique selon l'application recherchée et selon la matrice [49].

III.2. Propriétés

Les avantages des fibres naturelles par rapport aux fibres inorganiques synthétiques sont multiples. En effet, elles présentent une densité plus faible et permettent donc d'obtenir des composites plus légers [87]. Par ailleurs, celles-ci présentent une résistance spécifique élevée et comparable à celle des fibres de verre (Tableau 4). Parmi les fibres naturelles présentées dans le Tableau 4, les fibres de chanvre présentent, avec celles de lin, les propriétés mécaniques les plus favorables avec une résistance spécifique et un module d'Young particulièrement élevés.

Tableau 4 - Propriétés des fibres végétales (NS : Non spécifié) [30,88]

Fibres	Origine	Longueur (mm)	Diamètre (µm)	Résistance spécifique (MPa)	Résistance à la traction (MPa)	Module d'Young (GPa)	Densité ($g.cm^{-3}$)
Verre	Synthétique	-	<17	800-1400	2000-3500	70-76	2,5-2,59
Chanvre	Plante (Tige)	5-55	10-51	370-510	550-900	30-60	1,35
Lin	Plante (Tige)	10-65	5-38	345-620	580-1100	50-70	1,38
Sisal	Plante (Feuille)	0,8-8	7-47	55-580	507-855	9,22	1,20
Jute	Plante (Tige)	0,8-6	5-25	140-320	187-773	20-55	1,23
Coco	Fruit	0,3-3	7-30	92-152	175	6	1,2
Ramie	Plante (Tige)	900-1200	20-80	590	400-1000	60	1,0-1,55
Bois résineux	Tronc	1,0	30	NS	45,5-11,7	3,6-14,3	0,30-0,59
Abaca	Plante (Feuille)	4,6-5,2	10-30	NS	430-813	31,1-33,6	1,5

Enfin, une fibre est caractérisée par sa longueur L, son diamètre D et son rapport d'aspect L/D [89,90]. Ce dernier paramètre a une forte influence sur la capacité de transfert de charges entre fibres et matrice.

III.3. Composition chimique

Les fibres végétales contiennent des polymères naturels qui leur confèrent des propriétés mécaniques intéressantes. Ces polymères naturels sont la cellulose (α-cellulose), les hémicelluloses, la lignine et les composés extractibles (cires, pectines) auxquels s'ajoute la matière inorganique en très faible quantité [34,88,91,92]. Les structures chimiques des composés principaux confèrent un caractère hydrophile et une résistance thermo-mécanique plus ou moins importants aux fibres. La Figure 8 représente la composition chimique de certaines fibres lignocellulosiques. Les valeurs correspondent aux moyennes des valeurs extrêmes minimales et maximales reportées dans la littérature [30,88]. En plus des différents constituants, il est nécessaire de prendre en compte la teneur en eau ainsi que les produits solubles et/ou la matière inorganique. En effet, l'humidité absorbée par les fibres de ramie par exemple peut atteindre 12 voire 17% de la masse totale. Cependant, la composition des fibres peut varier fortement en fonction du climat [93], du champ de récolte et des procédés de transformation qu'elles subissent après récolte [92].

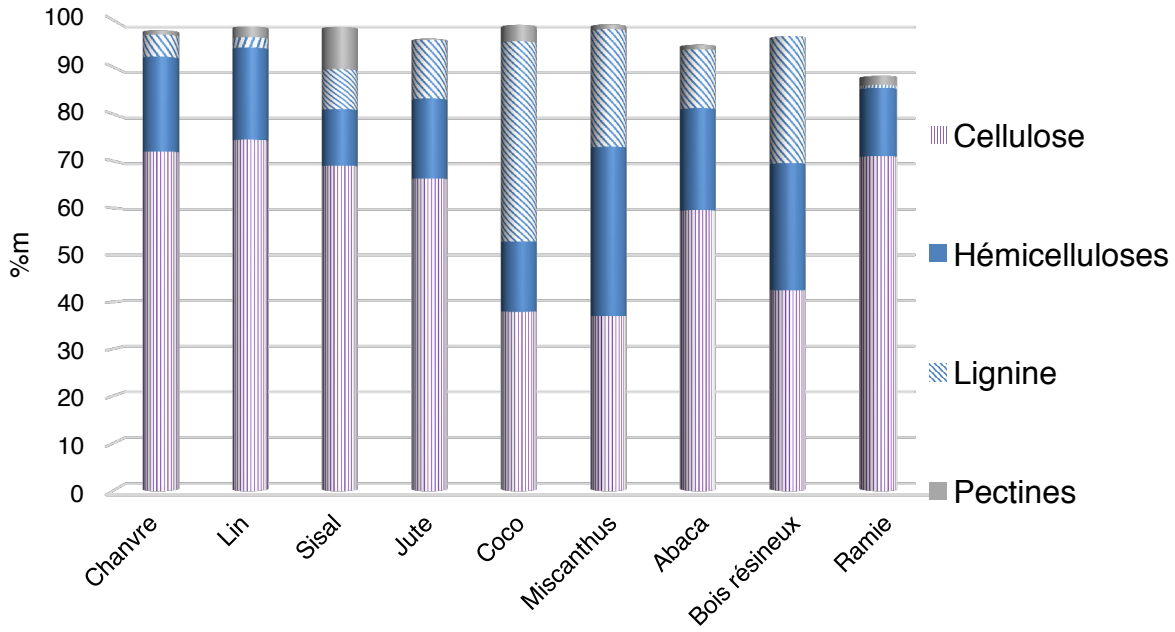

Figure 8 - Composition chimique des fibres végétales (%m) (composants principaux) [30,88,94]

III.3.1 Cellulose

La cellulose, polymère le plus abondant dans la nature, est le constituant principal des fibres végétales. Elle fait partie de la famille des polysaccharides $(C_6H_{12}O_5)_n$ [92] et détermine la plupart des propriétés physico-chimiques des fibres. Celle-ci se présente sous forme de macromolécules dont les entités répétitives de cellobiose $(C_6H_{11}O_5)_2O$ constituées chacune de deux monomères β-D-glucose sont liées entre elles par des liaisons β-1,4-glycosidiques générant une chaîne de polymère linéaire (Figure 9) [88]. La cellulose forme une structure microcristalline, avec des régions cristallines pouvant atteindre 80% de la part totale, et des régions amorphes moins ordonnées [92]. Les liaisons glycosidiques peuvent être dégradées sous l'effet de la température ou des microorganismes. Les composés volatils issus de cette dégradation sont présentés sur la Figure 12. Cependant, la cellulose se dégrade à plus haute température que les autres composants lignocellulosiques [95].

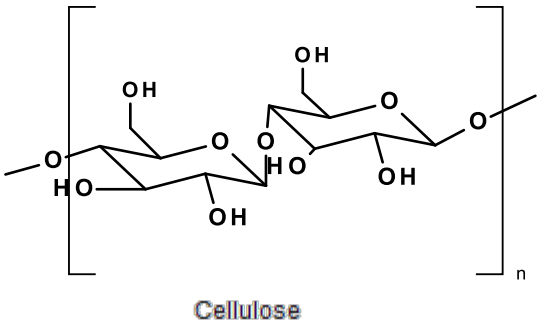

Figure 9 - Structure de la cellulose

III.3.2 Hémicelluloses

Les hémicelluloses sont les polysaccharides les plus présents dans le monde végétal après la cellulose et font partie, en plus de la cellulose, de la fraction carbohydratée des fibres. Les hémicelluloses sont constituées de polymères ramifiés contenant des groupes latéraux à l'origine de sa structure chimique amorphe et variée [96]. Elles contiennent des sucres à 5-6 atomes de carbone [53]. En effet, contrairement à la cellulose, les hémicelluloses ne sont pas seulement constituées de glucose. Les monomères sont principalement des xyloses, mannoses et galactoses selon la plante d'origine et leur condition de synthèse dans la nature (Figure 10) [97]. Se situant à l'interface entre les microfibrilles de cellulose et la lignine, celles-ci jouent le rôle de liant entre ces composants. Par ailleurs, les hémicelluloses sont facilement hydrolysables conduisant à la formation de sous-produits tels que les furanes et cyclopentanones [98].

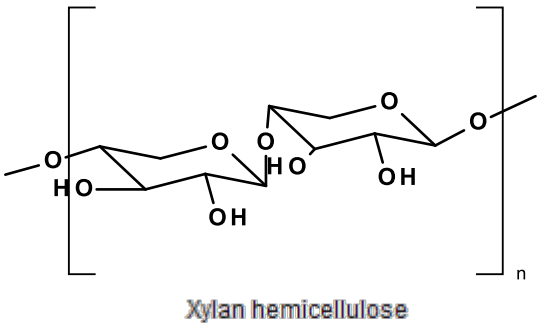

Figure 10 - Structures chimique de l'hémicellulose xylane

III.3.3 Lignine

La lignine, troisième constituant, est un polymère amorphe de structure complexe tridimensionnelle le plus abondant sur terre après les polysaccharides [99]. Elle est constituée d'unités aromatiques phénylpropane [100]. Contrairement à la cellulose et aux hémicelluloses, la lignine est hydrophobe et contribue à la rigidité des fibres [53]. Les unités primaires constituant la lignine, autrement appelés monolignols, sont l'alcool conifé rylique (G), l'alcool sinapylique (S) et l'alcool *p*-coumarylique (H) (Figure 11) [92]. La lignine ne se structure pas de la même façon selon les différents types de fibres. Les propriétés d'une lignine sont alors souvent caractérisées par le rapport des taux S/G notamment pour définir la dégradabilité de la lignine. Cependant, les monomères représentés sur la figure sont communs à toutes les lignines [101]. Des sous-produits issus de la décomposition thermique de la lignine tels que les acides sinapylique, p-coumarylique et vanillique peuvent être formés [102].

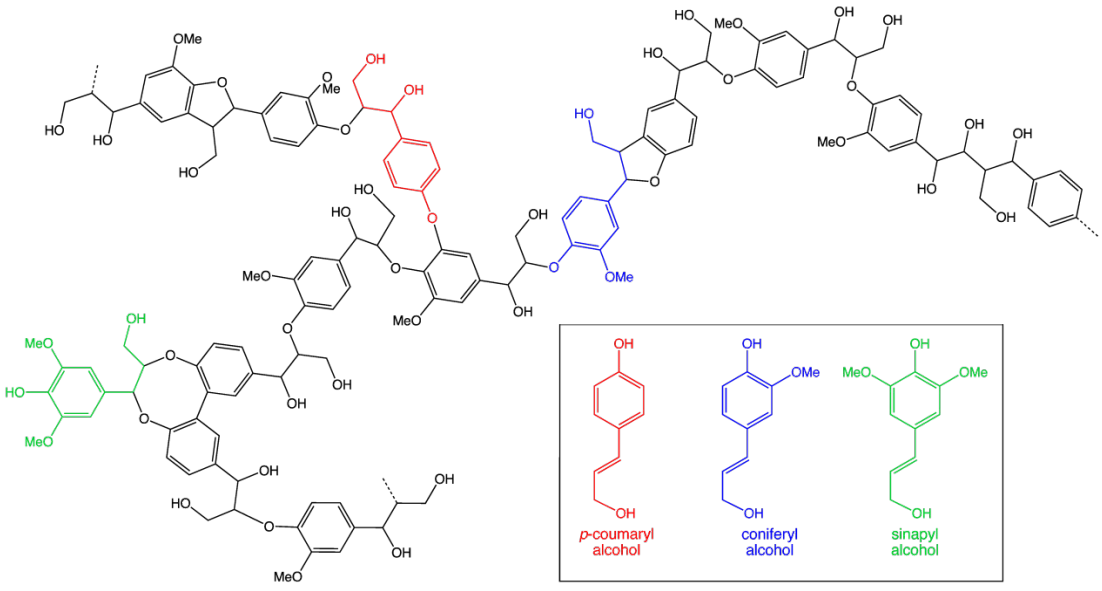

Figure 11 – Structure générale de la lignine [103]

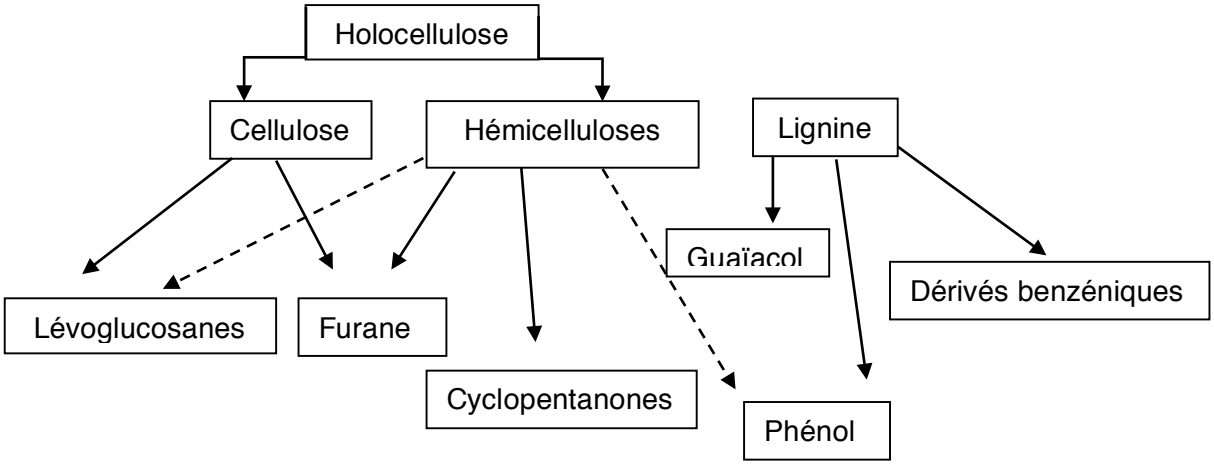

Figure 12 - Substances issues de la lignocellulose [7,98,104,105]

III.3.4 Pectines

Les pectines appartenant aussi à la famille des polysaccharides sont généralement retrouvées à faible teneur dans les fibres végétales [97]. Les fibres sont liées à la tige par les pectines. Ces dernières sont essentiellement éliminées au cours du rouissage consistant en un pré-traitement de défibrage pour favoriser la séparation des fibres de la tige [97].

III.3.5 Minéraux

Les minéraux constituent la part inorganique des fibres regroupant la silice et les sels métalliques [92]. Pour les fibres présentées sur le diagramme de la Figure 8, le taux est généralement inférieur ou égal à 1%. Par ailleurs, les sels de potassium peuvent accélérer la réaction de décomposition de la lignocellulose. En effet, leur activité catalytique a été démontrée au cours d'une pyrolyse des fibres, pendant laquelle la formation de coke était favorisée en présence d'acétate de potassium [106].

III.4. Structure et morphologie

Les fibres naturelles peuvent être définies comme des matériaux composites pluristratifiés. Leurs différents composants décrits précédemment s'organisent selon un schéma bien défini. Les fibres sont composées d'une paroi cellulaire primaire hydrophile souple (P) et de trois parois cellulaires secondaires plus hydrophobes et rigides (S1, S2, S3) (Figure 13) [62,97]. Ces parois cellulaires incluent des microfibrilles cristallines (chaînes de cellulose assemblées) orientées de manière hélicoïdale et reliées entre elles par la lignine et les

hémicelluloses. La paroi secondaire, assimilée à un composite organisé constitué de plusieurs polymères tels que les microfibrilles de cellulose et une matrice amorphe lignine/hémicellulose [7], joue un rôle majeur dans les propriétés physico-chimiques et mécaniques des fibres puisqu'elle présente le plus faible angle microfibrillaire. Ce dernier définit l'angle que forment les microfibrilles avec l'axe principal de la fibre et conditionne les caractéristiques des fibres de renforts puisque de petits angles favoriseront une force et une rigidité élevées des fibres alors que de larges angles induiront une ductilité [107]. Les fibres de chanvre présentent un angle microfibrillaire particulièrement étroit (2-6,2°) comparé aux autres fibres naturelles telles que le lin (5-10°), la banane (30-49°) ou le sisal (10-22°) justifiant certainement leur résistance spécifique élevée (Tableau 4).

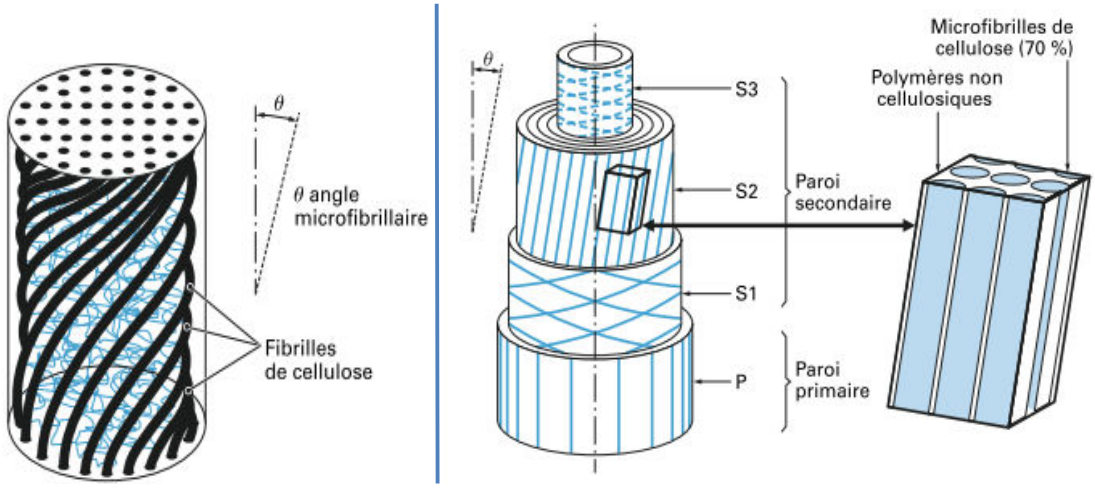

Figure 13 - Organisation structurelle d'une fibre élémentaire [97]

Ainsi, dans ce groupe de plantes à fibres, le chanvre a été retenu pour notre étude du fait de ses propriétés spécifiques intéressantes, de son degré de connaissance important et de son utilisation dans les deux secteurs de la construction et de l'automobile étudiés.

IV. Les biocomposites

IV.1. Propriétés mécaniques

La possibilité d'utiliser des biocomposites en remplacement des composites conventionnels pour des pièces de panneaux intérieurs de composants automobiles a été évaluée par Ahmad et al [34]. Les matériaux furent comparés selon leur indice de performance évalué selon le rapport entre le module d'Young $E^{1/3}$ ou la résistance à la traction $S^{1/2}$ et leur densité

ρ. Ainsi, un matériau rigide ou résistant et peu dense possède un indice élevé. Le composite époxy/fibres de carbone fut le matériau satisfaisant au mieux les exigences requises évaluées selon les indices $E^{1/3}/\rho$ et $S^{1/2}/\rho$. Cependant, le PP renforcé de fibres de chanvre se manifesta comme un candidat plus adapté que le PP renforcé de fibres de verre puisque son indice plus élevé démontra une force et une rigidité élevées tout en étant plus léger. Donc les biocomposites présentent un fort potentiel de remplacement des composites à fibres de verre. Cependant, bien que les propriétés spécifiques des fibres végétales, notamment leur rigidité, soient comparables à celles des fibres synthétiques, les propriétés mécaniques des biocomposites restent plus faibles à cause d'une différence de polarité entre la fibre naturelle et la matrice et donc à une interface fibre/matrice moins favorable (Figure 14). Par ailleurs, même si les fibres végétales représentent un coût massique moins élevé [37], les coûts de production des deux types de composites restent comparables [52]. Cependant, ceci peut dépendre de plusieurs facteurs. En effet, selon les paramètres pris en compte dans le coût (consommation d'énergie, matières premières, impact sur l'appareillage de mise en œuvre, résultats de récolte des fibres naturelles, …), le coût de valorisation des fibres peut fluctuer [108].

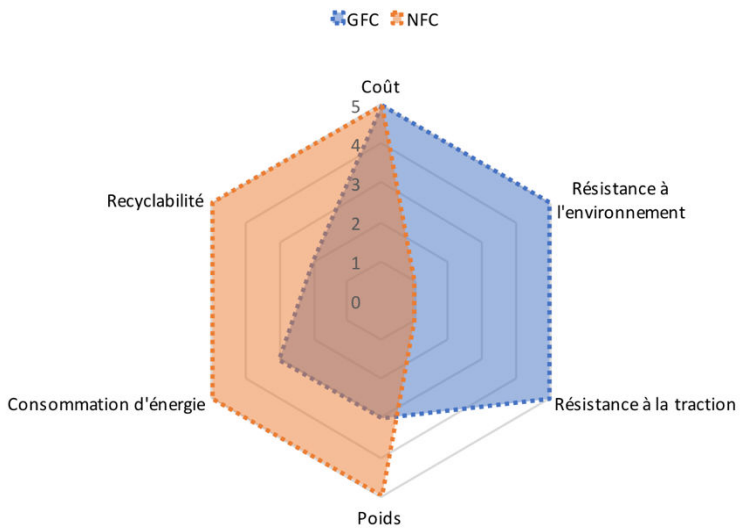

Figure 14 - Comparaison de mérite entre les composites renforcés de fibres naturelles (NFC) et les composites renforcés de fibres de verre (GFC) (moyenne) [30]

Toutefois, le nombre croissant de publications récentes traitant des propriétés des biocomposites reflète l'intérêt grandissant pour ce type de matériaux [7]. Plusieurs études traitent de la comparaison entre un polymère vierge et renforcé par des fibres naturelles

telles que les fibres de chanvre choisies pour cette étude. La Figure 15 résume l'influence de différentes fibres végétales et de verre inclues dans différentes résines pétrosourcées (PP, PE) et biosourcées (PLA, PBS) sur le module et la résistance à la flexion (test de flexion 3 points) mesurés avant et après incorporation de fibres végétales dans la matrice polymère à un même taux (30 %m). A noter que la comparaison avec les composites renforcés de fibre de verre est à analyser avec précaution étant donné les différences de densité. De même, les mêmes fibres de renforts ont été sélectionnées dans la littérature afin de comparer l'influence de la matrice. En général, plus le taux de fibres augmente, meilleure est la performance mécanique des composites. Par ailleurs, la composition chimique des fibres naturelles (proportion en cellulose, hémicellulose, lignine, et cires et pectines) a un effet conséquent sur la rigidification et le renforcement du composite. On peut noter que la résistance à la flexion augmente avec le taux de cellulose. En effet, au sein d'une même résine (ici le PP), la cellulose pure renforce davantage le matériau présentant une résistance plus élevée que les composites renforcés de fibres lignocellulosiques. Une même tendance a été reportée par Bledzki et al après un test en traction [96]. Toutefois, ceci n'est pas valable pour le composite PLA/cellulose recyclée. En effet, l'étape de recyclage de la cellulose a sûrement fortement affecté la structure cristalline du composé carbohydraté et donc dégradé ses propriétés. La lignine rigidifie les parois cellulaires des fibres et agit comme une barrière protectrice pour la cellulose [65,109]. Ceci pourrait notamment justifier le module plus élevé des composites PP et PLA renforcés par des fibres d'abaca par rapport aux autres fibres. En effet, l'abaca contient plus de lignine que le chanvre et le lin (Figure 8). Par ailleurs, les propriétés des biocomposites restent comparables aux composites à fibre de verre [110].

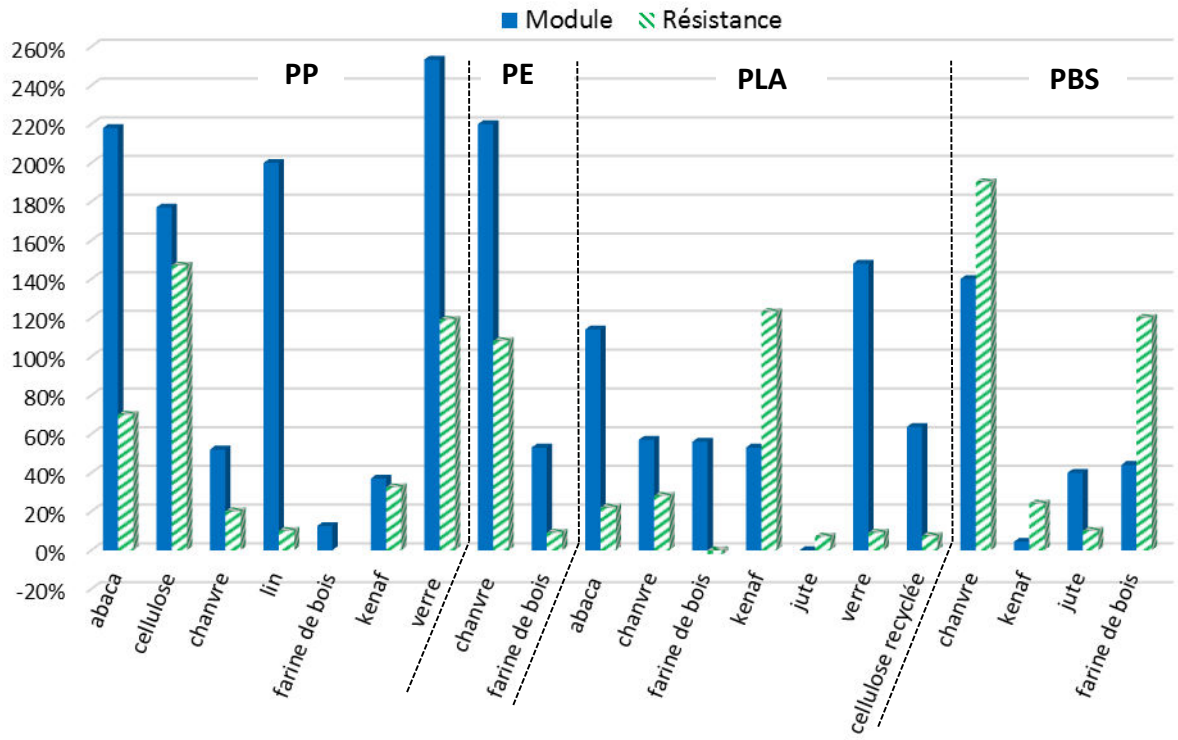

Figure 15 – Pourcentage d'augmentation des propriétés mécaniques en flexion de biocomposites pour un même taux massique de fibre de 30% [55,87,110–121]

IV.2. Procédés de mise en œuvre et mise en forme

Généralement, des produits semi-finis sont utilisés pour mettre en forme les biocomposites [31]. Ces produits peuvent être sous plusieurs formes :

- les fibres seules non mélangées à la résine sous forme de mats obtenus par la méthode de cardage pour démêler les fibres ou sous forme de tissés.
- les mélanges fibres/matrices obtenus par extrusion en voie fondue.

Différentes technologies de mise en forme des produits semi-finis existent via des procédés couramment utilisés pour des composites plus conventionnels. Les moulages par compression et par injection utilisés sont ceux principalement développés pour les composites à matrice thermoplastique [31,90]. Le moulage par injection est le procédé le plus largement utilisé en raison notamment de ses temps de cycle courts et sa reproductibilité. Ce procédé permet de fabriquer des formes complexes en injectant une matière fondue dans un moule [31]. D'autres procédés tels que le moulage par transfert de résine (RTM) et l'infusion [3] sont réservés à la mise en œuvre de biocomposites à matrice thermodurcissable.

Plusieurs travaux ont été reportés dans la littérature sur les biocomposites à matrice PP obtenus par moulage par compression [90,111,112,122,123] et moulage par injection [124–127] généralement précédés d'une étape d'extrusion dont les propriétés mécaniques, thermiques, microstructurales ou de durabilité ont été mesurées. Des études comparatives entre les différents procédés de mise en œuvre des biocomposites, tous types de matrices confondus, ont aussi été menées. Par exemple, Liu et al ont formulé des biocomposites dont la matrice biosourcée est à base de protéines de soja renforcée de fibres de kénaf. Ils ont relevé une température de fléchissement sous charge (HDT) et une résistance au choc Izod entaillé des biocomposites mis en forme par compression plus élevées que ceux injectés. Cela signifie que le moulage par compression permet de mieux préserver les propriétés thermiques et mécaniques des biocomposites car les efforts de cisaillement sont plus faibles qu'en injection. Les propriétés mécaniques de PVC renforcé de fibres de verre et fibres de bois obtenus après procédé d'extrusion bi-vis ont été comparées à celles de PVC obtenu par un procédé de compression [128]. Le composite était plus dense après compression évitant les propagations de défauts liés aux espaces vides éventuellement formés à l'interface fibre/matrice. Bledzki et al ont aussi examiné l'impact du choix de la technique de mise en forme parmi les mélangeur-moulage par injection, mélangeur-moulage par compression et moulage par compression directe sur les propriétés mécaniques (résistance à l'essai de résilience Charpy, traction, flexion) de PP renforcé de fibres d'abaca [129]. Le procédé de mélangeur-moulage par injection a garanti un composite de meilleure résistance à la traction (environ 90%) que les autres procédés. Cependant, le moulage par compression directe (sans mélange préalable) a induit une meilleure résistance à l'essai Charpy que les deux autres procédés de mise en œuvre. Tous ces faits démontrent l'importance du choix rigoureux des techniques et paramètres de formulation appropriés afin d'obtenir un composite aux performances optimales.

De plus, il n'est possible de profiter des propriétés mécaniques du renfort que si le transfert de contraintes entre la matrice et le renfort est efficace. Une bonne cohésion est alors indispensable. Cependant, la différence de polarité entre la fibre naturelle polaire et la matrice de polymère généralement non polaire induit une liaison interfaciale faible [130] et donc une limitation des propriétés finales du biocomposite. Des solutions permettent de pallier ce problème, telles que le traitement chimique en surface des fibres avant

incorporation dans la matrice [131,132] pour favoriser les liaisons chimiques. Aussi, l'ajout d'un agent de compatibilisation évite d'avoir recours à un pré-traitement chimique des fibres végétales [67,112,133]. Les agents à base d'anhydride maléique s'avèrent notamment être efficaces pour les biocomposites à matrice polyoléfine comme le PP [130].

Cependant, des limites non négligeables entravent l'utilisation de fibres naturelles et donc leur émergence dans les domaines d'application cités précédemment. En effet, les fibres végétales sont très hydrophiles de par leur composition chimique et sont donc sensibles aux conditions environnantes (lorsque le taux d'humidité est élevé, par exemple). Aussi, la structure des composés lignocellulosiques rend les fibres très sensibles aux conditions extérieures telles que l'exposition aux rayonnements UV provenant du soleil, à la chaleur ou un fort taux d'humidité. Ainsi, il est crucial de déterminer les causes de l'altération de la performance des biocomposites et leur conséquence sur les variations de leurs propriétés.

V. Les différents types de vieillissement : impact sur les propriétés mécaniques et microstructurale des biocomposites

Le vieillissement peut être défini selon son mécanisme, physique ou chimique, ou selon son mode d'action qui peut être principalement de nature hydrolytique, thermique ou photochimique. Les vieillissements présentés par la suite sont des causes de dégradation dues aux contraintes extérieures et conduisent donc à des modifications ou des ruptures de chaînes de polymère.

V.1. Vieillissement photochimique

Lorsqu'un matériau polymère est exposé au soleil, celui-ci absorbe l'énergie de la lumière solaire et passe de son état fondamental à un état excité. Ce passage à un nouvel état lui confère une réactivité qu'il n'avait pas auparavant. Ceci se traduit par la formation de radicaux libres qui sont des composés instables et propagent le phénomène de dégradation du matériau. Ces radicaux peuvent notamment réagir avec l'oxygène présent dans l'air et former des composés radicaux peroxydes POO° et hydroperoxydes POOH (Figure 16). L'abstraction d'hydrogène par les espèces radicalaires POO° ou OH° pour générer le radical P° durant la propagation se fera préférentiellement sur le carbone tertiaire [134,135]. Cette

génération de radicaux supplémentaires consiste donc en un processus d'auto-dégradation photochimique.

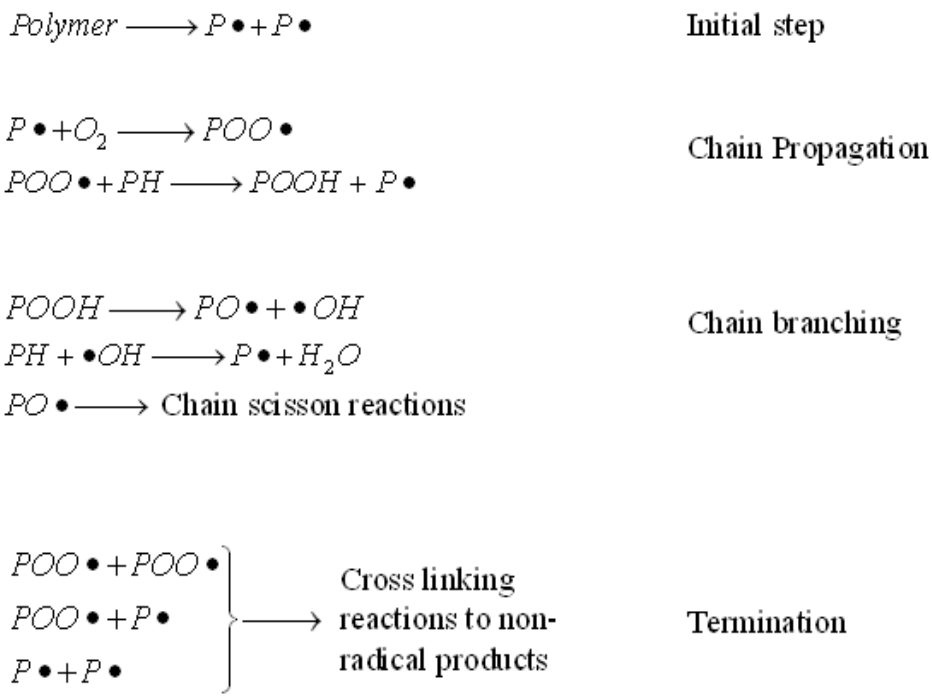

Figure 16 - Mécanisme de photodégradation des polymères [135]

De même, la faible énergie de dissociation de PO-OH (42 kJ.mol^{-1}) justifie sa très forte réactivité [135]. De par la présence d'électrons non appariés, dits électrons célibataires, dans la couche externe des radicaux oxy PO° formés, ces derniers présentent eux aussi une très forte instabilité qui provoque leur décomposition en composés carbonylés accompagnée d'un clivage de chaînes macromoléculaires [136]. En effet, les espèces PO° peuvent subir une β-scission ou former un groupement carbonyle intra-chaîne [135]. Ces carbonyles instables se décomposent par photolyse via les mécanismes de type Norrish. La réaction de type Norrish I implique une β-scission des composés carbonylés formés avec dégagement de CO et formation de deux alkyles radicaux [136]. La réaction de type Norrish II est un processus intramoléculaire via l'abstraction d'un γ-hydrogène générant des espèces carbonyles et vinyles [137,138].

Les polymères thermoplastiques sont soumis à ce type de vieillissement durant leur cycle de vie. Leur exposition à la lumière solaire résulte en des scissions de chaîne et réticulations

pour le PE ou scissions de chaîne seulement pour le PP [136]. Cela induit une diminution de la masse moléculaire et donc des chaînes plus courtes et plus mobiles cristallisant plus facilement [7]. Cependant, au sein d'un biocomposite à matrice polyoléfine, la dégradation photochimique affecte particulièrement les fibres naturelles. En effet, à l'état non dégradé, les composés lignocellulosiques contiennent des molécules avec des groupements fonctionnels cétones capables d'absorber des photons, autrement qualifiées chromophores. Ces espèces peuvent absorber la lumière UV initiant des réactions de photo-oxydation [119]. Le schéma simplifié suivant proposé par Azwa et al résume le chemin mécanistique dans lequel sont impliquées la photodégradation du polymère et des fibres et l'activité catalytique des groupements chromophores et des hydropéroxydes POOH [7].

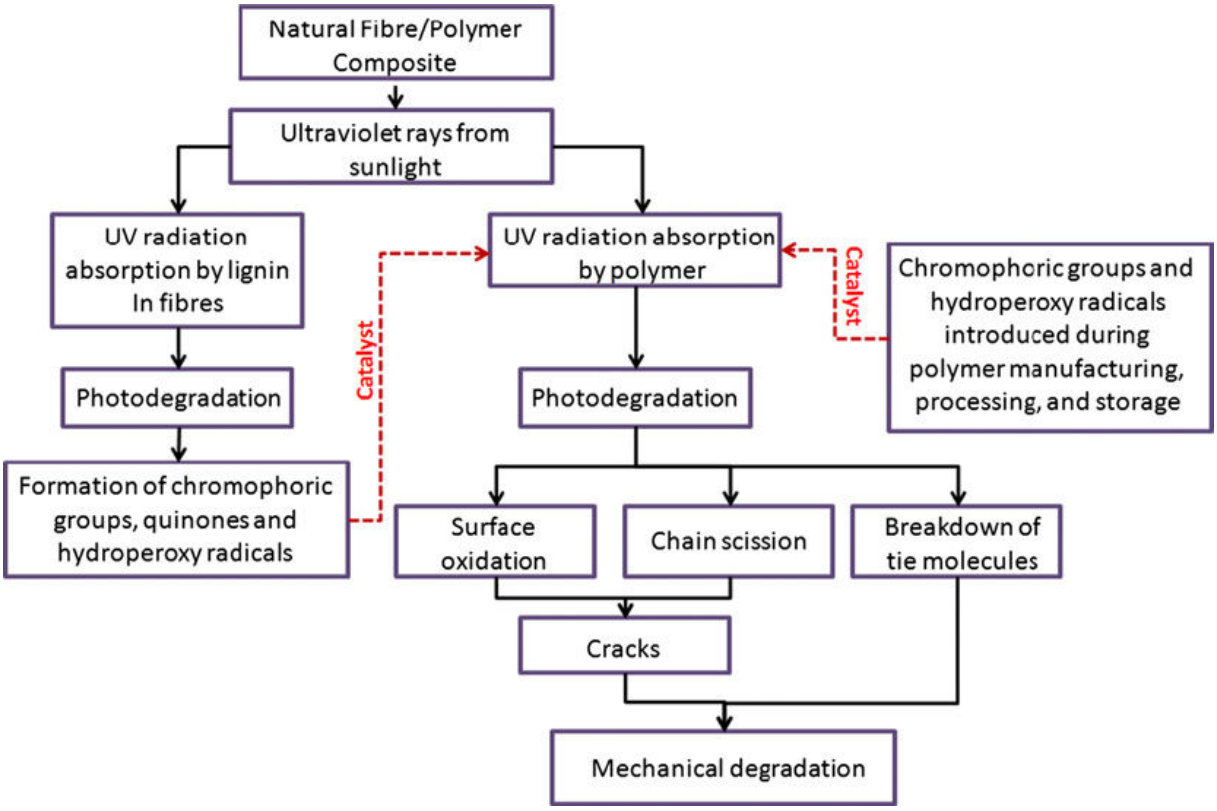

Figure 17 - Photodégradation des biocomposites et leurs composants

Sachant que le rayonnement UV proche (λ = 315-400 nm) est principalement responsable des modifications de structure chimique, de nombreux chercheurs ont procédé à ce type de dégradation en enceinte en imposant une radiance UV fixe à l'aide de lampes à fluorescence ou xénon. Les variations des propriétés mécaniques et microstructurales de biocomposites ont été ainsi mesurées après vieillissement accéléré en fonction du type de fibres et de farines naturelles. Lors d'une exposition UV, les propriétés mécaniques telles que le module

d'Young et la résistance à la traction ou à la flexion sont généralement affectées. En effet, le module a augmenté d'environ 4%, 25% et 7% pour les composites PLA/25%m de balles de riz en 1000h, PE/50%m de farine de bois en 3000h et PP/30%m de lignine en 960h respectivement après leur exposition sous rayons UV [100,139–141]. Ceci résulte d'une rigidification des matériaux liée à la cristallisation des chaînes plus courtes formées après scissions de chaînes du polymère. Cette hypothèse est confirmée par les mesures du degré de cristallinité des matrices ayant augmenté de 3,71% à 26,02% en 1000h et de 13,62% à 20,85% en 600h pour le composite à matrice PLA renforcé de balles de riz et de fibres de cellulose respectivement [139,142].

Les lois de réciprocité sont communément utilisées pour décrire l'effet de l'intensité de la lumière sur les polymères à partir de paramètres empiriques [143,144]. Bien qu'elles conviennent pour décrire des phénomènes dont les intensités ne varient pas significativement entre les conditions expérimentales de vieillissement et les conditions réelles d'usage, ces lois ne peuvent être appliquées lorsque le coefficient de proportionnalité varie avec l'intensité de la lumière. En effet, l'intensité de la lumière solaire filtrée par l'atmosphère ne sera pas filtrée en même quantité en enceinte. Schwarzschild a modifié la loi de réciprocité classique en considérant l'indice p (coefficient de Schwarzschild), paramètre supplémentaire permettant de considérer l'influence du matériau et des conditions expérimentales mais indépendant de la longueur d'onde de la lumière [143–145]:

$$Q = I^p \times t \qquad \text{Eq. 1}$$

avec Q l'énergie de rayonnement cumulatif ($J.m^{-2}$) (constant), t le temps (h), I l'intensité ($W.m^{-2}$) et p le paramètre de Schwarzschild. Ainsi, des sources de lumière d'intensité différente provoquent le même degré de dégradation sous différentes expositions si leurs produits $I^p \times t$ sont équivalents.

Ceci permet d'établir une corrélation entre les sources lumineuses de vieillissements artificiel et naturel.

V.2. Vieillissement thermique

Les fibres naturelles et les matrices de polymère sont soumises à une dégradation thermique lors de l'étape de mise en œuvre des biocomposites durant laquelle la température peut

s'élever à 220°C. Cependant, le vieillissement thermique peut être également observé lors du cycle de vie du biocomposite. Ce processus s'enclenche par la génération d'un radical soit par la présence de défauts de structure (irrégularités structurales) soit par rupture de liaisons des chaînes macromoléculaires, soit par la présence d'impuretés (amorceurs, résidus de catalyseurs de polymère, …). Les mécanismes de dégradation sont similaires à ceux se déroulant au cours d'une dégradation photochimique. Ainsi, la composition chimique des biocomposites est affectée et des composés oxygénés tels que des alcools, cétones, acides, péroxydes et aldéhydes sont formés et peuvent être détectés par analyse infrarouge.

Joseph et al ont étudié le vieillissement thermique effectué à 80°C de polyéthylène basse densité (PEBD) renforcé de fibres de sisal d'une part, et de fibres de verre d'autre part, pendant 7 jours [146]. Le dernier composite a présenté une meilleure stabilité dimensionnelle que le biocomposite grâce à une meilleure interface fibres synthétiques/matrice.

La prédiction de la durée de vie d'un matériau a été largement étudiée notamment selon le modèle type Arrhénius. Dans un cas simple de vieillissement thermique accéléré, l'extrapolation de la performance du matériau sous conditions ambiantes la plus communément appliquée implique que le taux de dégradation soit contrôlé par un taux réactionnel k exprimé comme suit [48,144,147] :

$$k = Aexp(-\frac{Ea}{RT}) \quad \text{Eq. 2}$$

avec k la constante de vitesse réactionnelle, A le coefficient pré-exponentiel, E_a l'énergie d'activation ($J.mol^{-1}$), R constante universelle des gaz parfaits (8,314 $J.mol^{-1}.K^{-1}$), T la température absolue (K). Cependant, l'extrapolation d'Arrhénius linéaire est controversée [144,147]. En effet, une relation type Arrhénius non-linéaire serait plus adaptée notamment à cause de la diffusion d'oxygène. En effet, des changements mécanistiques avec deux régimes différents à température faible et à température élevée induisent des variations de l'énergie d'activation devant être prises en compte dans la relation précédente :

$$k1 + k2 = A1exp\left(-\frac{E_{a1}}{RT}\right) + A2exp\left(-\frac{E_{a2}}{RT}\right) \quad \text{Eq. 3}$$

avec k_1 et k_2 les taux réactionnels des deux régimes. Par ailleurs, la température accentue le phénomène de photo-oxydation des polymères présenté précédemment. Dans un cas simple de photo-vieillissement, le modèle cinétique peut être décrit d'après la loi d'additivité, inspiré de la loi d'Arrhénius cité précédemment en incluant l'intensité de la lumière I [148]. Cependant, même si le temps d'induction de la photo-oxydation est réduit quand la température augmente [148], le taux de photo-oxydation évalué à partir de mesures spectroscopiques montre une dépendance n'obéissant pas à la relation d'Arrhénius [143,148].

V.3. Vieillissement hydrolytique

En conditions naturelles, la dégradation par rupture hydrolytique est causée par la pluie ou un fort taux d'humidité. La présence d'eau peut ainsi induire des scissions de chaîne du polymère et un gain en masse lorsque l'eau se fixe de manière irréversible aux chaînes de polymère compromettant la stabilité dimensionnelle du matériau [149]. L'absorption d'eau par les biocomposites est gouvernée par les groupements hydroxyles présents dans les fibres. De ce fait, un taux élevé en hémicelluloses dans les fibres favorisera l'absorption du fluide. Le mécanisme d'absorption d'eau par les biocomposites peut être décrit par la loi de diffusion de Fick puisque l'eau diffuse selon un gradient de concentration. L'équation de la loi de Fick a été simplifiée par Shen et Springer pour démontrer que l'absorption initiale est exprimée selon la formule suivante [150] :

$$\frac{M_t}{M_\infty} = \frac{4}{h} \times \left(\frac{D \times t}{\pi} \right)^{1/2} \qquad \text{Eq. 4}$$

avec M_t le taux de gain massique à l'instant t (%), M_∞ le taux maximal d'eau absorbée à saturation (%), D le coefficient de diffusion dans le composite ($cm^2.s^{-1}$), h l'épaisseur de l'échantillon (cm) et t le temps d'immersion (s). Ainsi, selon la Figure 18 représentant le taux d'humidité du matériau en fonction de $t^{1/2}$, l'absorption d'eau augmente linéairement au début puis atteint un plateau de saturation [151].

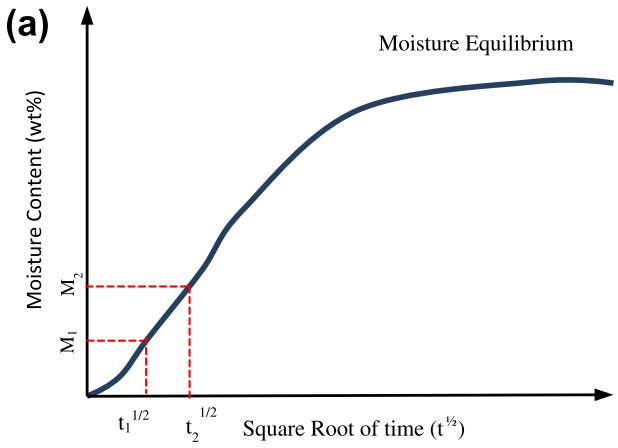

Figure 18 - Allure de la courbe d'absorption d'eau par les biocomposites [7]

La migration de l'eau au sein du polymère est favorisée dans les zones amorphes qui sont perméables aux molécules d'eau. Par ailleurs, les polyesters (PLA, PBS) sont particulièrement sensibles à l'hydrolyse [152]. En effet, le clivage des groupements esters est favorisé par les molécules d'eau. Ce caractère peut d'autant plus fragiliser les biocomposites. L'immersion dans l'eau chauffée à 60°C de PLA renforcé de fibres de ramie à un faible taux (10 %m) a induit une diminution drastique des résistances à la traction et à la flexion de 87% et 77% respectivement en moins de 3 semaines [149]. Par contre, le PP chargé à 40 %m de fibres Kraft, fibres plus sensibles à l'absorption d'eau que les fibres de ramie puisque principalement carbohydratées, présente pourtant un taux de diminution de la résistance à la traction de seulement 30% après immersion à température plus élevée (70°C) [153]. Ceci suggère que le PLA a été fortement affecté par le vieillissement hydrolytique.

Aussi, la capacité d'absorption d'eau dépend de l'affinité qu'a le polymère vis-à-vis de l'eau et cette affinité peut être déterminée à partir de son paramètre de solubilité : plus ce paramètre est proche de celui de l'eau, plus le polymère a une affinité avec ce solvant. La température de transition vitreuse Tg du polymère déterminée par analyse thermique DSC peut aussi être modifiée : le matériau présente alors un aspect caoutchouteux à une température plus faible que sa Tg initiale, on parle de plastification du polymère. Cela engendre un matériau plus ductile, d'où une diminution du module d'élasticité et une augmentation de l'allongement à la rupture [152].

La vulnérabilité d'un biocomposite face à un vieillissement hydrolytique est principalement liée à l'interface fibre/matrice qui est une zone très fragile (Figure 19). En effet, un

vieillissement par immersion dans l'eau de composites PP/lin a été effectué par Arbelaiz et al afin d'étudier les cinétiques de gain en masse par ces derniers [125]. Cette immersion a alors provoqué un gonflement de la cellulose. Ceci a généré des contraintes de cisaillement à l'interface matrice/fibre, et donc leur décohésion affectant les propriétés mécaniques (module et résistance à la traction) des biocomposites après immersion [7].

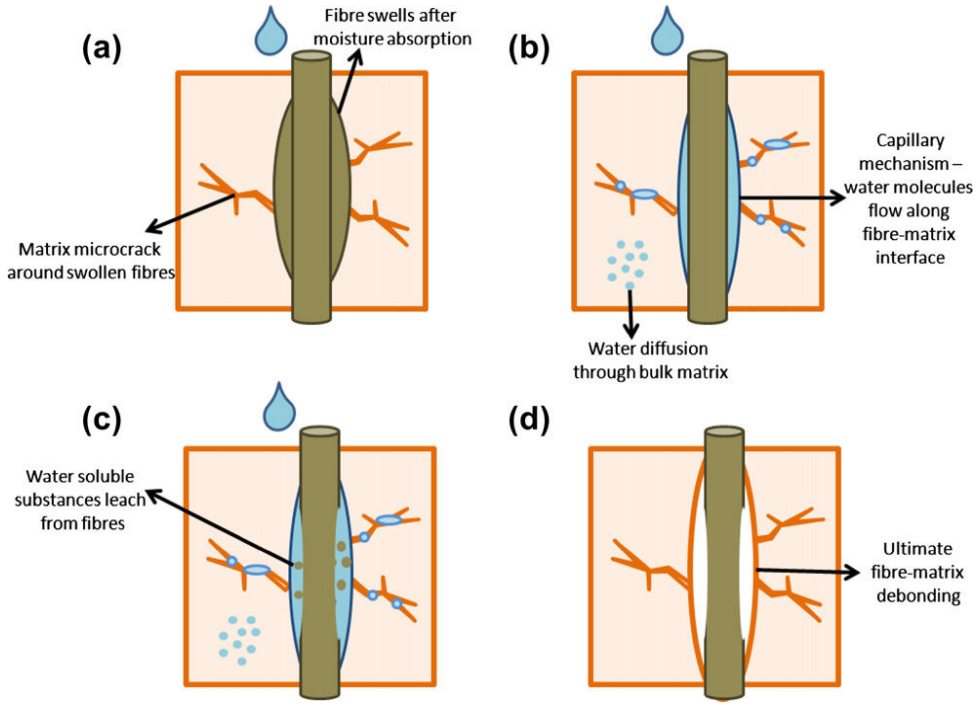

Figure 19 - Mécanisme d'absorption d'eau par les biocomposites [7]

De plus, la température peut faciliter la diffusion des molécules d'eau au sein du matériau. Par exemple, Joseph et al ont observé une prise en eau de composites PP/sisal plus rapide une fois l'eau chauffée à 70°C [154]. Afin de limiter l'absorption d'eau en environnement humide par les composites renforcés de fibres naturelles, la méthode communément utilisée consiste à augmenter l'hydrophobicité des fibres et améliorer l'adhésion interfaciale par traitement des fibres. Par exemple, l'ajout d'agent de couplage a permis de limiter la prise en eau des biocomposites [37,111,155].

V.4. Vieillissement des biocomposites par effet synergique

V.4.1 Vieillissement artificiel

Des vieillissements accélérés incluant les paramètres rayonnement UV, température, humidité et/ou pulvérisation d'eau sont généralement réalisés en enceinte de vieillissement

spécifique pour refléter les conditions extérieures auxquelles seront potentiellement soumis les biocomposites. Des cycles de vieillissement sont répétés plusieurs fois pour correspondre à une durée totale de vieillissement souhaitée. Puisque les lampes intégrées dans ces enceintes doivent refléter la lumière solaire, le spectre des lumières artificielles doit correspondre à celui de la lumière solaire et être donc continu dans la gamme 300 à 400 nm. Trois types de sources UV sont particulièrement utilisés. En effet, les chambres de photo-vieillissement ARTACC et SEPAP sont équipées d'une lampe à vapeur de mercure alors que les lampes fluorescentes sont favorisées dans l'enceinte QUV et les lampes à arc-xénon dans l'enceinte Xenostest. Les lampes les plus courantes ont des irradiances à 340 nm de 0,35 à 0,55 $W.m^{-2}$. Les conditions hygrothermiques peuvent aussi être contrôlées. Les résultats peuvent dépendre du type de lampe utilisé.

Plusieurs travaux extraits de la littérature sont présentés dans le Tableau 5 résumant la perte (en %) des propriétés mécaniques (modules et contrainte à la rupture en traction et en flexion) et les variations des propriétés microstructurales (taux de cristallinité) de biocomposites après vieillissement artificiel.

Les résultats du Tableau 5 montrent que, selon les conditions de vieillissement, les variations de propriétés mécaniques et de microstructure sont plus ou moins significatives. On observe que, lorsque tous les paramètres (rayons UV, chaleur, pulvérisation et condensation) sont considérés, l'impact sur les propriétés peut être très important. Par exemple, l'exposition à tous ces facteurs d'un composite PLA renforcé à 30 %m de fibres de chanvre a provoqué une réduction drastique de 83% de la contrainte à la rupture en flexion et en traction et du module en traction et flexion de 74-84% en 1000h [115]. Cependant, des conditions d'exposition similaires ont beaucoup moins endommagé le composite PP chargé à 40 %m de fibres de pin Kraft avec une chute de modules en traction ou flexion de 11-13% [156]. Ce résultat suggère que dans des mêmes conditions de vieillissement les biocomposites à matrice PP disposeraient d'une meilleure durabilité que ceux à matrice polyester.

Par ailleurs, les données de ce tableau de synthèse montrent que, pour un même matériau, chaque paramètre de vieillissement aurait plus ou moins d'impact sur les propriétés mécaniques du biocomposite. Par exemple, Stark et Matuana ont démontré par un simple essai UV et un essai UV + pulvérisation que l'étape de pulvérisation d'eau contribuait

fortement à la cinétique de dégradation de PEHD renforcé de farine de bois (50 m%) [140]. En effet, l'exposition aux rayons UV a induit une rigidification du biocomposite vérifiée par une augmentation du module de +25% alors que le module chute de 33% après un vieillissement combinant UV et pulvérisation. Cela peut être dû à la présence d'eau facilitant la pénétration de la lumière dans le bois et donc accélérant la photo-oxydation du composite. Une autre étude a montré que l'humidité relative affecte davantage la contrainte à la rupture en flexion et le module d'élasticité que la température et les rayons UV dans le cas de composites PEHD/farine de bois (60 %m) [157]. Ces auteurs proposent l'hypothèse qu'une humidité presque saturante amplifie la dégradation photochimique des composites. Ce résultat corrobore celui observé par Bergeret et al qui ont mis en évidence une plus forte sensibilité du biocomposite PLA/balles de riz sous cycle de24h pendant 3 jours (16h à 85°C sous une humidité de 45% puis 8h à 40°C sous une humidité de 95%) que sous simple rayonnement UV de 1000h [139]. Joseph et al [154], dans le cas d'un matériau PP/sisal (30 %m) immergé dans l'eau à 70 °C pendant seulement 7h, ont mis en évidence une fragilisation, quantifiée après essai à la traction, à peu près comparable à celle observée après 2016h d'irradiation UV à 30°C. On peut noter que d'autres auteurs ont montré des résultats cohérents à ces derniers avec une immersion de 2h à 70°C [154,155].

Parallèlement, Lopez et al se sont intéressés au vieillissement hygrothermique sans irradiation (40°C à 93% d'humidité) de PEHD/farine de bois (60 %m) [157]. Il en a résulté une réduction de la contrainte à la rupture en flexion de 25% alors qu'un vieillissement dans les mêmes conditions hygrothermiques mais avec rayonnement UV résulte en une variation de -32% de la même contrainte. Ainsi, les propriétés mécaniques sont moins affectées lorsque les composites sont seulement exposés à un taux d'humidité élevé. Donc une action synergique des paramètres peut considérablement amplifier les effets.

Les composants lignocellulosiques jouent un rôle prépondérant dans l'évolution des propriétés mécaniques et microstructurale des biocomposites au cours du vieillissement. D'après l'étude de Peng et al, le composite PP/lignine (30 %m) présente une meilleure conservation de la résistance à la rupture et du module à la flexion que les composites PP/farine de bois (40 %m) et surtout PP/cellulose (40 %m) [141]. En effet, il a été suggéré que les régions cristallines de la cellulose pouvaient être significativement affectées par l'exposition aux rayons UV et à l'absorption d'eau. Au contraire, les composés phénoliques

structurant la lignine et leur effet antioxydant pourraient prévenir la dégradation oxydative du matériau. Ainsi, même si des modifications de structure ont été confirmées par des variations de couleur, la lignine peut permettre de conserver les propriétés mécaniques du composite [141]. De plus, l'augmentation du taux de cristallinité est significativement atténuée en présence de lignine suggérant que les scissions de chaîne ont été retardées. Plusieurs chercheurs ont confirmé cette activité stabilisante de la lignine [65]. Cependant, la proportion en lignine doit être assez importante pour que les caractéristiques mécaniques du composite soient optimisées. En effet, Spiridon et al ont testé au cours de deux travaux distincts la réponse mécanique à la traction de PLA renforcé de 30 %m de cellulose d'une part et de 7 %m de lignine extraite du bois d'autre part [65,142]. Les deux composites furent exposés à un même vieillissement soit à 30°C sous 60% d'humidité et sous UV. Il a été constaté que la dégradation des propriétés mécaniques en traction est légèrement plus marquée pour le PLA/lignine.

Pour conclure, des fibres contenant des taux de cellulose et lignine différents se comporteront différemment dans des conditions d'usage similaires.

V.4.2 Vieillissement naturel

Les vieillissements effectués en laboratoire ne permettent pas de simuler tous les paramètres extérieurs susceptibles d'altérer les propriétés des biocomposites au cours de leur cycle de vie. En effet, les pluies acides, la pollution extérieure ou le développement de bactéries peuvent catalyser la cinétique de dégradation. De ce fait, les vieillissements naturels sont plus fiables quant à la représentation des conditions réelles. Cependant, ce type de vieillissement est moins reporté dans la littérature (Tableau 6). En effet, un temps d'exposition très long est souvent nécessaire pour détecter une dégradation effective du matériau. Par ailleurs, on peut remarquer que les travaux sur les vieillissements extérieurs de biocomposites incluent principalement des propriétés de surface telles que la composition chimique et l'aspect visuel (couleur, brillance). Parmi ces études, beaucoup concernent le comportement de WPCs en environnement extérieur, ce qui peut être expliqué par leur principale application extérieure (decking).

Les matrices de composites PP de WPC (60 %m) placés dans un environnement tempéré froid durant 4 mois ont subi une augmentation du taux de cristallinité de 10% alors que

l'exposition sous le même climat pendant 12 mois d'un composite équivalent mais avec un taux de charge de 70 %m a induit une diminution du taux de cristallinité de 17% [158,159]. En effet, les temps de vieillissement courts provoquent généralement une chimi-cristallisation du PP due aux scissions de chaîne. A long terme, la photodégradation atteint les zones cristallines réduisant le degré de cristallinité [140,160].

Des différences principalement en flexion de biocomposites PP/bambou (environ 35 %m) exposés à Xi'an en Chine (climat subtropical) pendant des durées comparables (10 à 12 mois) mais des années différentes ont été mesurées [161,162]. Ceci a été attribué à des conditions météorologiques différentes régnant au moment du test de vieillissement.

Les composites PEHD renforcés de 60 %m de fibres de bambou moulés par compression présentent un taux de cristallinité plus élevé qu'à l'état non vieilli même au bout de 3 ans d'exposition à Taichung (Taïwan) [163]. Ceci est dû à une stabilisation du taux de cristallinité après 4 mois d'augmentation, période après laquelle la proportion de la phase cristalline n'a sûrement pas été affectée. La dégradation s'est certainement manifestée par des réticulations des chaînes macromoléculaires du PE.

Par ailleurs, les vieillissements artificiels effectués en enceinte peuvent être corrélés aux vieillissements naturels. Les variations d'aspect visuel tel que la couleur peuvent notamment être suivies pour comparer les mécanismes de dégradation mises en jeu au cours des deux types de vieillissement afin d'évaluer la représentativité des conditions de vieillissement naturelles en enceinte [145].

Tableau 5 - Variations des propriétés mécaniques et microstructurale de biocomposites après un vieillissement accéléré (NS : non spécifié, Tamb : température ambiante) – *X_{c1} et X_{c2} taux de cristallinité mesurés par DSC à partir de l'enthalpie de fusion déterminée selon la 1ère et 2ème rampe de température respectivement*

Renforts	Matrice	Taux de renfort (%m)	Durée totale (h)	Irradiation UV ($W.m^{-2}$ @ 340nm)	Humidité relative (%)	Température (°C)	Pulvérisation (P)/ Condensation (C)/ Immersion (I)	Traction (%)		Flexion (%)		X_c (%)		Source
								contrainte à la rupture	module	contrainte à la rupture	module	X_{c1}	X_{c2}	
fibre de chanvre	PP	40	3624	-	-	Tamb	I	-35	-56	-	-	-	-	[172]
	PLA	30	1000	0,68 (1h)	-	50	P (1min) C (2h)	-83	-84	-83	-74	-	-	[121]
fibre de sisal	PP	30	2	-	-	70	I	-4	-16	-	-	-	-	[163]
			7	-	-	70	I	-11	-21	-	-	-	-	[162]
			2016	NS	-	30		-24	-35	-	-	-	-	
	PEBD	20	168	-	-	80	-	-20	-45	-	-	-	-	[154]
balles de riz	PLA	25	1000	NS	-	65		-	-	-47	+4	+600	-	[147]
			72	-	- 45% (16h,85°C) - 95% (8h, 40°C)		-	-	-	-90	-34	-	-	
fibre de pin Kraft	PP	40	1000	0,68 (1h,	-	50	P (1min) C (2h)	-13	-11	-	-	-7	-	[164]
			5712	-	-	70	I	-30	-69	-	-	-	-	[161]
farine de bois	PP	40	960	0,89 (8h)	-	60	C (4h)	-	-	-10	-30	+167	-	[106,149]
		30	120	NS (8h, 55 °C)	-		C (4h, 35°C)	-30	-10	-	-			[17]
	PEHD	60	2000	8,5	93% (avec UV)	40	-	-	-	-32	-20	-	-	[165]
				-	93%	40	-	-	-	-25	-15	-	-	
				-	34%	40	-	-	-	-17	-11	-	-	
				8,5	-	40	-	-	-	-4	-7	-	-	
				8,5	34%	NS	-	-	-	-3	-3	-	-	
		50	3000	NS (1,8h)	-		P (12min,avec UV)	-	-	-27	-33	-	-	[148]
							-	-	-	-2	+25	-	-	
		50	2000	NS (1,8h)	-		P (12min,avec UV)	-	-	-22	-26	-	-	[173]

Tableau 5 - Variations des propriétés mécaniques et microstructurale de biocomposites après un vieillissement accéléré (NS : non spécifié, Tamb : température ambiante) – *X_{c1} et X_{c2} taux de cristallinité mesurés par DSC à partir de l'enthalpie de fusion déterminée selon la 1ère et 2ème rampe de température respectivement*

Renforts	Matrice	Taux de renfort (%m)	Durée totale (h)	Irradiation UV ($W.m^{-2}$ @ 340nm)	Humidité relative (%)	Température (°C)	Pulvérisation (P)/ Condensation (C)/ Immersion (I)	Traction (%)		Flexion (%)		X_c (%)		Source
								contrainte à la rupture	module	contrainte à la rupture	module	X_{c1}	X_{c2}	
ramie	PLA	10	504	-	-	60	I	-87	-	-77	+25	+18	-	[157]
fibre de kénaf	PEHD	50	4000	0,35 (1,7h)	NS (1,8h)	62	P (18min,avec UV)	-	-	-37	-62	-	-	[174]
		40	1000	0,55 (0,66h)	65 (40min, avec UV)	62	P (60min)	-29	-36	-	-	-	-	[175]
lignine	PP	30	960	0,89 (8h, 60°C)	-		C (4h, 50°C)	-	-	+19	+7	+13	-	[106,149]
	PLA	7	600	NS	60	30	-	-15	+4	-	-	-	+17	[69]
fibres de cellulose	PP	40	960	0,89 (8h, 60°C)			C (4h, 50°C)	-	-	-60	-78	+30	-	[106,149]
	PP	30	500	NS (22h)		50	C (2h)	-14	-10	-	-			[132]
	PLA	30	600	NS	60	30	-	-11	+1	-	-	+53	-	[150]
fibre de bambou	PP	20	2016	-	-	75	I	-12	-38	-	-	-	-	[176]
fibre de lin	PLA	30	2160	-	-	40	I	-30	-55	-	-		-15	[63]
	PP	30	5040	-	-	Tamb	I	-7	-30	-	-	-	-	[131]

Tableau 6 - Variations des propriétés mécaniques et microstructurale de biocomposites après un vieillissement naturel – *X_{c1} et X_{c2} taux de cristallinité mesurés par DSC à partir de l'enthalpie de fusion déterminée selon la 1ère et 2ème rampe de température respectivement*

Renforts	Matrice	Taux de renfort (%)	Durée (mois)	Climat	Traction (%)		Flexion (%)		Xc (%)		Source
					contrainte à la rupture	module	contrainte à la rupture	module	X_{c1}	X_{c2}	
farine de paille de colza	PEHD	50	4	subtropical humide	-	-	-	-	+1		[169]
farine de bois	PEHD	40	3	continental humide	-	-	-	-			[136]
		60	18	tempéré froid			-9	-18			[157]
	PP	70	12	tempéré froid	-	-	-	-	-17	-35	[159]
		30	12	Méditerranéen	-14	-	-	-	-11	-7	[170]
		35,3	12	tropical	-	-	-4	-11	-	-	[160]
		60	4	tempéré froid	-	-	-	-	+10	-	[158]
fibre de kénaf	PBS	30	6	équatorial tempéré	-	-	-46	-37	-	-	[87]
fibre de bambou	PP	33	12	subtropical	-10	-	-3	-11	-	-	[161]
		35	10	subtropical humide	-18	-	-26	-7	-	-	[162]
	PEHD	60	36	subtropical humide	-	-	-17	-34	+42	-	[163]

VI. L'aspect visuel

L'aspect visuel d'un matériau est un critère esthétique important qui peut conditionner le choix d'un objet. La maîtrise de la perception des produits est donc aujourd'hui un enjeu industriel majeur, qui nécessite de connaître les propriétés de surface des produits et les interactions avec leur environnement lumineux.

Par ailleurs, des variations d'aspect des matériaux peuvent se manifester au cours du temps. Bien qu'elles soient généralement non souhaitées par l'utilisateur, celles-ci peuvent fournir des informations quant aux éventuelles modifications des propriétés physico-chimiques d'un matériau mais aussi indiquer quels composants entrent en jeu dans un processus de vieillissement d'un biocomposite par exemple.

VI.1. L'interaction lumière-matière

L'aspect visuel d'un objet est une propriété multi-critères. Il est le résultat perçu de l'interaction entre un rayon lumineux incident et la surface d'un objet. Plusieurs phénomènes de surface et de volume peuvent être mis en jeu lors de l'interaction d'une onde lumineuse avec la matière. Ces processus optiques sont présentés sur la Figure 20 et détaillés dans l'Annexe I de ce manuscrit.

Lorsque le rayon lumineux rencontre la surface d'un matériau polymère ou d'un biocomposite, une partie du rayonnement est réfléchie sans pénétrer dans le matériau : c'est la réflexion spéculaire, qui est quasi unidirectionnelle si la surface est très lisse (de dimension de rugosité très inférieure à la longueur de la lumière). Si le matériau est plus rugueux, la lumière est réfléchie selon toutes les directions de l'espace, on parle alors de réflexion diffuse. L'autre part du rayonnement lumineux pénètre dans le matériau et se propage. La présence d'éléments comme les fibres, d'indice de réfraction différent de la matrice de PP, provoque la diffusion de la lumière. La présence de chromophores dans les fibres végétales, capables d'absorber certaines longueurs d'onde du rayonnement visible, peut priver le rayonnement diffusé de ces longueurs d'onde et donc générer une couleur. C'est pour cette raison que la couleur peut consister en un témoin de l'évolution du matériau au cours du vieillissement, puisque les structures chimiques et donc les propriétés

d'absorption varient. Pour le PP, ce sont les phases cristallisées qui vont générer la diffusion car elles aussi ont un indice de réfraction différent des zones amorphes.

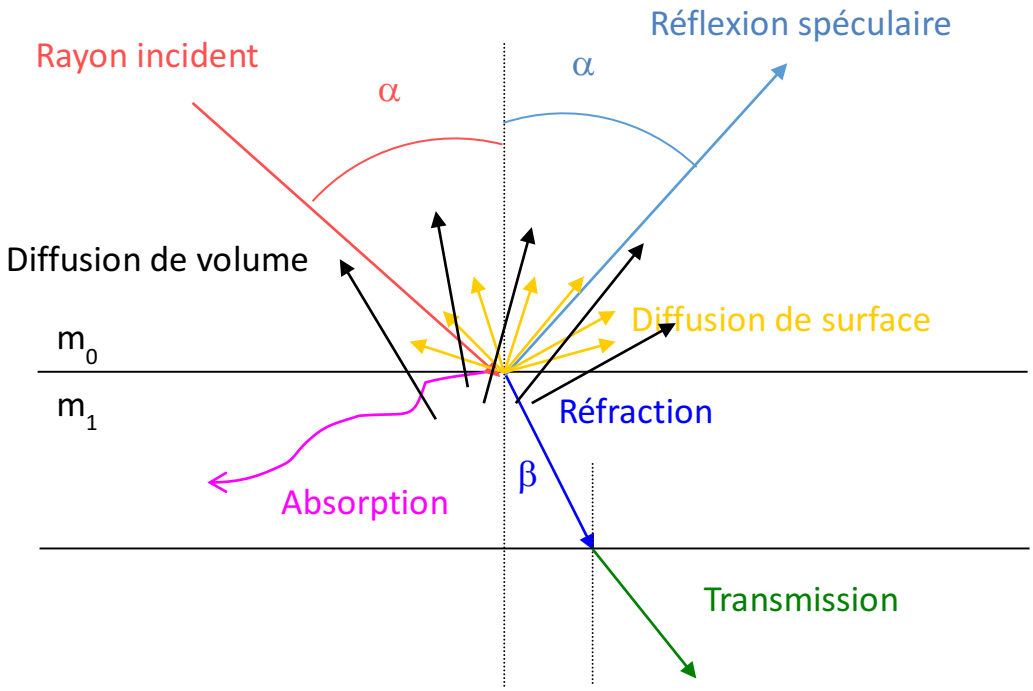

Figure 20 - Interaction lumière-matière

VI.2. La couleur

VI.2.1 Colorimétrie et calcul des valeurs tristimulaires

La colorimétrie permet de quantifier la couleur, en essayant autant que possible de tenir compte de la manière dont on perçoit les couleurs. Cependant, il faut être vigilant sur le fait que la couleur n'est pas une propriété propre de l'objet. En effet, la couleur d'un objet dépend de l'objet, de la source lumineuse et de l'observateur. De même, la contribution de ces trois critères dans la perception de la couleur est abordée dans l'Annexe I. Elle peut être caractérisée et quantifiée par spectrocolorimétrie et son résultat sera exprimé dans un système de référence faisant appel à un espace de couleurs dont deux coordonnées représentent la chromaticité et une coordonnée représente la clarté [171]. Plusieurs systèmes existent, mais nous nous limiterons au détail d'un seul système retrouvé dans la littérature et traitant des variations de couleur des biocomposites au cours du vieillissement, soit l'espace tridimensionnel L*a*b*. Celui-ci est défini selon le modèle proposé par la Commission Internationale de l'Eclairage (CIE) adopté en 1976 [172]. Une couleur,

représentée par un point dans l'espace tridimensionnel (Figure 21), est donc définie par les trois coordonnées suivantes :

- L* la clarté qui peut être comprise entre 0 pour et 100,
- a* qui est la position chromatique sur un axe allant du vert au rouge (entre -300 pour le vert et 300 pour le rouge),
- b* qui représente la position chromatique sur un axe bleu-jaune (entre -300 pour le bleu et 300 pour le jaune).

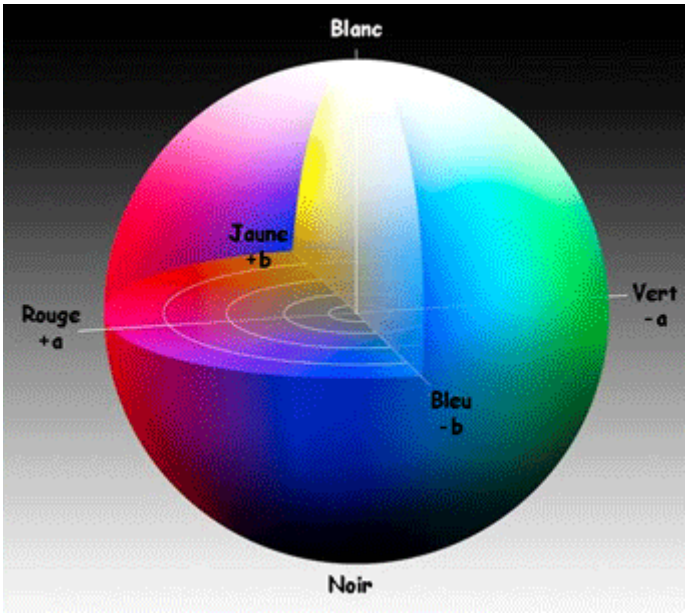

Figure 21 - Espace tridimensionnel colorimétrique L*a*b*

Ces coordonnées sont obtenues à partir des courbes de réflectance étant définies par la quantité d'énergie réémise par rapport à la quantité d'énergie reçue à toutes les longueurs d'onde (200-700nm). Par ailleurs, l'écart total basé sur la distance euclidienne des coordonnées est souvent calculé en industrie pour comparer différentes pièces fabriquées afin de vérifier la reproductibilité des couleurs par exemple. Il peut être déterminé selon la formule suivante :

$$\Delta E = \sqrt{\Delta L *^2 + \Delta a *^2 + \Delta b *^2} \qquad \text{Eq. 5}$$

VI.3. La brillance

VI.3.1 Définition et relation avec l'aspect de surface

Le brillant est défini par la CIE comme « l'aspect dans lequel on perçoit des reflets lumineux d'objets comme superposés à la surface par suite des propriétés directionnelles sélectives de cette surface » [173]. La brillance d'un matériau est d'autant plus marquée que la lumière est réfléchie de manière dirigée. Ainsi, lorsque la lumière illumine la surface d'un objet, elle peut être complètement réfléchie (réflexion spéculaire) ou réfléchie dans toutes les directions (réflexion diffuse) [174]. Lorsqu'un matériau est rugueux, sa surface n'est pas complètement plane et présente des zones d'inclinaison différente. Ces inclinaisons d'angles différents qui peuvent être causées par la présence de fibres naturelles en surface pour les biocomposites, induisent une réflexion des rayons lumineux dans toutes les directions. Les directions des ondes réfléchies dépendent ainsi des irrégularités de surface. Deux paramètres représentant le brillant seront suivis au cours de cette étude :

- le brillant de contraste. Celui-ci correspond au rapport entre la luminosité apparente de la surface à un angle spéculaire et celle mesurées à un angle éloigné de la zone spéculaire.
- le haze déterminé au voisinage de la direction spéculaire. L'aspect flou et brumeux peu contrasté qualifié par ce paramètre peut être problématique car il peut affecter la qualité d'apparence.

VI.4. Impact du vieillissement sur l'apparence visuelle des biocomposites

Plusieurs travaux ont traité de l'évolution de la couleur de biocomposites sous vieillissement naturel ou accéléré en enceinte. Les biocomposites les plus étudiés sont à base de farine de bois et le suivi des paramètres L*, a* et b* de ces WPC (Wood Plastic Composites) a permis d'en déduire l'influence majeure de l'exposition extérieure sur la couleur du composite [100,141,175]. En effet, Peng et al ont pu démontrer que les composites PP/farine de bois, présentant une couleur brune avant exposition, blanchissaient au fur et à mesure du vieillissement [100]. Cette variation de couleur est due notamment à une décomposition des constituants lignocellulosiques sensibles aux rayonnements solaires et à la pluie. Par ailleurs, la lignine semble être très réactive face aux rayons UV et se dégrade plus facilement que les

polysaccharides. En effet, celle-ci présente des groupes chromophoriques, structures très sensibles à la lumière [176]. La décomposition photochimique se déroule en deux étapes:

- Formation de composés paraquinoniques suite à une oxydation des chaînes de polymère de la lignine qui se manifeste par un jaunissement du matériau. Les réactions mises en jeu sont une scission de chaîne de la lignine et/ou une déméthoxylation [176,177]. Ce dernier processus de décomposition est mis en évidence par une diminution du taux de groupements méthoxy -OCH_3 après exposition à la lumière ultraviolette [176]. Par ailleurs, ces composés peuvent être présents dans la lignine avant son exposition aux conditions climatiques. En effet, les composés paraquinones et/ou orthoquinones peuvent aussi être retrouvés dans les biocomposites non exposés aux conditions climatiques. La décomposition de ces produits en d'autres molécules peut justifier l'absence de jaunissement des biocomposites après vieillissement [136].
- Réduction des paraquinones en hydroquinones causant un blanchiment en surface [61,100].

La dégradation repose donc sur un processus d'oxydo-réduction pour lequel Muasher et Sain proposent le schéma réactionnel présenté sur la Figure 22 [136].

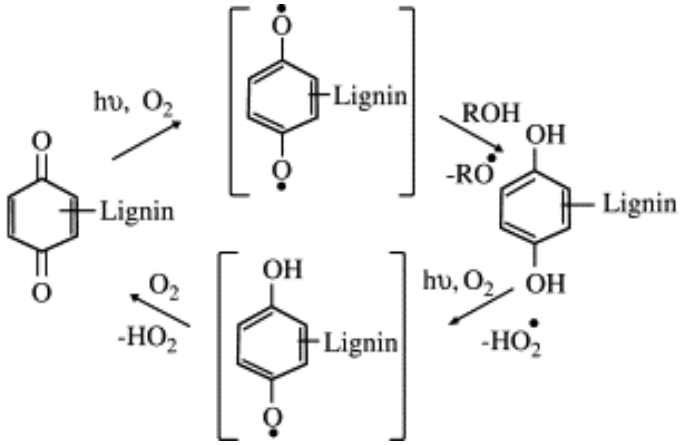

Figure 22 - Processus d'oxydo-réduction des composés phénoliques issus de la lignine [136]

Afin de comprendre l'influence de la lignine sur la dégradation de composites formulés à base de PP et de bois, Peng et al ont comparé l'évolution de la couleur de différents composites formulés à partir de différents taux de farine de bois, cellulose et lignine incorporés dans une même matrice PP durant un vieillissement artificiel en enceinte QUV selon la norme ASTM G154 (Figure 23) [100]. Ils ont constaté un blanchiment (augmentation

de ΔL) durant les 250 premières heures de vieillissement pour tous les composites, phénomène observé par d'autres chercheurs tels que Muasher et Sain [136], Butylina et al [159] ou encore Fabiyi et McDonald [178] après vieillissement de WPC. Aussi, les cinétiques de blanchiment étaient plus rapides pour les composites L1 et L2 pour lesquels le renfort a été effectué par ajout de lignine (Figure 23). Seul le matériau formulé à partir de PP renforcé du plus fort taux de charge en lignine pure (30 %m) se décolore plus lentement. Cette observation se justifie par un effet antioxydant des groupements phénols de la lignine s'activant lorsqu'elle est présente en grande proportion dans le composite. Cette propriété a aussi été mise en avant sur des biocomposites PLA/lignine formulés par Spiridon et al [65].

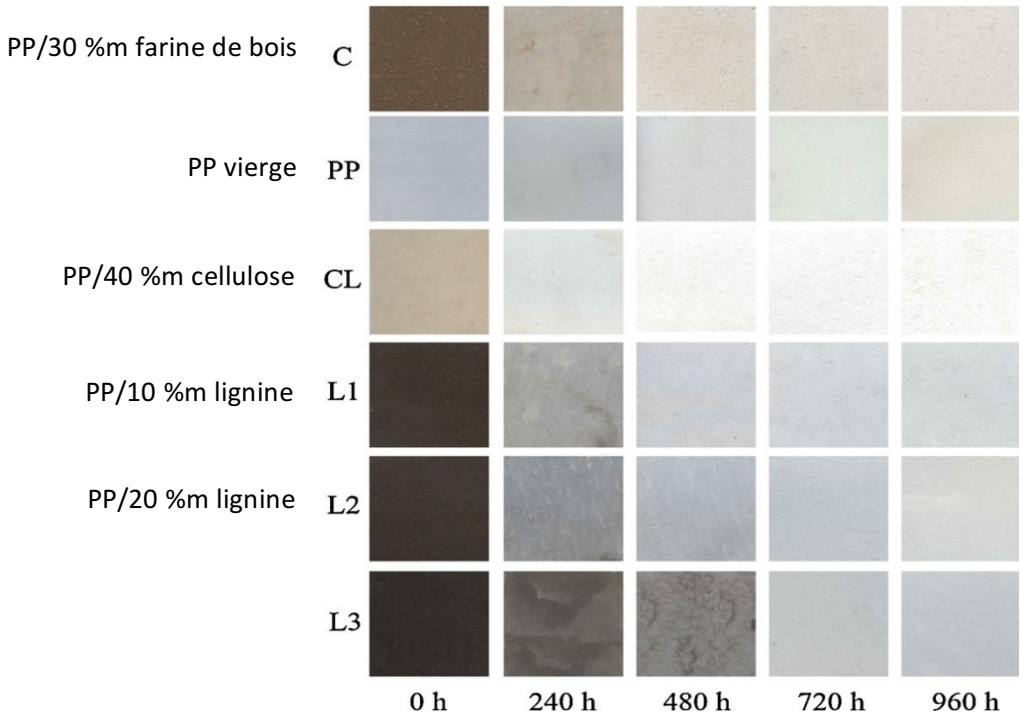

Figure 23 - Evolution de la couleur de composites au cours d'un vieillissement accéléré [100]

Parallèlement, les valeurs de Δb relevées au cours du vieillissement ont diminué, indiquant une perte de la couleur jaune et donc une réduction des composés paraquinoniques en composés hydroquinoniques correspondant à la deuxième phase de la dégradation photochimique. De même, le matériau L3 évolue différemment des autres biocomposites au cours du vieillissement puisque la variation de Δb est très peu prononcée. Ceci peut aussi être lié à la propriété de barrière attribuée à la lignine face à la dégradation oxydative. Toutefois, d'autres ont observé un jaunissement. Fabiyi a démontré que les variations de couleur et clarté évaluées par le calcul de ΔE étaient liées à la formation d'espèces

carbonyles et à la dégradation de la lignine [179]. La fraction carbohydratée des fibres végétales est aussi responsable du jaunissement des biocomposites [180]. En effet, des composés carbonyles chromophores peuvent être issus de l'oxydation des chaînes de polymère de cellulose et hémicelluloses. Aussi, la présence de structures chromophoriques de couleur rouge a été expliquée par la formation des structures quinoïdes due à la photo-dégradation de la lignine [180]. Cependant, le paramètre chromatique a* n'est généralement pas significativement modifié au cours des vieillissements [87,100].

Par ailleurs, l'eau accentue la décoloration des biocomposites. En effet, les WPCs blanchissent plus rapidement lorsqu'ils sont exposés à la radiation et à la pulvérisation d'eau que sous radiation seulement [181].

Outre les analyses colorimétriques, Peng et al ont procédé à des mesures de brillance des biocomposites par détermination de la réflectivité. Pour cela, un brillancemètre a été utilisé dont l'échelle de mesure s'étend de 0 à 100, 100 étant le niveau de brillant spéculaire de l'étalon de référence. Les unités de brillance (GU : Gloss Units) sont représentées en fonction de l'échantillon. Il a été constaté que tous les matériaux C, CL, PP, L1, L2 et L3 (Figure 23) ont perdu de leur brillance initiale après seulement 240h de vieillissement artificiel. Les images obtenues par microscopie électronique à balayage (MEB) ont confirmé l'apparition de microfissures en surface ainsi que des creux induisant une réflexion plus diffuse et donc une surface matte. En plus des brillancemètres qui mesurent en général la brillance selon 3 angles, les spectrogoniomètres peuvent aussi être utilisés afin de quantifier la brillance de plastiques [63]. En effet, l'énergie radiométrique de la lumière détectée étant collectée en fonction de l'angle de détection (détecteur mobile), ceci permet d'évaluer la répartition angulaire de l'intensité de la lumière réfléchie et d'ainsi déterminer le type de réflexion du matériau.

Ainsi, les composés chromophoriques et sensibles à l'humidité de nature lignocellulosique et présents dans les fibres naturelles induisent des modifications de couleur et de clarté des biocomposites et WPCs de par des changements structuraux et peuvent affecter leur brillance durant leur cycle de vie.

VII. Emission de Composés Organiques Volatils (COV) et qualité de l'air des habitacles automobiles

Les biocomposites sont de plus en plus utilisés comme pièces intérieures de véhicules et peuvent donc avoir un impact, comme les autres matériaux de l'habitacle, sur la qualité de l'air intérieur, devenue depuis une trentaine d'années, un enjeu important de santé publique. En effet, dans les pays industrialisés tels que les États-Unis ou l'Union Européenne, nous passons environ 80% de notre temps dans les environnements clos [182] et, après les lieux d'habitation et les lieux de travail, les moyens de transport sont le troisième environnement auquel nous sommes le plus longtemps exposés : plus d'1h chaque jour [183]. Ainsi, depuis 1970, des recherches ont été entreprises sur la qualité de l'air en intérieur de véhicule (VIAQ) notamment en Allemagne [184]. Aujourd'hui, la pollution retrouvée dans nos habitacles de voiture est considérée par l'Organisation Mondiale de la Santé (OMS) comme une menace potentielle pour la santé humaine [185,186]. En effet, selon l'enquête menée par l'Association Santé Environnement de France (ASEF), l'air intérieur de l'habitacle d'un véhicule présenterait un degré de pollution plus élevé qu'à l'extérieur [187]. Les taux de particules fines, de dioxyde d'azote et de benzène relevés ont montré un phénomène d'accumulation dans cet espace clos impliquant des taux d'exposition élevés [187,188]. Mais récemment, l'identification de polluants toxiques émis par les composants intérieurs d'habitacle tels que les tableaux de bords, panneaux de porte, revêtement des sièges et matériaux de planchers suggère que les sources intérieures contribuent aussi à la dégradation de la qualité de l'air [189,190]. De ce fait, l'impact sur la santé des pièces intérieures d'automobile devient un intérêt sociétal majeur [183]. Les polluants émis par ces matériaux sont principalement des Composés Organiques Volatils (COV) que l'OMS a classé en 4 catégories listées dans le Tableau 7 ci-après :

Tableau 7 - Classification des composés organiques selon l'OMS [191]

Composés	Abréviations	Gamme de températures d'ébullition
Composés organiques très volatils	COTV	<0°C à 50-100°C
Composés organiques volatils	COV	50-100°C à 240-260°C
Composés organiques semi volatils	COSV	240-260°C à 380-400°C
Composés organiques associés aux particules	POM	>380°C

Ces composés peuvent causer des irritations des yeux du nez et des voies respiratoires (asthme, notamment) ainsi que des réactions allergiques [190]. Des expositions très longues et régulières à des taux significativement élevés de certains polluants classés cancérigène, mutagène ou toxiques pour la reproduction (CMR) pourraient causer des problèmes plus graves à long terme tels que le développement de cancer, la baisse de fertilité ou des problèmes thyroïdiens [186,192,193]. A l'instar du « Sick Building Syndrome » mis en évidence dans des immeubles de bureaux aux USA dans les années 1980s, le « Sick Car Syndrome » a également été largement reconnu : il désigne un ensemble de symptômes diffus (fatigue, maux de tête, irritations, asthme…), dus aux polluants présents dans les habitacles [186][194]. D'ailleurs, suite à la reconnaissance étendue de ce syndrome, plusieurs constructeurs automobiles ont dû racheter ou rembourser l'achat de véhicules [195].

Outre leurs effets potentiels sur la santé, les COV peuvent également être responsables de nuisances olfactives [196,197]. L'odeur de voiture neuve (« new car smell » en anglais) peut en effet devenir désagréable et entêtante à long terme [189,198]. Des études portant sur l'évaluation sensorielle couplée à l'analyse physico-chimique de l'air ont révélé que l'odeur dans un véhicule neuf résulte de l'émission de plus de 200 substances provenant de différentes parties de l'habitacle [186,197]. Les travaux sur les odeurs sont nombreux mais la relation chimie-odeur reste très difficile à établir, surtout dans le cas de sources multiples et complexes comme les composants d'un habitacle automobile.

VII.1. Règlementations et guides

En raison de l'impact des COV sur la qualité de l'air des habitacles, des réglementations et des normes sont instaurées. Dans l'ordre chronologique, la Corée suivie de la Chine puis du

Japon se sont engagés à mettre en œuvre des valeurs limites de concentrations en polluants afin d'améliorer la VIAQ. Ainsi, la Corée a établi en 2007 la notification No. 2007-539 spécifiant les concentrations limites de 6 substances dont les valeurs maximales permises listées dans le Tableau 8 doivent être respectées par les constructeurs et équipementiers automobiles [199]. Les concentrations se situent entre 30 $\mu g.m^{-3}$ pour le benzène et 1600 $\mu g.m^{-3}$ pour l'éthylbenzène [194,200]. Suite à cette initiative, les résultats ont été positifs puisque la concentration mesurée dans les véhicules neufs a diminué en 7 années jusqu'à 87% pour l'éthylbenzène [201]. En Chine, la norme GB/T 27630 a été introduite en 2012 [202,203]. Elle propose des valeurs limites de concentration pour l'acétaldéhyde et l'acroléine en plus des 6 polluants listés dans la No. 2007-539. Récemment, les associations de fabricants automobiles du Japon (JAMA), d'Europe (ACEA) et du monde (AIAM) se sont également engagées dans la démarche d'amélioration de la VIAQ [204–206]. Toutefois, la concentration maximale autorisée pour une même substance diffère entre chaque norme issue de chaque pays (Tableau 9). De plus, on note que, quelle que soit la réglementation ou recommandation, les composés cancérogènes tel que le benzène font l'objet de mesures plus restrictives.

Tableau 8 - Concentrations limites des COV dans les recommandations et règlementations et leur classement par le Centre International de Recherche sur le Cancer (CIRC) ((1 : cancérogène pour l'Homme, 2B : probablement cancérogène pour l'Homme, 3 : inclassable) [194,200,203,204]

	Concentrations limites ($\mu g.m^{-3}$)			
	JAMA (Japon)	**GB/T 27630 (Chine)**	**No 2007-539 (Corée)**	**Catégorie CIRC**
Formaldéhyde	100	100	250	1
Acétaldéhyde	48	50	-	2B
Benzène	-	110	30	1
Toluène	260	1100	1000	3
Styrène	220	260	300	2B
Xylène	870	1500	870	3
Acroléine	-	50	-	3
Éthylbenzène	3800	1500	1600	2B

Des travaux sont aussi menés en Europe pour une législation de la VIAQ. La commission européenne s'engage à impliquer des experts compétents en matière de législation sur les polluants chimiques [201]. Cependant, toutes ces instructions ne concernent pour l'instant que l'évaluation globale de l'air du véhicule. Des valeurs seuils ou valeurs guides à l'échelle des matériaux d'intérieur d'automobile ne sont pas disponibles.

VII.2. Normalisation des méthodes de prélèvement et d'analyse

Afin de proposer des véhicules conformes aux valeurs limites VIAQ, des normes décrivant les méthodes d'essai pour la détermination des émissions de COV par les composants automobiles sont mises à disposition des industriels. Au cours des années, des méthodes spécifiques aux fabricants pour les mesures de COV et COSV en air intérieur de véhicules telles que la norme américaine General Motors GMW1564, la norme allemande Volkswagen PB VWL 709 ou la norme française Renault D42 3109 ont été adoptées, employant de nombreuses techniques analytiques [206,207]. Par ailleurs, les normes ISO 12219 dont la plus ancienne est publiée en 2012 ont harmonisé les normes européennes et décrivent différents protocoles de mesure des COV à différentes échelles, depuis le taux d'émission des matériaux jusqu'à la concentration dans l'air intérieur des véhicules [208–211]. L'industrie automobile européenne a aussi adopté des méthodes telles que celles décrites dans la VDA 278 pour mesurer les émissions des pièces intérieures.

VII.3. Emissions dans les véhicules

Quelques travaux traitent des émissions de COV dans les véhicules et de l'influence de différents facteurs sur leurs taux d'émission. Certaines études décrivent une analyse exhaustive des COV [212] alors que d'autres portent sur la mesure de COV spécifiques [189] correspondant aux polluants potentiellement dangereux et listés dans les règlementations. Outre la concentration des COV individuels, la concentration en COV totaux (COVT) est aussi déterminée pour évaluer la VIAQ [189,194,212–215]. Les COVT sont définis dans la norme ISO 16000-6 comme la somme des COV dont le temps de rétention se situe entre ceux de l'hexane et l'hexadécane dans des conditions d'analyse par chromatographie en phase gazeuse bien définies [216,217].

Les résultats d'une dizaine d'études sont résumés dans le Tableau 9 où chaque véhicule ou lot de véhicules est arbitrairement désigné par les appellations VE1 à VE19. On remarque que le toluène et l'éthylbenzène sont systématiquement détectés. Il a été montré que ces émissions de COV dépendent fortement de la température [189,218]. En effet, une diminution de 4°C par l'activation du conditionnement d'air (AC) dans le véhicule peut réduire de 4 à 6 fois les concentrations mesurées en toluène et éthylbenzène respectivement [189]. Par ailleurs, il a été montré que les concentrations étaient plus élevées dans les véhicules placés en conditions statiques (garés, non-ventilés) que dans ceux en conditions de conduite et de ventilation (Figure 24) [215]. L'introduction d'air extérieur dans l'habitacle fait généralement baisser le taux de COV par effet de dilution. En effet, il a été démontré que dans des conditions de ventilation (fan) off et recirculation d'air (RC) off (Cf. VE10 dans le Tableau 9) ou fan on et RC on (Cf. VE11), la VIAQ était plus affectée que sous condition de ventilation fan on RC off (Cf. VE12). Cependant, bien que le taux de renouvellement d'air réduise les niveaux de COV intérieurs, d'autres COV peuvent être apportés via l'air extérieur en fonction de la densité du trafic routier. Ceci est particulièrement vérifié pour le toluène [215].

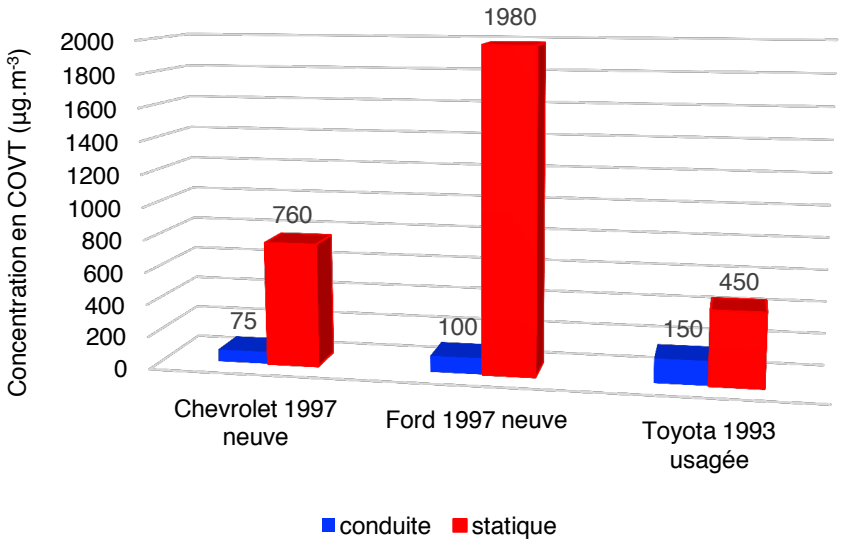

Figure 24 - Concentrations en COVT de 3 modèles de voiture en condition statique et de conduite pendant 90 minutes [215]

Par ailleurs, une étude comparative menée sur 12 COV a montré que les concentrations dans les habitacles de véhicules neufs de différentes marques et différents lieux de fabrication pouvaient, pour un même composé, varier d'un facteur 1000 voire plus (de quelques $\mu g.m^{-3}$

à environ 8000 µg.m^{-3} pour les m,p-xylènes) [189]. Une étude a été menée par Yoshida et al sur 50 véhicules de 6 marques différentes pour évaluer l'influence du constructeur, des spécifications (matériaux utilisés, prix catalogue) ainsi que l'état d'utilisation des voitures (distance parcourue, ventilation) sur la pollution de l'air intérieur par ces composés [219]. Ce travail montre que l'hétérogénéité des concentrations mesurées avant (VE18) et après livraison et utilisation des véhicules (VE19) était principalement due aux différents matériaux intérieurs utilisés ou la qualité (luxe ou bon marché) plus que dépendante du constructeur. En effet, la composition des pièces intérieures influence le profil d'émission, notamment le type de revêtement couvrant les sièges. Les pièces en cuir émettent des quantités plus élevées que des pièces en tissu avec un fort impact sur la concentration de toluène qui peut augmenter de 39% [189,214]. Mais d'autres produits (peintures, revêtement de surface) peuvent aussi contribuer aux émissions de polluants et impacter la VIAQ [220].

En complément de l'analyse de l'air des habitacles, des études sur la mesure des émissions des matériaux constitutifs des intérieurs automobiles sont donc nécessaires pour identifier et caractériser les sources de polluants. La technique de l'espace de tête (Head-Space) couplé à la Micro-Extraction sur Phase Solide (SPME) reposant sur un prélèvement passif des COV, a été employée pour évaluer les sources potentielles de COV en analysant individuellement (et hors véhicule) des échantillons de chaque composant intérieur [189]. L'antioxydant 2,6-di-tert-butyl-4-methylphénol (BHT) a été détecté comme composé majeur émis par les produits pétrosourcés. Il a été montré que des hydrocarbures aliphatiques tels que l'heptadécane ou le tétradécane proviennent principalement des graisses (lubrifiants par exemple) alors que les plus longues chaînes telles que l'éicosane ou le docosane étaient émis par des matériaux plastiques. Cette famille chimique (hydrocarbures aliphatiques) représente 52 % des COVT. Des composés aromatiques, tels que le toluène et les xylènes issus des adhésifs, ont aussi été identifiés et représentent 42 % de la concentration en COVT. D'autres familles chimiques comme des composés halogénés, des espèces carbonylées et des esters ont aussi été détectées en plus faible proportion. Le PVC peut notamment être à l'origine de la pollution de l'air par des composés chlorés [189]. Dans une étude différente, 275 COV ont été détectés avec une grande proportion d'hydrocarbures aliphatiques et aromatiques [221], ce qui corrobore les résultats de l'étude présentée précédemment [189].

Pour des véhicules usagés, les concentrations peuvent être beaucoup plus faibles qu'à l'état neuf [189]. Cela est probablement dû à la diminution du taux d'émission des matériaux de l'habitacle au cours du temps. Par exemple, Yoshida et Matsunga ont montré une décroissance exponentielle de la concentration en COVT au cours du temps avec une diminution de 1/10ème après une année (Cf. VE1 dans le Tableau 9) [212]. Après 5 années, les concentrations sont significativement réduites (VE8 et VE9) [214].

Les différentes études présentées ci-dessus montrent que la qualité de l'air des habitacles automobiles doit être améliorée et qu'une sélection de matériaux peu émetteurs en amont de la construction pourrait fortement y contribuer, de même que la mise en place de réglementations. En effet, on remarque que les véhicules examinés lors d'études récentes effectuées en Chine satisfont les limites imposées par la norme chinoise GB/T 27630 [214,222].

Tableau 9 - Concentration de COV dans plusieurs habitacles de véhicules neufs et usagés en conditions statiques et de conduite (TMB : triméthylbenzène, NM : non mesuré)

Désignation	Etat véhicule	Conditions prélèvement	Concentration (µg.m^{-3})									Source
			toluène	benzène	éthylbenzène	1,2,4-TMB	*m&p*-xylène	*o*-xylène	∑xylènes	styrène	COVT	
VE1	neuf	ventilation off, statique	226	6	361	212	3104	899	4003	74	14 000	[212]
VE2	neuf	conduite (90min)	12	2	2	NM	4	1	5	NM	NM	[215]
VE3	neuf	conduite (26min)	5	2	1	3	4	2	6	NM	NM	[223]
VE4	neuf	ventilation off, statique	34	NM	66	73	140	53	193	130	NM	[189]
VE5	neuf	ventilation off, statique	2000	NM	35	41	2500	1400	3900	1500	NM	[189]
VE6	neuf	ventilation off, statique	210	NM	42	30	78	39	117	54	NM	[189]
VE7	neuf	ventilation off, statique	2700	NM	170	500	230	140	370	140	NM	[189]
VE8	neuf	ventilation off, statique	105	20	23	NM	NM	NM	NM	13	NM	[214]
VE9	usagé (5 ans)	ventilation off, statique	49	14	10	NM	NM	NM	NM	10	NM	[214]
VE10	neuf	ventilation off, statique	66	17	14	NM	NM	NM	28	7	612	[214]
VE11	neuf	ventilation on, recirculation on statique	85	18	16	NM	NM	NM	30	4	NM	[214]
VE12	neuf	ventilation on, recirculation off, statique	47	14	10	NM	NM	NM	17	5	NM	[214]
VE13	neuf	ventilation off, statique	82	48	85	NM	346	95	441	155	4940	[222]
VE14	usagé (1 an)	ventilation off, statique	50	10	10	NM	20	10	30	10	1240	[222]
VE15	neuf	ventilation off, statique	72	5	9	NM	-	-	100	4	NM	[202]
VE16	neuf		68	8	11	NM	-	-	134	4	NM	
VE17	usagé (2,6 ans)	ventilation off, statique	151	60	54	NM	NM	NM	133	NM	NM	[220]
VE18	neufs	ventilation on/off, statique	12-368	1-53	3-62	6-186	5-163	2-83	NM	1-675	556-11398	[219]
VE19	usagés (<3 ans)	ventilation on/off, statique	12-356	1-33	2-59	2-98	3-65	1-25	NM	0-79	136-3968	[221]

VII.4. Emission de COV par les polymères

Parmi les matériaux émetteurs mis en évidence dans les paragraphes précédents, les polymères peuvent contribuer de façon importante à la pollution de l'air intérieur des véhicules [191]. Ces matériaux émettent généralement des COV à des taux élevés au début de leur cycle de vie, puis l'émission se stabilise au bout de quelques jours (10 à 30 jours) à température et humidité ambiantes [191]. Cependant, lorsque les matières plastiques sont utilisées dans des milieux dont les conditions peuvent en dégrader la matrice primaire, la structure de ces dernières et donc la nature des composés émis peuvent être altérées et conduire à la libération de polluants volatils. Ainsi, dans plusieurs études, le PP, très utilisé dans des pièces d'habitacle, a été soumis à des dégradations artificielles (photo-chimique [224], thermique [225], radiative [134] ou photo-thermique [143]) afin d'apporter des informations mécanistiques de dégradation. Des composés volatils issus de la décomposition du polymère tels que les alcanes, alcènes, alcools, aldéhydes sont formés. Les COV appartenant aux deux dernières familles chimiques sont générés suite à l'oxydation des chaînes de polymère. Des schémas réactionnels ont été proposés impliquant principalement les réactions radicalaires précédemment exposées (partie V.1) [134,225].

VII.5. Emission de COV par les biocomposites

Comme détaillé dans la partie V, les fibres végétales retrouvées dans les biocomposites sont sensibles aux conditions climatiques telles que le rayonnement UV, l'humidité ou la chaleur. Leur dégradation peut induire l'émission de sous-produits issus de la décomposition des composés lignocellulosiques [226]. Quelques articles scientifiques reportent des résultats relatifs aux émissions de COV et au dégagement d'odeurs par des biocomposites. Comme observé sur la Figure 25, le composite comportant des fibres d'abaca émet des odeurs à plus forte concentration que ceux renforcés par des fibres de lin ou de jute.

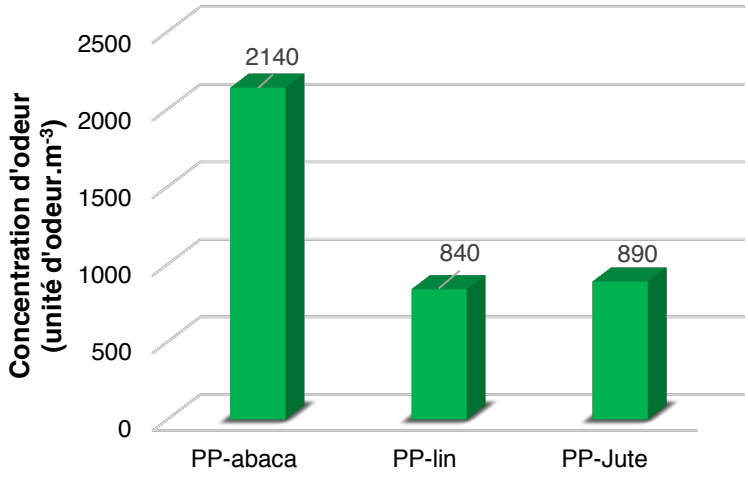

Figure 25 - Concentrations d'odeur de biocomposites à matrice PP renforcée par différents types de fibres végétales (abaca, lin, jute) [31]

Afin de limiter l'impact des biocomposites sur la qualité de l'air, K.W. Kim et al ont étudié la réduction de l'émission de COV par des biocomposites à matrice biodégradable PLA et PBS renforcées de fibres d'ananas et de fibres de manioc par le procédé de « bake-out » [213]. Cela consiste à chauffer les matériaux sous un flux d'air avant leur utilisation afin de réduire les COV (sorte de « dégazage ») [213]. Au-delà de 70 °C, les composites PLA/fibres d'ananas et PLA/fibres de manioc présentent des facteurs d'émission de COVT plus élevés que le PLA pur en raison de l'émission plus importante de COV dégagés par les renforts naturels tels que le 2-furancarboxaldéhyde (furfural) provenant des fibres, et le 1,4-dioxane issu du PLA, ces deux composés étant classés CMR [193]. En Corée, la température maximale intérieure d'une automobile durant les deux saisons de printemps et automne est d'environ 50 °C et peut atteindre 90 °C en été [213]. Cela montre donc l'importance de la température dans l'évaluation de l'impact des biocomposites sur la VIAQ.

Dans un même objectif, H.S. Kim et al ont quantifié la réduction d'odeur et les émissions de COV de biocomposites, dont les matrices PLA et PBS renforcées de farine végétale étaient similaires, en incorporant des charges inorganiques poreuses pouvant piéger les substances gazeuses [227]. Les émissions de COV tels que le tridécane provenant de la matrice et le furfural émis par la farine de bambou ont été réduites. Des analyses olfactométriques couplées à des analyses chimiques ont permis de constater que l'odeur était due aux COV oxygénés émis par la matrice thermoplastique et les farines [196].

Un article concerne les émissions de COV dérivant de la dégradation thermique de composites PP/fibres de cellulose et fibres de chanvre et ayant été analysés par espace de tête (Headspace)-SPME (HS-SPME) [226]. Plusieurs COV ont été identifiés à l'état initial et à l'état vieilli (hydrocarbures aliphatiques, acides carboxyliques, alcools). Des COV spécifiques aux fibres végétales comme des composés carbohydratés et le 2-furanmethanol issu de la déshydratation et la décarboxylation du glucopyranose et xylopyranose, structures primaires de la cellulose et des hémicelluloses [228,229] ont été détectés. Ce dérivé furanique est suspecté être cancérogène selon la classification CMR [193]. Il a été constaté une augmentation du nombre et de la concentration des COV après le traitement thermique [226]. Donc, un processus thermo-oxydatif ayant dégradé la structure primaire du polymère et de la cellulose a certainement favorisé le dégagement de sous-produits de décomposition.

VII.6. Analyse des COV émis par les matériaux

Dans la plupart des études décrites précédemment concernant les atmosphères de véhicules, les COV ont été analysés directement dans l'air des habitacles par des techniques de prélèvements actifs décrites dans des normes telles que l'ISO 12219-1 [208]. Les travaux traitant de la caractérisation des émissions de matériaux sont moins fréquemment reportés dans la littérature. La technique classiquement utilisée pour prélever les COV émis par des matériaux est l'espace de tête couplé à la SPME (HS-SPME) [196,226,230–232]. Cette technique d'extraction consiste à prélever les polluants dans la partie supérieure d'un flacon hermétiquement scellé contenant le matériau à caractériser. Cette mesure est simple et rapide avec des temps d'extraction courts. Mais l'HS-SPME implique souvent une destruction du matériau puisqu'une découpe en morceaux de petite dimension est nécessaire pour introduire l'échantillon dans le flacon d'espace de tête. Par conséquent, cette procédure d'échantillonnage ne convient pas pour fournir des données quantitatives liées aux émissions de surface (taux d'émission, par exemple). Pour la détermination de ces derniers, des tests en chambre d'émission sont effectués. Selon le type d'usage du matériau (tableau de bord, garnissage de portière…), des chambres de volumes supérieurs à 4 m^3 peuvent être utilisées et les essais peuvent durer plusieurs jours selon le temps de stabilisation requis par les normes [209–211]. Ces protocoles sont donc complexes et longs à mettre en œuvre. Ils sont par conséquent peu adaptés à un suivi fréquent du vieillissement d'un matériau, par

exemple.

En alternative à ces mesures en chambre d'émission, notre laboratoire a développé une méthode d'échantillonnage passif par couplage d'une cellule d'émission à la technique SPME [233,234].

VII.6.1 La MicroExtraction sur Phase Solide (SPME)

La technique de MicroExtraction sur Phase Solide (SPME) développée par Pawliszyn et al repose sur un prélèvement passif des polluants [233]. Le dispositif de piégeage impliqué est basé sur l'ad- (ou l'ab-)sorption des COV à la surface d'une fibre constituée d'un barreau de silice fondue recouvert d'une phase stationnaire. Cette phase peut être constituée de polydiméthylsiloxane (PDMS), de divinylbenzène (DVB) et/ou de Carboxen (CAR) selon les propriétés physico-chimiques des polluants à analyser. Durant la phase de prélèvement, les COV diffusent de l'air vers la fibre : la première loi de Fick s'applique et la quantité de matière extraite peut être déterminée selon l'équation 6 [235]:

$$n_f = D_i \times \frac{S_{ad}}{z} \int_0^t (C_i - C_{sorb}) dt \qquad \text{Eq. 6}$$

avec n_f la quantité de matière extraite sur l'adsorbant (µg), D_i le coefficient de diffusion moléculaire du composé i dans l'air ($m^2.s^{-1}$), S_{ad} la section de l'adsorbant (m^2), z la longueur de diffusion (m), C_i la concentration du composé dans l'air ($\mu g.m^{-3}$), C_{sorb} la concentration du composé à la surface de l'adsorbant ($\mu g.m^{-3}$) et t la durée d'échantillonnage (s).
Au début de l'échantillonnage, C_{sorb} peut être négligé. L'intégration de l'équation précédente conduit donc à :

$$n_f = k \times C_i \times t \qquad \text{Eq. 7}$$

Avec $k = D_i \times \frac{S_{ad}}{z}$, nf est donc proportionnel au produit produit $C_i \times t$, autrement désigné dose d'exposition et exprimé en $\mu g.m^{-3}.s$ [236]. n_f étant déterminé par chromatographie en phase gazeuse après désorption thermique de la fibre SPME dans l'injecteur, il est alors possible de déterminer Ci, connaissant t, le temps d'extraction sur fibre.

VII.6.2 Couplage cellules d'émission - Echantillonnage passif

VII.6.2.1 Device for On Site Emission Control (DOSEC) couplée à la SPME

Un premier dispositif a été réalisé au laboratoire pour mesurer de façon simple les émissions surfaciques de matériaux : il consistait à coupler une cellule d'émission FLEC (Field and Laboratory Emission Cell) recommandée par la norme ISO 16000-10 à la SPME [237]. Ce couplage a ensuite été optimisé par Bourdin et al afin d'en améliorer les performances [234]. Une nouvelle cellule en verre (DOSEC) a ainsi été développée (Figure 26).

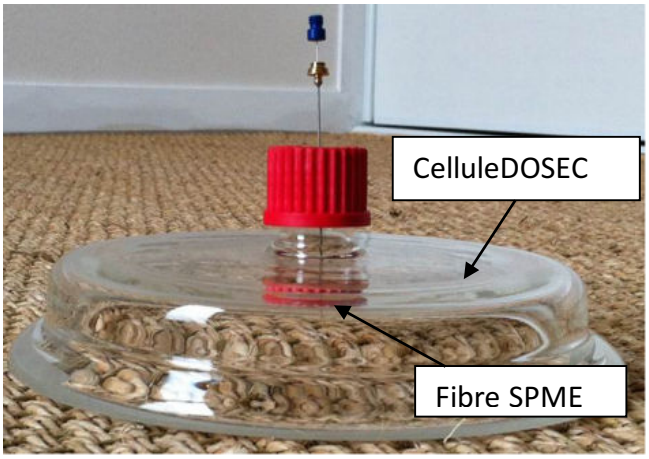

Figure 26 - Cellule DOSEC couplée à la SPME

Cette méthode d'échantillonnage passif permet de déterminer la concentration des COV à l'interface matériau/air (C_{is}) liée au taux d'émission (EF) par la première loi de diffusion de Fick dans des conditions de régime stationnaire [238] selon l'équation 8 [239]:

$$EF = -D_i \frac{dC}{dx} = -D_i \frac{C_i - C_{is}}{L} \qquad \text{Eq. 8}$$

avec EF le taux d'émission ($\mu g.m^{-3}.s^{-1}$), D_i le coefficient de diffusion du polluant i dans l'air ($m^2.s^{-1}$), C_i la concentration du composé dans l'air ($\mu g.m^{-3}$), C_{is} la concentration en phase gazeuse à la surface du matériau ($\mu g.m^{-3}$) et L l'épaisseur de la couche limite de diffusion (m).

La mesure de l'émission d'un matériau se déroule en deux étapes. Premièrement, la cellule est placée sur le matériau afin d'isoler la surface à analyser. Les COV diffusent alors du matériau vers l'air enfermé dans la cellule jusqu'à l'établissement de l'équilibre des

concentrations des COV à l'interface matériau/air. Une fois l'équilibre matériau/air établi, la fibre SPME est exposée aux COV émis et la concentration à la surface du matériau C_{is} est déterminée après extraction sur fibre SPME en mode statique (Cf. paragraphe VII.6.1).

Ce dispositif a déjà été appliqué pour la mesure des émissions de COV par des matériaux de construction dans une salle de classe d'un collège [235,238] et pour l'étude de la qualité de l'air intérieur de maisons [240] afin d'en vérifier la faisabilité. Ce dispositif sera transposé à notre étude pour le prélèvement de COV émis par des biocomposites pouvant être utilisés en équipements intérieurs de véhicule et dont l'impact sur la qualité de l'air intérieur doit être caractérisé.

VIII. Relations pouvant exister entre indicateurs de vieillissement obtenus à partir d'essais non destructifs et destructifs

L'évaluation des relations entre les grandeurs intensives propres aux matériaux peut avoir plusieurs intérêts. Premièrement, puisque la mesure des propriétés mécaniques implique souvent un endommagement, voire une destruction du matériau, des indicateurs de dégradation à partir d'essais non destructifs pourraient permettre d'estimer la perte de la stabilité et de la performance de plastiques. Aussi, cela permet d'apporter une compréhension aux mécanismes de vieillissement. Cette partie abordera tout d'abord un état de l'art sur les polymères puis sur les biocomposites.

VIII.1. Les polymères

Le premier intérêt s'est manifesté à travers la détermination de relations existant entre des paramètres quantitatifs non mécaniques et les propriétés mécaniques, par exemple entre la formation de produits de photo-oxydation comme les espèces carbonylés (mesurées par spectroscopie infrarouge) et l'élongation et la force à la rupture obtenues par test en traction [241]. Les matériaux PEBD non réticulé et réticulé soumis à une exposition UV ont présenté un même profil bien que la relation était non linéaire suggérant que le suivi des variations du taux d'espèces carbonyle peut servir à prédire la tenue mécanique de PE de différentes structures. Cependant, d'autres études ont montré qu'aucune relation simple n'existait entre les modifications de la composition chimique et de structure du PE et ses

propriétés mécaniques. En effet, lors d'une autre étude sur le vieillissement de PEBD, l'élongation à la rupture apparait comme stable au début du vieillissement accéléré puis diminue de façon importante alors que l'intensité de la bande infrarouge liée aux carbonyle (1715 cm^{-1}) augmente continuellement [242]. Cette stabilisation durant les temps courts de vieillissement serait due aux réactions de réticulation entre les chaînes de PE. Parallèlement, lors du vieillissement naturel de ces mêmes matériaux, une diminution de l'élongation à la rupture est observée dès les temps courts d'exposition suggérant que les phénomènes de scission de chaîne ont prédominé. Donc, selon les conditions d'exposition, les relations entre l'élongation et le taux de carbonyle serait différent. Aussi, après avoir répertorié les données de déformation en fonction de l'augmentation relative des groupements carbonyles au cours du vieillissement naturel du PEBD, Akay et al remarquent aussi que la corrélation n'est pas évidente [243]. La diminution de la déformation à la rupture est plus prononcée lorsque le taux de formation de composés oxygénés est faible, c'est-à-dire lorsque log ($I+\Delta I^{1725}$) ≤0,1 généralement (Figure 27). Ensuite, l'évolution est plus complexe. Donc, les changements de structure chimique du polymère n'influencent pas significativement les propriétés générales. De plus, pendant la saison hivernale, aucune variation significative du taux de carbonyle n'a été détectée par spectroscopie infrarouge alors que la contrainte et la déformation à la rupture avaient augmenté et le module d'élasticité diminué. Ces tendances suggèrent que la réticulation avait prédominé au détriment des scissions de chaîne.

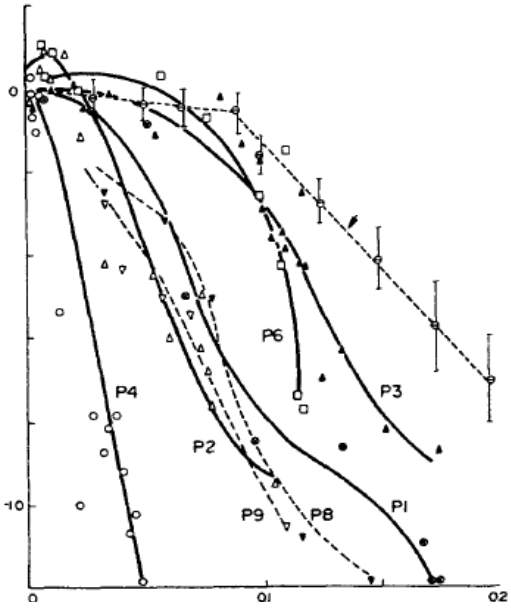

Figure 27 – Variation du logarithme de l'élongation à la rupture de PEBD $\frac{\varepsilon}{\varepsilon_0}$ en fonction du logarithme du taux de carbonyles $I + \Delta I^{1725}$ (les échantillons P1 à P9 représentent différents taux de stabilisants UV) [243]

Beaucoup moins d'études concernent l'approche corrélative des propriétés physico-chimiques aux propriétés mécaniques du PP. L'évolution de la force résiduelle a été comparée à celle de la viscosité intrinsèque durant 3 vieillissements artificiels (exposition à différents rayonnements UV) et un vieillissement naturel [244] (Figure 28). Quel que soit le mode de dégradation, la viscosité a évolué linéairement avec la résistance. Ceci suggère que les modifications à l'échelle moléculaire telles que le poids moléculaire gouvernent les propriétés mécaniques.

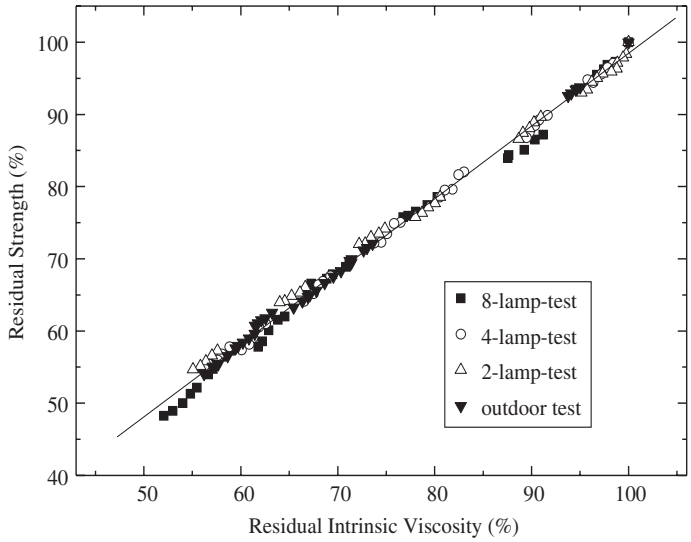

Figure 28 - Relation entre l'augmentation de la viscosité intrinsèque et de la force résiduelle en traction du PP au cours de différents photo-vieillissements [244]

Quelques études existent sur les relations entre propriétés microstructurales au cours du vieillissement du PE. L'interdépendance entre les paramètres a été quantifiée pour proposer des hypothèses sur les mécanismes de dégradation ou apporter des informations de compréhension. Comme démontré sur la Figure 30, une relation linéaire entre le taux de cristallinité χ_c et l'inverse de la racine carrée de la masse moléculaire en poids $\frac{1}{\sqrt{Mw}}$ de PEHD a été établie dans la revue de Fayolle et al qui ont tenté de valider cette relation dans plusieurs travaux menés par d'autres chercheurs [245]. Ceci permettait de vérifier si les variations de longueur de chaîne du polymère pouvaient être exclusivement expliquées par le phénomène de chimi-cristallisation estimé par le taux de cristallinité. La pente et l'ordonnée à l'origine dépendent de la structure chimique du polymère et des conditions de cristallisation. Cependant, même si une dépendance linéaire peut être supposée dans certains cas, les résultats sont relativement dispersés pour d'autres et la dépendance ne peut être tout le temps représentée ou vérifiée par une linéarité entre les grandeurs.

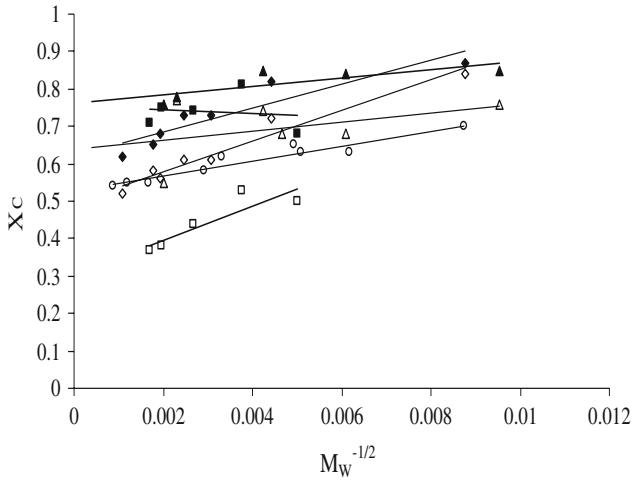

Figure 30 - Variation de X_c en fonction de $M_w^{-1/2}$ de PEHD (les différentes courbes correspondant aux différents travaux réalisés par différents chercheurs) symboles remplis : cristallisation par trempe, symboles vides : cristallisation isotherme [245]

Le taux de cristallinité peut être aussi déterminé par spectroscopie infrarouge à partir des bandes d'absorption attribuées aux phases amorphe et cristalline [246]. Au cours d'un vieillissement hivernal de PEHD de 3 mois, ces bandes se sont révélées être linéairement corrélées (r^2 = 0,98) à l'enthalpie de fusion ΔH_m [246]. Ceci témoigne de la dépendance de la microstructure à la composition chimique. Akay et al ont constaté que l'indice vinyle (910 cm^{-1}) et l'indice de carbonyle (1725 cm^{-1}) variaient de façon proportionnelle au cours de la dégradation naturelle du PE [243]. Cependant, cette étude de cas ne vérifie pas le mécanisme de conversion de groupements vinyle en groupements carbonyle (Norrish II) [247,248] qui, généralement, induit la stabilisation de la teneur en groupements vinyles à partir d'un certain temps de vieillissement puisque ces espèces peuvent se réarranger pour former des espèces carbonyles. Ceci suggère que, soit un mode de dégradation différent s'est déroulé au cours du vieillissement, soit le temps de vieillissement était trop court dans ces conditions d'exposition pour apercevoir une stagnation de l'indice vinyle.

L'évolution des émissions de COV a été comparée à d'autres propriétés au cours du vieillissement de polymères, telle que les variations de couleur/clarté, de microstructure ou de propriétés mécaniques, ceci afin de déterminer si les dommages physiques des matériaux polymères peuvent être associés aux modifications des profils d'émission de COV. Par exemple, l'étude de Carlsson et al sur le vieillissement photochimique de PVC a mis en évidence un lien direct entre le blanchiment des échantillons et la libération de COV chlorés

tels que le 1-chlorobutane et la 1,1-dichloroacétone [249–251]. Par ailleurs, il a été démontré que le degré de dégradation estimé à partir du taux de scissions de chaîne et de la chute de la masse moléculaire après thermo-oxydation de matériaux polymères était relié au taux de COV oxygénés tels que les acides carboxyliques et lactones [252]. Plus précisément, l'acide butanedioïque pouvait servir d'indicateur de vieillissement permettant d'éviter le suivi d'une famille chimique complète de composés volatils. De même, une corrélation a été établie entre l'émission du produit de dégradation 1-pentyl-2,5-pyrrolidinedione dérivant du polyamide PA 6,6 recyclé et les propriétés mécaniques du matériau après vieillissement thermique [253]. En effet, la diminution rapide de la résistance à la traction après une période d'induction coïncidait avec la quantité élevée de produits de dégradation formés.

VIII.2. Les biocomposites et matériaux lignocellulosiques

Peu de travaux sont reportés sur les relations entre les propriétés de biocomposites déterminées au cours du vieillissement. Fabiyi et al ont dégagé des corrélations linéaires entre le blanchiment exprimé par ΔL et la concentration en acides carboxyliques et la concentration en esters à la surface de WPC (R^2 de 0,93 et 0,87 respectivement) [138]. Donc, une simple évaluation de la clarté du matériau dans ces conditions spécifiques d'exposition pourrait indiquer des modifications à l'échelle moléculaire puisqu'un lien de causalité entre la formation de composés oxygénés et la décoloration est établi. Au cours d'un autre travail réalisé sur le même type de matériaux, une relation linéaire est établie entre le degré de cristallinité et la masse moléculaire en poids de la matrice PP de WPC validée au cours de vieillissements artificiel sous arc xenon (R^2 = 0,90) et en extérieur (R^2 = 0,99) [158]. Ceci suggère que la diminution du poids moléculaire était responsable de l'augmentation de la cristallinité. Des tendances corrélatives pour une même propriété évaluée selon différents paramètres peuvent aussi être vérifiées. En effet, un degré de dépendance élevé a été déterminé entre les deux paramètres liés à la couleur a* et b* au cours d'un vieillissement accéléré de WPC indépendamment du temps de vieillissement [254]. Cela pourrait être certainement dû à la formation de paraquinones de couleur jaune et de composés de couleur rouge tels que les orthoquinones suite à la décomposition de la lignine.

La dégradation de la lignocellulose seule permet de comprendre la contribution des fibres aux variations des propriétés physico-chimiques des biocomposites mais aussi de déterminer le rôle de chaque composant sur les évolutions des propriétés. De même que pour les polymères, l'éventuelle existence de relations entre différentes propriétés, comme la couleur et la microstructure, a été étudiée. En effet, il a été montré que les variations de la valeur ΔE d'échantillons de bois sont bien corrélées avec le rapport des absorbances à 1509 et 897 cm^{-1} de liaisons C=C. Celles-ci correspondent aux composés phénoliques de la lignine qui apparaît en surface au cours d'un vieillissement artificiel à rayonnement UV [255]. Cette relation suggère que les variations de couleur sont principalement attribuées à la formation de chromophores résultant de la dégradation photochimique de la lignine. De même, Bonifazi a établi une corrélation, validée par analyse statistique, des changements de couleur tel que le blanchiment (augmentation de L*) et la coloration rouge (augmentation de a*) dus à la photo-dégradation des composants en bois, notamment la lignine, et les changements observés par analyse spectrale [256]. Une autre étude portait sur la dégradation de la cellulose. Son degré de polymérisation a été déterminé à partir de la viscosité intrinsèque représenté en fonction de la résistance à la traction en mode zero-span, essai mécanique donnant des indications sur la résistance des fibres de papier, sous différentes conditions de vieillissement accéléré. Cela implique que la longueur de chaîne de la cellulose affecte considérablement la résistance mécanique [257].

Les émissions de COV par des matériaux lignocellulosiques et leur rapport aux autres propriétés ont notamment été évalués pour vérifier si des mesures effectuées selon des méthodes de caractérisation non invasives telles que l'échantillonnage de COV sur des objets de valeur par exemple (pièces de musée) peuvent indiquer l'état de dégradation avancé. La dégradation de papiers historiques contenant principalement de la cellulose et une très faible proportion en lignine a été étudiée [258]. Une relation quantitative s'est dégagée entre les produits volatils pouvant servir de marqueurs de dégradation et la teneur en lignine. En outre, la teneur en groupements carbonyles était corrélée positivement avec la teneur en lignine fournissant des informations sur la composition. Tous ces derniers faits témoignent de la contribution de la lignine, même à faible taux, dans l'évolution des propriétés de polymères à base de lignocellulose.

IX. Synthèse bibliographique et problématique

La société actuelle connaît une expansion croissante du développement de matériaux biosourcés sur le marché. Suite à une volonté de préservation de l'environnement, des intérêts sont portés par les industriels aux biocomposites en alternative aux composites traditionnels, notamment dans les secteurs de la construction et de l'automobile. En effet, les fibres naturelles sont biodégradables, issus de ressources renouvelables et requièrent peu d'énergie pour être produites. De plus, la structure organisée des composantes des fibres confère aux fibres des propriétés spécifiques comparables à celles des fibres de verre.

Cependant, ce développement se heurte à une forte dépendance des propriétés des biocomposites aux conditions d'usage et donc à une variabilité non négligeable. Même si de nombreux moyens sont déployés et largement utilisés pour s'affranchir de ces limites (stabilisants, protection, revêtements, …), comprendre les mécanismes de dégradation et s'intéresser aux phénomènes impliqués dans la dégradation reste le meilleur moyen de maîtriser leur comportement face aux conditions d'usage.

Dans les deux types d'applications précités (bâtiment et automobile), les polymères de type PP renforcés de fibres de chanvre sont très utilisés et seront donc étudiés ici avec différents taux de charge. Leur durabilité sera évaluée au travers de deux types de vieillissements naturels adaptés aux applications visées : une exposition directe aux intempéries et une exposition sous vitre pare-brise. Les propriétés mécaniques, de microstructure, d'aspect visuel seront suivies tout au long du processus. Au vu du nombre restreint d'études reportées dans la littérature sur les émissions de COV par les biocomposites, des prélèvements des substances émises par les matériaux seront effectués tout au long du vieillissement sous vitrage. Cela permettra de contribuer à l'évaluation du risque d'exposition dans les habitacles. De plus, ces nouvelles données pourront aussi contribuer à expliquer, voire à proposer certains mécanismes de dégradation.

Des corrélations interprétées par certains auteurs entre les propriétés de matériaux thermoplastiques au cours de leur vieillissement ont permis d'évaluer la possibilité de s'affranchir de mesures invasives au profit de techniques non destructives (mesure d'aspect visuel et d'émission de COV, par exemple) pour déterminer l'état de dégradation.

Cependant, des études similaires extrapolées au comportement des biocomposites et incluant plusieurs types de propriétés n'ont pas encore été abordées. C'est pourquoi la nature des corrélations entre les propriétés physico-chimiques des biocomposites au cours de leurs conditions d'usage sera interprétée afin de rendre compte des relations existant entre tous les paramètres étudiés. Une partie développée en Annexes détaille l'outil statistique utilisé afin de trouver les liens entre ces derniers.

Enfin, l'objectif sera de comparer les résultats issus d'un vieillissement en enceinte à ceux obtenus après vieillissement naturel extérieur afin de vérifier si l'exposition en laboratoire reflète réellement les conditions naturelles d'exposition et s'il est donc possible de mettre en évidence une équivalence temporelle.

Références

[1] J. Aspling, H. Oxfall, S. Danielsson, A. Segerborg, K. Segerholm, S. Wännström, RISE report on roadmap 2015 to 2025: Bio-based composites, (2017) 1–11.

[2] Nova Institut, Feature Wind Energy, n°99, JEC Compos. Mag. (2015) 18–19.

[3] Denzil Walton, Markets: the bio-based composites in Asia JEC Asia business review, JEC Compos. Mag. (2017).

[4] MarketsandMarkets, Report on natural fiber composites market: Global trends & forecasts to 2019, Mark. Res. (2014).

[5] Grand View Research Inc, Natural fiber composites market analysis and segment forecasts to 2024 report, 2015.

[6] Grand View Research Inc, Research report on natural fiber composites market analysis by raw material, by matrix, by technology, by application and segment forecasts to 2024, 2016.

[7] Z.N. Azwa, B.F. Yousif, A.C. Manalo, W. Karunasena, A review on the degradability of polymeric composites based on natural fibres, Mater. Des. 47 (2013) 424–442. doi:10.1016/j.matdes.2012.11.025.

[8] A. Eder, M. Carus, Global Trends in Composites (WPC), Build. Constr. 8 (2013) 16–17.

[9] Kebony, Choosing the best low maintenance decking option, (2017). http://kebony.com/fr/blog/best-low-maintenance-decking/ (accessed August 3, 2017).

[10] B.J. Davis, Global overview WPC decking market, Eko-Tek Consult. (2015).

[11] BuildDirect, Different types of composite decking: hollow vs solid core boards, (n.d.). https://www.builddirect.com/ (accessed June 1, 2017).

[12] Ecodeck, Hollow vs solid composites decking, (2013). http://ecodek.co.uk/blog/hollow-solid-composite-decking/ (accessed August 3, 2017).

[13] Nathan Johnson, Composite and plastic decking: product in review, Architecture Design, (2014).

[14] F.P. La Mantia, M. Morreale, Accelerated weathering of polypropylene/wood flour composites, Polym. Degrad. Stab. 93 (2008) 1252–1258. doi:10.1016/j.polymdegradstab.2008.04.006.

[15] A.A. Klyosov, Composition of Wood Plastic Composites deck boards: thermoplastics, in: Wood Plast. Compos., John Wiley & Sons, 2007: pp. 50–58. doi:10.1002/9780470165935.ch2.

[16] A.A. Klyosov, Foreword-overview : wood plastic composites, in: Wood Plast. Compos., John Wiley & Sons, 2007. doi:10.1002/9780470165935.ch1.

[17] K. Wood, Wood-filled composites jump off the deck, CompositesWorld. (2007).

[18] J.H. Schut, Beyond decking: wood composites branch out, Plactics Technol. (2004).

[19] A. Kerr, Potential of industrial hemp to displace fiber from forests, (1998). http://www.andykerr.net/hemp-replacing-wood/.

[20] S. Grahams, 10 materials that could replace wood one day, Mercur. News. (2011).

[21] A. El-Sabbagh, A. Ramzy, L. Steuernagel, D. Meiners, Flowability and fiber content homogeneity of natural fiber polypropylene composites in injection molding, AIP Conf. Proc. 1779 (2016). doi:10.1063/1.4965531.

[22] F. Sarasini, Biocomposites for high-performance applications - current barriers and future needs towards industrial development, Woodhead publishing, 2017.

[23] Y. Regnier, Le pic de Hubbert: Mieux comprendre le débat actuel sur la « fin » du pétrole, Attac. (2005) 1–8.

[24] K. Aleklett, C. Campbell, J. Lahèrrere, Peak Oil, Assoc. Study Peak Oil. (n.d.). https://www.peakoil.net.

[25] O. Akampumuza, P.M. Wambua, A. Ahmed, W. Li, X. Qin, Review of the applications of biocomposites in the automotive industry, Polym. Compos. 16 (2016) 101–113. doi:10.1002/pc.23847.

[26] G. Marsh, Next step for automotive materials, Mater. Today. 6 (2003) 36–43. doi:10.1016/S1369-7021(03)00429-2.

[27] D.H. Mueller, Improving the impact strength of natural fiber reinforced composites by specifically designed material and process parameters, Int. Nonwovens J. 13 (2004) 31–38.

[28] M. Saxena, A. Pappu, A. Sharma, R. Haque, S. Wankhede, Composite materials from natural resources: Recent trends and future potentials, in: P. Tesinova (Ed.), Adv.

Compos. Mater. - Anal. Nat. Man-Made Mater., InTech, 2011. doi:10.5772/50570.

[29] W.C. Inc., Ward's Motor Vehicle Facts and Figures, Standford Libraries, 2008.

[30] S. Shibata, Natural Fiber Composites, in: R.D.S.G. Campilho (Ed.), Nat. Fiber Compos., 2016: pp. 157–173.

[31] O. Faruk, A.K. Bledzki, H.-P. Fink, M. Sain, Biocomposites reinforced with natural fibers: 2000–2010, Prog. Polym. Sci. 37 (2012) 1552–1596. doi:10.1016/j.progpolymsci.2012.04.003.

[32] G. Koronis, A. Silva, M. Fontul, Green composites: A review of adequate materials for automotive applications, Compos. Part B Eng. 44 (2013) 120–127. doi:10.1016/j.compositesb.2012.07.004.

[33] K. Hill, B. Swiecki, J. Cregger, The bio-based materials automotive value chain, Cent. Automot. Res. (2012) 1–92.

[34] F. Ahmad, H.S. Choi, M.K. Park, A Review : Natural Fiber Composites Selection in View of Mechanical , Light Weight , and Economic Properties, (2015) 10–24. doi:10.1002/mame.201400089.

[35] D. Brosius, Natural fiber composites slowly take root, Compos. Technol. 12 (2006) 32–37.

[36] U. Vaidya, Biocomposites, recycling and environmental aspects, in: Compos. Automotive, Truck Mass Transit, 2011: pp. 373–400.

[37] L. Mohammed, M.N.M. Ansari, G. Pua, M. Jawaid, M.S. Islam, A Review on Natural Fiber Reinforced Polymer Composite and Its Applications, Int. J. Polym. Sci. 2015 (2015). doi:10.1155/2015/243947.

[38] P. Malnati, Interior innovation: The value proposition, CompositesWorld. (2010). http://www.compositesworld.com/articles/interior-innovation-the-value-proposition (accessed June 20, 2017).

[39] N. Mavi, R. Döflemeler, Peugeot 308, Frankfurt Mot. Show. (2013) 5–6.

[40] Lotus Eco Elise, (n.d.). http://www.lotuscars.com/engineering/eco-elise (accessed August 10, 2017).

[41] Amanda Jacob, BioConcept car wins Composites Europe award, Reinf. Plast. (2009).

[42] ProShift Inc., Renault Megane bio-concept car has first racing success with new PS3, (2010). http://www.proshift.com.

[43] Citroën Jordan Inc., Sustainability, (n.d.). http://www.citroen-jo.com/citroen-universe/environnement/durable-developement/ (accessed June 15, 2017).

[44] Industrial applications for natural fibre reinforced composites, JEC Mag. (2011).

[45] J. Thoin-Bousquié, Les 100 équipementiers automobiles mondiaux les plus

performants en 2016, L'UsineNouvelle. (2017).

[46] Amanda Jacob, Faurecia develops hemp-based materials for automotive applications, Reinf. Plast. (2014).

[47] Faurecia, Faurecia's living garden at Frankfurt Motor Show demonstrates rapidly growing choices in bio-materials, Bio-Based News. (2015).

[48] Feature, construction, solutions, medical, biocomposites, n°111, JEC Compos. Mag. (2017) 1–122.

[49] Fibres Recherche et Développement (FRD), Mémento 2016: Panorama des marchés « fibres végétales techniques matériaux (hors bois) », (2016).

[50] Faurecia Corporate, (n.d.). http://www.faurecia.com/fr.

[51] O. Le Friec, Communiqué de presse: Faurecia FlaxpregTM remporte le prix de l'innovation JEC Europe 2015 dans la catégorie produits semi-finis, Faurecia News. (2015).

[52] C. Alves, P.M.C. Ferrão, A.J. Silva, L.G. Reis, M. Freitas, L.B. Rodrigues, D.E. Alves, Ecodesign of automotive components making use of natural jute fiber composites, J. Clean. Prod. 18 (2010) 313–327. doi:10.1016/j.jclepro.2009.10.022.

[53] M. John, S. Thomas, Biofibres and biocomposites, Carbohydr. Polym. 71 (2008) 343–364. doi:10.1016/j.carbpol.2007.05.040.

[54] MarketsandMarkets Inc, Natural fiber composites market by type, manufacturing process, application, and region - Global forecasts to 2021, (2016).

[55] A. Shahzad, Hemp fiber and its composites - a review, J. Compos. Mater. 46 (2012) 973–986. doi:10.1177/0021998311413623.

[56] A.N. Netravali, C.M. Pastore, Sustainable composites, DEStech, 2015.

[57] Osborne Industries Inc, The difference between thermoplastic and thermosetting plastic, (2017).

[58] E. Adamopoulou, Poly(butylene succinate): a promising polymer, PhD thesis, School of chemical engineering, 2012.

[59] A. Le Duigou, P. Davies, C. Baley, Seawater ageing of flax/poly(lactic acid) biocomposites, Polym. Degrad. Stab. 94 (2009) 1151–1162. doi:10.1016/j.polymdegradstab.2009.03.025.

[60] D. Rusu, S.A.E. Boyer, M.F. Lacrampe, P. Krawczak, Bioplastics and Vegetal Fiber Reinforced Bioplastics for Automotive Applications, Handb. Bioplastics Biocomposites Eng. Appl. (2011) 397–449. doi:10.1002/9781118203699.ch15.

[61] L. Soccalingame, D. Perrin, J.-C. Bénézet, S. Mani, F. Coiffier, E. Richaud, A. Bergeret, Reprocessing of artificial UV-weathered wood flour reinforced polypropylene composites, Polym. Degrad. Stab. 120 (2015) 313–327.

doi:10.1016/j.polymdegradstab.2015.07.013.

[62] F. Ilczyszyn, Caractérisation expérimentale et numérique du comportement mécanique des agro-composites renforcés par des fibres de chanvre, Thèse de doctorat, Université de technologie de Troyes, 2013.

[63] C. Badji, L. Soccalingame, H. Garay, A. Bergeret, J.C. Bénézet, Influence of weathering on visual and surface aspect of wood plastic composites: Correlation approach with mechanical properties and microstructure, Polym. Degrad. Stab. 137 (2017) 162–172. doi:10.1016/j.polymdegradstab.2017.01.010.

[64] Y. Feng, H. Shen, J. Qu, B. Liu, H. He, L. Han, Preparation and properties of PBS/sisal-fiber composites, Polym. Eng. Sci. 51 (2011) 474–481. doi:10.1002/pen.21852.

[65] I. Spiridon, K. Leluk, A.M. Resmerita, R.N. Darie, Evaluation of PLA–lignin bioplastics properties before and after accelerated weathering, Compos. Part B Eng. 69 (2015) 342–349. doi:10.1016/j.compositesb.2014.10.006.

[66] J. Bausset, M. Loyaux, Intégrez des produits biosourcés dans vos composites, JEC Eur. (2014) 1–36.

[67] L. Soccalingame, Etude des scénarios de fin de vie de biocomposites, Thèse de doctorat, Université de Montpellier II, 2014.

[68] S. Lee, D. Cho, W. Park, S. Han, L. Drzal, Novel silk/poly(butylene succinate) biocomposites: the effect of short fibre content on their mechanical and thermal properties, Compos. Sci. Technol. 65 (2005) 647–657. doi:10.1016/j.compscitech.2004.09.023.

[69] World plastics materials demand 2015 by types, Plast. Mark. Res. Gr. (2015) 3.

[70] Service Public de Wallonie (SPW), Fiche technique n°1.09: Le Polypropylène (PP), (2010) 1–2.

[71] J.A. Garde, R. Catala, R. Gavara, Analysis of antioxidants extracted from polypropylene by supercritical fluid extraction, Food Addit. Contam. 15 (1998) 701–708. doi:10.1080/02652039809374700.

[72] V. Ambrogi, P. Cerruti, C. Carfagna, M. Malinconico, V. Marturano, M. Perrotti, P. Persico, Natural antioxidants for polypropylene stabilization, Polym. Degrad. Stab. 96 (2011) 2152–2158. doi:10.1016/j.polymdegradstab.2011.09.015.

[73] N. Billon, Cours sur le comportement mécanique des polymères (chapitre XVII), Matériaux Pour L'ingénieur l'Ecole Des Mines Paris. (2006).

[74] M. Denac, V. Musil, I. Šmit, F. Ranogajec, Effects of talc and gamma irradiation on mechanical properties and morphology of isotactic polypropylene/talc composites, Polym. Degrad. Stab. 82 (2003) 263–270. doi:10.1016/S0141-3910(03)00220-9.

[75] P. Wambua, J. Ivens, I. Verpoest, Natural fibres: Can they replace glass in fibre reinforced plastics?, Compos. Sci. Technol. 63 (2003) 1259–1264. doi:10.1016/S0266-

3538(03)00096-4.

[76] J. Maida, Growth in housing and construction industries will drive the Wood Plastic Composites market, Bus. Wire. (n.d.). https://www.technavio.com/ (accessed May 13, 2017).

[77] C. Hindle, Polypropylene, Br. Plast. Fed. (n.d.). http://www.bpf.co.uk/plastipedia/polymers/PP.aspx.

[78] L. Garnier, Relations entre élaboration, structure et propriétés de mélanges de polypropylènes isotactique et syndiotactique: Application aux procédés d'élaboration de fils élastiques, Thèse de doctorat, Université Lille 1: Sciences et technologie, 2009.

[79] M. Vite, Relations entre microstructure , propriétés mécaniques et résistance à la rayure du polypropylène injecté, Thèse de doctorat, Université de Savoie, 2009.

[80] N. Ljungberg, J.Y. Cavaillé, L. Heux, Nanocomposites of isotactic polypropylene reinforced with rod-like cellulose whiskers, Polymer (Guildf). 47 (2006) 6285–6292. doi:10.1016/j.polymer.2006.07.013.

[81] Lenzing Corporation, The global fiber market in 2016, (2015) 6–7. http://www.lenzing.com/en/investors/equity-story/global-fiber-market.html.

[82] M. Jaque, Coton : la Chine liquide une partie de ses immenses stocks, LesEchos.fr. (2016).

[83] C. Meirhaeghe, H. Bewa, F.R. et D. (FRD), Etude du gisement accessible de fibres végétales à usages matériaux en France, 2011.

[84] A. Dureuil, Agrocomposites - Une structuration nécessaire de la filière en France, Agrobiobase. (2012).

[85] Initiative Discover Natural Fibres (DNFI) organization, Natural fibers are sustainable, (n.d.). dnfi.org (accessed May 3, 2017).

[86] Consoglobe Planétoscope, (2015). https://www.planetoscope.com/agriculture-alimentation/1178-production-mondiale-de-coton.html (accessed August 11, 2017).

[87] M.Z. Ahmad Thirmizir, Z.A. Mohd Ishak, R. Mat Taib, S. Rahim, S. Mohamad Jani, Natural Weathering of kenaf bast fibre-filled poly(butylene succinate) composites: Effect of fibre loading and compatibiliser addition, J. Polym. Environ. 19 (2010) 263–273. doi:10.1007/s10924-010-0272-2.

[88] T. Gurunathan, S. Mohanty, S.K. Nayak, Composites : Part A A review of the recent developments in biocomposites based on natural fibres and their application perspectives, Compos. PART A. 77 (2015) 1–25. doi:10.1016/j.compositesa.2015.06.007.

[89] L. Soccalingame, A. Bourmaud, D. Perrin, J.-C. Bénézet, A. Bergeret, Reprocessing of wood flour reinforced polypropylene composites: Impact of particle size and coupling agent on composite and particle properties, Polym. Degrad. Stab. 113 (2015) 72–85.

doi:10.1016/j.polymdegradstab.2015.01.020.

[90] P. Joseph, Effect of processing variables on the mechanical properties of sisal-fiber-reinforced polypropylene composites, Compos. Sci. Technol. 59 (1999) 1625–1640. doi:10.1016/S0266-3538(99)00024-X.

[91] A. Shahzad, Hemp fiber and its composites - a review, J. Compos. Mater. 46 (2011) 973–986. doi:10.1177/0021998311413623.

[92] J.S. Han, J.S. Rowell, Chemical Composition of Fibers, in: R.M. Rowell, R.A. Young, J.K. Rowell. (Eds.), Pap. Compos. from Agro-Based Resour., CRC/Lewis Publishers, 1996: pp. 84–134.

[93] M.S. Huda, D. Ray, A.K. Mohanty, M. Misra, Properties and performance of natural fibre composites, Woodhead Publishing, 2008. doi:10.1016/B978-0-323-05712-7.00031-3.

[94] J.M. Yatim, N. Hafizah, B. Abd, R. Mahjoub, Biocomposites for the construction materials and structures, in: CIDB Semin. Sarawak, 2011: pp. 1–29.

[95] C. Courgneau, D. Rusu, C. Henneuse, V. Ducruet, M.F. Lacrampe, P. Krawczak, Characterisation of low-odour emissive polylactide/cellulose fibre biocomposites for car interior, Express Polym. Lett. 7 (2013) 787–804. doi:10.3144/expresspolymlett.2013.76.

[96] A.K. Bledzki, J. Gassan, Composites reinforced with cellulose based fibres, Prog. Polym. Sci. 24 (1999) 221–274. doi:10.1016/S0079-6700(98)00018-5.

[97] C. Baley, Fibres naturelles de renfort pour matériaux composites, Tech. l'Ingénieur. (2013) 1–17.

[98] C. He, C.L. Chen, A. Giannis, Y. Yang, J.Y. Wang, Hydrothermal gasification of sewage sludge and model compounds for renewable hydrogen production: A review, Renew. Sustain. Energy Rev. 39 (2014) 1127–1142. doi:10.1016/j.rser.2014.07.141.

[99] N. Sallem-Idrissi, C. Vanderghem, T. Pacary, A. Richel, D.P. Debecker, J. Devaux, M. Sclavons, Lignin degradation and stability: Volatile Organic Compounds (VOCs) analysis throughout processing, Polym. Degrad. Stab. 130 (2016) 30–37. doi:10.1016/j.polymdegradstab.2016.05.028.

[100] Y. Peng, R. Liu, J. Cao, Y. Chen, Effects of UV weathering on surface properties of polypropylene composites reinforced with wood flour, lignin, and cellulose, Appl. Surf. Sci. 317 (2014) 385–392. doi:10.1016/j.apsusc.2014.08.140.

[101] J.S. Lupoi, S. Singh, R. Parthasarathi, B. a. Simmons, R.J. Henry, Recent innovations in analytical methods for the qualitative and quantitative assessment of lignin, Renew. Sustain. Energy Rev. 49 (2015) 871–906. doi:10.1016/j.rser.2015.04.091.

[102] G. Dorez, L. Ferry, R. Sonnier, A. Taguet, J.-M. Lopez-Cuesta, Effect of cellulose, hemicellulose and lignin contents on pyrolysis and combustion of natural fibers, J. Anal. Appl. Pyrolysis. 107 (2014) 323–331. doi:10.1016/j.jaap.2014.03.017.

[103] C.B. Clifford, Alternative fuels from biomass sources, (n.d.). https://www.e-education.psu.edu/egee439/node/670 (accessed August 31, 2017).

[104] L. Pollegioni, F. Tonin, E. Rosini, Lignin-degrading enzymes, FEBS J. 282 (2015) 1190–1213. doi:10.1111/febs.13224.

[105] K. Katō, H. Komorita, Pyrolysis of Cellulose, Agric. Biol. Chem. 32 (1968) 21–26. doi:10.1080/00021369.1968.10859016.

[106] D.J. Nowakowski, J.M. Jones, Uncatalysed and potassium-catalysed pyrolysis of the cell-wall constituents of biomass and their model compounds, J. Anal. Appl. Pyrolysis. 83 (2008) 12–25. doi:10.1016/j.jaap.2008.05.007.

[107] J.R. Barnett, V. a Bonham, Cellulose microfibril angle in the cell wall of wood fibres., Biol. Rev. Camb. Philos. Soc. 79 (2004) 461–472. doi:Doi 10.1017/S1464793103006377.

[108] W.D. Brouwer, Natural fibre composites: Saving weight and cost with renewable materials, in: Thirteen. Int. Conf. Compos. Mater. Beijing, 2001.

[109] M. Ho, H. Wang, J.-H. Lee, C.-K. Ho, K.-T. Lau, J. Leng, D. Hui, Critical factors on manufacturing processes of natural fibre composites, Compos. Part B. 8 (2012) 3549–3562. doi:10.1016/j.compositesb.2011.10.001.

[110] M.S. Huda, L.T. Drzal, A.K. Mohanty, M. Misra, Chopped glass and recycled newspaper as reinforcement fibers in injection molded poly(lactic acid) (PLA) composites: A comparative study, Compos. Sci. Technol. 66 (2006) 1813–1824. doi:10.1016/j.compscitech.2005.10.015.

[111] T.T. Law, Z.A.M. Ishak, Absorption and Dimensional Stability of Short Kenaf Fiber-Filled Polypropylene Composites Treated with Maleated Polypropylene, Polym. Polym. Compos. 21 (2013) 449–456. doi:10.1002/app.

[112] G. Cantero, A. Arbelaiz, F. Mugika, A. Valea, I. Mondragon, Mechanical Behavior of Wood/Polypropylene Composites: Effects of Fibre Treatments and Ageing Processes, J. Reinf. Plast. Compos. 22 (2003) 37–50. doi:10.1106/073168403021495.

[113] K.B. Adhikary, S. Pang, M.P. Staiger, Dimensional stability and mechanical behaviour of wood-plastic composites based on recycled and virgin high-density polyethylene (HDPE), Compos. Part B Eng. 39 (2008) 807–815. doi:10.1016/j.compositesb.2007.10.005.

[114] A.K. Bledzki, A. Jaszkiewicz, D. Scherzer, Mechanical properties of PLA composites with man-made cellulose and abaca fibres, Compos. Part A Appl. Sci. Manuf. 40 (2009) 404–412. doi:10.1016/j.compositesa.2009.01.002.

[115] M.S. Islam, K.L. Pickering, N.J. Foreman, Influence of accelerated ageing on the physico-mechanical properties of alkali-treated industrial hemp fibre reinforced poly(lactic acid) (PLA) composites, Polym. Degrad. Stab. 95 (2010) 59–65. doi:10.1016/j.polymdegradstab.2009.10.010.

[116] S. Ochi, Mechanical properties of kenaf fibers and kenaf/PLA composites, Mech. Mater. 40 (2008) 446–452. doi:10.1016/j.mechmat.2007.10.006.

[117] L. Sisti, G. Totaro, M. Vannini, P. Fabbri, S. Kalia, A. Zatta, A. Celli, Evaluation of the retting process as a pre-treatment of vegetable fibers for the preparation of high-performance polymer biocomposites, Ind. Crops Prod. 81 (2016) 56–65. doi:10.1016/j.indcrop.2015.11.045.

[118] C.-F. Kuan, C.-C.M. Ma, H.-C. Kuan, H.-L. Wu, Y.-M. Liao, Preparation and characterization of the novel water-crosslinked cellulose reinforced poly(butylene succinate) composites, Compos. Sci. Technol. 66 (2006) 2231–2241. doi:10.1016/j.compscitech.2005.12.011.

[119] N. Lu, S. Oza, A comparative study of the mechanical properties of hemp fiber with virgin and recycled high density polyethylene matrix, Compos. Part B Eng. 45 (2013) 1651–1656. doi:10.1016/j.compositesb.2012.09.076.

[120] L. Liu, J. Yu, L. Cheng, W. Qu, Mechanical properties of poly(butylene succinate) (PBS) biocomposites reinforced with surface modified jute fibre, Compos. Part A Appl. Sci. Manuf. 40 (2009) 669–674. doi:10.1016/j.compositesa.2009.03.002.

[121] B.L. Shah, S.E. Selke, M.B. Walters, P.A. Heiden, Effects of wood flour and chitosan on mechanical, chemical, and thermal properties of polylactide, Polym. Compos. 16 (2008) 101–113. doi:10.1002/pc.

[122] K.B. Adhikary, S. Pang, M.P. Staiger, Accelerated Ultraviolet Weathering of Recycled Polypropylene--Sawdust Composites, J. Thermoplast. Compos. Mater. 22 (2009) 661–679. doi:10.1177/0892705709096550.

[123] S. Mukhopadhyay, R. Srikanta, Effect of ageing of sisal fibres on properties of sisal – Polypropylene composites, Polym. Degrad. Stab. 93 (2008) 2048–2051. doi:10.1016/j.polymdegradstab.2008.02.018.

[124] A. Bourmaud, C. Baley, Rigidity analysis of polypropylene/vegetal fibre composites after recycling, Polym. Degrad. Stab. 94 (2009) 297–305. doi:10.1016/j.polymdegradstab.2008.12.010.

[125] A. Arbelaiz, B. Fernández, J.A. Ramos, A. Retegi, R. Llano-Ponte, I. Mondragon, Mechanical properties of short flax fibre bundle/polypropylene composites: Influence of matrix/fibre modification, fibre content, water uptake and recycling, Compos. Sci. Technol. 65 (2005) 1582–1592. doi:10.1016/j.compscitech.2005.01.008.

[126] R. Gadioli, J.A. Morais, W.R. Waldman, M.-A. De Paoli, The role of lignin in polypropylene composites with semi-bleached cellulose fibers: Mechanical properties and its activity as antioxidant, Polym. Degrad. Stab. 108 (2014) 23–34. doi:10.1016/j.polymdegradstab.2014.06.005.

[127] N.S. Egute, P.L. Forster, F.D. Parra, D.M. Fermino, S. Santana, A.B. Lugão, Mechanical and thermal properties of polypropylene composites with curaua fibre, in: Int. Nucl. Atl. Conf., 2009.

[128] S. Tungjitpornkull, N. Sombatsompop, Processing technique and fiber orientation angle affecting the mechanical properties of E-glass fiber reinforced wood/PVC composites, J. Mater. Process. Technol. 209 (2009) 3079–3088. doi:10.1016/j.jmatprotec.2008.07.021.

[129] A.K. Bledzki, O. Faruk, A.A. Mamun, Influence of compounding processes and fibre length on the mechanical properties of abaca fibre-polypropylene composites, Polimery/Polymers. 53 (2008) 120–125.

[130] K.L. Fung, X.S. Xing, R.K.Y. Li, S.C. Tjong, Y.-W. Mai, An investigation on the processing of sisal fibre reinforced polypropylene composites, Compos. Sci. Technol. 63 (2003) 1255–1258. doi:10.1016/S0266-3538(03)00095-2.

[131] N. Le Moigne, M. Longerey, J.-M. Taulemesse, J.-C. Bénézet, A. Bergeret, Study of the interface in natural fibres reinforced poly(lactic acid) biocomposites modified by optimized organosilane treatments, Ind. Crops Prod. 52 (2014) 481–494. doi:10.1016/j.indcrop.2013.11.022.

[132] D. Chen, J. Li, J. Ren, Influence of fiber surface-treatment on interfacial property of poly(l-lactic acid)/ramie fabric biocomposites under UV-irradiation hydrothermal aging, Mater. Chem. Phys. 126 (2011) 524–531. doi:10.1016/j.matchemphys.2011.01.035.

[133] N. Petchwattana, S. Covavisaruch, S. Chanakul, Mechanical properties, thermal degradation and natural weathering of high density polyethylene/rice hull composites compatibilized with maleic anhydride grafted polyethylene, J. Polym. Res. 19 (2012) 9921. doi:10.1007/s10965-012-9921-6.

[134] R. Bernstein, S.M. Thornberg, A.N. Irwin, J.M. Hochrein, D.K. Derzon, S.B. Klamo, R.L. Clough, Radiation-oxidation mechanisms: Volatile organic degradation products from polypropylene having selective C-13 labeling studied by GC/MS, Polym. Degrad. Stab. 93 (2008) 854–870. doi:10.1016/j.polymdegradstab.2008.01.020.

[135] J.F. Rabek, Photostabilization of Polymers: Principles and applications, Elsevier Applied Science, 1990. doi:10.1007/978-94-009-07-47-8.

[136] M. Muasher, M. Sain, The efficacy of photostabilizers on the color change of wood filled plastic composites, Polym. Degrad. Stab. 91 (2006) 1156–1165. doi:10.1016/j.polymdegradstab.2005.06.024.

[137] T. Salthammer, Emissions of Volatile Organic Compounds from Products, 4 (2004) 37–71. doi:10.1007/b94830.

[138] J.S. Fabiyi, A.G. McDonald, M.P. Wolcott, P.R. Griffiths, Wood plastic composites weathering: Visual appearance and chemical changes, Polym. Degrad. Stab. 93 (2008) 1405–1414. doi:10.1016/j.polymdegradstab.2008.05.024.

[139] A. Bergeret, J. Benezet, T.P.T. Tran, G.C. Papanicolaou, A. Koutsomitopoulou, Valorization of agricultural by-products in poly (lactic acid) to develop biocomposites, in: V.K. Thakur (Ed.), Green Compos. from Nat. Resour., CRC Press, Taylor & Francis

LLC, 2013. doi:10.13140/2.1.1271.2969.

[140] N.M. Stark, L.M. Matuana, Influence of photostabilizers on wood flour-HDPE composites exposed to xenon-arc radiation with and without water spray, Polym. Degrad. Stab. 91 (2006) 3048–3056. doi:10.1016/j.polymdegradstab.2006.08.003.

[141] Y. Peng, R. Liu, J. Cao, Characterization of surface chemistry and crystallization behaviour of polypropylene composites reinforced with wood flour, cellulose, and lignin during accelerated weathering, Appl. Surf. Sci. (2015). doi:10.1016/j.apsusc.2015.01.147.

[142] I. Spiridon, R.N. Darie, H. Kangas, Influence of fiber modifications on PLA/fiber composites. Behavior to accelerated weathering, Compos. Part B Eng. 92 (2016) 19–27. doi:10.1016/j.compositesb.2016.02.032.

[143] A. François-Heude, E. Richaud, E. Desnoux, X. Colin, Influence of temperature, UV-light wavelength and intensity on polypropylene photothermal oxidation, Polym. Degrad. Stab. 100 (2014) 10–20. doi:10.1016/j.polymdegradstab.2013.12.038.

[144] J.W. Martin, R.A. Ryntz, J. Chin, R.A. Dickie, Service life prediction of polymeric materials: Global perspectives, in: R.A. Ryntz, J. Chin, R.A. Dickie (Eds.), Springer Science & Business Media, 2008: p. 537. doi:10.1007/978-0-387-84876-1.

[145] X. Yang, X. Jiang, J. Hu, F. Wang, C. Hu, Relationship between physical and mechanical properties of accelerated weathering and outdoor weathering of PVC-coated membrane material under tensile stress, J. Ind. Text. (2016). doi:10.1177/1528083716639062.

[146] K. Joseph, S. Thomas, C. Pavithran, Effect of ageing on the physical and mechanical properties of sisal fiber reinforced polyethylene composites, Compos. Sci. Technol. 53 (1995) 99–110. doi:10.1016/0266-3538(94)00074-3.

[147] M. Celina, K.T. Gillen, R.A. Assink, Accelerated aging and lifetime prediction: Review of non-Arrhenius behaviour due to two competing processes, Polym. Degrad. Stab. 90 (2005) 395–404. doi:10.1016/j.polymdegradstab.2005.05.004.

[148] L. Audouin, S. Girois, L. Achimsky, J. Verdu, Effect of temperature on the photooxidation of polypropylene films, Polym. Degrad. Stab. 60 (1998) 137–143. doi:10.1016/S0141-3910(97)00042-6.

[149] T. Yu, F. Sun, M. Lu, Y. Li, Water absorption and hygrothermal aging behavior of short ramie fiber reinforced poly(lactic acid) composites, Polym. Compos. (2016) 1–7. doi:10.1002/pc.24038.

[150] C.-H. Shen, G.S. Springer, Moisture absorption and desorption of composite materials, J. Compos. Mater. 10 (1976) 2–20. doi:10.1177/002199837601000101.

[151] H. Han, Study of agro-composite hemp/Polypropylene : Treatment of fibers , morphological and mechanical characterization, PhD thesis, Université de technologie de Troyes, 2015.

[152] Y.J. Phua, W.S. Chow, Z. a. Mohd Ishak, The hydrolytic effect of moisture and hygrothermal aging on poly(butylene succinate)/organo-montmorillonite nanocomposites, Polym. Degrad. Stab. 96 (2011) 1194–1203. doi:10.1016/j.polymdegradstab.2011.04.017.

[153] M.D.H. Beg, K.L. Pickering, Mechanical performance of Kraft fibre reinforced polypropylene composites: Influence of fibre length, fibre beating and hygrothermal ageing, Compos. Part A Appl. Sci. Manuf. 39 (2008) 1748–1755. doi:10.1016/j.compositesa.2008.08.003.

[154] P. V. Joseph, M.S. Rabello, L.H.C. Mattoso, K. Joseph, S. Thomas, Environmental effects on the degradation behaviour of sisal fibre reinforced polypropylene composites, Compos. Sci. Technol. 62 (2002) 1357–1372. doi:10.1016/S0266-3538(02)00080-5.

[155] D.F. Caulfield, D. Feng, S. Prabawa, R.A. Young, A.R. Sanadi, Interphase effects on the mechanical and physical aspects of natural fiber composites, Die Angew. Makromol. Chemie. 272 (1999) 57–64. doi:10.1002/(SICI)1522-9505(19991201)272:1<57::AID-APMC57>3.0.CO;2-W.

[156] M.D.H. Beg, K.L. Pickering, Accelerated weathering of unbleached and bleached Kraft wood fibre reinforced polypropylene composites, Polym. Degrad. Stab. 93 (2008) 1939–1946. doi:10.1016/j.polymdegradstab.2008.06.012.

[157] J.L. Lopez, M. Sain, P. Cooper, Performance of natural-fiber-plastic composites under stress for outdoor applications: Effect of moisture, temperature, and ultraviolet light exposure, J. Appl. Polym. Sci. 99 (2006) 2570–2577. doi:10.1002/app.22884.

[158] J.S. Fabiyi, A.G. McDonald, Degradation of polypropylene in naturally and artificially weathered plastic matrix composites, Maderas. Cienc. Y Tecnol. 16 (2014) 0–0. doi:10.4067/S0718-221X2014005000021.

[159] S. Butylina, M. Hyvärinen, T. Kärki, A study of surface changes of wood-polypropylene composites as the result of exterior weathering, Polym. Degrad. Stab. 97 (2012) 337–345. doi:10.1016/j.polymdegradstab.2011.12.014.

[160] C. Homkhiew, T. Ratanawilai, W. Thongruang, Effects of natural weathering on the properties of recycled polypropylene composites reinforced with rubberwood flour, Ind. Crops Prod. 56 (2014) 52–59. doi:10.1016/j.indcrop.2014.02.034.

[161] X. Zhou, S. Huang, L. Chen, Effect of antiaging agents on the outdoor natural weathering of bamboo powder/polypropylene foamed composites, J. Vinyl Addit. Technol. 22 (2014) 311–319. doi:10.1002/vnl.21433.

[162] X. Zhou, S. Huang, Y. Yu, J. Li, L. Chen, Outdoor natural weathering of bamboo flour/polypropylene foamed composites, J. Reinf. Plast. Compos. 33 (2014) 1835–1846. doi:10.1177/0731684414548611.

[163] K.C. Hung, Y.L. Chen, J.H. Wu, Natural weathering properties of acetylated bamboo plastic composites, Polym. Degrad. Stab. 97 (2012) 1680–1685.

doi:10.1016/j.polymdegradstab.2012.06.016.

[164] S. Panthapulakkal, M. Sain, Injection-molded short hemp fiber/glass fiber-reinforced polypropylene hybrid composites—Mechanical, water absorption and thermal properties, J. Appl. Polym. Sci. 103 (2006) 2432–2441. doi:10.1002/app.

[165] N.M. Stark, L.M. Matuana, Ultraviolet weathering of photostabilized wood-flour-filled high-density polyethylene composites, J. Appl. Polym. Sci. 90 (2003) 2609–2617. doi:10.1002/app.12886.

[166] T. Lundin, S.M. Cramer, R.H. Falk, C. Felton, Accelerated weathering of natural fiber-filled polyethylene composites, J. Mater. Civ. Eng. 16 (2004) 547–555. doi:10.1061/(ASCE)0899-1561(2004)16.

[167] A.H. Umar, E.S. Zainudin, S.M. Sapuan, Effect of accelerated weathering on tensile properties of kenaf reinforced high-density polyethylene composites, J. Mech. Eng. Sci. 2 (2012) 198–205. doi:http://dx.doi.org/10.15282/jmes.2.2012.7.0018.

[168] M.M. Thwe, K. Liao, Durability of bamboo-glass fiber reinforced polymer matrix hybrid composites, Compos. Sci. Technol. 63 (2003) 375–387. doi:10.1016/S0266-3538(02)00225-7.

[169] P. Zou, H. Xiong, S. Tang, Natural weathering of rape straw flour (RSF)/HDPE and nano-SiO2/RSF/HDPE composites, Carbohydr. Polym. 73 (2008) 378–383. doi:10.1016/j.carbpol.2007.12.002.

[170] L. Soccalingame, D. Perrin, J.-C. Bénézet, A. Bergeret, Reprocessing of UV-weathered wood flour reinforced polypropylene composites: Study of a natural outdoor exposure, Polym. Degrad. Stab. 133 (2016) 389–398. doi:10.1016/j.polymdegradstab.2016.09.011.

[171] M. Sablier, M. Perraudeau, Lumière et couleur, Tech. l'Ingénieur. (2004).

[172] P. Callet, Couleur et apparence visuelle - Le transparent et l'opaque, Tech. L'ingénieur. (2004).

[173] Commission Internationale de l'Eclairage, Vocabulaire international de l'Eclairage, Rapport technique 17.4, CIE Publ. (1987).

[174] V. Domurado, Étude et modélisation de la réflectance de la surface d'objets réels, Mémoire de fin d'études, 2001.

[175] M. Kiguchi, Y. Kataoka, H. Matsunaga, K. Yamamoto, P.D. Evans, Surface deterioration of wood-flour polypropylene composites by weathering trials, J. Wood Sci. 53 (2006) 234–238. doi:10.1007/s10086-006-0838-8.

[176] D.N.-S. Hon, S.-T. Chang, Surface degradation of wood by ultraviolet light, J. Polym. Sci. Polym. Chem. Ed. 22 (1984) 2227–2241. doi:10.1002/pol.1984.170220923.

[177] K. Srinivas, K.K. Pandey, Photodegradation of thermally modified wood, J. Photochem. Photobiol. B Biol. 117 (2012) 140–145. doi:10.1016/j.jphotobiol.2012.09.013.

[178] J.S. Fabiyi, A.G. McDonald, Physical morphology and quantitative characterization of chemical changes of weathered PVC/Pine composites, J. Polym. Environ. 18 (2009) 57–64. doi:10.1007/s10924-009-0152-9.

[179] J.S. Fabiyi, D. McIlroy, A.G. McDonald, Wood modification effects on weathering of HDPE-based Wood Plastic Composites, J. Polym Env. 17 (2009) 34–48. doi:10.1007/s10924-009-0118-y.

[180] D. Rosu, R. Bodîrləu, C.A. Teacə, L. Rosu, C.D. Varganici, Epoxy and succinic anhydride functionalized soybean oil for wood protection against UV light action, J. Clean. Prod. 112 (2016) 1175–1183. doi:10.1016/j.jclepro.2015.07.092.

[181] N.M. Stark, Effect of weathering cycle and manufacturing method on performance of wood flour and high-density polyethylene composites, J. Appl. Polym. Sci. 100 (2006) 3131–3140. doi:10.1002/app.23035.

[182] N.E. Klepeis, W.C. Nelson, W.R. Ott, J.P. Robinson, a M. Tsang, P. Switzer, J. V Behar, S.C. Hern, W.H. Engelmann, The National Human Activity Pattern Survey (NHAPS): a resource for assessing exposure to environmental pollutants., J. Expo. Anal. Environ. Epidemiol. 11 (2001) 231–252. doi:10.1038/sj.jea.7500165.

[183] D. Müller, D. Klingelhöfer, S. Uibel, D. a Groneberg, Car indoor air pollution - analysis of potential sources., J. Occup. Med. Toxicol. 6 (2011) 33. doi:10.1186/1745-6673-6-33.

[184] Korean Automobile Testing & Research Institute, Ministry of Land Infrastructure and Transport, Proposal for a New GTR on Vehicle Indoor Air Quality (VIAQ), (n.d.) 25–28.

[185] X. Chen, G. Zhang, H. Chen, Controlling strategies and technologies of volatile organic compounds pollution in interior air of cars, Proc. - 2010 Int. Conf. Digit. Manuf. Autom. ICDMA 2010. 1 (2010) 450–453. doi:10.1109/ICDMA.2010.375.

[186] MCS-Aware, Sick Car Syndrome, (2015). http://www.mcs-aware.org/general-articles/189-sick-car-syndrome (accessed January 5, 2017).

[187] Automobile : un concentré de pollution à l'intérieur des voitures, LeParisien. (2015).

[188] B. Xu, X. Chen, J. Xiong, Air quality inside motor vehicles' cabins: A review, Indoor Built Environ. (2016) 1–14. doi:10.1177/1420326X16679217.

[189] Y.C. Chien, Variations in amounts and potential sources of volatile organic chemicals in new cars, Sci. Total Environ. 382 (2007) 228–239. doi:10.1016/j.scitotenv.2007.04.022.

[190] Air quality sciences Inc., Indoor Air Quality hazards of new cars, (2006) 47–51.

[191] C. Yu, D. Crump, A review of the emission of VOCs from polymeric materials used in buildings, Build. Environ. 33 (1998) 357–374. doi:10.1016/S0360-1323(97)00055-3.

[192] C. Weathers, Is that New Car Smell killing you ?, AlterNet. (2014). http://www.alternet.org/new-car-smell-killing-you (accessed September 4, 2017).

[193] Chemical Risk Prevention Unit, CNRS, European harmonised classification and labelling of carcinogenic, mutagenic and toxic for reproduction (CMR) substances according to the criteria of the CLP Regulation, (2015).

[194] H. Kim, B. Lee, S. Choi, Sustainable biocomposites for automotive interior parts, in: 18TH Int. Conf. Compos. Mater., 2011: pp. 1–4.

[195] R. Grisanti, Is your car making you sick?, Funct. Med. Univ. (2012).

[196] J.S. Félix, C. Domeño, C. Nerín, Characterization of wood plastic composites made from landfill-derived plastic and sawdust: volatile compounds and olfactometric analysis, Waste Manag. 33 (2013) 645–55. doi:10.1016/j.wasman.2012.11.005.

[197] K. Sakakibara, K. Kaitani, C. Hamada, S. Sato, M. Matsuo, Analysis of odor in car cabin, JSAE Rev. 20 (1999) 237–241. doi:10.1016/S0389-4304(98)00073-3.

[198] C. Weathers, Is that New Car Smell killing you ?, AlterNet. (2014).

[199] Infrastructure and Transportation Ministry of Labor, MLIT 2007–539: Newly manufactured vehicle indoor air quality management standard, South Korea, (2007).

[200] Underwriters Laboratories UL LLC, Vehicle Interior Air Quality: Addressing chemical exposure in automobiles, (2015).

[201] Korean Automobile Testing & Research Institute, Proposal for Vehicle Indoor Air Quality (VIAQ), GRPE-69-28, (2014) 5–6.

[202] J. Xiong, T. Yang, J. Tan, L. Li, Y. Ge, Characterization of VOC emission from materials in vehicular environment at varied temperatures: Correlation development and validation, PLoS One. 10 (2015) 1–21. doi:10.1371/journal.pone.0140081.

[203] Ministry of environmental protection, GB/T 27630-2011 Chinese national standard: Guideline for air quality assesment of passenger car, (2011).

[204] JAMA, Announces Voluntary Guidelines for Reducing Vehicle Cabin VOC Concentration Levels, 2005. http://www.jama-english.jp/.

[205] European Automobile Manufacturers Association, (n.d.). http://www.acea.be/.

[206] C.S. Widdowson, Vehicle interior air quality - (S)VOC emission from materials: regulation, standard methods and analytical implementation, Top. C7 Transp. Cabin Environ. (2017).

[207] Bureau Veritas Services, Vérification des émissions des matériaux et produits, (2009). www.bureauveritas.fr.

[208] ISO 12219-1: Whole vehicle test chamber — Specification and method for the determination of volatile organic compounds in cabin interiors, (2012).

[209] ISO 12219-2: Screening method for the determination of the emissions of volatile organic compounds from vehicle interior parts and materials — Bag method, (2012).

[210] ISO 12219-3: Screening method for the determination of the emissions of volatile organic compounds from vehicle interior parts and materials — Micro-scale chamber method, (2012).

[211] ISO 12219-4: Interior air of road vehicles – Method for the determination of the emissions of volatile organic compounds from vehicle interior parts and materials – Small chamber method., (2013).

[212] T. Yoshida, I. Matsunaga, A case study on identification of airborne organic compounds and time courses of their concentrations in the cabin of a new car for private use, Environ. Int. 32 (2006) 58–79. doi:10.1016/j.envint.2005.04.009.

[213] K.-W. Kim, B.-H. Lee, S. Kim, H.-J. Kim, J.-H. Yun, S.-E. Yoo, J.R. Sohn, Reduction of VOC emission from natural flours filled biodegradable bio-composites for automobile interior, J. Hazard. Mater. 187 (2011) 37–43. doi:10.1016/j.jhazmat.2010.07.075.

[214] B. Xu, Y. Wu, Y. Gong, S. Wu, X. Wu, S. Zhu, T. Liu, Investigation of volatile organic compounds exposure inside vehicle cabins in China, Atmos. Pollut. Res. 7 (2015) 215–220. doi:10.1016/j.apr.2015.09.005.

[215] M.J. Fedoruk, B.D. Kerger, Measurement of volatile organic compounds inside automobiles, J. Expo. Anal. Environ. Epidemiol. 13 (2003) 31–41. doi:10.1038/sj.jea.7500250.

[216] S. Kim, J.-A. Kim, H.-J. Kim, S. Do Kim, Determination of formaldehyde and TVOC emission factor from wood-based composites by small chamber method, Polym. Test. 25 (2006) 605–614. doi:10.1016/j.polymertesting.2006.04.008.

[217] ISO 16000-6: Indoor air -- Part 6: Determination of volatile organic compounds in indoor and test chamber air by active sampling on Tenax TA sorbent, thermal desorption and gas chromatography using MS or MS-FID, (2011).

[218] S. Overton, J. Manura, Identification of volatile organic compounds in a new automobile, Sci. Instrum. Serv. Inc. (1999) 1–6.

[219] T. Yoshida, I. Matsunaga, K. Tomioka, S. Kumagai, Interior air pollution in automotive cabins by Volatile Organic Compounds diffusing from interior materials: II. influence of manufacturer, specifications and usage status on air pollution, and estimation of air pollution levels in initial phases of deliv, Indoor Built Environ. 15 (2006) 425–444. doi:10.1177/1420326X06069395.

[220] X. Chen, G. Zhang, Q. Zhang, H. Chen, Mass concentrations of BTEX inside air environment of buses in Changsha, China, Build. Environ. 46 (2011) 421–427. doi:10.1016/j.buildenv.2010.08.005.

[221] T. Yoshida, I. Matsunaga, K. Tomioka, S. Kumagai, Interior air pollution in automotive cabins by Volatile Organic Compounds diffusing from interior materials: I. Survey of 101 Types of Japanese domestically produced cars for private use, Indoor Built Environ. 15 (2006) 425–444. doi:10.1177/1420326X06069395.

[222] K. You, Y. Ge, B. Hu, Z. Ning, S. Zhao, Y. Zhang, P. Xie, Measurement of in-vehicle

volatile organic compounds under static conditions, J. Environ. Sci. 19 (2007) 1208–1213. doi:10.1016/S1001-0742(07)60197-1.

[223] C.C. Chan, H. Özkaynak, J.D. Spengler, L. Sheldon, Driver exposure to Volatile Organic Compounds, CO, Ozone, and NO2 under different driving conditions, Environ. Sci. Technol. 25 (1991) 964–972. doi:10.1021/es00017a021.

[224] C. Rouillon, P.-O. Bussiere, E. Desnoux, S. Collin, C. Vial, S. Therias, J.-L. Gardette, Is Carbonyl Index a quantitative probe to monitor polypropylene photodegradation?, Polym. Degrad. Stab. 128 (2016) 200–208. doi:10.1016/j.polymdegradstab.2015.12.011.

[225] A. François-Heude, E. Richaud, J. Leprovost, M. Heninger, H. Mestdagh, E. Desnoux, X. Colin, Real-time quantitative analysis of volatile products generated during solid-state polypropylene thermal oxidation, Polym. Test. 32 (2013) 907–917. doi:10.1016/j.polymertesting.2013.04.008.

[226] A. Espert, L.A. de las Heras, S. Karlsson, Emission of possible odourous low molecular weight compounds in recycled biofibre/polypropylene composites monitored by head-space SPME-GC–MS, Polym. Degrad. Stab. 90 (2005) 555–562. doi:10.1016/j.polymdegradstab.2005.03.009.

[227] H.-S. Kim, B.-H. Lee, H.-J. Kim, H.-S. Yang, Mechanical–thermal properties and VOC emissions of natural-flour-filled biodegradable polymer hybrid bio-composites, J. Polym. Environ. 19 (2011) 628–636. doi:10.1007/s10924-011-0313-5.

[228] M.G. Al-Shaal, W. Ciptonugroho, F.J. Holzhäuser, J.B. Mensah, P.J.C. Hausoul, R. Palkovits, Catalytic upgrading of α-angelica lactone to levulinic acid esters under mild conditions over heterogeneous catalysts, Catal. Sci. Technol. 5 (2015) 5168–5173. doi:10.1039/C5CY00446B.

[229] R.F. Perez, M.A. Fraga, Hemicellulose-derived chemicals: one-step production of furfuryl alcohol from xylose, Green Chem. 16 (2014) 3942. doi:10.1039/C4GC00398E.

[230] Ó. Ezquerro, B. Pons, M.T. Tena, Development of a headspace solid-phase microextraction–gas chromatography–mass spectrometry method for the identification of odour-causing volatile compounds in packaging materials, J. Chromatogr. A. 963 (2002) 381–392. doi:10.1016/S0021-9673(02)00211-X.

[231] J. Salafranca, I. Clemente, F. Isella, C. Nerín, O. Bosetti, Influence of oxygen and long term storage on the profile of volatile compounds released from polymeric multilayer food contact materials sterilized by gamma irradiation, Anal. Chim. Acta. 878 (2015) 118–130. doi:10.1016/j.aca.2015.03.055.

[232] P. Kusch, G. Knupp, Headspace-SPME-GC-MS Identification of Volatile Organic Compounds released from expanded polystyrene, 12 (2004) 83–87.

[233] C.L. Arthur, J. Pawliszyn, Solid Phase Microextraction with thermal desorption using fused silica optical fibers, Anal. Chem. 62 (1990) 2145–2148.

[234] D. Bourdin, P. Mocho, V. Desauziers, H. Plaisance, Formaldehyde emission behavior of

building materials: on-site measurements and modeling approach to predict indoor air pollution., J. Hazard. Mater. 280 (2014) 164–73. doi:10.1016/j.jhazmat.2014.07.065.

[235] D. Bourdin, Composés Organiques Volatils émis par les matériaux de construction : impact sur la qualité de l'air intérieur, Thèse de doctorat, Université de Pau et des pays de l'Adour, 2013.

[236] V. Desauziers, Analyse des COV en traces dans l'air, Tech. l'Ingénieur. 33 (2009).

[237] J. Nicolle, V. Desauziers, P. Mocho, Solid phase microextraction sampling for a rapid and simple on-site evaluation of volatile organic compounds emitted from building materials, J. Chromatogr. A. 1208 (2008) 10–15. doi:10.1016/j.chroma.2008.08.061.

[238] V. Desauziers, D. Bourdin, P. Mocho, H. Plaisance, Innovative tools and modeling methodology for impact prediction and assessment of the contribution of materials on indoor air quality, Herit. Sci. 3 (2015) 1. doi:10.1186/s40494-015-0057-y.

[239] N. Shinohara, M. Fujii, A. Yamasaki, Y. Yanagisawa, Passive flux sampler for measurement of formaldehyde emission rates, Atmos. Environ. 41 (2007) 4018–4028. doi:10.1016/j.atmosenv.2007.01.028.

[240] APR ADEME CORTEA 2013, Projet COVBAT-BOIS - Nature et déterminants de la contamination aux composés organiques volatils et prédiction de la qualité de l'air intérieur dans les logements à ossature bois, 2016.

[241] A. Torikai, A. Takeuchi, S. Nagaya, K. Fueki, Photodegradation of polyethylene : effect of crosslinking on the oxygenated products and mechanical properties, Polym. Photochem. 7 (1986) 199–211.

[242] A. Tidjani, R. Arnaud, A. Dasilva, Natural and accelerated photoaging of linear low density polyethylene: Changes of the elongation at break, J. Appl. Polym. Sci. 47 (1993) 211–216. doi:10.1002/app.1993.070470203.

[243] G. Akay, T. Tinçer, H.E. Ergöz, A study of degradation of low density polyethylene under natural weathering conditions, Eur. Polym. J. 16 (1980) 601–605. doi:10.1016/0014-3057(80)90095-6.

[244] X. Yang, X. Ding, Prediction of outdoor weathering performance of polypropylene filaments by accelerated weathering tests, Geotext. Geomembranes. 24 (2006) 103–109. doi:10.1016/j.geotexmem.2005.11.002.

[245] B. Fayolle, E. Richaud, X. Colin, J. Verdu, Review : degradation-induced embrittlement in semi-crystalline polymers having their amorphous phase in rubbery state, (2008) 6999–7012. doi:10.1007/s10853-008-3005-3.

[246] P. Pagès, F.C.J. Saurina, X. Colom, FTIR and DSC study of HDPE structural changes and mechanical properties variation when exposed to weathering aging during Canadian winter, J. Appl. Polym. Sci. 60 (1996) 153–159.

[247] N.M. Stark, L.M. Matuana, Surface chemistry changes of weathered HDPE/wood-flour

composites studied by XPS and FTIR spectroscopy, Polym. Degrad. Stab. 86 (2004) 1–9. doi:10.1016/j.polymdegradstab.2003.11.002.

[248] S.A. Jabarin, E.A. Lofgren, Photooxidative effects on properties and structure of high-density polyethylene, J. Appl. Polym. Sci. 53 (1994) 411–423. doi:10.1002/app.1994.070530404.

[249] D.J. Carlsson, M. Krzymien, J. Worsfold, Volatiles released during the weathering of PVC, J. Vinyl Addit. Technol. 3 (1997) 100–106.

[250] K. Curran, M. Strlic, Polymers and volatiles : Using VOC analysis for the conservation of plastic and rubber objects, Stud. Conserv. 0 (2014) 1–14. doi:10.1179/2047058413Y.0000000125.

[251] D.J. Carlsson, M.E. Krzymien, D.J. Pleizier, G., Worsfold, M. Day, Volatiles released from PVC during photochemical degradation. The fate of chlorine., in: Society of Plastics Engineers (Ed.), Conf. Soc. Plast. Eng., 1999.

[252] M. Hakkarainen, A.-C. Albertsson, Indicator products: A new tool for lifetime prediction of polymeric materials, Biomacromolecules. 6 (2005) 775–779. doi:10.1021/bm049483f.

[253] M. Groning, M. Hakkarainen, Headspace solid-phase microextraction with gas chromatography/mass spectrometry reveals a correlation between the degradation product pattern and changes in the mechanical properties during the thermooxidation of in-plant recycled polyamide 6,6, J. Appl. Polym. Sci. 86 (2002) 3396–3407. doi:10.1002/app.11345.

[254] J.S. Fabiyi, A.G. McDonald, Effect of wood species on property and weathering performance of wood plastic composites, Compos. Part A Appl. Sci. Manuf. 41 (2010) 1434–1440. doi:10.1016/j.compositesa.2010.06.004.

[255] D. Rosu, C.A. Teaca, R. Bodirlau, L. Rosu, FTIR and color change of the modified wood as a result of artificial light irradiation, J. Photochem. Photobiol. B Biol. 99 (2010) 144–149. doi:10.1016/j.jphotobiol.2010.03.010.

[256] G. Bonifazi, L. Calienno, G. Capobianco, A. Lo, C. Pelosi, R. Picchio, S. Serranti, Modeling color and chemical changes on normal and red heart beech wood by re fl ectance spectrophotometry, Fourier Transform Infrared spectroscopy and hyperspectral imaging, Polym. Degrad. Stab. 113 (2015) 10–21. doi:10.1016/j.polymdegradstab.2015.01.001.

[257] X. Zou, N. Gurnagul, T. Uesaka, J. Bouchard, Accelerated aging of papers of pure cellulose: mechanism of cellulose degradation and paper embrittlement, Polym. Degrad. Stab. 43 (1994) 393–402. doi:10.1016/0141-3910(94)90011-6.

[258] M. Strlič, J. Thomas, T. Trafela, L. Cséfalvayová, I.K. Cigić, J. Kolar, M. Cassar, Material degradomics: On the smell of old books, Anal. Chem. 81 (2009) 8617–8622. doi:10.1021/ac9016049.

CHAPITRE II

VIEILLISSEMENTS NATURELS EN EXTÉRIEUR ET SOUS VITRE PARE-BRISE DE BIOCOMPOSITES PP/CHANVRE :

IMPACT SUR LES PROPRIETES PHYSICO-CHIMIQUES ET LES RELATIONS ENTRE LES PROPRIÉTÉS

Chapitre II

Vieillissements naturels en extérieur et sous vitre pare-brise de biocomposites PP/chanvre : Impact sur les propriétés physico-chimiques et les relations entre les propriétés

Ce chapitre comprend deux parties.

La première partie s'intéresse à l'impact de deux conditions d'usage du polypropylène vierge (PP) et des biocomposites PP renforcé de fibres de chanvre (10 et 30% en masse) simulant pendant une année un vieillissement en habitacle automobile (vieillissement naturel sous vitre pare-brise) et de lames de terrasse (vieillissement naturel en extérieur). Différentes propriétés ont été suivies au cours du vieillissement comme les propriétés mécaniques en flexion, la structure chimique par spectroscopie infrarouge, l'apparence visuelle (couleur, rugosité), la microstructure (taux de cristallinité). Les résultats ont montré que les biocomposites PP/chanvre sont d'une manière générale plus sensibles auxvieillissements que la matrice PP seule, et cela quel que soit le type de vieillissement naturel. Toutefois, chacun des vieillissements a permis de comprendre la contribution de différents facteurs de dégradation dans les mécanismes observés. Ainsi, la pluie et les rayonnements UV conduisent pour tous les matériaux à un accroissement en composés vinyliques et à la formation de micro-fissures de surface. La concentration en composés carbonylés n'est par contre pas affectée. Des températures élevées comme celles rencontrées lors du vieillissement sous vitrage favorisent la chimi-cristallisation du PP et un fort jaunissement des biocomposites, alors que le vieillissement en extérieur conduit à une perte des nuances de teinte rouge des biocomposites.

Dans la seconde partie de ce chapitre, les corrélations entre les différentes propriétés mesurées au cours des vieillissements sont étudiées à travers une analyse statistique en composantes principales (ACP) dont le principe est détaillé dans l'Annexe II. Ainsi, les résultats ont montré une dépendance entre la chute des propriétés mécaniques (module en flexion, contrainte à la flèche conventionnelle) et l'évolution du taux de composés oxygénés

(acides carboxyliques, cétones, lactones) évalué par spectroscopie infrarouge. De plus, il a été démontré que le blanchiment des biocomposites (paramètre L*) évalué par spectrocolorimétrie est fortement relié au taux de liaisons vinyliques C=C mesuré par spectroscopie infrarouge. Outre les scissions de chaines responsables de la formation de ce type de liaison, les composés aromatiques de la lignine contribuent aussi à l'augmentation du taux de liaisons C=C. Donc cette analyse a aussi permis de confirmer de façon quantitative que la lignine était en partie responsable des variations de clarté de surface des biocomposites.

Ce chapitre fait l'objet de deux publications, la première étant soumise au journal Polymer Degradation and Stability et la deuxième à soumettre à Composite Science and Technology.

I. Exterior and under glass natural weathering of hemp fibers reinforced polypropylene biocomposites: impact on mechanical, chemical, microstructural and visual aspect properties

Célia Badji, Joana Beigbeder, Hélène Garay, Anne Bergeret, Jean-Charles Bénézet and Valérie Desauziers

Ecole des Mines d'Alès, C2MA, 6 Avenue de Clavières, 30319 Alès, Cedex France

Abstract

This work aims to investigate two types of natural weathering, exterior and under glass weathering, representing respectively decking and car interior end uses of hemp fibers reinforced polypropylene (PP) biocomposites. Mechanical flexural tests were firstly performed. Then, the evolution of the PP matrix microstructure was determined through Differential Scanning Calorimetry (DSC). The chemical composition was followed by infrared spectroscopy to understand the photo- and thermo-chemical mechanisms. CIELab system-based colorimetric measurements were carried out to determine the evolution of the chromaticity and lightness. Through a new approach, gloss was obtained by determining the type of reflection of materials either specular or diffuse. Also, the surface aspect was characterized by rugosimetry. The influence of the hemp fibers rate (from 0 to 30 wt%) was studied. Results showed that biocomposites were generally more sensitive than neat PP whatever the weathering conditions. However, each type of weathering assessment allowed understanding the contribution of each degradation factor. Indeed, rainfall or UV-A rays induced an increase of vinyl concentration and the formation of cracks on surface whatever the material whereas the carbonyl functional groups rate was not influenced by the type of weathering. The high temperatures found under windshield glass favored a chemicrystallization at the first period of exposition and a stronger color instability (yellowing) whereas outdoor exposure induced red color loss.

Keywords: hemp fibers, degradation, gloss, roughness, oxidation, rain, temperature

I.1. Introduction

Due to environment and sustainability issues, biocomposites have encountered remarkable interest in the last decades. They are developed in numerous industrial sectors such as construction (decking), automobile (door panels, dashboards) and sport (surfboard) in replacement of glass or carbon fibers reinforced composites materials [1]. Although they present lower mechanical performances than glass fibers reinforced polymer composites, their specific mechanical properties are excellent. Composites based on thermoplastics such as polypropylene (PP), polyethylene (PE), polyvinyl chloride (PVC) or polylactic acid (PLA) are widely used in modern society [2–4]. PP is besides. The global production of PP is near 60 million MT per year and could reach 75 million MT in 2022 [5].

The high sensitivity face to climatic conditions of vegetal fibers used for the biocomposites reinforcement constitutes a drag for their use. Lots of recent studies deal with the natural fibers composites exterior weathering in different countries and environments such as Mediterranean [3], tropical [6,7] and continental [8,9] climates to test their durability. The exposition induced their degradation and hypotheses were brought to explain the extrinsic variations. Indeed, radical-based oxidative processes due to high temperature or ultraviolet (UV) rays are responsible to the physico-chemical properties alteration. During the weathering, the polymer matrix degrades into lower molecular weight products by Norrish type I and II reactions chain scissions [9,10]. As regards vegetal fibers, formation of quinoid structures, UV radiation absorption by lignin, Norrish reactions and photo-yellowing reactions occur and lead to the formation of chromophoric groups. Also, the thermal degradation could particularly affect the hemicelluloses stability [11]. These chemical mechanisms resulted in a mechanical performance loss, visual aspect and microstructural changes [7,12,13]. The degradation can be reduced by stabilizers incorporated during processing and slowing down the photo-oxidation rate [14].

The influence of each exterior degradation factor was assessed by weathering realized in laboratories allowing to uncouple these parameters in order to understand their contribution on biocomposites properties evolution. Depending on the studied property, either UV rays, temperature or water had a more severe impact. Indeed, UV exposure of rice husks reinforced PLA biocomposites was studied in accordance with potential final

applications [15]. It was compared to immersion and hygrothermal conditions. UV and hygrothermal ageing carried out at 65 °C and 85 °C respectively presented a more significant effect on the polymer crystallinity rate than immersion way. The observed increase was due to a chemicrystallization mechanism of PLA macromolecular chains favored at high temperature [16]. Otherwise, molecular weights and bending strength exhibited a stronger decrease under hygrothermal ageing conditions than under other weathering ones. Thwe and Liao [17] also worked on the hygrothermal ageing of bamboo fibers reinforced PP composites. Samples were immersed in water at 25 °C for 6 months and at 75 °C for 3 months. Tensile strength and modulus showed a slight decrease after ageing at 25 °C after 6 months. However, they were highly reduced after immersion at 75 °C. The interfacial adhesion was also impacted due to debonding caused by the incompatibility between thermal and moisture expansion coefficients. The temperature promoted the water saturation phenomenon [18,19]. The immersion representing extreme water absorption conditions was also studied by Arbelaiz et al [20]. The water uptake induced a fibers swelling until reaching saturation that affected the interfacial adhesion and the mechanical properties. This also led to microcracking of the composite and dimensional instability. Otherwise, Bauer suggested that the rate of photo-oxidation due to UV rays exposition increased with the temperature with an Arrenhius rate dependence [21]. The photo-oxidation rate of natural fibers reinforced composites also increased with the humidity [11], the water facilitating the light penetration into the vegetal matter. Thus, a synergistic effect could also enlarge the degradation phenomenon during the weathering.

The contribution of each vegetal fibers component (lignin, hemicellulose, non-cellulosic componets for example) on variations of biocomposites properties during the weathering has been investigated. Beg et al. evaluated the effects of lignin and hemicelluloses presence on composite properties. A better interfacial bonding and higher tensile strength were observed whenbleached Kraft wood fibers are incorporated in PP all along the ageing thanks to the removal of non-cellulosic compounds [11]. Also, Peng et al. showed that the cellulose favored the formation of microcracks on the surface of cellulose fibers reinforced PP composites but any significant discoloration was observed [22]. Indeed, the high hygroscopicity of cellulose may induce a composite swelling and thus a higher surface roughness compared to neat PP. The discoloration of composites was accelerated by the

presence of lignin, especially at high content. Indeed, it is widely accepted that a phenoxy quinone redox mechanism is implied in lignin decomposition [14]. In fact, the paraquinone structures with a characteristic yellow color formed after ageing are further decomposed into hydroquinone molecules responsible for the composites bleaching. However, it was recently demonstrated that the carbohydrate part of lignocellulosic materials could also undergone yellowing due to chromophoric carbonyl formation after photo-oxidation [23]. Otherwise, Peng et al. also noted that the presence of lignin induced a lower decrease in flexural strength and modulus of PP composites, as well as a low number of microcracks at the composite surface and a better surface hydrophobicity towards weathering than in presence of cellulose or wood flour [22]. The same improvement of mechanical properties in presence of lignin in cellulose fibers reinforced PP composites was noted by Gadioli et al. [24]. This anti-oxidant role of lignin can be explained by the presence of hindered phenols that prevent free radical-based reactions during the polymer stabilization process [22,24]. Otherwise, infrared spectroscopy revealed that an oxidative degradation of materials occurred whatever the lignocellulosic component chosen for the composite reinforcement. Nevertheless, hemicelluloses reinforced thermoplastic composites were not studied because of their very low thermal stability limiting their process.

Several studies were investigated about natural and artificial weathering of car exterior and interior pieces made of paints and coatings [21,25–27]. The main works reported in the literature dealing with the car interior pieces behaviour examine their Volatile Organic Compounds (VOCs) emissions and their impact on indoor air quality [28–30]. To our knowledge, any exterior ageing of natural fibers reinforced composites representing a car interior environment was reported in the literature.

The objective of this work is to assess the influence of the type of weathering, either exterior or under windshield glass, on the evolution of physico-chemical properties of hemp fibers reinforced PP biocomposites. Flexural properties as well as microstructure and chemical composition were followed over the weathering. Visual and surface aspects were analyzed thanks to optical measurements. A comparison between the two weathering was done for each material and each characterization to understand the effects of the weathering exterior parameters.

I.2. Materials and Methods

I.2.1 Materials

Polypropylene grade H733-07 with a melt flow rate of 7.5 g/10 min (230 °C, 2.16 kg) purchased from Braskem Co. (Sao Paulo, Brazil) was used as thermoplastic matrix. Hemp fibers (2-6 mm) were provided by AgroChanvre (Barenton, France). After the retting process (38 days), their cellulose, hemicelluloses and lignin rates displayed in Table 1 were determined by successive chemical extractions based on TAPPI T264, ASTM D1104 standards [31,32]. Two hemp fibers loading 10 wt% (PP10) and 30 wt% (PP30) were chosen (Table 2). Maleic anhydride grafted polypropylene (MA-g-PP) with a 1 wt% grafting rate (Orevac CA100) and supplied by Arkema (France), was added at 3.1 wt% of PP as coupling agent.

Table 1 - Hemp fibers chemical composition

	Cellulose	Hemicelluloses	Lignin	Liphophilic extractives	Ash
(wt%)	82.1	8.5	4.5	2.7	2.1

Table 2 - Designation of materials

	Composition (wt%)		
	PP	Hemp fibers	MA-g-PP
PP	100	-	-
PP10	87.3	10	2.7
PP30	67.9	30	2.1

I.2.2 Material processing

Hemp fibers and MA-g-PP have been dried before processing for 15 h at 60 °C in an oven to remove residual water. Granules of PP and MA-g-PP were mixed with hemp fibers in a BC21 Clextral co-rotating twin-screw extruder (L/D = 36 with the diameter D = 25 mm) (Clextral, France) with the temperature profile 190-190-190-180-175-175-175 °C from feed to die and a screw speed of 220 rpm. Once dried for 3 days at 60 °C, extruded pellets were injection molded in a Krauss Maffei KM50-T180CX at 210 °C (Krauss Maffei, Germany) with an

injection speed of 30 $cm^3.s^{-1}$ to obtain square specimens of 100 × 100 × 2 mm and ISO 1 dog-bone specimens (Figure 1).

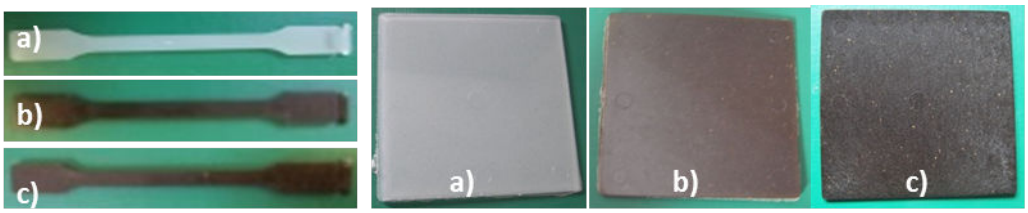

Figure 1 - PP (a), PP10 (b) and PP30 (c) materials: dog-bone specimens (left) and square specimens (right)

I.2.3 Weathering conditions

Two types of natural weathering were carried out in the south west of France (Pau) between September 2015 and September 2016 allowing to include climatic conditions from the four annual seasons and consider the contribution of each season to the degradation. The first exterior exposition corresponded to a decking use and the second one simulated a car interior environment. These two weathering conditions satisfied with ISO 877-1:2011 and ISO 877-2:2011 respectively [33,34]. The samples were fixed on galvanized racks at an angle of 45° with the ground and directed toward the south. Laminated windshield glasses protected the materials for the automotive application (Figure 2). The designation of non-weathered and weathered materials is featured in Table 3. Dog-bone and square specimens were sampled after 1, 2, 3, 6, 9 and 12 months for laboratory characterizations. Seasonal data such as solar radiation and pluviometry were recorded from Pau-Uzein station [35] whereas laboratory-sensors were used for monitoring temperature and relative humidity (Figure 3 and Figure 4). All along the ageing, mean temperature was slightly higher under glass than outside with the biggest difference in August 2015. Otherwise, the min-max temperature values amplitude was greater under windshield glass. On the contrary, relative humidity was obviously lower under glass due to higher temperatures drying the interior air. Thus, under glass weathering simulates a hot and dry climate whereas exterior ageing represented moderate and humid climate.

Figure 2 - Exposure racks

Table 3- Designation of non-weathered and PP, PP10 and PP30 weathered materials

	Non-weathered materials	Exterior weathered materials	Under glass weathered materials
Designation	PP-UW, PP10-UW, PP30-UW	PP-EW, PP10-EW, PP30-EW	PP-GW, PP10-GW, PP30-GW

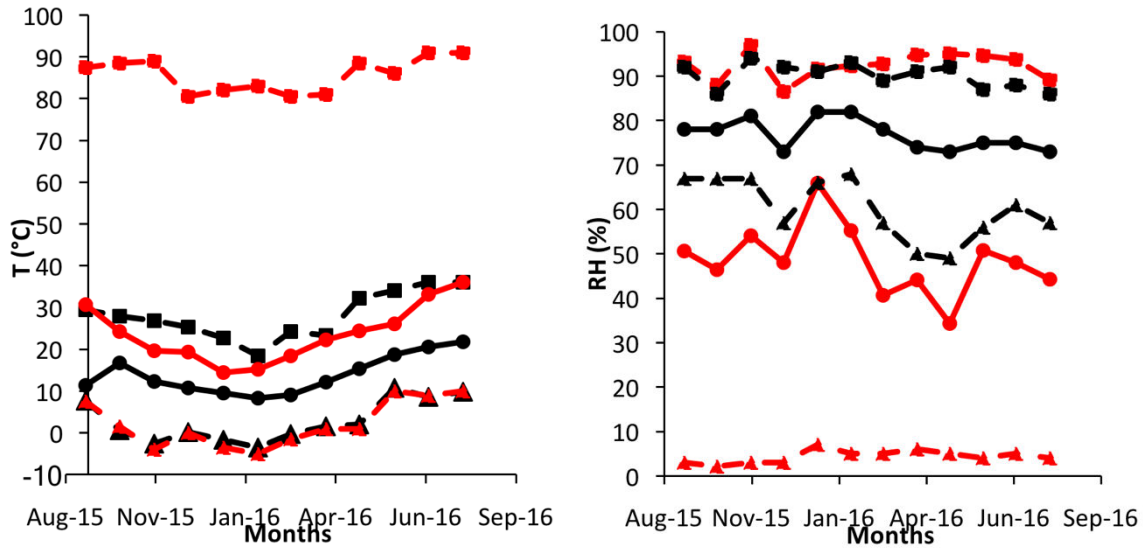

A B

Figure 3 – Mean (rounds), minimum (triangles) and maximum (squares) temperature (A) and relative humidity (B) (red: under glass weathering, dark: exterior weathering)

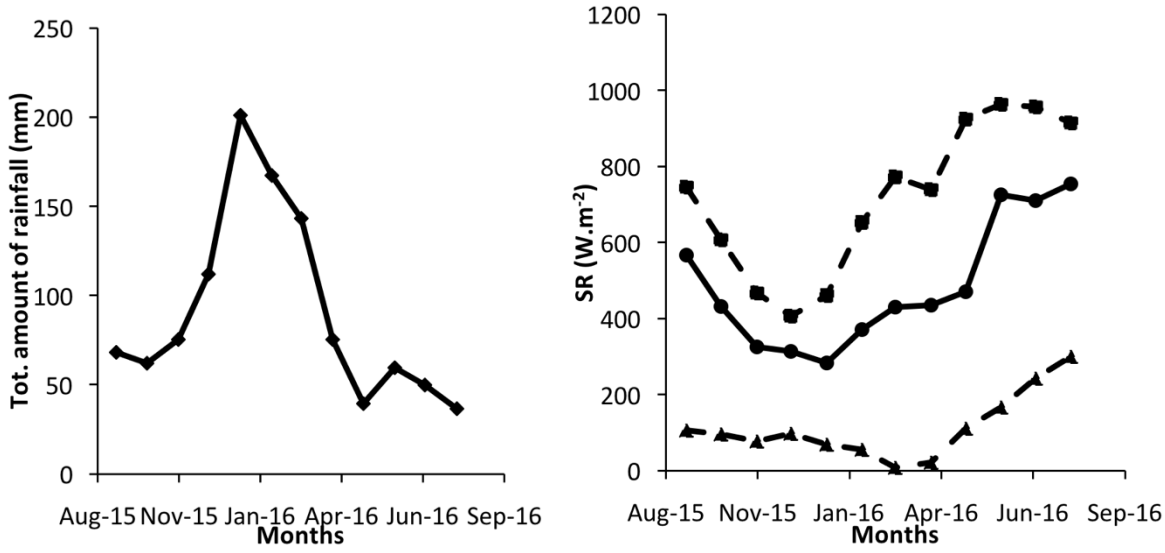

A B

Figure 4 – Total amount of rainfall (A) and mean (round), minimum (triangles) and instantaneous global solar radiation SR values maximum (squares) (B)

I.2.4 Mechanical characterization

Before mechanical test, samples were conditioned for 3 days at 23 ± 2 °C and 50 ± 10% RH. Then, flexural properties characterization was performed by three point bending test carried out in the same hygrothermal conditions on ISO 1A dog-bone samples in accordance to the ISO 178:2010 standard [36]. A Zwick TH 010 press apparatus was used with a 2.5 kN load cell. Elastic modulus E_f calculated between 0.05 and 0.25 % of strain and the stress at the conventional deflection σ_{fc} corresponding to the stress at a strain of 3.5 % were deduced from stress-strain curves. The cross-head speeds were set at 2 and 100 $mm.min^{-1}$ for the modulus and flexural stress at the conventional deflection measurements respectively. Eight samples of each material were tested to evaluate the reproducibility.

I.2.5 Visual aspect characterization

I.2.5.1 Spectrocolorimetry

The surface color analysis was performed with a Chroma Sensor 3 spectrocolorimeter (Datacolor, United States). The configuration illuminant/observer chosen was D65/10°. The CIE 1976 *L*, a*, b** uniform system was used. L*, a* and b* were deduced from the reflectance curves. The L* coordinate represents the lightness whereas a* and b* represent the chromaticity. An increase of L* (from 0 to 100) witnesses a material lightening. a* and b*

are the chromaticity positions on axes from -300 to +300 which are green (-a*) to red (+a*) and blue (-b*) to yellow (+b*) axes respectively. Values were obtained from the analysis of four areas of three samples.

I.2.5.2 Spectrophotogoniometry

The distribution of the intensity of light reflected by a material according to the angle of detection can be related to the surface aspect of a material [37]. Indeed the gloss of a material is more pronounced as the light is reflected directionally. On the contrary, a rough surface induces a diffuse reflection since the reflected light is not concentrated in a narrow bundle (Figure 5). A GON 360 goniometer (Instrument Systems GmbH) coupled to a MAS 40 spectrometer with a halogen lamp and a power supply of 12V was used to collect the radiometric power. The source angle was fixed at 20° according to ISO 2813 standard [38]. Detector angles varied from 5° to -60° with an angular step smaller in the specular zone in order to detect the high variations of intensity in this zone. The spectral range of analysis was 380-780 nm and from every spectrum I=f(λ(nm)) obtained for every detector angle, the total intensity can be represented versus the detector angle: I(u.a.) = f(Θ(°)).

Figure 5 - Diffuse (a) and specular (b) reflections (from ISO 2813)

G_1 corresponding to haze gloss was detemined from the ratio of the maximum intensity obtained for the angle of detection of -20° I(Θ = -20°) to the intensity obtained for the angle of -22° I(Θ = -20 + -2°) both situated in the specular zone was calculated for all samples (Eq. 1). The ratio G_2 of I(Θ = -20°) to the intensity collected for the angle of -35° I(Θ = -20 + -15°) of a diffusely reflected light far away from the specular zone so was also calculated (Eq. 2) and corresponds to contrast gloss. The higher the value of G_1 and G_2 are, the glossier and smoother the surface seems. The gloss was computed for three replicates at four locations on each material.

$$G_1 = \frac{I(\Theta = -20°)}{I(\Theta = -22°)} \quad \text{Eq. 1}$$

$$G_2 = \frac{I(\Theta = -20°)}{I(\Theta = -35°)} \quad \text{Eq. 2}$$

I.2.6 Microstructure characterization

I.2.6.1 Differential scanning calorimetry (DSC)

A PYRIS Diamond calorimeter (Perkin Elmer, United States) was employed for the determination of the polymer crystallinity behavior during the weathering. The measurements were carried out under nitrogen atmosphere at a 20 mL.min^{-1} flow. The temperature ranged from 30 to 210 °C with a heating ramp at 10 °C.min^{-1}. Two heating steps with an intermediate cooling step at -10 °C.min^{-1} were performed. Fragments of almost 10 mg sampled at the materials surface were placed into standard aluminium pans. Two replicate samples per material were analyzed. The crystallinity ratio was calculated according to the following equation taking into account the melting enthalpy:

$$\chi_{c1}\,(\%) = \frac{\Delta H_{m1}}{W \times \Delta H_{m_{100}}} \times 100 \quad \text{Eq. 3}$$

$$\chi_{c2}\,(\%) = \frac{\Delta H_{m2}}{W \times \Delta H_{m_{100}}} \times 100 \quad \text{Eq. 4}$$

where W is the PP mass fraction, ΔHm_1 and ΔHm_2 (J.g^{-1}) are the melting enthalpy determined from the 1st and 2nd heating steps respectively and ΔHm_{100} corresponds to the estimated melting enthalpy of a fully crystalline PP (209 J.g^{-1}) [39,40].

I.2.7 Chemical composition characterization

I.2.7.1 Fourier Transform InfraRed spectroscopy (FTIR)

A IFS66 spectrometer (Bruker, United States) operating in the Attenuated Total Reflectance (ATR) mode was used to follow the functional groups specific to the polymer and biocomposites degradation. The device was equipped with a single reflection diamond crystal accessory. Thin slices of exposed surfaces were analyzed and the spectra were

recorded as a result of the average of 32 scans in the 400 to 4000 cm^{-1} spectral range with a resolution of 1 cm^{-1}. Infrared spectra were normalized according to the Min-Max normalization method with the 2925 cm^{-1} reference band assigned to the CH_2 methylene groups.

I.2.8 Surface characterization

I.2.8.1 Confocal rugosimetric measurement

A MICROMESURE STIL system equipped with a STIL CHR150 optical sensor (STIL, France) was used to evaluate the roughness by altitude measurement of each surface point on the sample without contact with the sample according to the ISO 25178 international standard. More details are given in a previous paper [12]. A bidimensional scanning allows obtaining the image of the sample surface located at a precise distance from the STIL optical sensor. Acquisition software SurfaceMap® allowed the control of the station and the post-treatment MountainsMap® software was used to analyze the surface geometry and to calculate roughness parameters. The micrometric range of the optical pen was 285 µm. It permits a tridimensional analysis and the analyzed area X*Y was 5 mm * 5 mm with an analysis step of 10 µm in X and Y directions. The tridimensional roughness parameter Sa followed during the weathering corresponds to the arithmetic mean of the absolute of the height values (Eq. 4):

$$\mathrm{Sa} = \frac{1}{NM}\sum_{x=0}^{N-1}\sum_{y=0}^{M-1}|z(x,y)| \qquad \text{Eq. 5}$$

with M the number of points along the X axis, N the number of points along the Y axis, and $z_{x,y}$ the altitude in µm. Mean values and standard deviations were obtained from the analysis of four areas of three samples.

I.3. Results and Discussion

I.3.1 Mechanical performance

Stress-strain curves of PP, PP10 and PP30 are plotted in Figure 6 before and after exterior and under glass one-year weathering. At non-weathered state, the stress increased with the fiber loading for a same strain value. However, PP and PP10 presented a continuous increase of stress until 5% of deformation whereas the flexural strain at break of PP30 almost

equalled to 3.5%. This early break is explained by the stiffness provided by the vegetal fibers. A similar behavior was observed after weathering except for virgin PP that broke after 12 months of exterior weathering at lower stress (46 MPa) than exterior weathered PP30 (71 MPa). This rupture suggests that the strength of neat PP was mostly affected by the exterior weathering than by under glass exposition. However, although the one-year exposition overthrew the flexural properties of biocomposites, the type of weathering had no significant influence on their mechanical behavior.

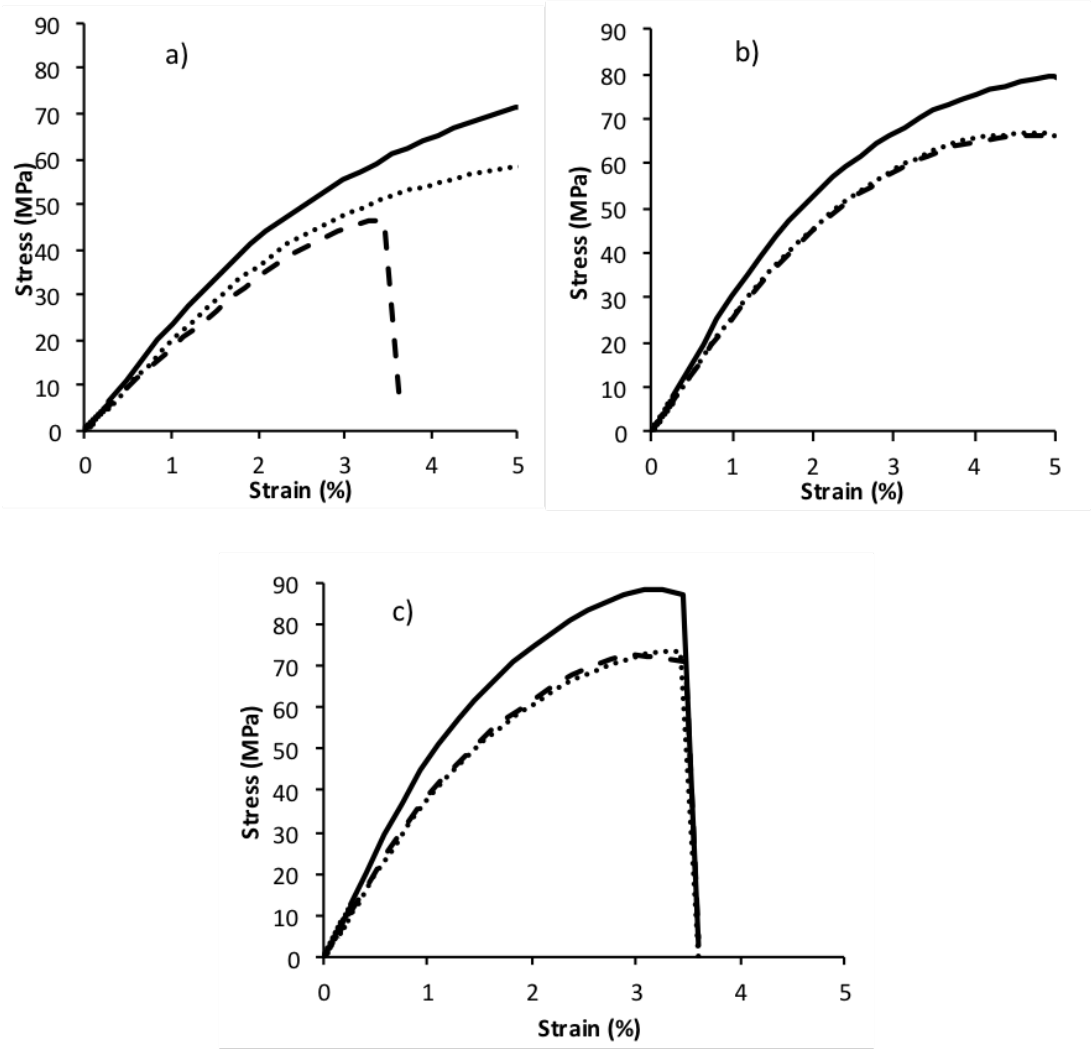

Figure 6 - Stress-strain curves of PP (a), PP10 (b) and PP30 (c) before (full line) and after one-year exterior (dashed line) and one-year under windshield glass (dotted line) weathering

The elastic modulus E_f and the stress at the conventional deflection σ_{fc} have also been recorded during the ageing and their evolution is represented in Figure 7.

At non-weathered state, E_f increased from 19 ±0.15 to 47 ±0.5 GPa with the fiber loading. Moreover, the modulus value of biocomposites was higher than virgin PP whatever the weathering state. Thus, the material stiffening effect of the fibers was maintained over the exposition. However, higher significant variations all along the ageing were noted for the highest loading with a first moderate increase during the first 2 months of 1% and 5% for PP30-EW and PP30-GW respectively. Therefore, this trend was more pronounced under windshield glass. This increase was followed by a decrease until 12 months which was barely more significant after exterior exposition of PP30, and seems thus to be more harmful than under glass weathering.

The conventional deflection flexural stress σ_{fc} showed an equivalent increasing trend with the fiber rate, meaning that the fibers have a reinforcement effect. However, σ_{fc} decreased with the time of exposition whatever the material due to the degradation of both polymer and hemp fibers. As well as for E_f, σ_{fc} of PP30 underwent a higher drop during the first 9 months than PP and PP10 confirming that the presence of vegetal fibers weakened the mechanical stability. However, PP showed a drastic decrease of σ_{fc} after 12 months of exterior weathering. Indeed, it decreased by 18% whereas it came down by 4% for PP30 in the last 3 months of exterior exposition. This was certainly due to the rainfall or the exposition to long and short waves UV-A, B or C rays that were filtered by laminated windshield glasses at about 98% [41]. Nevertheless, in view of climatic conditions observed between June and August 2016 corresponding to the 10^{th} and 12^{th} months of ageing, it can be assumed that the photo-oxidation of the polymer could mainly be responsible to this embrittlement at the end of the year (Figure 4). Indeed, this three-month period particularly suffered from the solar radiation reaching an average solar radiation of almost 760 $W.m^{-2}$ for the last month. Finally, PP10-EW and PP10-GW evolutions presented less significant difference and variations than PP and PP30.

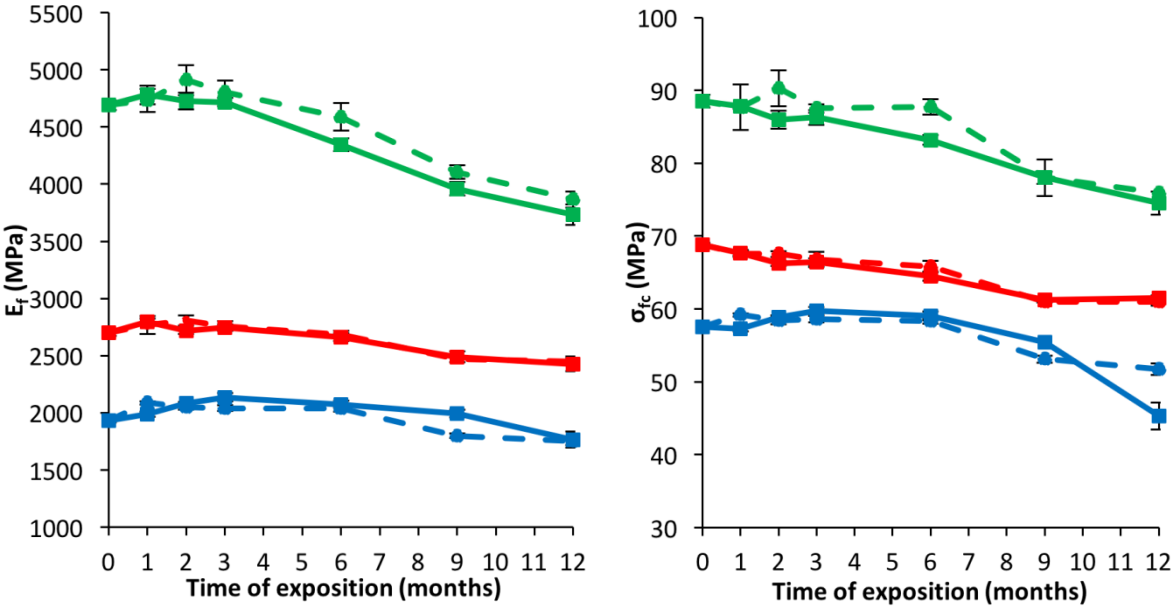

Figure 1 – Evolution of the elastic modulus E_f (a) and the stress at the conventional deflection σ_{fc} (b) during one-year exposition (blue: PP, red: PP10, PP30: green, full line: exterior weathering, dashed line: under glass weathering)

I.3.2 Microstructure

Since the elastic modulus evolution can be related to the crystallization behaviour of the polymer, the crystallinity degree was determined from the first and the second heating ramps (Figure 8).

Globally, crystallinity percentages of materials are lower for the first heating step than the second one. Moreover, at non-weathered state, PP30 exhibited 2% and 4% higher χ_{c1} and χ_{c2} crystallinity rates respectively than virgin PP. A same increase with the fiber content of the crystallinity percentage of polymer matrices deduced from the first [3,42] and the second heating ramp [43,44] was observed at initial state. This implies that lignocellulosic compounds played the role of nucleating agents favouring the crystallization of the polymer [44,45].

Otherwise, the evolution of the crystallinity rate over the weathering firstly shows that the exposition did not have considerable influence on PP and PP10. However, PP30 underwent higher variations with a slight increase until 2 months and a decrease during 10 months. Indeed, this first increase is more important for the highest fiber reinforced composite suggesting that the nucleation effect of the fibers improved the crystallinty rate [24].

Moreover, the increase was more pronounced under windshield glass where temperatures almost reached 90 °C. As regards under glass weathered PP30, the values increased by 11% for χ_{c1} against 9% for χ_{c2}. So a same trend as Young's modulus evolution was registered and is ascribed to the polymer chemicrystallization in the amorphous phase favored under high temperatures due to the reduction of the macromolecular chains length inducing their higher mobility [46]. However, the exterior exposition generally induced a higher drop of χ_c than under glass one, especially for χ_{c2} during the 10 last months of ageing. Indeed, χ_{c1} and χ_{c2} of PP30-EW decreased by 20% and 23% whereas it declined by 3 and 6% for PP30-GW. Otherwise, no significant difference was noted between χ_{c1} and χ_{c2} evolution tendencies.

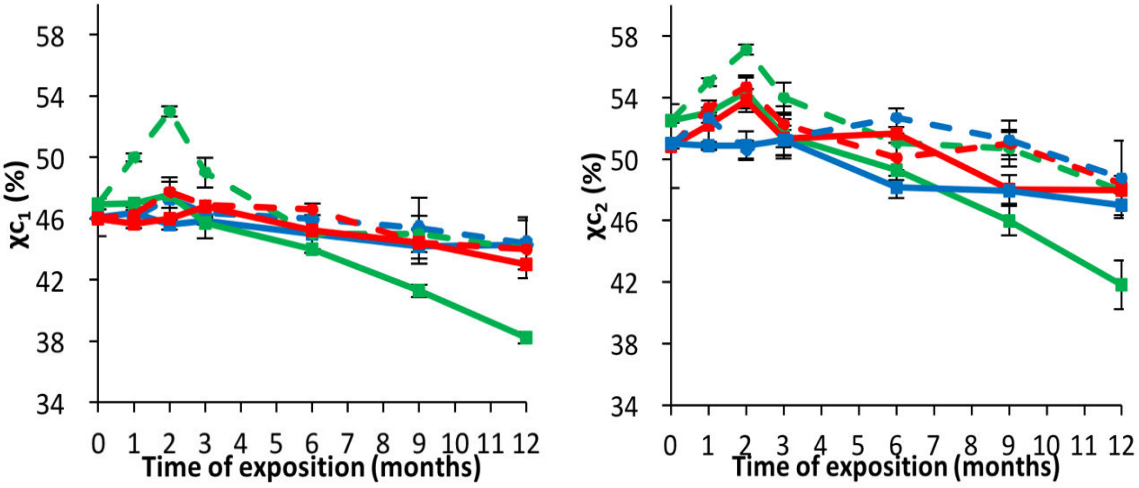

Figure 8 - Evolution of the crystalinity rate (χ_{c1} from the first heating run and χ_{c2} from the second one) during one-year exposition (blue: PP, red: PP10, PP30: green, full line: exterior weathering, dashed line: under glass weathering)

I.3.3 Chemical structure

The evolution of the infrared peaks of carbonyl groups such as γ-lactones (1780 cm^{-1}), esters and aliphatic aldehydes (1740 cm^{-1}), carboxylic acids and ketones (1711 cm^{-1}) specific to oxidative degradation and ethenyl functional groups (1650 cm^{-1}) for polymer and fibers chain scissions are depicted in Figure 9 before and after one-year exposition [9,40,47]. The spectra were zoomed in the wavenumber range of interest 1490-1820 cm^{-1}. Before weathering, the increase of the intensity of absorption bands assigned to C=O and C=C bonds vibration with the fiber loading was due to the presence of carbonyl and carbon double bonds naturally present in holocellulose and lignin [48,49].

During the weathering, the continuous linear increase of the intensity of carboxylic acids and esters absorbance on the PP spectrum with the weathering time mainly indicates a photo and thermo-oxidative degradation of the polymer under UV rays and high temperatures (Figure 10) involving reaction with oxygen from the atmosphere. As regards γ-lactones, the absorbance did not vary a lot during the first 6 months. Then it suddenly rose from 0.02 to 0.16 in 6 months. The carbonyls absorbance increase was more drastic for biocomposites which suggests that hemp fibers also underwent photo and thermo-oxidation. The proportion of vegetal fibers at the surface exceeding the PP proportion over the ageing due to a polymer decomposition could also contribute to this increase. Among all the carbonyl containing derivatives, ketones and carboxylic acids were preferentially formed during the weathering contrary to non-weathered state. It is supposed that the hydrolysis of esters products occurred leading to the formation of carboxylic acids. Moreover, this characterization allowed to highlight that, contrary to carbonyl concentration presenting a similar evolution under the two types of weathering, the exterior ageing promoted a greater generation of carbon double bonds than under glass one. This trend was more pronounced for weathered PP10 and PP30 implying that the vegetal fibers contributed to the C=C bonds formation. The rising protrusion of fibers on surface, including lignin containing aromatic ring-based structure, may involve the C=C stretching detection [3]. Also, their increasing formation during the first 6 months might be favored by hydrolytic effect of heavy rainfall increasing during this period (Figure 4) leading to chain scissions along the early exposition. Otherwise, the evolution of vinyl tended to stabilize after 6 months whatever the weathering conditions, especially for biocomposites. Also, a conversion of C=C towards C=O groups via Norrish type II reaction may explain this formed plateau [10]. Moreover, the increasing temperature and solar radiation observed during this stage could encourage their conversion.

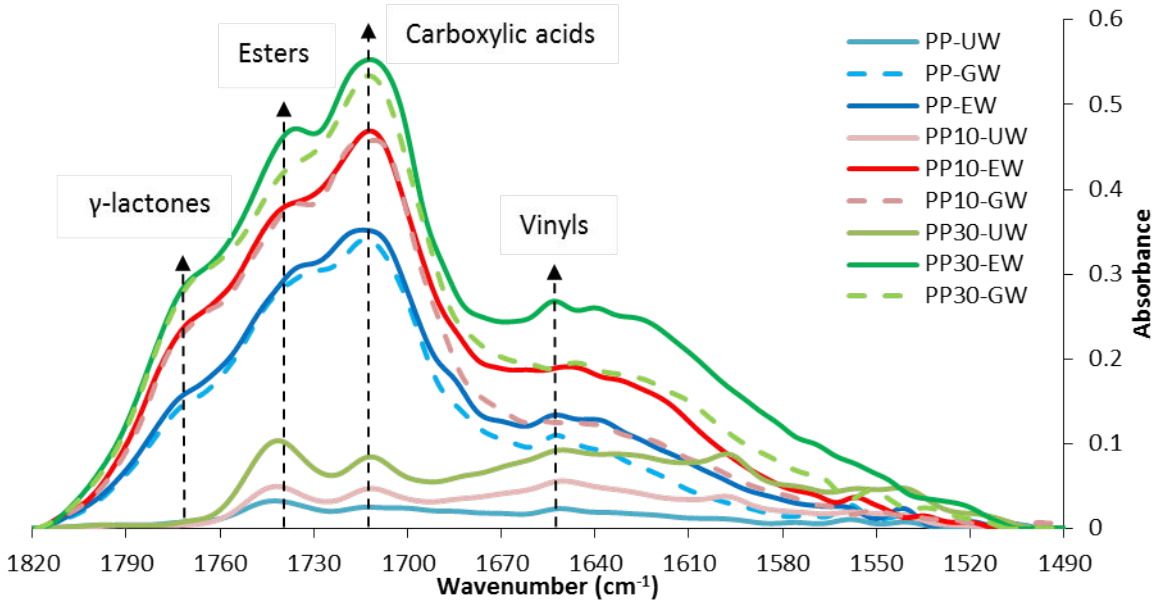

Figure 9 - Infrared spectra of unweathered and one-year weathered PP, PP10 and PP30 in 1490-1820 cm^{-1} region

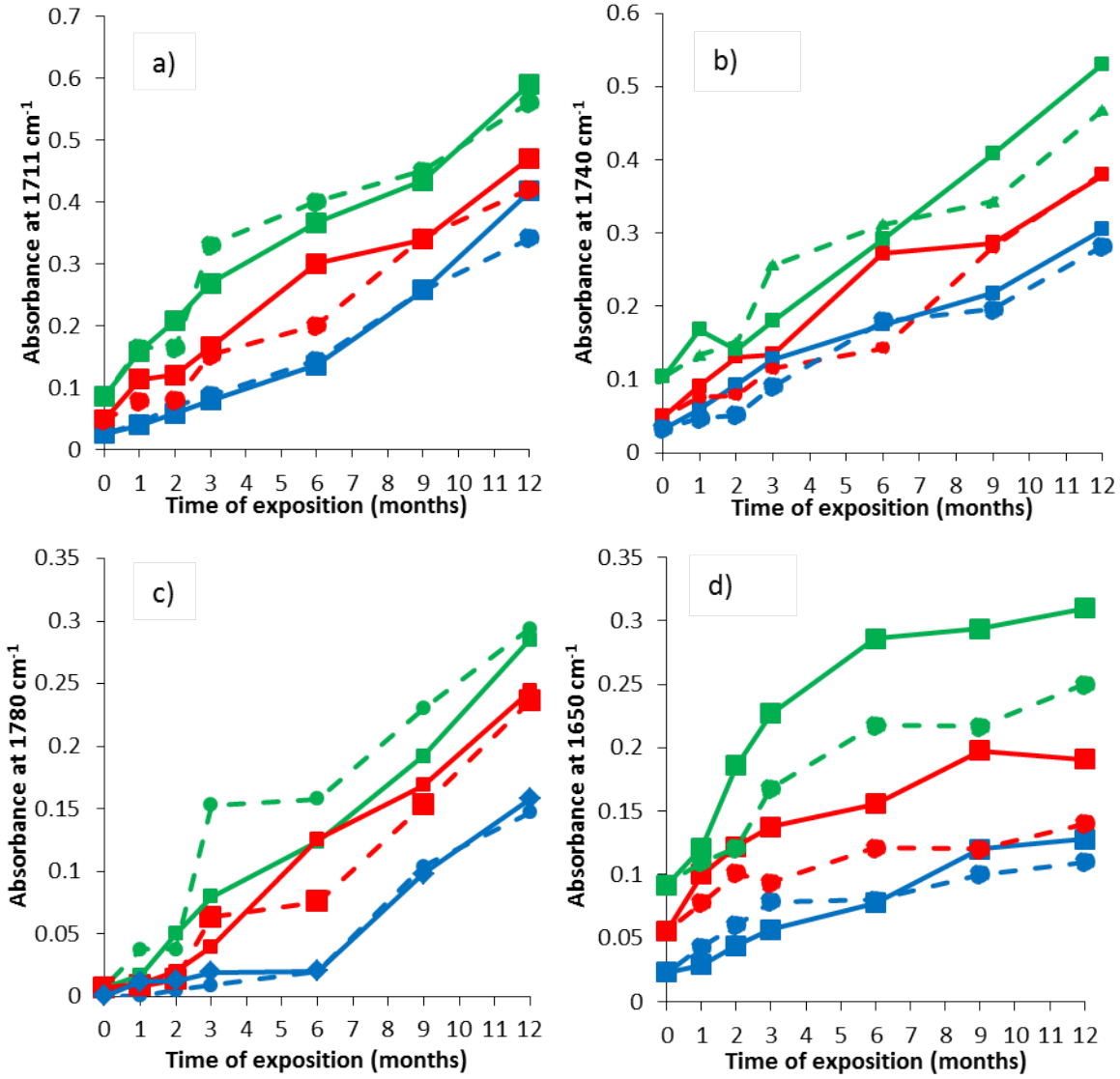

Figure 10 - Absorbance values of C=O (at 1711 cm^{-1} (a), 1740 cm^{-1} (b), 1780 cm^{-1} (c)) and C=C (1650 cm^{-1} (d)) versus the weathering time (blue: PP, red: PP10, PP30: green, full line: exterior weathering, dashed line: under glass weathering)

I.3.4 Visual aspect

I.3.4.1 Color

Contrary to virgin PP, the weathering had a great impact on biocomposites lightness evolution (Figure 11). Indeed, the lightness of PP30 varied in a wide range of L* values in the first months, especially by exterior weathering since its bleaching kinetic was higher than by under windshield glass one. The degradation of lignin is responsible to this bleaching and is explained by the reduction mechanism of paraquinone to hydroquinone molecules due to UV radiation [3]. Then, L* remained constant until 12 months. Indeed, PP30 reached a L*

coordinate maximum at approximately 75 after 3 months of exterior weathering and 6 months of under glass weathering. This lightness saturation is in agreement with previous color studies of natural fibers reinforced plastic composites [8,22,50,51]. Here, it is assumed to be due to the increasing proportion of holocellulose at the analyzed surface which is completely uncovered after the second half of the year.

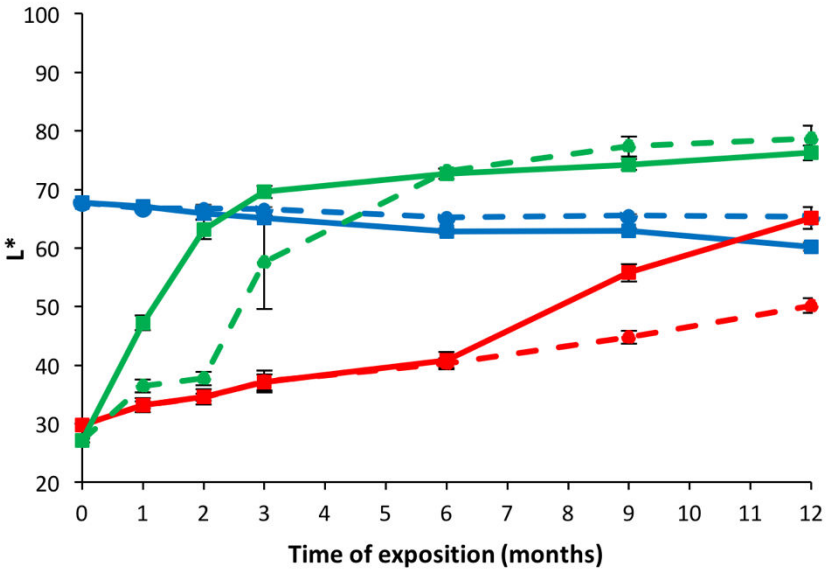

Figure 11 - L* coordinate evolution over the weathering (blue: PP, red: PP10, PP30: green, full line: exterior weathering, dashed line: under glass weathering)

The color was monitored during the two types of weathering and the coordinates a* and b* are represented in the chromatic plane in the Figure 12 for each material at each weathering state. Firstly, this graph clearly shows that three main groups can be formed according to the fiber loading.

Secondly, biocomposites experienced higher variations in color than PP, in particular by yellowing. Moreover, under glass weathering implied a higher yellowing kinetic than exterior exposition. For instance, b* of PP30-GW increased by 10 units whereas it only increased by 1 unit after one-year of exposition. This was certainly due to the higher temperatures. As well as for the bleaching, this yellowing was due to the decomposition of the lignin structure present in hemp fibers into paraquinones whose characteristic color is yellow. Thus, the temperature may favor the formation of paraquinones, which will be consequently favored during under glass ageing and the redox cycle previously mentioned might be shifted towards the oxidation of hydroquinones to paraquinones. However, as mentioned in the

introductory part, holocellulose at high content in long-time retted hemp fibers, could undergo yellowing due to its oxidation. Indeed, hemicelluloses, well-known as thermally sensitive substances, may preferentially oxidize and thus yellow faster under high temperature than UV radiation. As regards a* evolution, its decrease witnessed a loss of red color of biocomposites due to orthoquinones or phenolic extractives degradation [52]. Otherwise, PP10 was particularly subjected to the red color loss after 9 and 12 months of exterior ageing, stage during which temperatures and UV radiation were the highest. So an exterior weathering promoted a* decrease whereas under glass exposure promoted the b* increase. This observation leads to presume that chromophoric yellowing structures are sensitive to high temperatures whereas UV rays and water absorption could induce reddish quinones and extractives decomposition.

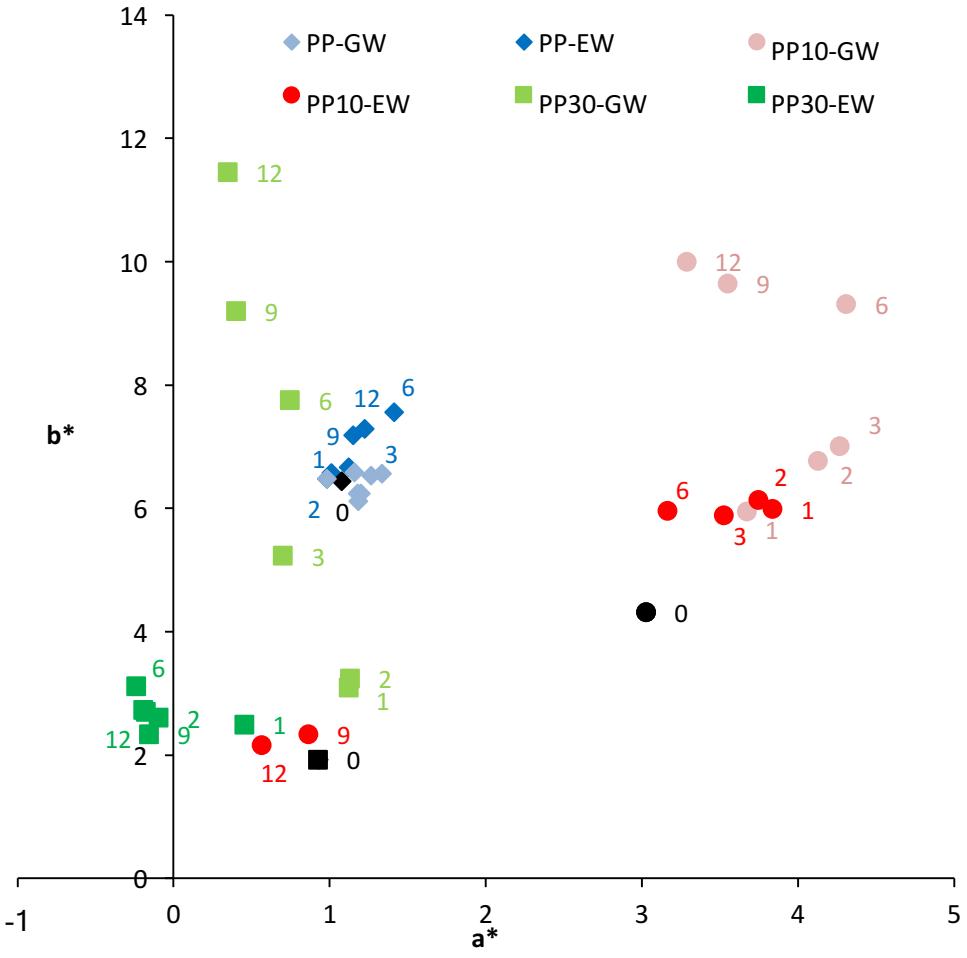

Figure 12 - a* and b* chromatic coordinates evolution over the weathering of PP (diamonds), PP10 (spheres) and PP30 (squares) (the numbers corresponding to the time of exposition (months))

I.3.4.2 Gloss

The intensity of the light reflected by non-weathered and one-year weathered materials is represented as a function of the angle of detection in Figure 13. Focusing on the non-weathering state, the maximum intensity of the specular peak decreased with the hemp fibers rate. This means that gloss diminished with the fiber loading because of the presence of hemp fibers at the surface leading to a less smooth surface [12]. Otherwise, the peak decreased by 5 times between PP10 and PP30. Moreover, the specular peak of the highest fiber loaded composite is extended on a wider range of detection angles than PP and PP30 and demonstrates a more diffuse reflection of the light induced by the presence of the fibers.

As regards PP, PP10 and PP30 weathered samples, the specular peak becomes wider and extended on several angles. PP underwent a great relative decrease of gloss after exterior weathering, the maximum intensity decreasing by almost 5 times. The specular peak of exterior and under glass weathered PP30 was hardly visible. It firstly suggests that the exposition induced a loss of matter at the surface impacting on the brightness. The next part will permit to analyze the surface aspect. Also, it can be assumed that hemp fibers were partly responsible of the surface aspect alteration. The asymmetric repartition of the light intensity according to -20 ° can be explained by the non-flat surface of biocomposites.

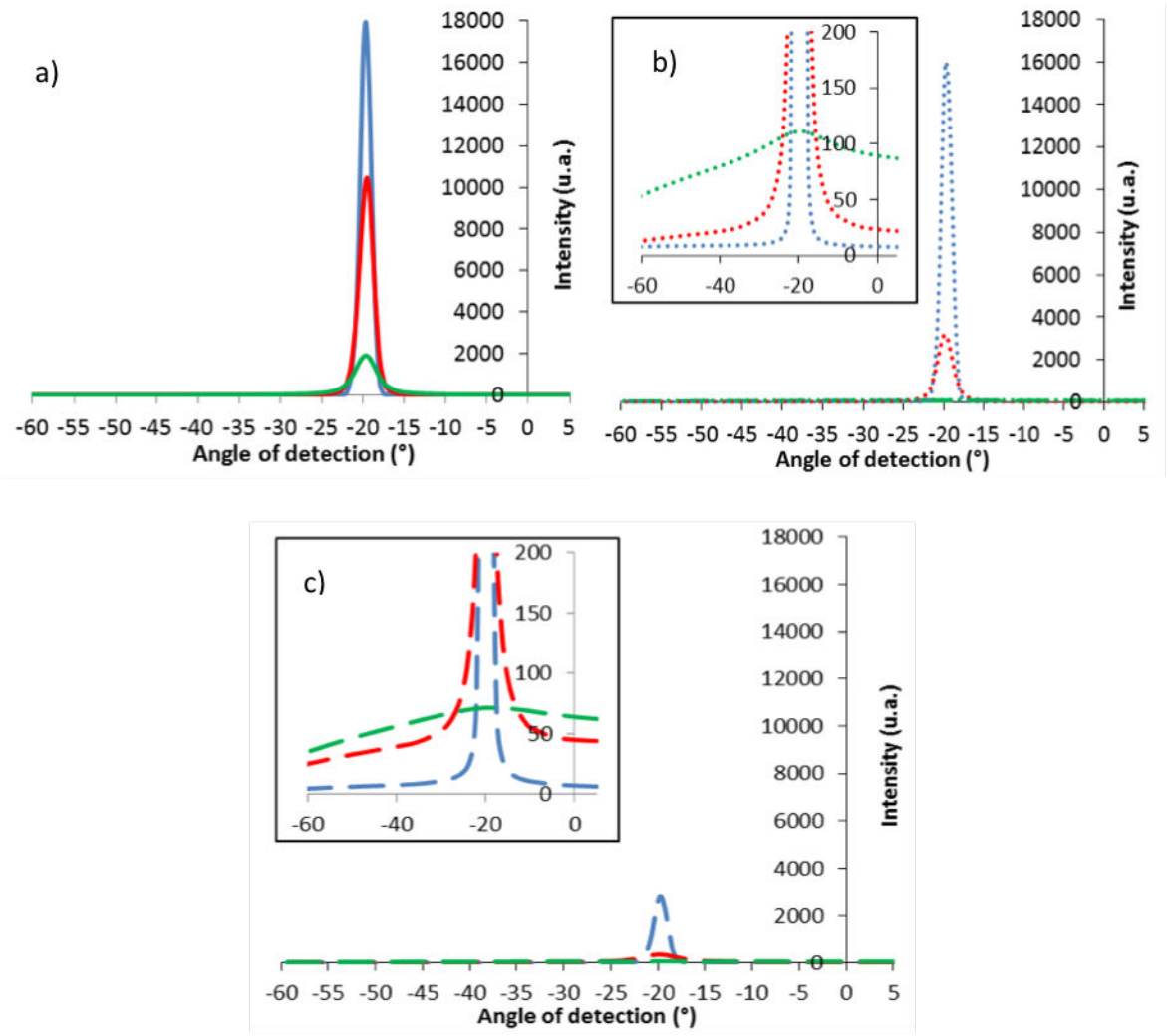

Figure 13 – Angular repartition of the light reflected by non-weathered (a), one-year under glass weathered (b) and one-year exterior weathered (c) PP (blue), PP10 (red) and PP30 (green)

The variations of G_1 and G_2 values are displayed in Figure 14 for all materials. The influence of the type of weathering was mainly observed for neat PP all along the ageing whose the gloss mostly suffered from the exterior parameters such as UV rays or rainfall than extreme temperatures. The loss of gloss of neat PP-EW could originate from the dust and other impurities deposits and the formation of microcracks issued from the degradation of the polymer. As regards biocomposites, the degradation of both hemp fibers and the polymer matrix at the surface induced a drop of both G_1 and G_2. Gloss values of PP30-EW and PP30-GW tended towards a G_1 and G_2 minimum ratio of 1 at an early stage of the weathering demonstrating the severe impact on the biocomposite gloss. Otherwise, G_1 of non-weathered PP10 equivalent to 44 was close to PP30 one equaling 12 unlike the G_2 ratio value decreasing from 2418 for PP10 to 30 for PP30. This means that its specular peak shape is

close to PP30. Otherwise, the non-flat surface could be responsible to the high standard deviations.

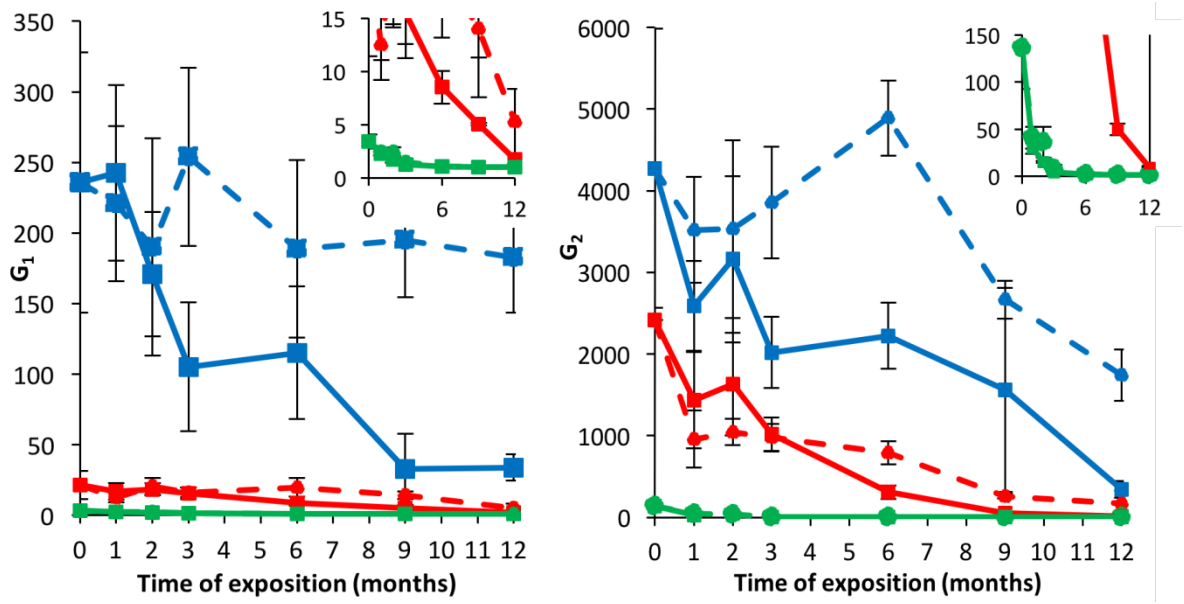

Figure 14 – Variations of G_1 and G_2 parameters during the weathering (blue: PP, red: PP10, PP30: green, full line: exterior weathering, dashed line: under glass weathering)

I.3.5 Topography

I.3.5.1 Roughness

Since the gloss is related to the surface aspect, the roughness has been qualitatively and quantitatively assessed to understand the gloss variations. The surface images are gathered in Table 4. Altitudes variations are represented by false colors. It is worth noting that the difference in color between images is not to be taken into account. Before weathering, materials exhibited a relative smooth surface. Then, regular microcracks were distinguished at the surface of exterior weathered neat PP. Otherwise, these microcracks followed the same direction as the injected matter flow one during molding processing whatever the specimen of virgin PP-EW meaning that the process step had an influence. The polymer matrix was probably weakened by macromolecular chain scissions [53] and these microcracks could contribute to the embrittlement of PP. PP10-EW presented both microcraks and some hollows probably issued from the removal of vegetal fibers due to exterior factors whereas the topography of PP10-GW was not significantly influenced by the

ageing. Weathered PP30 surface presented more and deeper slots than other materials. So the presence of fibers damaged the surface of the reinforced material.

Table 4 – Altitude images of surfaces of non-weathered and one-year weathered PP, PP10 and PP30

	PP	PP10	PP30
UW	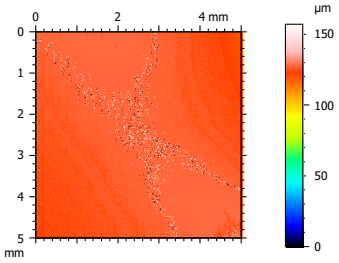	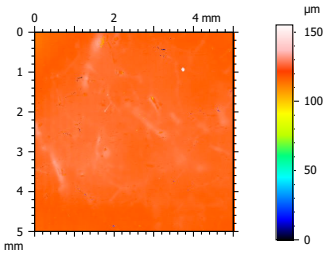	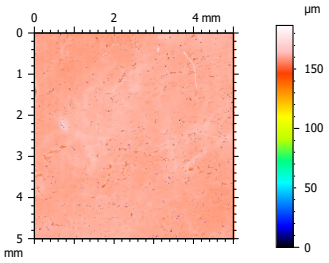
EW	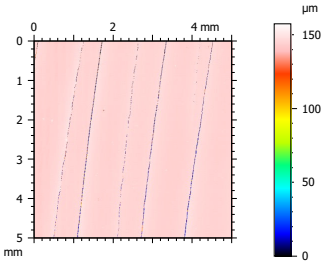	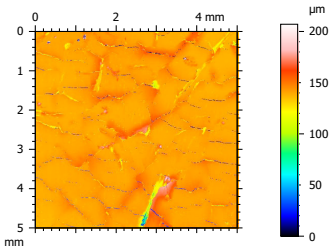	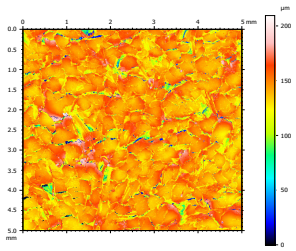
GW	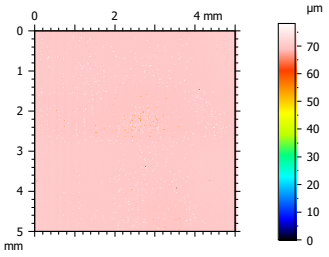	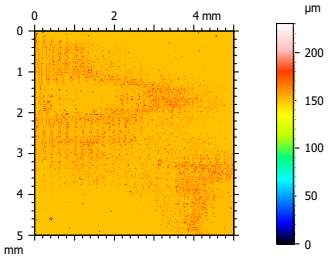	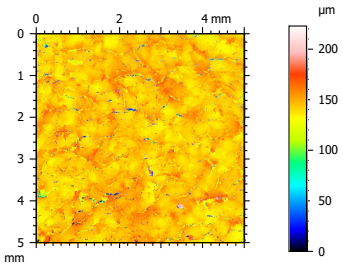

The changes in average roughness parameter Sa are shown in Figure 15. Before ageing, Sa increased from 0.45 ±0.33 µm for PP to 1.89 ±0.54 µm for PP30 since the presence of vegetal fibers at the biocomposites surface led to a less smooth surface [12]. This observation corroborates with the gloss measurement. After the exposition, any significative variation of Sa was observed for PP during 9 months. Then the roughness parameter of exterior weathered PP increased from 0.31 ±0.14 µm to 1.98 ±0.22 µm in 3 months whereas it remained at the same roughness level under windshield glass. This may be explained by the increasing solar radiation during this period responsible to photo-oxidation inducing polymer chain scission and create thereby surface cracks [9]. Also, this trend is in agreement with the

evolution of the stress at the conventional deflection and the appearance of this cracks on surface may brittle the mechanical resistance. Nevertheless, the formation of these microcracks was expected to occur on surfaces of under glasses weathered samples for which the crystallinity rate mostly increased at the beginning of exposition due to chain scission. But these microcracks were only distinguished for exterior weathered samples. This could be linked to rainfall and UV rays synergetic effect accelerating the degradation of the polymer after the first two-month short period favoring microcracks for outdoor exposed materials. Sa values of biocomposites exhibited a cubic continuous growth. This increase was due to the degradation of the polymer matrix and fibers inducing an appearance of fibers on the surface. Also, a water uptake could provoke fiber-matrix debonding despite of the presence of coupling agent. Contrary to other studied properties, PP10-EW and PP10-GW did not exhibit similar evolutions. Indeed Sa of the intermediate loading biocomposite that was exteriorly weathered increased faster from Februray to August 2016.

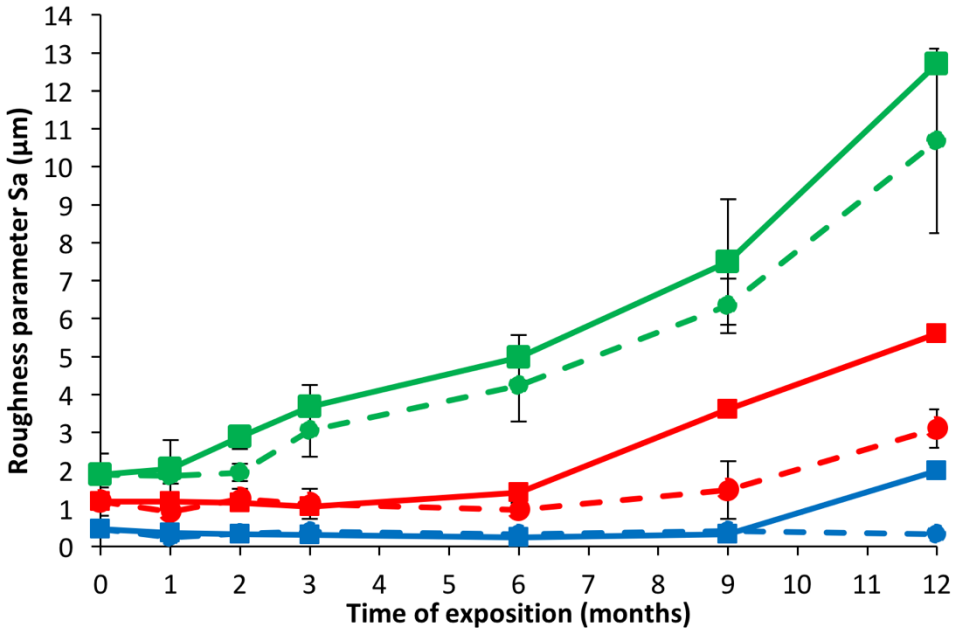

Figure 15 - Sa roughness parameter evolution over the exposition (blue: PP, red: PP10, PP30: green, full line: exterior weathering, dashed line: under glass weathering)

I.4. Conclusion

The objective of this work was to understand the influence of the type of weathering (exterior versus under glass weathering) on PP and PP/hemp fibers biocomposites (10 and

30wt%) properties such as mechanical, chemical, microstructural and visual aspect properties.

Even if flexural mechanical properties (modulus and stress at the conventional deflection) are improved thanks to vegetal fiber reinforcement as already shown in literature, the biocomposites modulus seems to be less stable over the weathering whatever the kind of exposition. Similarly, under glass ageing (GW) induced stronger changes of conventional deflection stress of PP30 than PP one. Also, the exterior ageing (EW) more affected the strength of biocomposites during the first 9 months. Then, the stress at the conventional deflection of exterior aged PP drastically decreased by 18% whereas it slightly decreased for exterior aged PP30 after 12 months. Hence, PP was certainly highly sensitive to high UV light intensity at this stage of exposition highly deteriorating the synthetic polymer.

Physical properties were mostly affected for biocomposites than PP because of their sensitivity face to climatic conditions. However, even if they bleached at the same level under the two expositions, some differences in color instability, especially by yellowing during GW and red color loss during EW, was observed for weathered biocomposites. This was explained by the possible different sensitivities of the hemp fibers components under the different factors.

As regards chemical and microstructural properties, even if all materials underwent oxidation, a higher kinetic of chemical structure degradation was recorded for PP30 suggesting that either carbonyl-containing lignocellulosic compounds appeared at the surface or hemp fibers oxidized faster. Otherwise, the exterior weathering more favored the formation of carbon double bonds and the decrease of the crystallinity rate either caused by solar radiation, rainfall or their synergetic effect.

Also, it highly altered the surface aspect (gloss, roughness) at different degradation kinetics according to the fiber content. The assessment of G_1 and G_2 parameters allowed to understand the contribution of the presence of hemp fibers to the reflection in the specular or diffuse zones. The carbonyl absorbance increasing during the ageing was not influenced by the type of weathering conditions. Otherwise, analyses showed that either under windshield glass or exterior weathering had the highest impact according to the property. All these properties will be faced together to bring out relationships.

In summary, according to the property, either under glass or outdoor ageing induced the highest variations. Also, visual appearance and chemical stability of biocomposites were more affected. Thus, UV stabilizers or pigments should be incorporated during the process to limit the variations and allow their use in decking or automobile structures. Nonetheless, in view of the properties changes over the exposition, PP10 material raised as a good compromise between mechanical performance and visuals aspect changes. Indeed, its mechanical performance was enhanced compared to neat PP. Moreover, this material underwent lower drastic variations (in particular by bleaching and yellowing) than those observed for PP30.

I.5. Acknowledgements

This research did not receive any specific grant from funding agencies in the public, commercial, or not-for-profit sectors.

I.6. References

[1] G. Marsh, Next step for automotive materials, Mater. Today. 6 (2003) 36–43. doi:10.1016/S1369-7021(03)00429-2.

[2] X. Zhou, S. Huang, L. Chen, Effect of antiaging agents on the outdoor natural weathering of bamboo powder/polypropylene foamed composites, J. Vinyl Addit. Technol. 22 (2014) 311–319. doi:10.1002/vnl.21433.

[3] L. Soccalingame, D. Perrin, J.-C. Bénézet, A. Bergeret, Reprocessing of UV-weathered wood flour reinforced polypropylene composites: Study of a natural outdoor exposure, Polym. Degrad. Stab. 133 (2016) 389–398. doi:10.1016/j.polymdegradstab.2016.09.011.

[4] N. Le Moigne, M. Longerey, J.-M. Taulemesse, J.-C. Bénézet, A. Bergeret, Study of the interface in natural fibres reinforced poly(lactic acid) biocomposites modified by optimized organosilane treatments, Ind. Crops Prod. 52 (2014) 481–494. doi:10.1016/j.indcrop.2013.11.022.

[5] Platts petrochemical Analytics, Report: Global polyolefins outlook: 2014-2025, 2016. www.platts.com/ppa (accessed June 16, 2017).

[6] L. Belec, T.H. Nguyen, D.L. Nguyen, J.F. Chailan, Comparative effects of humid tropical weathering and artificial ageing on a model composite properties from nano- to macro-scale, Compos. Part A Appl. Sci. Manuf. 68 (2015) 235–241. doi:10.1016/j.compositesa.2014.09.028.

[7] M.Z. Ahmad Thirmizir, Z.A. Mohd Ishak, R. Mat Taib, S. Rahim, S. Mohamad Jani,

Natural Weathering of Kenaf Bast Fibre-Filled Poly(Butylene Succinate) Composites: Effect of Fibre Loading and Compatibiliser Addition, J. Polym. Environ. 19 (2010) 263–273. doi:10.1007/s10924-010-0272-2.

[8] S. Butylina, M. Hyvärinen, T. Kärki, A study of surface changes of wood-polypropylene composites as the result of exterior weathering, Polym. Degrad. Stab. 97 (2012) 337–345. doi:10.1016/j.polymdegradstab.2011.12.014.

[9] J.S. Fabiyi, A.G. McDonald, M.P. Wolcott, P.R. Griffiths, Wood plastic composites weathering: Visual appearance and chemical changes, Polym. Degrad. Stab. 93 (2008) 1405–1414. doi:10.1016/j.polymdegradstab.2008.05.024.

[10] N.M. Stark, L.M. Matuana, Surface chemistry changes of weathered HDPE/wood-flour composites studied by XPS and FTIR spectroscopy, Polym. Degrad. Stab. 86 (2004) 1–9. doi:10.1016/j.polymdegradstab.2003.11.002.

[11] M.D.H. Beg, K.L. Pickering, Accelerated weathering of unbleached and bleached Kraft wood fibre reinforced polypropylene composites, Polym. Degrad. Stab. 93 (2008) 1939–1946. doi:10.1016/j.polymdegradstab.2008.06.012.

[12] C. Badji, L. Soccalingame, H. Garay, A. Bergeret, J.-C. Bénézet, Influence of weathering on visual and surface aspect of wood plastic composites: Correlation approach with mechanical properties and microstructure, Polym. Degrad. Stab. 137 (2017) 162–172. doi:10.1016/j.polymdegradstab.2017.01.010.

[13] M.I. Popa, S. Pernevan, C. Sirghie, I. Spiridon, D. Chambre, D.M. Copolovici, N. Popa, Mechanical Properties and Weathering Behavior of Polypropylene-Hemp Shives Composites, J. Chem. 2013 (2013) 1–8. doi:10.1155/2013/343068.

[14] M. Muasher, M. Sain, The efficacy of photostabilizers on the color change of wood filled plastic composites, Polym. Degrad. Stab. 91 (2006) 1156–1165. doi:10.1016/j.polymdegradstab.2005.06.024.

[15] A. Bergeret, J. Benezet, T.P.T. Tran, G.C. Papanicolaou, A. Koutsomitopoulou, Valorization of agricultural by-products in poly (lactic acid) to develop biocomposites, in: V.K. Thakur (Ed.), Green Compos. from Nat. Resour., CRC Press, Taylor & Francis LLC, 2013. doi:10.13140/2.1.1271.2969.

[16] M.S. Islam, K.L. Pickering, N.J. Foreman, Influence of accelerated ageing on the physico-mechanical properties of alkali-treated industrial hemp fibre reinforced poly(lactic acid) (PLA) composites, Polym. Degrad. Stab. 95 (2010) 59–65. doi:10.1016/j.polymdegradstab.2009.10.010.

[17] M.M. Thwe, K. Liao, Durability of bamboo-glass fiber reinforced polymer matrix hybrid composites, Compos. Sci. Technol. 63 (2003) 375–387. doi:10.1016/S0266-3538(02)00225-7.

[18] O. Gil-Castell, J.D. Badia, T. Kittikorn, E. Strömberg, A. Martínez-Felipe, M. Ek, S. Karlsson, A. Ribes-Greus, Hydrothermal ageing of polylactide/sisal biocomposites. Studies of water absorption behaviour and Physico-Chemical performance, Polym.

Degrad. Stab. 108 (2014) 212–222. doi:10.1016/j.polymdegradstab.2014.06.010.

[19] A. Le Duigou, P. Davies, C. Baley, Seawater ageing of flax/poly(lactic acid) biocomposites, Polym. Degrad. Stab. 94 (2009) 1151–1162. doi:10.1016/j.polymdegradstab.2009.03.025.

[20] A. Arbelaiz, B. Fernández, J.A. Ramos, A. Retegi, R. Llano-Ponte, I. Mondragon, Mechanical properties of short flax fibre bundle/polypropylene composites: Influence of matrix/fibre modification, fibre content, water uptake and recycling, Compos. Sci. Technol. 65 (2005) 1582–1592. doi:10.1016/j.compscitech.2005.01.008.

[21] D.R. Bauer, Interpreting weathering acceleration factors for automotive coatings using exposure models, Polym. Degrad. Stab. 69 (2000) 307–316. doi:10.1016/S0141-3910(00)00074-4.

[22] Y. Peng, R. Liu, J. Cao, Y. Chen, Effects of UV weathering on surface properties of polypropylene composites reinforced with wood flour, lignin, and cellulose, Appl. Surf. Sci. 317 (2014) 385–392. doi:10.1016/j.apsusc.2014.08.140.

[23] D. Rosu, R. Bodîrlău, C.A. Teacă, L. Rosu, C.D. Varganici, Epoxy and succinic anhydride functionalized soybean oil for wood protection against UV light action, J. Clean. Prod. 112 (2016) 1175–1183. doi:10.1016/j.jclepro.2015.07.092.

[24] R. Gadioli, J.A. Morais, W.R. Waldman, M.-A. De Paoli, The role of lignin in polypropylene composites with semi-bleached cellulose fibers: Mechanical properties and its activity as antioxidant, Polym. Degrad. Stab. 108 (2014) 23–34. doi:10.1016/j.polymdegradstab.2014.06.005.

[25] U. Schulz, V. Wachtendorf, T. Klimmasch, P. Alers, The influence of weathering on scratches and on scratch and mar resistance of automotive coatings, Prog. Org. Coatings. 42 (2001) 38–48. doi:10.1016/S0300-9440(01)00148-5.

[26] N. Tahmassebi, S. Moradian, S.M. Mirabedini, Evaluation of the weathering performance of basecoat/clearcoat automotive paint systems by electrochemical properties measurements, Prog. Org. Coatings. 54 (2005) 384–389. doi:10.1016/j.porgcoat.2005.08.004.

[27] P. Šimon, M. Fratričová, P. Schwarzer, H.W. Wilde, Evaluation of the residual stability of polyurethane automotive coatings by DSC: Equivalence of Xenotest and desert weathering tests and the synergism of stabilizers, J. Therm. Anal. Calorim. 84 (2006) 679–692. doi:10.1007/s10973-005-7549-z.

[28] S. Overton, J. Manura, Identification of volatile organic compounds in a new automobile, 1999.

[29] B. Xu, Y. Wu, Y. Gong, S. Wu, X. Wu, S. Zhu, T. Liu, Investigation of volatile organic compounds exposure inside vehicle cabins in China, Atmos. Pollut. Res. 7 (2015) 215–220. doi:10.1016/j.apr.2015.09.005.

[30] M.J. Fedoruk, B.D. Kerger, Measurement of volatile organic compounds inside automobiles, J. Expo. Anal. Environ. Epidemiol. 13 (2003) 31–41.

doi:10.1038/sj.jea.7500250.

[31] J.S. Han, J.S. Rowell, Chemical Composition of Fibers, in: R.M. Rowell, R.A. Young, J.K. Rowell. (Eds.), Pap. Compos. from Agro-Based Resour., CRC/Lewis Publishers, 1996: pp. 84–134.

[32] J. Acera Fernández, N. Le Moigne, A.S. Caro-Bretelle, R. El Hage, A. Le Duc, M. Lozachmeur, P. Bono, A. Bergeret, Role of flax cell wall components on the microstructure and transverse mechanical behaviour of flax fabrics reinforced epoxy biocomposites, Ind. Crops Prod. 85 (2016) 93–108. doi:10.1016/j.indcrop.2016.02.047.

[33] ISO 877-1: Plastics -- Methods of exposure to solar radiation -- Part 1: General guidance, (2011).

[34] ISO 877-2: Plastics -- Methods of exposure to solar radiation -- Part 2: Direct weathering and exposure behind window glass, (2011).

[35] Pau-Uzein meteorological station, Real-time weather reports, (2016). http://www.infoclimat.fr/observations-meteo/temps-reel/pau-uzein/07610.html (accessed June 16, 2017).

[36] ISO 178:2010, Plastics – Determination of flexural properties, (2010).

[37] R. Alexander-Katz, R.G. Barrera, Surface correlation effects on gloss, J. Polym. Sci. 36 (1997) 1321–1334.

[38] ISO 2813: Coatings: Determination of gloss value at 20°, 60° and 85°, (2014) 1–31.

[39] Sperling L.H., Introduction to physical polymer science, 4th ed., John Wiley & Sons, 2006. doi:10.1002/0471757128.ch9.

[40] C. Rouillon, P.O. Bussiere, E. Desnoux, S. Collin, C. Vial, S. Therias, J.L. Gardette, Is carbonyl index a quantitative probe to monitor polypropylene photodegradation?, Polym. Degrad. Stab. 128 (2016) 200–208. doi:10.1016/j.polymdegradstab.2015.12.011.

[41] Joanne Will, Does my windshield protect me from the sun ?, Globe Mail. (2013). https://www.theglobeandmail.com/globe-drive/culture/commuting/does-my-windshield-protect-me-from-the-sun/article12495123 (accessed August 16, 2017).

[42] L. Běhálek, M. Maršálková, P. Lenfeld, J. Habr, J. Bobek, M. Seidl, Study of crystallization of polylactic acid composites and nanocomposites with natural Fibres by DSC method, in: NANOCON Conf., 2013: pp. 1–6.

[43] L. Soccalingame, A. Bourmaud, D. Perrin, J.-C. Bénézet, A. Bergeret, Reprocessing of wood flour reinforced polypropylene composites: Impact of particle size and coupling agent on composite and particle properties, Polym. Degrad. Stab. 113 (2015) 72–85. doi:10.1016/j.polymdegradstab.2015.01.020.

[44] N.S. Egute, P.L. Forster, F.D. Parra, D.M. Fermino, S. Santana, A.B. Lugão, Mechanical

and thermal properties of polypropylene composites with curaua fibre, in: Int. Nucl. Atl. Conf., 2009.

[45] M. John, S. Thomas, Biofibres and biocomposites, Carbohydr. Polym. 71 (2008) 343–364. doi:10.1016/j.carbpol.2007.05.040.

[46] B. Fayolle, E. Richaud, J. Verdu, F. Farcas, Embrittlement of polypropylene fibre during thermal oxidation, J. Mater. Sci. 43 (2007) 1026–1032. doi:10.1007/s10853-007-2242-1.

[47] L. Wei, A.G. McDonald, C. Freitag, J.J. Morrell, Effects of wood fiber esterification on properties, weatherability and biodurability of wood plastic composites, Polym. Degrad. Stab. 98 (2013) 1348–1361. doi:10.1016/j.polymdegradstab.2013.03.027.

[48] J.S. Félix, C. Domeño, C. Nerín, Characterization of wood plastic composites made from landfill-derived plastic and sawdust: volatile compounds and olfactometric analysis, Waste Manag. 33 (2013) 645–55. doi:10.1016/j.wasman.2012.11.005.

[49] J. Li, H.-C. Hu, X.-S. Chai, Rapid method for determination of carbonyl groups in lignin compounds by headspace gas chromatography., J. Chromatogr. A. 1404 (2015) 39–43. doi:10.1016/j.chroma.2015.05.055.

[50] K. Srinivas, K.K. Pandey, Photodegradation of thermally modified wood, J. Photochem. Photobiol. B Biol. 117 (2012) 140–145. doi:10.1016/j.jphotobiol.2012.09.013.

[51] H. Du, W. Wang, Q. Wang, S. Sui, Y. Song, Effects of ultraviolet absorbers on the ultraviolet degradation of rice-hull/high-density polyethylene composites, J. Appl. Polym. Sci. 126 (2012) 906–915. doi:10.1002/app.36558.

[52] A.J. Vinha, A.G. Carvalho, M. Teixeira de Souza, C. Marangon Jardim, A. de Cassia Oliveira Carneiro, J. Luiz Colodette, Effect of extractives on wood color of heat treated Pinus radiata and Eucalyptus pellita, Maderas. Cienc. Y Tecnol. 17 (2015) 857–864. doi:10.4067/S0718-221X2015005000074.

[53] J.S. Fabiyi, D. McIlroy, A.G. McDonald, Wood modification effects on weathering of HDPE-based Wood Plastic Composites, J. Polym Env. 17 (2009) 34–48. doi:10.1007/s10924-009-0118-y.

II. Natural weathering of hemp fibers reinforced polypropylene biocomposites: Relationships between visual and surface aspects, mechanical properties and microstructure based on PCA statistical approach

Célia Badji, Joana Beigbeder, Hélène Garay, Anne Bergeret, Jean-Charles Bénézet and Valérie Desauziers

C2MA, Ecole des mines d'Alès, 6 avenue de Clavières, 30319 Cedex France

Keywords: ageing, statistical method, hemp fibers, relationships, similarities

Abstract

Exterior and under windshield glass natural weathering of neat polypropylene (PP) and hemp fibers reinforced PP biocomposites were investigated. The objective was to emphasize the relationships between the properties of materials according to the weathering type, the fiber loading and the weathering time in order to bring new insights of degradation mechanisms understanding. For this purpose, a Principal Component Analysis (PCA) statistical method was applied to the whole data. Hence, the contribution of the different properties to the principal components drawing was determined. Properties that discriminated the most the samples and the relationships between them were deduced. Otherwise, specific groups of individuals to which samples were assigned as well as similitudes between them characterized by variables were highlighted. As regards global calculation, properties linked to chemical composition, surface aspect and mechanical performance merged as significant variables. The treatment carried out by isolating materials loaded by the three different hemp fiber rates particularly outstand the link between mechanical properties and products issued from oxidation. The close correlation between whitening parameter and C=C bond level also confirmed the lignin degradation way. Finally, depending on the weathering duration, the properties characterized either fiber loading or weathering state (unweathered or weathered) whereas mechanical performance differentiated the different fiber rate containing non-weathered samples whatever the exposure time.

II.1. Introduction

The use of natural fibers for thermoplastics reinforcement results from the will of developing materials based on renewable resources as alternatives for fossil ones. In 2015, the construction industry dominated the worldwide market of natural fibers reinforced composites in terms of application followed by the automotive industry [1]. The regulations and standards implemented by the Corporate Average Fuel Economy (CAFE) to reduce vehicle weight are likely to prompt a positive impact on demand of biocomposites by automotive industries over the next years [2].

Biocomposites combine advantages such as stiffness and recyclability. However, the high sensitivity of vegetal fibers impedes their extensive application. Indeed, UV rays sensitivity, thermal instability and moisture absorption are the main characteristics responsible to the broad variability of their properties. Since several decades, their durability has been studied and several works investigated the influence of biocomposites ageing on mechanical and visual aspect properties. Results obviously showed that the degradation of the materials affected their mechanical behavior. Biocomposites strongly lost strength and stiffness depending on the degradation conditions [3–7]. The presence of natural fibers were evidenced to give rise to materials surface defects, particularly due to fibers swelling face to rainfall provoking roughening and cracking. The gloss, important appearance parameter, is besides mainly compromised by these surface aspect changes [3,8,9]. Moreover, the natural reinforcing part also instigated the biocomposites discoloration by photo-induced oxidation via yellowing and bleaching [3,9,10]. Some solutions can be brought to avert these variations, for example by adding chemical stabilizers that can prolong their lifetime [11]. However, in order to effectively intervene, the degradation mechanisms must be handled. The elucidation of relationships between the different properties governing the variations in biocomposites during weathering is required to assess durability.

Well-known relationships exist between structure and properties of thermoplastic polymers [12–15]. Relationships between properties evolutions of thermoplastics determined all along their weathering have been investigated. An interesting correlation between modification of crystalline fraction and detection of micro-cracks after polypropylene (PP) accelerated ageing was deduced from microscopy and calorimetry analyses [8]. But this observation

cannot be verified by regression and remains crude correlation. On the contrary, interdependence between parameters was sometimes quantified. For instance, a linear relationship between the crystallinity ratio χ_c and the inverse of the square root of weight-average molecular weight M_w of high density polyethylene (HDPE) was assumed for quenched HDPE [16]. However, this linear relationship could not describe crystallisation behaviour of other HDPE samples. Also, the absorption bands corresponding to crystalline and amorphous phases and allowing to measure the crystallinity of HDPE were proved to be well correlated with the melting enthalpy over a natural weathering during Canadian winter [17]. So a close link between chemical composition and microstructure evolution was verified and demonstrated that ageing was caused by chemical structure modification leading to configuration changes such as chain breaking, chain branching and oxidation. The rheological and mechanical behavior of PP were interrelated since the intrinsic viscosity linearly evolved with tensile strength under different UV-weathering conditions indicating the dominant role played by the reduction in molecular weight of the samples in mechanical properties changes [18]. Akay et al considered vinyl index as a function of carbonyl index throughout PE natural degradation [19]. The resulting plot fitted a linear regression. Torikai et al demonstrated that for different PE samples having the same structure, the amount of oxidation products versus elongation and strength at break after photodegradation lie on a same curve [20]. Hence, a simple method such as infrared spectroscopy could allow predicting the photostability of polymer materials. In contrast to this approach and after having attempted to find correlation, other authors reported that no simple relation exists between the changes in chemical structure and mechanical properties [13,19,21].

Fewer studies focused on relationships between properties evolutions of biocomposites determined all along their weathering. Fabiyi evidenced strong correlations between lightness and chemical composition (carboxylic acid and ester concentrations) evolutions over an exterior weathering of wood plastic composites (WPC) by equations with good correlation coefficients [22]. Indeed, lightness proportionally increased with the carbonyl groups containing molecules concentration. Thus, in these degradation conditions, lightness could be a useful direct predictive indicator of chemical structure changes. The same team established a linear relationship existing between the crystallinity and molecular weight in mass taking place over xenon-arc and outside weathering. This suggests that the decrease in

chain length due to chain scission induced a simultaneous increase of the crystallinity ratio [23]. A linear regression between a* and b* chromatic coordinates was observed after accelerated ageing of thermoplastic/white oak composites irrespectively to the exposure time [24]. Indeed, as yellowness increased, so did the redness. Some studies on correlations after lignocellulosic materials degradation were also assessed. For example, overall color changes (ΔE) occurred as absorbance of C=C bonds in aromatic structure containing lignin increased during UV light irradiation of wood [25]. This relationship suggests that the color variations during irradiation were mainly due to the formation of chromophores resulting from photochemical degradation of lignin. More precisely, another paper reporting results dealing with regression analyses during artificial photo-irradiation of indicated that infrared peak intensity related to lignin containing bonds vibrations has a significant statistical relation with the chromatic and lightness coordinates, in particular with L* and a* [26]. Another study dealt with cellulose degradation. The graphing of its degree of polymerization determined from the intrinsic viscosity as a function of zero-span tensile strength felt on a common line over different accelerated ageing conditions. This implies that chain length of cellulose impacts the strength [27].

Most of the time, statistical analyses reported in works regarding weathering of natural fillers and fibers reinforced materials were used to evaluate the significance of variations of physico-chemical properties before and after materials degradation. This allowed emphasizing through statistical means the properties that significantly evolved. Besides, Student's t-test was conducted as recurrent relevant method [10,28–30]. Also, a comparison between the influence of two artificial ageings on wood loss from WPC surface was statistically computed by Fabiyi and his co-workers [22].

Principal Component Analysis (PCA) is also a useful statistical technique that has found application in fields such as biology, health and agriculture, etc. This common technique is required for finding patterns in high-dimensional dataset. As regards application of PCA for lignocellulosic materials ageing studies, Bonifazi et al. employed this method to distinguish the main groups of samples of different wood species that were formed over the ageing and presenting same features [26]. The degradation of both cellulose and lignin was suspected to be mainly responsible to chemical evolution. Indeed, principal components explained

cellulose/lignin absorption band during the ageing. Also, in a previous paper, the relationships between properties of PP and WPC were assessed before and after natural and artificial weathering thanks to this analysis [3]. Depending on the considered parameter (wood loading, weathering state), either mechanical or chemical composition property was highly discriminating.

Nevertheless, the progressive evolution of relationships between chemical, physical and mechanical properties of materials over their exposition under real conditions representing their end use and the influence of components has not been studied. This work aims to carry out PCA on two types of weathering simulating car interior and decking of PP and PP/hemp fibers biocomposites towards different criteria consideration (fiber rate, type and time of exposure) to determine the influence of the different parameters. The objective is to determine the relationships existing between properties for a better understanding of their degradation mechanisms. Also, the samples grouping or remoteness and their contribution to principal components drawing will be interpreted.

II.2. Materials and methods

II.2.1 Raw materials

Polypropylene (PP, grade H733-07) with a melt flow rate of 7.5 g/10 min (230 °C, 2.16 kg) obtained from Braskem (Brazil) in the form of pellets was used as homopolymer matrix. Hemp fibers provided by AgroChanvre (France) were sifted to obtain 2 to 6-mm length range. After the 38-days retting process, their cellulose, hemicelluloses and lignin rates were determined by chemical extractions based on TAPPI T264, ASTM D1104 standards [31,32]. anhydride grafted polypropylene (MA-g-PP, Orevac CA100) with a 1 wt% grafting rate purchased from Arkema (France), was added at 3.1 wt% of PP as coupling agent. The hemp fibers were added at 10 wt% (PP10) and 30 wt% (PP30) in the (PP+MA-g-PP) part.

II.2.2 Process conditions

Raw materials have been oven-dried before processing for 15 h at 60 °C. PP and MA-g-PP granules were mixed with hemp fibers in a BC21 Clextral co-rotating twin-screw extruder (L/D = 36 with the diameter D = 25 mm and L= 900 mm) (Clextral, France) with the

temperature ranging from 190 to 175 °C from feed to die and a screw speed of 220 rpm. Once dried for 3 days at 60 °C in an air-circulating oven, extruded pellets were injection molded in a Krauss Maffei KM50-T180CX at 210 °C (Krauss Maffei, Germany) with an injection speed of 30 $cm^3.s^{-1}$ and a mold kept at 40 °C. ISO 1 dog-bone specimens and square specimens of 100 × 100 × 2 mm^3 and were obtained for both mechanical performance and visual appearance characterizations respectively (Figure 1).

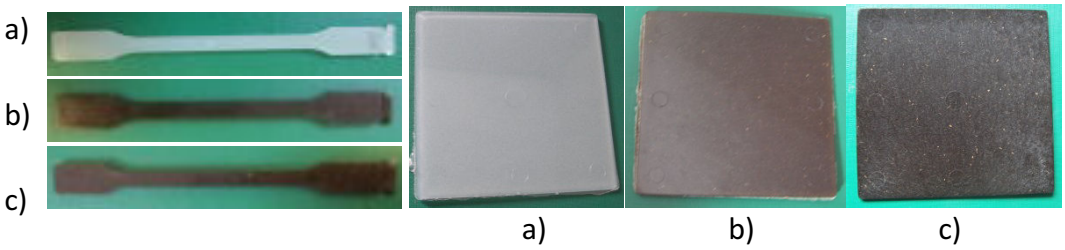

Figure 1 - (a) PP, (b) PP10 and (c) PP30 materials: dog-bone specimens (left) and square specimens (right)

II.2.3 Weathering

Weathering tests were operated in Pau in the south west of France. Exterior and under windshield glass one-year expositions were chosen to represent exterior and interior applications of materials. Samples were exposed according to ISO 877-2011 standard [33,34]. The samples were fixed on galvanized racks at an angle of 45° with the ground and directed toward the south direction. Laminated windshield glasses covered the materials for the automotive application (Figure 2). Meteorological data from September 2015 to September 2016 were provided from Pau-Uzein station for outdoor parameters [35] whereas laboratory-sensors were used for under windshields glasses monitoring. Data evolutions monitored all along the exposition are shown in Figure 3. Changes in materials properties were measured after 1, 2, 3, 6, 9 and 12 months.

Figure 2 - Exterior and under glass exposure racks

Table 1- Designation of non-weathered and weathered PP, PP10 and PP30 materials

Ageing time (Months)	Non-weathered materials	Exterior weathered materials	Under glass weathered materials
0	PP-UW, PP10-UW, PP30-UW	-	-
1	-	PP-EW1, PP10-EW1, PP30-EW1	PP-GW1, PP10-GW1, PP30-GW1
2	-	PP-EW2, PP10-EW2, PP30-EW2	PP-GW2, PP10-GW2, PP30-GW2
3	-	PP-EW3, PP10-EW3, PP30-EW3	PP-GW3, PP10-GW3, PP30-GW3
6	-	PP-EW6, PP10-EW6, PP30-EW6	PP-GW6, PP10-GW6, PP30-GW6
9	-	PP-EW9, PP10-EW9, PP30-EW9	PP-GW9, PP10-GW9, PP30-GW9
12	-	PP-EW12, PP10-EW12, PP30-EW12	PP-GW12, PP10-GW12, PP30-GW12

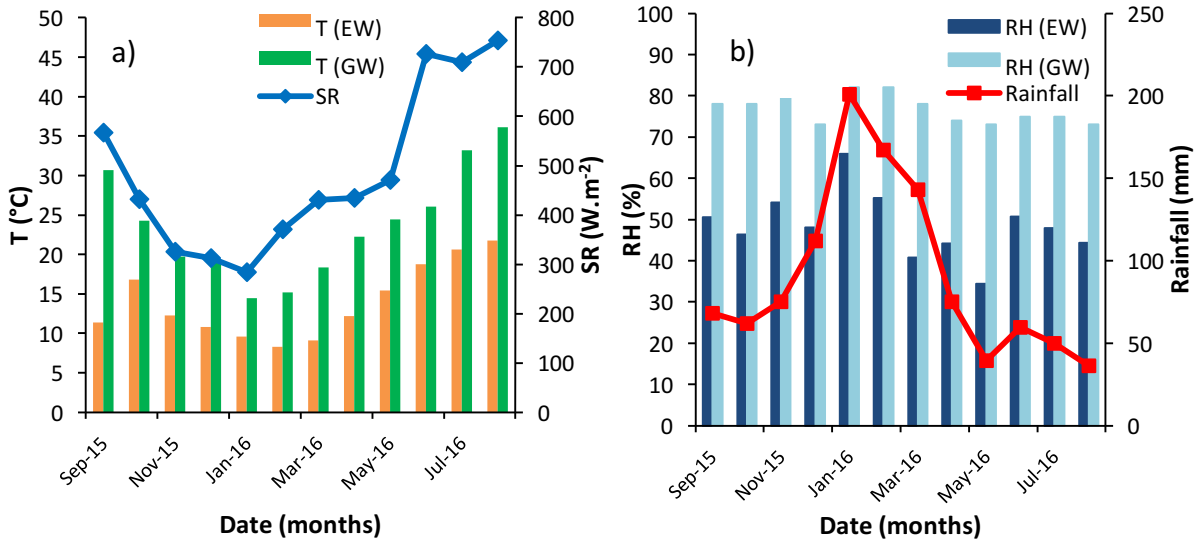

Figure 3 – Mean temperature and mean solar radiation SR (blue curve) (a) and mean relative humidity and rainfall (b)

II.2.4 Flexural tests

Mechanical properties were measured by three-point bending test at 23 ± 2 °C and 50 ± 10% RH on ISO 1A dog-bone samples in accordance to the ISO 178:2010 standard. A Zwick TH 010 press apparatus and a 2.5 kN load cell were used to characterize flexural properties. Values of elastic modulus E_f and the stress at the conventional deflection σ_{fc} corresponding to the stress at a strain of 3.5 % were calculated from stress-strain curves. The cross-head speeds were set at 2 and 100 mm.min^{-1} for the modulus and flexural stress at the conventional deflection measurements respectively. Eight samples of each material were tested.

II.2.5 Differential Scanning Calorimetry (DSC)

Calorimetric data were obtained through Differential Scanning Calorimetry (DSC) by means of a PYRIS Diamond calorimeter (Perkin Elmer, United States). The analysis was conducted under nitrogen atmosphere at a 20 mL.min^{-1} constant flow. Surface fragments of almost 10 mg were analysed. Samples were heated from 30 to 210 °C with a heating ramp at 10 °C.min^{-1}. Two heating steps with an intermediate cooling step at -10 °C.min^{-1} were performed. Two replicate samples per material were analysed. The crystallinity rate was calculated according to the following equation from the melting enthalpy:

$$\chi_c\ (\%) = \frac{\Delta H_m}{W \times \Delta H_{m_{100}}} \times 100 \qquad \text{Eq. 1}$$

with W the PP mass fraction, ΔHm (J.g^{-1}) the melting enthalpy determined from the 2nd heating step and ΔHm_{100} the standard melting enthalpy of a 100% crystalline PP (209 J.g^{-1}) [36,37]. The 2nd heating cycle was chosen in order to overcome the crystallinity related to the thermal background of the polymer (processing). Otherwise, the second run provides information about the ability of degraded chains of the polymer to crystallize [10,37–40]. Moreover, same evolution tendencies of χ_c deduced from 1st and 2nd heating cycles were observed during the weathering.

II.2.6 Infrared spectroscopy

A IFS66 spectrometer (Bruker, Unites States) operating in the Attenuated Total Reflectance (ATR) mode was used to follow vinyl and carbonyl bonds formation witnessing outdoor degradation. The device was equipped with a single reflection diamond crystal accessory. Thin slices of exposed surfaces were analyzed and the spectra were recorded as a result of the average of 32 scans in the 400 to 4000 cm^{-1} spectral range with a resolution of 1 cm^{-1}. Infrared spectra were normalized according to the Min-Max normalization method with the 2925 cm^{-1} reference band assigned to the methylene groups. Absorbance values for specific peaks (1711 cm^{-1} for C=O of carboxylic acids/ketones; 1740 cm^{-1} for C=O of esters/aldehydes; 1780 cm^{-1} for C=O of γ-lactones; 1650 cm^{-1} for C=C of vinyls) were recorded.

II.2.7 Spectrocolorimetry

The surface color analysis was performed by spectrocolorimetry on a Chroma Sensor CS3 (DataColor, United States). The illuminant/observer configuration was D65/10°. The CIE 1976 *L*, a*, b** uniform system was used to determine the lightness and the color. L*, a* and b* were obtained from the reflectance curves. The L* coordinate represents the lightness whereas a* and b* represent the chromaticity. An increase of L* (from 0 to 100) demonstrates a material lightening. a* and b* are the chromaticity positions on axes from -300 to +300 axes from green (-a*) to red (+a*) and from blue (-b*) to yellow (+b*). Values were obtained from the analysis of four areas of three samples.

II.2.8 Spectrophotogoniometry

A GON 360 goniometer (Instrument Service, Germany) coupled to a MAS 40 spectrometer equipped with a halogen lamp was used to collect the radiometric power. The source angle was fixed at 20° according to ISO 2813 standard [41]. Detector angles varied from 5° to -60° with an angular step smaller in the specular zone to detect the high variations of intensity in this zone. The distribution of the intensity of light reflected by a material according to the angle of detection allowed to characterize the gloss aspect [42]. G_1 corresponding to the haze gloss was determined from the ratio between the maximum intensity obtained for the angle of detection of -20° I(Θ = -20°) and the intensity obtained for the angle of -22° I(Θ = -20

+ -2°) both situated in the specular zone (Eq. 2). The ratio between I(Θ = -20°) and the intensity collected for the angle of -35° I(Θ = -20 + -15°) of a diffusely reflected light far away from the specular zone was also calculated and correspond the contrast gloss (Eq. 3). The higher the value of G_1 and G_2 are, the glossier and smoother the surface seems. The gloss was computed for three replicates at four locations on each material.

$$G1 = \frac{I(\Theta = -20°)}{I(\Theta = -22°)} \quad \text{Eq. 2}$$

$$G2 = \frac{I(\Theta = -20°)}{I(\Theta = -35°)} \quad \text{Eq. 3}$$

II.2.9 Rugosimetry

A MICROMESURE STIL system equipped with a STIL CHR150 optical sensor was used to evaluate the roughness by altitude measurement of each surface point on the sample without contact with the sample according to the ISO 25178 international standard. More details are given in a previous paper [3]. A bidimensional scanning allows obtaining the image of the sample surface located at a precise distance from the STIL optical sensor. Acquisition software SurfaceMap® allowed the control of the station and the post-treatment MountainsMap® software was used to analyze the surface geometry and to calculate roughness parameters. The micrometric range of the optical pen was 285 µm. It permits a tridimensional analysis and the analyzed area X*Y was 5 mm * 5 mm with an analysis step of 10 µm in X and Y directions. The tridimensional roughness parameter Sa followed during the weathering corresponds to the arithmetic mean of the absolute of the height values (Eq. 4):

$$\mathrm{Sa} = \frac{1}{NM} \sum_{x=0}^{N-1} \sum_{y=0}^{M-1} |z(x,y)| \quad \text{Eq. 4}$$

with M the number of points along the X axis, N the number of points along the Y axis, and $z_{x,y}$ the altitude in µm. Mean values and standard deviations were obtained from the analysis of four areas of three samples.

II.2.10 Statistical analysis

Principal Component Analysis (PCA) was carried out on Statistica 13 software (Dell, France). This multivariate statistical technique is used to make the cloud of the whole data

(properties of all samples) easy to explore and visualize it in a reduced dimension. For this purpose, a set of orthogonal non-correlated principal components (axes) is built. More details of the calculation method principle are given elsewhere [3,43]. In order to overcome the difference of units between all the properties (variables) for correct interpretation, the standardization of the dataset by centering-reduction was used for the correlation circle representation:

$$X_i' = \frac{X_i - \bar{X}}{\sigma_x} \qquad \text{Eq. 5}$$

where X_i' is the centered-reduced variable, X_i is the variable and $\bar{X}$ and σ_x are the mean and standard deviation of the variable X respectively. The designations of variables (properties) are gathered in Table 2.

Table 2 - Designation of parameters

Designation	Parameter
E	Modulus of elasticity (MPa)
s	Stress at the conventional deflection (MPa)
Xc	Crystallinity rate (%)
A1	Absorbance C=O at 1711 cm^{-1} (carboxylic acids/ketones)
A2	Absorbance C=O at 1740 cm^{-1} (esters/aldehydes)
A3	Absorbance C=O at 1780 cm^{-1} (γ-lactones)
A4	Absorbance C=C at 1650 cm^{-1} (vinyls)
Sa	Roughness (µm)
G1	Haze gloss
G2	Contrast gloss
L*	Lightness (light-dark)
a*	Chromatic coordinate (red-green)
b*	Chromatic coordinate (yellow-blue)

II.3. Results and discussion

II.3.1 Global data treatment

The correlation circle allows explaining the contribution of variables (properties) to the provided information rate by their projection into a two-dimension subspace and verifying the correlations between properties. The correlation circle taking into account the overall dataset is represented in Figure 4. The first two principal components (axes) account for almost 70% of the total inertia. This means that a remaining part of 30% is carried by other

components that are not represented here. Otherwise, the horizontal first principal component PC1 accounts for almost 47% of the information and represents the highest inertia rate (two times higher than the second axis PC2).

Vector ends of chemical bonds absorbance values, followed over the weathering to understand the oxidative degradation and carbon-carbon double bond formation are near to the circle. This means that they are well represented by the correlation circle. Also, these variables are close to PC1 corresponding to the main principal axis meaning that they mostly contributed to the drawing of this factor. Thus, PC1 explains the differences linked to the chemical composition and surface aspect evolution. A further study of the individuals (materials) will show how the analysed samples influenced the variables representation.

Carbonyl absorption bands are strongly correlated with each other since they exhibit close correlation coefficients with both PC1 and PC2. This suggests that A1, A2 and A3 evolved in a same way throughout the weathering. Mechanical properties vectors (E and s), for their part, mostly head in the same direction as PC2. Also, the crystallinity rate Xc contributed to the drawing of PC2. So, flexural and microstructure properties bring a different or complementary information to the chemical composition. However, parameters linked to stiffness and stress are non-correlated with C=O maximal absorbance variables since they exhibit an angle of 90°. Thus, any relationship between chemical bonds evolution and mechanical performance can be concluded.

All the other parameters including the color and the lightness coordinates displayed low correlation coefficient absolute values according to PC1 and PC2 and are thus far away from the circle. This suggests that they were not well projected into the plan after the dimensions reducing calculation. This might be due to strong differences in color changes between materials explained by different loading of vegetal fibers in PP matrix.

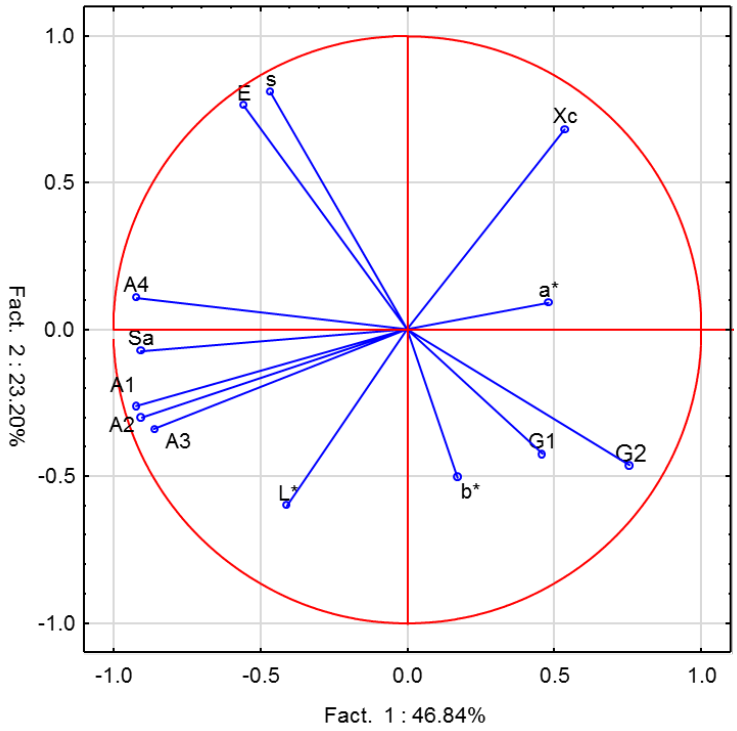

Figure 4 – Global data treatment: Correlation circle taking into account overall dataset

The projection of the individuals (samples) is shown in Figure 5. Their relative positions and their distance with the two PC axes allow identifying the groups of individuals having taken close values on variables. Also, the observed tendencies of variables will be used for the individuals graph interpretation. Firstly, three main groups according to the fiber loading represented by three different colors are easily distinguished. The group of the PP30 weathered during 1, 2, 3 months globally scores relatively high values according to the first and second axes by comparison with PP10 and PP weathered during the same time. This means that PP30 samples take higher values of mechanical properties and carbonyl and vinyl absorbance. However, whatever the type of weathering and the fiber rate, the materials take on increasingly low values according to PC1 and PC2 all along the ageing. Thus, by simultaneous analysis with the correlation circle, long-time exposed materials particularly exhibit high absorbance values and low mechanical performance.

Also, after 6, 9 and 12 months of weathering, the discrimination of the fiber loading is mainly made by PC1, so here, by the chemical composition parameters and the roughness property and no more by the mechanical performance. Indeed, the discrimination between the different fiber rates materials is mainly well represented by the second axis (E, s) at the

beginning of the exposition. Then, from 6 months of weathering, PC1 becomes the axis explicating the hemp fiber rate. So, depending on the weathering time, chemical structure and surface aspect or mechanical performance play a major role in discernment of neat thermoplastic and biocomposites. The next treatment by weathering time (paragraph 3.2) will allow understanding the evolution of properties discriminating power.

Also, materials weathered under windshield glass and outside during a same time of weathering load equally according to PC2 for a same fiber loading (Figure 5). This trend is observed for the three materials and suggests that mechanical properties are not influenced by the type of weathering. However, exterior weathered materials take lower values than under glass weathered ones according to PC1 whatever the weathering time, meaning that they underwent faster oxidation and gloss loss. Otherwise, the difference between the types of weathering EW and GW of each individual increases with the weathering time.

The individuals contributing the most to PC1 are PP-UW and PP30-EW12 whereas PP30-GW2 and PP-GW12 represent the endpoints of PC2. Therefore, followed absorption bands peaks and Sa mostly oppose non-weathered neat PP and one-year outdoor weathered PP30 that certainly present the more disparate behaviors of oxidation and surface deterioration. On the contrary, mechanical performance and crystallinity oppose PP-GW12 and low weathered PP30. Indeed, the last one particularly took high values in E and Xc due to chemicrystallization of PP occurring during short-times exposure [9,16].

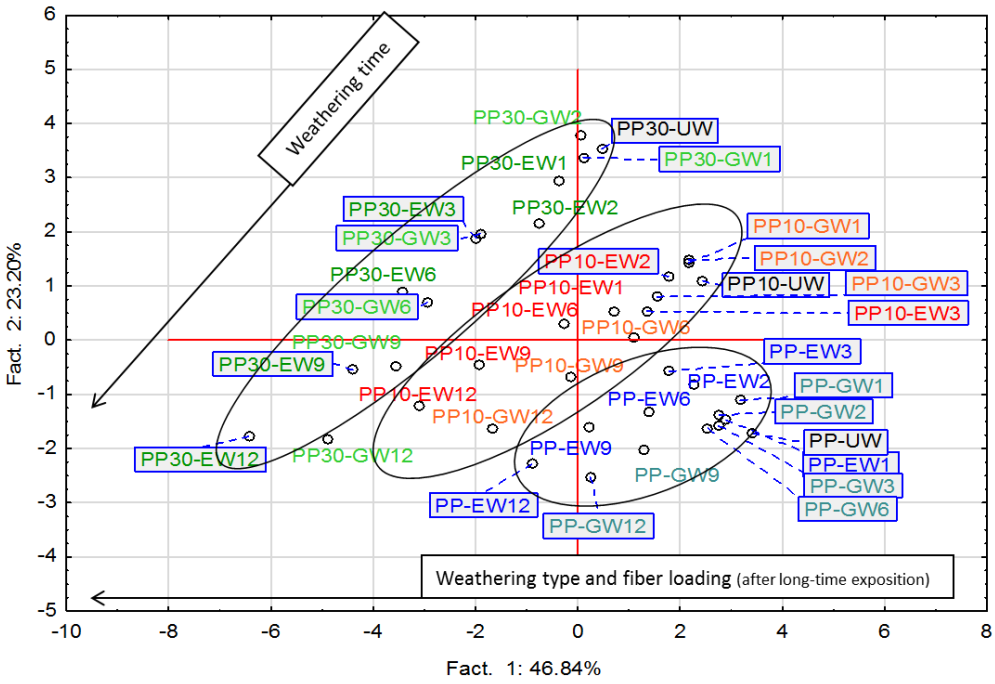

Figure 5 – Global data treatment: Projection of all individuals (PP30 materials: green, PP10 materials: red, PP materials: blue)

II.3.2 Data treatment by type of weathering

The correlation circles of exterior (EW) and under windshield glass (GW) weathering are represented in Figure 6. Firstly, roughly similar factorial coordinates of absorbance values, roughness parameter, contrast gloss and mechanical parameters are raised for the two types of weathering. Moreover, the correlations profile of variables issued from EW dataset does not significantly differentiate with the previous global treatment one. The main difference between global data and exterior exposure data analysis is the higher rate of variations brought by PC1 when only EW data is considered. Indeed, some variables such as b*, that is besides better represented than previously, bring more information in the degradation mechanisms since they get close to PC1 and their number values are high (close to the circle) in the case of EW. Otherwise, this colorimetric parameter seems to highly contribute to the drawing of PC2 for GW. Indeed, the inertia rate of PC2 increased from EW to GW explained by the move of b* parameter towards PC2.

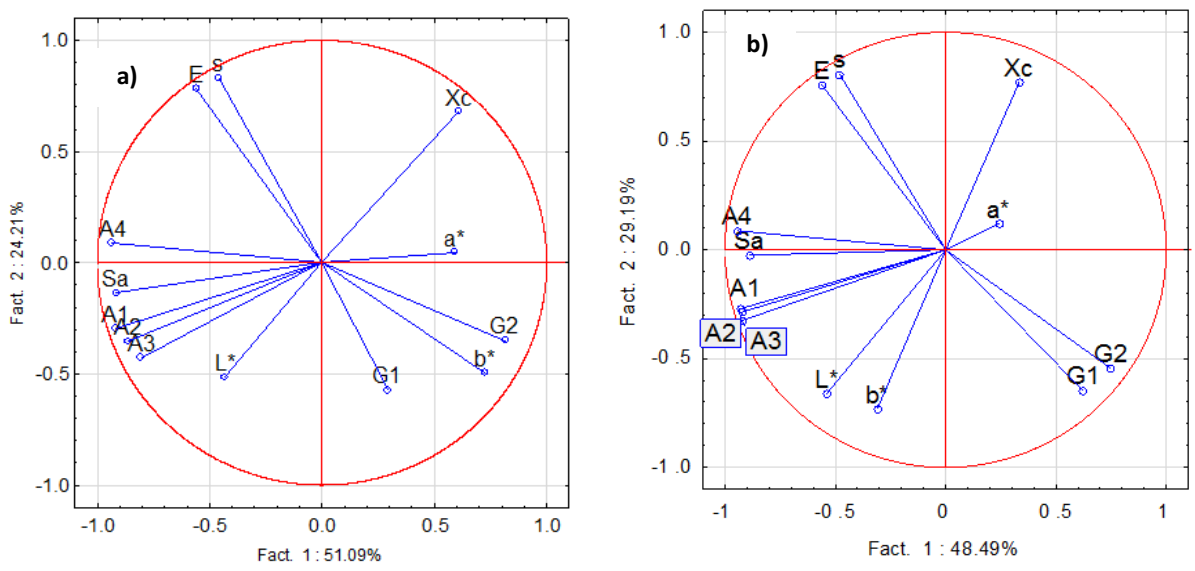

Figure 6 – Influence of the type of weathering: Correlation circles of EW (a) and GW (b)

The same three main clusters PP, PP10 and PP30 are emphasized whatever the conditions of exposition (Figure 7). Also, the individuals get increase in roughness and carbonyl and vinyl bonds formation as well as loss in stiffness, stress at deflection and crystallinity ratio over the exposure. However, some differences are noted between the two individuals' projections of EW samples in one hand and GW samples in another hand. For the three samples batches, the gaps between EW samples weathered at different times are equally important according to PC2 and PC1. However, they are differently organized with a more vertical evolution over the under glass weathering than over exterior one. Indeed, the gaps between GW samples weathered at different times of weathering are less important according to PC1 than for EW samples. This might be due to the fact that materials surface oxidation and alteration (roughness increase and gloss decrease) during GW occurred slower than during EW. However, b* and Xc tend to 1 and -1 values respectively according to PC2 for GW. This observation suggests that they also highly contribute to the main variations over GW since samples mainly arranged vertically. As regards non-weathered samples, b* decreases with the fiber loading. Otherwise, it is interesting to note that b* mainly differentiates the three fiber loadings after one-year exterior ageing (Figure 7a) according to PC1, whereas it rather represents the degradation evolution (from UW to GW12) over under glass exposition according to PC2 (Figure 7b). Indeed, concerning EW, b* value of biocomposites remained lower than PP one after one-year and did not significantly evolve

with the weathering. This observation can justify the main differentiation according to the fiber rate. However, a fast yellowing kinetic of biocomposites was observed due to higher temperatures under windshield glass (Figure 3A). Since temperature was the main degrading factor under glass, yellowing was certainly linked to hemp fibers thermal instability, especially hemicelluloses [44]. Thus, the exposition conditions influence correlations and visual aspect explains either hemp fiber rate or weathering time depending on the variation degree. Furthermore, as concluded previously, mainly oxygenated bonds concentration, surface roughness and gloss (PC1) oppose PP, PP10 and PP30 after long-duration of EW and GW since PC2 no longer differentiates the three materials.

Also, the gaps in PP30 samples (weathered at different times) between them are more important than between PP and PP10 ones. This is attributed to greater changes in physico-chemical properties. Hence, a further data analysis by fiber loading is required to verify more specifically the contribution of each variable to this variations enlargement.

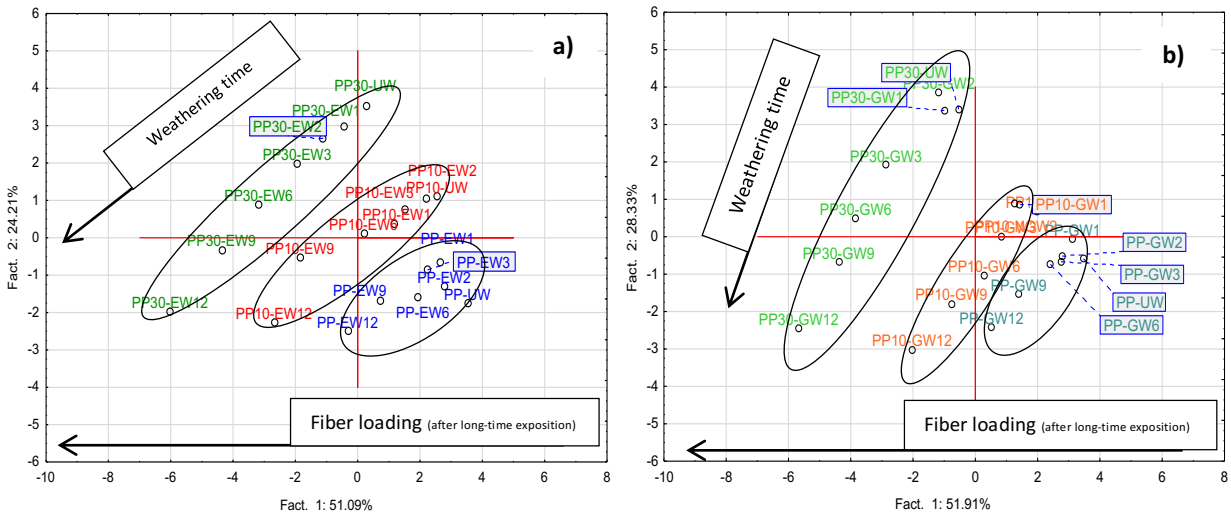

Figure 7 - Influence of the type of weathering: EW (a) and GW (b) individuals projection

II.3.3 Treatment by fiber loading

The correlation circles of PP, PP10 and PP30 gathering non-weathered and weathered samples are illustrated in Figure 8. It is interesting to note that a maximum variance is extracted from the bidimensional projection whose variables correlations are interpreted by fiber loading. This attests the importance of the materials split-up particularly depending on the fiber rate for the properties linking. As well as for global and weathering type analyses, the maximum absorbance of infrared bands characteristic to oxidative degradation and

chain scission and the surface aspect remain ones of the main parameters contributing to PC1. Moreover, the treatment by fiber loading induced an alignment of most of variables according to PC1, translating a higher variance rate of PC1. Indeed, Xc, E and s, that were previously linked to PC2 and mostly discriminated the differences between the different fiber rates, here contribute to the drawing of the most important component. Thus, plotting variables on these dimensions will allow discussing only the influence of time and type of weathering by the samples representation.

The greater the fiber loading, the higher the information share is retained by PC1. Thus, the higher vegetal fiber biocomposite, the better the data is graphically summarised. For both neat PP and biocomposites, an anti-correlation between mechanical properties and carboxylic acids, ketones and γ-lactones concentration is observed. Therefore, when materials are considered by their hemp fiber rate, the mechanical performance loss (elastic modulus and stress at conventional deflection decrease) could be linked to their oxidative degradation. This anti-correlation was not verified thanks to the previous representations. It can be supposed that mechanical properties that mostly brought information on the fiber loading role cannot explain this factor in this analysis since PP, PP10 and PP30 are dissociated. Also, a small angle between lightness (L*) and C=C vibration band (A4) vectors is raised on biocomposites correlation circles. This could witness the contribution of lignin degradation or surface emergence by the increase of C=C bonds in phenolic structures responsible to further bleaching due to chromophores molecules generation [4,10].

Unlike biocomposites, even if the elastic modulus of neat PP is well represented since its vector tip is close to the circle, it does not strongly contribute to PC1 inertia rate. Otherwise, the higher the fiber rate, the closer to PC2 b* chromatic coordinate is. Hence, b* brings information distinct to the other variables.

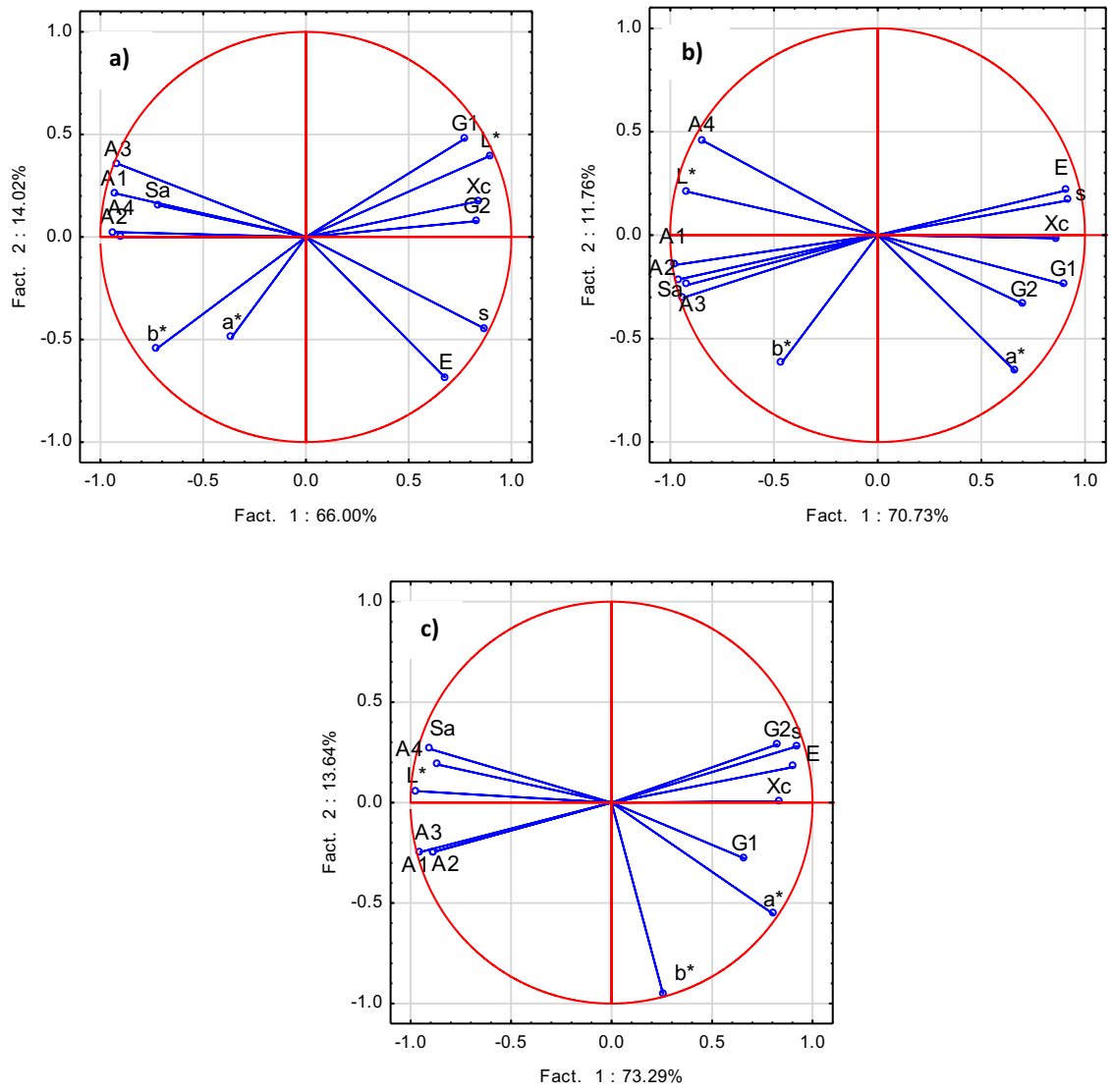

Figure 8 – Influence of the fiber loading: Correlation circles of PP (a), PP10 (b) and PP30 (c)

Factorial plans containing individuals are plotted in Figure 9. The oxidation process and mechanical performance loss qualify the evolution over the exposition (PC1) rather than the type of degradation. This observation reinforces our earlier interpretation. Otherwise, individuals belonging to PP30-GW group score high on the second component while PP30-EW2, PP30-EW3 and PP30-EW6 score low. Thus, the type of weathering is mainly classified by b* parameter due to the different rates of yellowing of the biocomposites outdoor and under glass. Indeed, yellowing was assigned to chromophore structures containing paraquinones whose formation seems to be favoured under the high temperatures recorded under windshield glass. Also, the weathering time factor is better represented since this evolves from 1 to 12 months according to the component carrying the most information.

Otherwise, PP30 samples are more organized according to PC1 than neat PP. Indeed, the two groups PP30-GW and PP30-EW are better distinguished than PP ones. This might be explained by the consequent influence of the type of weathering on the b* chromatic parameter value linked to degradation of hemp fibers that preferentially undergo yellowing under glass promoted by high temperatures [11]. Also, for a same time of ageing, PP-EW and PP-GW exhibit significantly different values according to PC1 with lower score for PP-EW, and hence high carbonyl and vinyl absorbance values, due to outdoor degradation factors that were more affected. Therefore, the type of weathering had globally a bigger influence on PP properties changes during the exposure than on PP30. Moreover, by comparison with PP30 samples, PP-EW and PP-GW weathered during 6, 9 and 12 months are also particularly distant according to PC2. This last assumption can justify the higher amount of variance carried by PC2 for virgin PP.

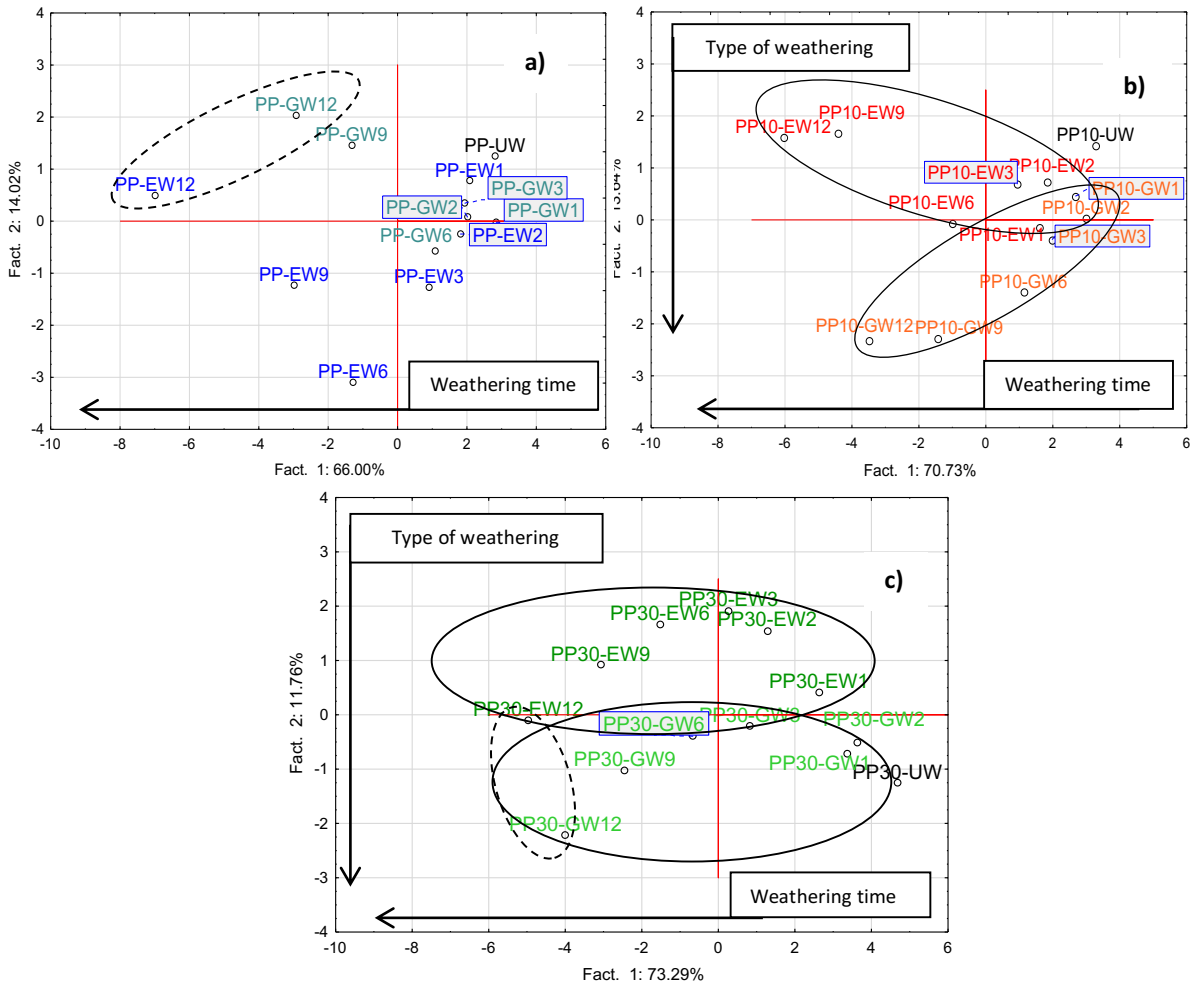

Figure 9 - Influence of the fiber loading: Individuals projection of PP (a), PP10 (b) and PP30 (c)

II.3.4 Treatment by time of weathering

The evolution over the weathering of the relationships between properties and their contribution to principal components are depicted in Figure 10. The inertia rate of PC1 globally decreased throughout the weathering to the benefit of PC2 one. Thus, information of different nature is provided. At early stage of exposition to climatic conditions, E, s, A1, A4, Sa on the one hand, and L*, G1, G2 on the other hand, are respectively positively and negatively correlated with PC1 whereas A3 (γ-lactones) and a* color coordinate are described by PC2. Indeed, at 1 month of weathering, A2 and A3 absorbance values are not as much as meaningful than for previous analyses since the farther to PC1 the variable, the lower the information rate captured by this variable. However, they rapidly join PC1. From 6 months of exposition, variables linked to the mechanical parameters come off PC1 and provide information through PC2. Individuals score plot will bring complementary insight to understand this evolution.

The average roughness is more and more anti-correlated with gloss parameters as the ageing time goes on. Moreover, it is an acknowledged fact that the surface topography has a direct impact on brightness [3,42], but Sa preferentially anti-correlates with G2 corresponding to contrast gloss. This may be justified through changes in gloss values all along the exposition. Indeed, gloss of PP-EW exhibited drastic decrease in G2 between 9 and 12 months whereas G1 remained almost constant. G2 decrease could justify the sudden increase of roughness parameter at the same period. Moreover, literature data revealed that contrast gloss was intimately related to average roughness and confirms our hypothesis [45]. Similarly, crystallinity degree Xc and carbonyl functional groups absorbance are anti-correlated after 9 and 12 months whereas Xc headed in the same way as A1 at the beginning. Indeed, the decomposition of polymer chains firstly induced an increase of the degree of crystallinity due to chain scission in the amorphous phase promoting formation of short chains which rearrange into a crystalline phase [9,16]. Nevertheless, when chain scission continues further, the crystalline regions are affected and the crystallinity ratio decreases due to oxidative degradation whatever the material [30,46]. The unstable and reactive molecules formed through polymer decomposition oxidized and thus carbonyl absorption bands could increase to the detriment of the well-organized crystalline phase.

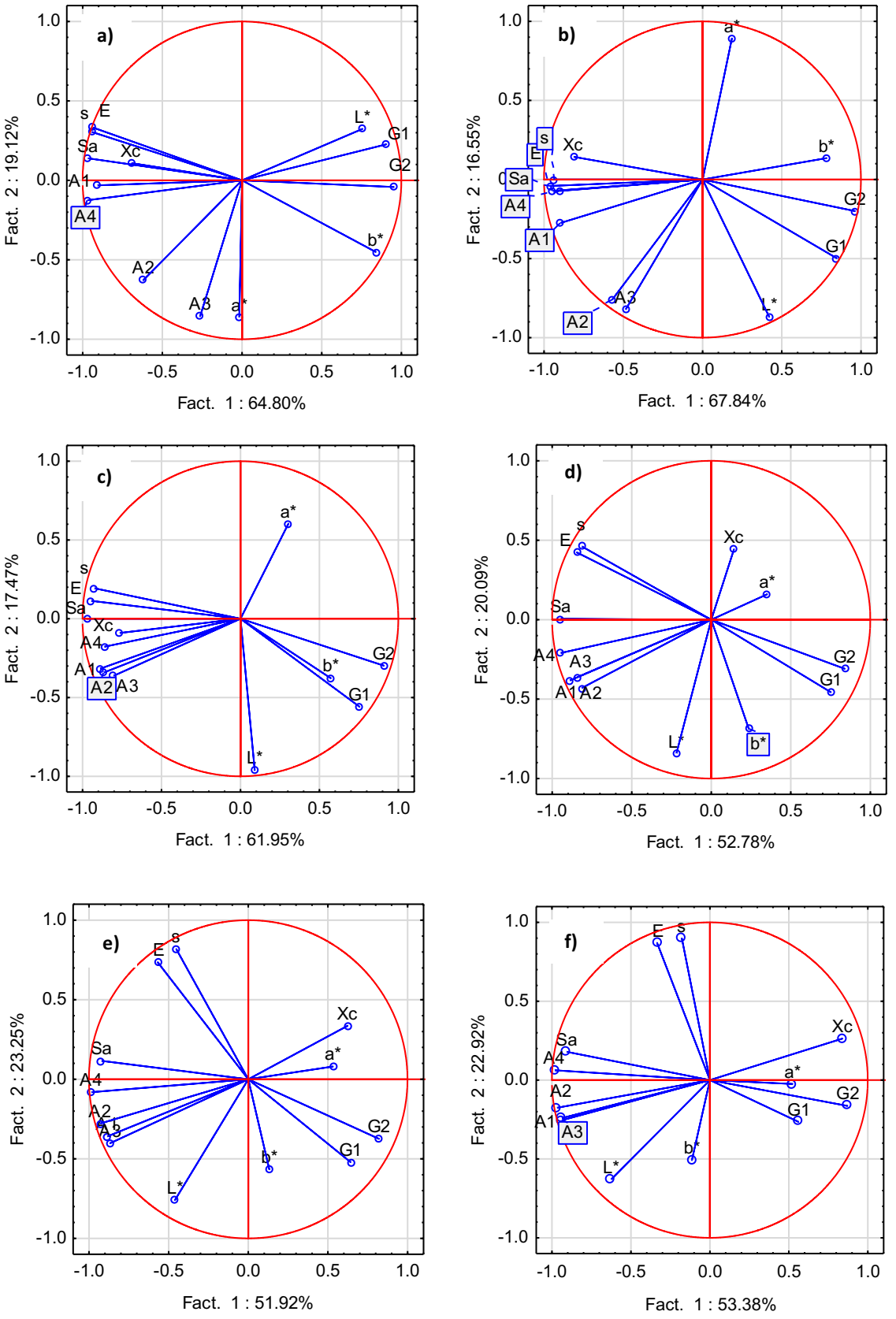

Figure 10 – Influence of the weathering duration: Correlation circles after 1 (a), 2 (b), 3 (c), 6 (d), 9 (e) and 12 (f) months of weathering

Scatterplots of individuals by weathering time are reported in Figure 11. After 1, 2 and 3 months of exposition, PP30 samples present lower values on PC1 than PP and PP10 ones i.e. high values in mechanical, C=O and C=C bonds, roughness properties. Thus, these properties demonstrate oxidation and surface aspect alteration due to presence of hemp fibers. The difference between the fiber loadings is better interpreted than weathering states at the beginning of exposition. Indeed, at early stage (1, 2, 3 months), all materials spread along PC1 whereas PC2 differences the states of weathering (UW, EW, GW) explained by a*, A2 and A3. This observation leads us to presume that aldehydes, esters and γ-lactones are particularly due to weathering rather than their naturally occurring presence in hemp fibers as ketones and carboxylic acids (PC1). Indeed EW materials take low scores on PC2 and thus high values of A2 and A3.

However, the different states of weathering tend to organize themselves according to PC1 throughout the ageing. So this reversal suggests that the variables linked to PC1 (absorbance, surface aspect including roughness, contrast gloss and crystallinity) further differentiate the states of the materials, either non-weathered or weathered, at a higher degree than at the beginning. So, long-term exposure obviously caused higher changes that are better characterized by PC1 whatever the material and the weathering type. As regards E and s, as they progress towards PC2, non-aged materials also progressively spread out along PC2 whereas EW and GW samples more and more align themselves on PC1. Therefore, mechanical performance defines the fiber loading mainly at non-weathered state. Indeed, difference of bulk properties (elastic modulus and conventional deflection stress values), between non-weathered PP, PP10 and PP30 is notable. On the contrary, their carbonyl and vinyl bonds peaks and crystallinity ratio, that are properties measured at the surface, are not so different. This can be explained by a major presence of polymer matrix at the material non-aged surface covering vegetal fibers and hence, leading to main analysis of PP properties. On the contrary, the exposition led to microstructure and absorbance differentiation between PP and biocomposites because of emergence of hemp fibers at the surface, to the detriment of distinction by bulk properties (mechanical performance) since their values were not as different as non-weathered state values.

Nevertheless, the gap between non-weathered and weathered states according to PC1 is higher than according to PC2 after 9 and 12-month exposition whereas the contrary is observed after 3 and 6 months. This can be due to degree of crystallinity and C=O absorption bands relating to PC1, parameters witnessing degradation rather than describing vegetal fibers rate.

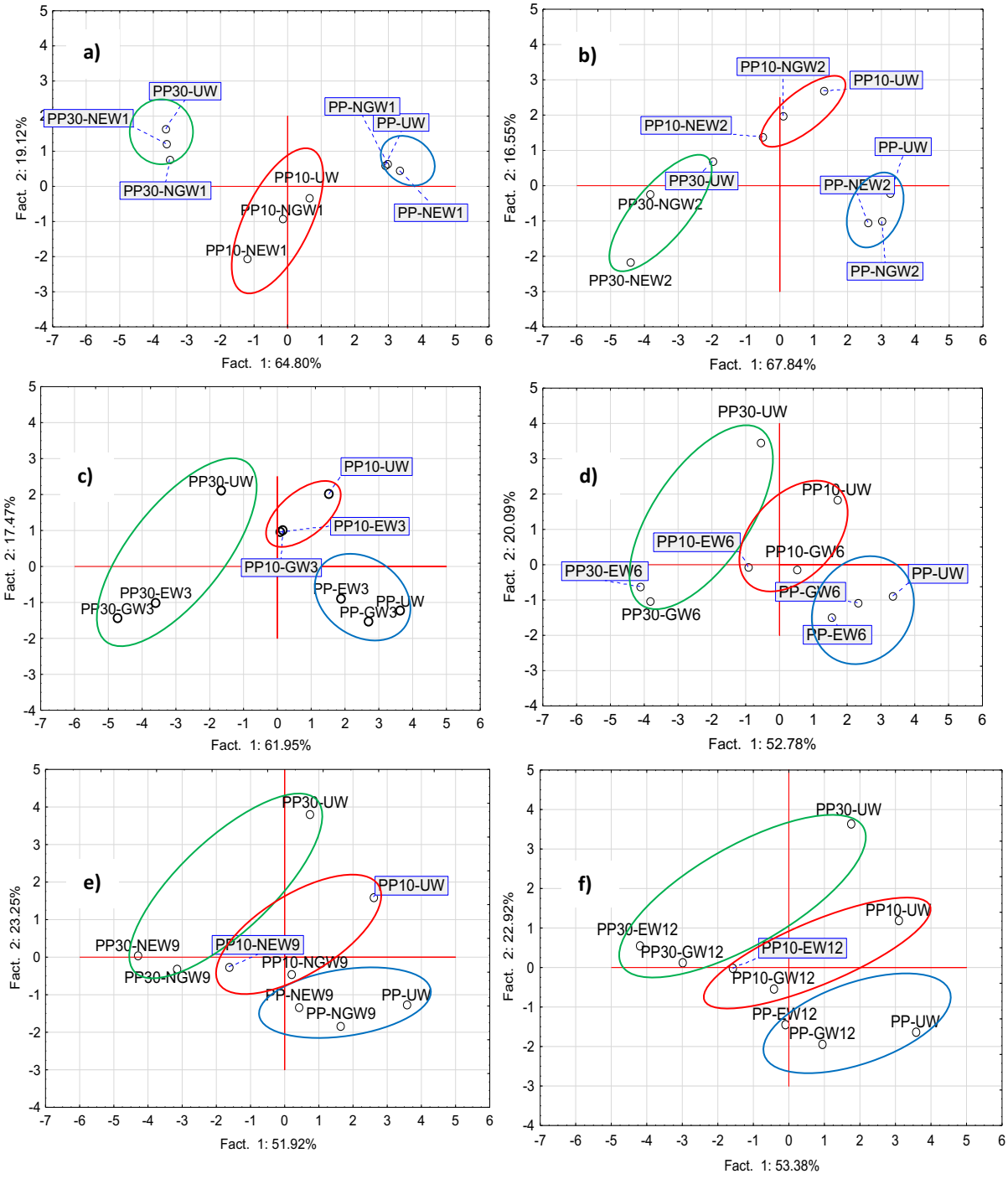

Figure 11 – Influence of the weathering duration: Individuals projections after 1 (a), 2 (b), 3 (c), 6 (d), 9 (e) and 12 (f) months of weathering

II.4. Conclusion

Principal Component Analysis (PCA) is a statistical method used to derive underlying variables and reduce the number of dimensions in order to consider more easily a dataset. In this work, the relationships between properties of neat PP and natural fibers reinforced composites were determined and the interpretation of samples grouping was carried out. According to the considered individuals, the measurements brought complementary information.

The global analysis allowed to give off the main parameters (C=O and C=C maximum absorbance measured through infrared spectrometry, roughness, bending mechanical performance) distinguishing the main aggregates corresponding to neat PP and PP reinforced by 10 wt% (PP10) and 30 wt% (PP30) of hemp fibers.

The treatment according to the type of weathering (exterior EW or under windshield glass GW) exhibited some differences between correlation profiles meaning that exterior or indoor conditions influenced links existing between the properties. Indeed, this showed that parameters sensitive to high temperature such as b* (blue-yellow chromatic coordinate measured through spectrocolorimetry) differentiated ageing times after under glass ageing than fiber rates whereas the contrary was observed for exterior ageing. Indeed, b* value of EW biocomposites remaining lower than PP one did not significantly change with the weathering time whereas a fast yellowing kinetic of biocomposites was observed with the ageing time. This yellowing can be explained by some by-products formation sensitive to temperature.

Statistical calculation by separation of materials by fiber loadings showed different profiles of individuals. PP30-EW and PP30-GW clusters were well distinguished according to b* coordinate meaning that the major parameter differentiating the biocomposites weathering conditions is the visual aspect (yellowing). However, PP-EW and PP-GW were differentiated by most of the variables suggesting that the type of weathering had a higher impact on the global changes kinetic in properties of PP than those of biocomposites. Also, as regards links between measured parameters, this representation could allow prediction of mechanical performance loss thanks to carbonyl bands monitoring. Also, the intimate relationship found

between L* and C-C double bond absorption band including C=C of lignin structure for biocomposites, confirmed the contribution of lignin degradation reported in literature.

Finally, an evolution of properties in the correlation circles and their contribution to principal components was observed over the weathering. Firstly, the fiber loading was discriminated by chemical bonds, surface aspect (roughness and contrast gloss) and crystallinity whereas state of weathering was characterized by these same variables after long-time exposition. Also, it was noted that, contrary to ketones and carboxylic acids, aldehydes and γ-lactones species were generated by weathering after short period rather than their naturally occurring presence in vegetal fibers. After one year, non-weathered PP, PP10 and PP30 samples considered as reference materials were mainly distinguished by flexural modulus and conventional deflection stress whereas weathered PP, PP10 and PP30 were distinguished by surface properties. This was certainly due to bulk properties distinction favoured at non-weathered state contrary to surface characteristics of materials differentiated after long-time exposition due to matrix decomposition. Thus, a long exposure time accentuated the difference between surface aspects of the three materials. An anti-correlation between C=O absorption bands and crystallinity ratio observed after long-time weathering was explained by the crystalline phase deterioration under oxidative degradation. After long-time exposition (9 to 12 months), degree of crystallinity and C=O absorption bands also witnessed degradation rather than distinguish vegetal fibers rate.

Therefore, the use of this statistical tool allowed taking into account 13 quantitative variables simultaneously and draw relationships between them at a same time.

II.5. References

[1] Grand View Research Inc, Natural fiber composites market analysis and segment forecasts to 2024 report, 2015.

[2] Flexform, Vehicle weight reduction and safety concerns for meeting CAFE standards, (2012). http://www.naturalfibersforautomotive.com/?p=84 (accessed June 1, 2017).

[3] C. Badji, L. Soccalingame, H. Garay, A. Bergeret, J.-C. Bénézet, Influence of weathering on visual and surface aspect of wood plastic composites: Correlation approach with mechanical properties and microstructure, Polym. Degrad. Stab. 137 (2017) 162–172. doi:10.1016/j.polymdegradstab.2017.01.010.

[4] L. Soccalingame, D. Perrin, J.-C. Bénézet, S. Mani, F. Coiffier, E. Richaud, A. Bergeret,

Reprocessing of artificial UV-weathered wood flour reinforced polypropylene composites, Polym. Degrad. Stab. 120 (2015) 313–327. doi:10.1016/j.polymdegradstab.2015.07.013.

[5] L. Soccalingame, D. Perrin, J.-C. Bénézet, A. Bergeret, Reprocessing of UV-weathered wood flour reinforced polypropylene composites: Study of a natural outdoor exposure, Polym. Degrad. Stab. 133 (2016) 389–398. doi:10.1016/j.polymdegradstab.2016.09.011.

[6] A. Le Duigou, P. Davies, C. Baley, Seawater ageing of flax/poly(lactic acid) biocomposites, Polym. Degrad. Stab. 94 (2009) 1151–1162. doi:10.1016/j.polymdegradstab.2009.03.025.

[7] A. Arbelaiz, B. Fernández, J.A. Ramos, A. Retegi, R. Llano-Ponte, I. Mondragon, Mechanical properties of short flax fibre bundle/polypropylene composites: Influence of matrix/fibre modification, fibre content, water uptake and recycling, Compos. Sci. Technol. 65 (2005) 1582–1592. doi:10.1016/j.compscitech.2005.01.008.

[8] C. Rouillon, P.-O. Bussiere, E. Desnoux, S. Collin, C. Vial, S. Therias, J.-L. Gardette, Is Carbonyl Index a quantitative probe to monitor polypropylene photodegradation?, Polym. Degrad. Stab. 128 (2016) 200–208. doi:10.1016/j.polymdegradstab.2015.12.011.

[9] Y. Peng, R. Liu, J. Cao, Y. Chen, Effects of UV weathering on surface properties of polypropylene composites reinforced with wood flour, lignin, and cellulose, Appl. Surf. Sci. 317 (2014) 385–392. doi:10.1016/j.apsusc.2014.08.140.

[10] S. Butylina, M. Hyvärinen, T. Kärki, A study of surface changes of wood-polypropylene composites as the result of exterior weathering, Polym. Degrad. Stab. 97 (2012) 337–345. doi:10.1016/j.polymdegradstab.2011.12.014.

[11] M. Muasher, M. Sain, The efficacy of photostabilizers on the color change of wood filled plastic composites, Polym. Degrad. Stab. 91 (2006) 1156–1165. doi:10.1016/j.polymdegradstab.2005.06.024.

[12] M.R. Kantz, H.D. Newman, F.H. Stigale, The skin-core morphology and structure-property relationships in injection-molded polypropylene, J. Appl. Polym. Sci. 16 (1972) 1249–1260. doi:10.1002/app.1972.070160516.

[13] N.M. Stark, L.M. Matuana, Surface chemistry and mechanical property changes of wood-flour/high-density-polyethylene composites after accelerated weathering, J. Appl. Polym. Sci. 94 (2004) 2263–2273. doi:10.1002/app.20996.

[14] D. Feng, D.F. Caulfield, A.R. Sanadi, Effect of compatibilizer on the structure-property relationships of kenaf-fiber/polypropylene composites, Polym. Compos. 22 (2001) 506–517. doi:10.1002/pc.10555.

[15] W.Y. Chiang, W.D. Yang, B. Pukánszky, Polypropylene composites. II: Structure-property relationships in two-and three-component polypropylene composites, Polym. Eng. Sci. 32 (1992) 641–648.

[16] B. Fayolle, E. Richaud, X. Colin, J. Verdu, Review : degradation-induced embrittlement in semi-crystalline polymers having their amorphous phase in rubbery state, (2008) 6999–7012. doi:10.1007/s10853-008-3005-3.

[17] P. Pagès, F.C.J. Saurina, X. Colom, FTIR and DSC study of HDPE structural changes and mechanical properties variation when exposed to weathering aging during Canadian winter, J. Appl. Polym. Sci. 60 (1996) 153–159.

[18] X. Yang, X. Ding, Prediction of outdoor weathering performance of polypropylene filaments by accelerated weathering tests, Geotext. Geomembranes. 24 (2006) 103–109. doi:10.1016/j.geotexmem.2005.11.002.

[19] G. Akay, T. Tinçer, H.E. Ergöz, A study of degradation of low density polyethylene under natural weathering conditions, Eur. Polym. J. 16 (1980) 601–605. doi:10.1016/0014-3057(80)90095-6.

[20] A. Torikai, A. Takeuchi, S. Nagaya, K. Fueki, Photodegradation of polyethylene : effect of crosslinking on the oxygenated products and mechanical properties, Polym. Photochem. 7 (1986) 199–211.

[21] A. Tidjani, R. Arnaud, A. Dasilva, Natural and accelerated photoaging of linear low-density polyethylene: Changes of the elongation at break, J. Appl. Polym. Sci. 47 (1993) 211–216. doi:10.1002/app.1993.070470203.

[22] J.S. Fabiyi, A.G. McDonald, M.P. Wolcott, P.R. Griffiths, Wood plastic composites weathering: Visual appearance and chemical changes, Polym. Degrad. Stab. 93 (2008) 1405–1414. doi:10.1016/j.polymdegradstab.2008.05.024.

[23] J.S. Fabiyi, A.G. McDonald, Degradation of polypropylene in naturally and artificially weathered plastic matrix composites, Maderas. Cienc. Y Tecnol. 16 (2014) 0–0. doi:10.4067/S0718-221X2014005000021.

[24] J.S. Fabiyi, A.G. McDonald, Effect of wood species on property and weathering performance of wood plastic composites, Compos. Part A Appl. Sci. Manuf. 41 (2010) 1434–1440. doi:10.1016/j.compositesa.2010.06.004.

[25] D. Rosu, C.A. Teaca, R. Bodirlau, L. Rosu, FTIR and color change of the modified wood as a result of artificial light irradiation, J. Photochem. Photobiol. B Biol. 99 (2010) 144–149. doi:10.1016/j.jphotobiol.2010.03.010.

[26] G. Bonifazi, L. Calienno, G. Capobianco, A. Lo, C. Pelosi, R. Picchio, S. Serranti, Modeling color and chemical changes on normal and red heart beech wood by re fl ectance spectrophotometry, Fourier Transform Infrared spectroscopy and hyperspectral imaging, Polym. Degrad. Stab. 113 (2015) 10–21. doi:10.1016/j.polymdegradstab.2015.01.001.

[27] X. Zou, N. Gurnagul, T. Uesaka, J. Bouchard, Accelerated aging of papers of pure cellulose: mechanism of cellulose degradation and paper embrittlement, Polym. Degrad. Stab. 43 (1994) 393–402. doi:10.1016/0141-3910(94)90011-6.

[28] N.M. Stark, L.M. Matuana, Ultraviolet weathering of photostabilized wood-flour-filled

high-density polyethylene composites, J. Appl. Polym. Sci. 90 (2003) 2609–2617. doi:10.1002/app.12886.

[29] N.M. Stark, L.M. Matuana, Surface chemistry changes of weathered HDPE/wood-flour composites studied by XPS and FTIR spectroscopy, Polym. Degrad. Stab. 86 (2004) 1–9. doi:10.1016/j.polymdegradstab.2003.11.002.

[30] C. Homkhiew, T. Ratanawilai, W. Thongruang, Effects of natural weathering on the properties of recycled polypropylene composites reinforced with rubberwood flour, Ind. Crops Prod. 56 (2014) 52–59. doi:10.1016/j.indcrop.2014.02.034.

[31] J.S. Han, J.S. Rowell, Chemical Composition of Fibers, in: R.M. Rowell, R.A. Young, J.K. Rowell. (Eds.), Pap. Compos. from Agro-Based Resour., CRC/Lewis Publishers, 1996: pp. 84–134.

[32] J. Acera Fernández, N. Le Moigne, A.S. Caro-Bretelle, R. El Hage, A. Le Duc, M. Lozachmeur, P. Bono, A. Bergeret, Role of flax cell wall components on the microstructure and transverse mechanical behaviour of flax fabrics reinforced epoxy biocomposites, Ind. Crops Prod. 85 (2016) 93–108. doi:10.1016/j.indcrop.2016.02.047.

[33] ISO 877-1: Plastics -- Methods of exposure to solar radiation -- Part 1: General guidance, (2011).

[34] ISO 877-2: Plastics -- Methods of exposure to solar radiation -- Part 2: Direct weathering and exposure behind window glass, (2011).

[35] Pau-Uzein meteorological station, Real-time weather reports, (2016). http://www.infoclimat.fr/observations-meteo/temps-reel/pau-uzein/07610.html (accessed June 16, 2017).

[36] Sperling L.H., Introduction to physical polymer science, 4th ed., John Wiley & Sons, 2006. doi:10.1002/0471757128.ch9.

[37] C. Rouillon, P.O. Bussiere, E. Desnoux, S. Collin, C. Vial, S. Therias, J.L. Gardette, Is carbonyl index a quantitative probe to monitor polypropylene photodegradation?, Polym. Degrad. Stab. 128 (2016) 200–208. doi:10.1016/j.polymdegradstab.2015.12.011.

[38] L. Sisti, G. Totaro, M. Vannini, P. Fabbri, S. Kalia, A. Zatta, A. Celli, Evaluation of the retting process as a pre-treatment of vegetable fibers for the preparation of high-performance polymer biocomposites, Ind. Crops Prod. 81 (2016) 56–65. doi:10.1016/j.indcrop.2015.11.045.

[39] M. Groning, M. Hakkarainen, Headspace solid-phase microextraction with gas chromatography/mass spectrometry reveals a correlation between the degradation product pattern and changes in the mechanical properties during the thermooxidation of in-plant recycled polyamide 6,6, J. Appl. Polym. Sci. 86 (2002) 3396–3407. doi:10.1002/app.11345.

[40] K.B. Adhikary, S. Pang, M.P. Staiger, Accelerated Ultraviolet Weathering of Recycled

Polypropylene--Sawdust Composites, J. Thermoplast. Compos. Mater. 22 (2009) 661–679. doi:10.1177/0892705709096550.

[41] ISO 2813: Coatings: Determination of gloss value at 20°, 60° and 85°, (2014) 1–31.

[42] R. Alexander-Katz, R.G. Barrera, Surface correlation effects on gloss, J. Polym. Sci. 36 (1997) 1321–1334.

[43] L.J. Williams, H. Abdi, Principal Component Analysis, Wiley Interdiscip. Rev. Comput. Stat. 2 (2010) 433–459. doi:10.1002/wics.101.

[44] J. Gassan, A.K. Bledzki, Thermal degradation of flax and jute fibers, J. Appl. Polym. Sci. 82 (2001) 1417–1422. doi:10.1002/app.1979.

[45] W.J. O'Brien, W.M. Johnston, F. Fanian, S. Lambert, The surface roughness and gloss of composites., J. Dent. Res. 63 (1984) 685–688. doi:10.1177/00220345840630051601.

[46] N.M. Stark, L.M. Matuana, Influence of photostabilizers on wood flour-HDPE composites exposed to xenon-arc radiation with and without water spray, Polym. Degrad. Stab. 91 (2006) 3048–3056. doi:10.1016/j.polymdegradstab.2006.08.003.

CHAPITRE III

VIEILLISSEMENT SOUS VITRE PARE-BRISE DE BIOCOMPOSITES PP/CHANVRE :

ETUDE DE L'ÉMISSION DE COMPOSÉS ORGANIQUES VOLATILS

Chapitre III

Vieillissement sous vitre pare-brise de biocomposites PP/chanvre : Etude de l'émission de Composés Organiques Volatils

Actuellement, un intérêt croissant pour l'impact des émissions de Composés Organiques Volatils (COV) sur la qualité de l'air intérieur émerge, en particulier dans le cas des véhicules. Les biocomposites étant de plus en plus intégrés dans les pièces d'habitacles, une étude quantitative de leurs émissions de COV en conditions d'usage présente tout son intérêt. En effet, à notre connaissance, aucune étude de ce type n'est à ce jourété reportée dans la littérature.

Ce chapitre comprend trois parties.

La première partie est consacrée à la mesure des émissions de COV par le polypropylène (PP) et les biocomposites à matrice PP renforcée de fibres de chanvre au cours d'une année d'exposition sous vitre pare-brise. L'objectif est d'évaluer l'influence des fibres végétales sur la qualité de l'air intérieur et de déterminer l'impact des facteurs environnementaux sur les variations d'émission. Pour cela, un protocole d'échantillonnage des COV émis par les matériaux précédemment développé au laboratoire a été appliqué. Cette étude a montré que la présence de renforts végétaux contribue fortement aux émissions de composés volatils. Après exposition, la présence de fibres végétales a principalement induit des émissions de composés oxygénés tels que des phénols, acides carboxyliques et furanes issus de la décomposition oxydative de la lignine et de l'holocellulose, en plus des alcanes provenant du polypropylène.

Dans la littérature, les mécanismes de décomposition de la biomasse sont étudiés à partir de l'identification de sous-produits volatils tels que les furanes issus de la décomposition des carbohydrates structurant les fibres et identifiés dans ce travail. La génération de ces COV est généralement provoquée par pyrolyse ou par réaction catalytique. Toutefois ces procédés impliquent des conditions énergétiques favorables à la formation de tels

composés, ce qui n'est pas le cas dans cette étude. Ainsi, la seconde partie du chapitre vise à démontrer que les réactions de Maillard peuvent être extrapolées à des conditions de vieillissement naturel. En effet, les protéines et les sucres naturellement présents dans les fibres et identifiés en tant que COV sont potentiellement responsables de la formation de certains furanes issus de la dégradation thermique. Par ailleurs, des réactions entre les substances oxygénées linéaires identifiées au cours de l'exposition ont été proposées afin d'expliquer la formation d'autres composés furaniques identifiés au cours du vieillissement. Ces réactions sont basées sur des interactions moléculaires entre les cétones et les acides carboxyliques et font intervenir des cyclisations et la déshydratation des molécules.

Finalement, la troisième partie vise à corréler les profils d'émissions de COV des matériaux aux propriétés dont les évolutions au cours du vieillissement ont été précédemment décrites (chapitre II). Ainsi, les taux d'émission sont inclus dans le calcul statistique de l'analyse en composantes principales (ACP) (Cf. Annexe II) et sont mis en relation avec la performance mécanique (module, contrainte en flexion), la microstructure (taux de cristallinité) et l'aspect de surface (couleur, rugosité, brillant). Les liens établis entre la variable représentant les émissions et celles correspondant aux autres propriétés au cours du vieillissement sont obtenus à travers l'interprétation des profils de corrélation obtenues par analyse statistique. L'étude statistique est effectuée en distinguant les différents matériaux selon leur taux de fibres (0, 10, 30 %m) d'une part, et les différents temps de vieillissement d'autre part. Lorsque l'étude statistique est effectuée par matériau, une relation émerge entre les émissions de COV et la performance mécanique (module et contrainte à la flèche conventionnelle). Ces résultats sont une ouverture au recours de techniques non destructives pour prédire la durée de vie des biocomposites.

La première partie de ce chapitre sous forme de publication a été soumise pour publication à Polymer Degradation and Stability. La publication incluse dans la deuxième partie a été soumise au Journal of Polymers and the Environment. Enfin, la troisième partie est à soumettre à Macromolecular Materials and Engineering.

I. Under glass weathering of hemp fibers reinforced polypropylene biocomposites: Impact of Volatile Organic Compounds emissions on indoor air quality

Célia Badji, Joana Beigbeder, Hélène Garay, Anne Bergeret, Jean-Charles Bénézet and Valérie Desauziers

C2MA, Ecole des Mines d'Alès, 6 Avenue de Clavières, 30319, Alès Cedex, France

Abstract

Nowadays, natural fibers reinforced composite materials can be used in closed environments such as car cabins. It has hence become a necessity to study their emissions of Volatile Organic Compounds (VOCs) to check their impact on indoor air quality. The purpose of this work was first to study the emissions of VOCs from hemp fibers reinforced polypropylene (PP) biocomposites in comparison with neat PP. The influence of under windshield glass weathering on VOCs release was then investigated. The exposition lasted one year and the fiber loading influence on emissions was studied all along the weathering. The VOCs concentration at the material/air interface was determined using a passive sampling method involving an emission cell coupled with Solid Phase MicroExtraction (SPME). VOCs analysis was then carried out by gas chromatography coupled to mass spectrometry and flame ionization detections. One of the most significant results is the drastic increase of oxygenated compounds concentration during the exposition, especially for biocomposites. Among these oxidation by-products, formaldehyde, acetaldehyde, furfural and 2-furanmethanol, recognized as Cancerogen, Mutagen and toxic for Reproduction (CMR), were detected. A broad range of alkanes, specific of PP matrix degradation was also identified. Finally, measured concentrations of substances found in this work and listed in Vehicle Indoor Air Quality (VIAQ) standards were gathered in order to discuss the biocomposites emissions impact on indoor air quality.

Keywords: vegetal fibers, polypropylene, automobile, Volatile Organic Compounds emission, weathering

I.1. Introduction

The development of natural fibers used as an alternative to glass fibers in the reinforcement of thermoplastic polymers has grown as the result of environmental concerns and the depletion of fossil resources. Indeed, their low density, good specific properties and low environmental impact make them attractive in fields like automobile and construction (decking). Moreover, the production of natural fibers composites could increase from 92,000 metric tons (MT) in 2012 to 370,000 MT in 2020 according to the incentives [1].

Concerning automotive sector, the use of biocomposite materials in vehicle interior parts is increasingly seen in replacement of glass fibers reinforced composites. They are mainly used in car binnacles like door panels and dashboards. Thermoplastics such as polypropylene (PP) and biopolyesters including mainly polylactic acid (PLA) and polybutylene succinate (PBS) are mainly used as polymer matrices. However, the highlighting of the time spent in vehicles induces more investigations on the health impact of car interior pieces [2]. Indeed, transportation is the third environment that humans attend after houses and work places, where they are subjected to indoor air pollution. Moreover, the World Health Organization (WHO) has recognised interior air pollution of vehicles as a major threat to human health [3]. Several sources like traffic emissions, tobacco smoke or interior materials can result in a poor binnacle air quality. Recently, the “Sick Car Syndrome” has been highlighted as a result of the identification of toxic products emitted by binnacle pieces [4]. They are issued from the dashboard, door panels, seat coverings and flooring materials. They can cause eye, nose and throat irritations, allergic skin reactions, headaches and fatigue. Emitted VOCs can also be responsible for olfactory annoyance and could limit end use application [5,6].

Currently, some national regulations and standardizations have been implemented to improve vehicle interior air quality (VIAQ). Korea government has been one of the first countries to manage VIAQ guideline. They have established the notification No. 2007-539 in 2007 specifying limit concentration levels for 6 substances which are benzene, toluene, formaldehyde, xylene, ethylbenzene and styrene with limit levels ranging from 30 $\mu g.m^{-3}$ for benzene to 1600 $\mu g.m^{-3}$ for ethylbenzene [7,8]. After that, a study made by Korea Automobile Testing & Research Institute showed a significant concentration decrease in 5 years [9]. Car interior VOCs emissions are also coming under more scrutiny in China. Indeed,

the standard GB/T 27630 implemented on 2012 is inspired from the recommendatory standard guideline for air quality assessment of passenger car issued on 2011 [10]. This applies the evaluation on binnacle air quality by proposing limit values for the previously mentioned 6 substances plus acetaldehyde and acrolein. Associations such as Japan Automobile Manufacturers Association (JAMA) and European Automobile Manufacturers Association (ACEA) recently made headway to improve VIAQ [11,12]. For instance, JAMA has drawn up the guideline "vehicle cabin VOC testing methods for passenger cars" for conducting the necessary VOC measurements. Nevertheless, the limit concentration levels are different between each country standard. Indeed, formaldehyde concentration limit ranges from 100 $\mu g.m^{-3}$ in Chinese and Japanese standards to 250 $\mu g.m^{-3}$ in Korean guideline. They only concern whole vehicle assessment whereas threshold values at the material scale are mostly imposed by automotive industries. In order to propose new vehicles complying with the VIAQ limit values, worldwide standards describing test methods for the determination of VOCs emissions from car trim components are already implemented. In Europe, ISO 12219 standards describe different protocols and scales for the determination of either VOCs concentrations in car indoor air or VOCs emission rate for materials [13–15].

Lots of studies dealt with pollutants emission in vehicles and the influence of different parameters on their concentrations. Most of the time, total VOCs (TVOCs) concentration is also measured, besides individual VOC levels, to evaluate indoor air quality [8,16–20]. In automotive and building industry, all VOCs whose retention times are between those of hexane and hexadecane under specific gas chromatographic conditions represent TVOCs [21]. It was shown that static conditions (parked, unventilated) favored higher TVOCs concentration in car cabins than specified driving conditions and ventilation. TVOCs level was decreased from 1980 $\mu g.m^{-3}$ in moderate-heat (almost 40 °C) and static conditions to 100 $\mu g.m^{-3}$ under 90-minutes driving conditions in a 1997 Ford vehicle [20]. Vehicle age also plays a role. Indeed, Chien compared measured levels in new cars for specified products with levels found in literature [18]. It was observed that they could be three orders of magnitude higher than those of older cars, but they decrease over time [22]. VOCs emission is strongly temperature dependent [22] but other parameters like relative humidity and interior trim compositions have also an influence. Indeed, leather pieces emit higher quantities than

fabric pieces with a big influence on toluene VIAQ concentration which can increase by 39 % [17,18]. The contribution of materials to the VIAQ is therefore very important. That is highlighted by a study only focused on VOCs emissions from materials [19]. Long-chain aliphatic hydrocarbons and aromatic compounds, like toluene and xylenes, were mostly identified and counted for 52 % and 42 % of TVOCs concentration respectively. Other chemical families like halocarbons, carbonyls and esters were also detected. This kind of study is not very widespread and to our knowledge, no work is published regarding emissions of VOCs emitted by car interior finished parts made of biocomposites.

Vegetal fibers used in biocomposites are known to be sensitive face to climatic conditions such as ultraviolet (UV) rays, high temperatures and humidity. Physico-chemical properties of natural fillers composites are thereby affected by water absorption and oxidation reactions leading to mechanical performance loss and chemical composition and visual aspect changes [23–30]. Some works described qualitative and semi-quantitative analysis of VOCs evolved from biocomposites. A study has been done on emissions of VOCs sampled by headspace solid phase micro-extraction (HS-SPME) after a thermal ageing of cellulose and hemp fibers reinforced polypropylene (PP) composites [31]. Different VOCs chemical families were identified such as aliphatic hydrocarbons, carboxylic acids and alcohols but also compounds specific to natural fibers like 2-furanmethanol. K.W. Kim et al. worked on the reduction of TVOCs emission from pineapple and destarched cassava flour reinforced polylactic acid (PLA) and polybutylene succinate (PBS) biocomposites by the bake-out process [16]. The study investigated the influence of temperature and baking time on TVOCs emission factor. They noted a factor increase with temperature and a decrease with baking time. Otherwise, neat PLA and PBS presented lower emission factor than loaded ones. In the same line, H.S. Kim et al. worked on the reduction of odor and VOC emissions of vegetal flour filled reinforced PLA and PBS composites by incorporating porous inorganic fillers [32]. Volatile products emissions caused by high temperature manufacturing like tridecane from the matrix and furfural from bamboo flour were decreased. Olfactometric analyses carried out on natural fillers composites allowed to understand the high responsibility of oxygenated compounds issued from both the polymer and natural fillers to unpleasant odor [5]. However, no study deals with the VOCs emissions of biocomposites under real conditions of use since the impact of natural fiber composites ageing on VOCs emission is

poorly documented. Indeed, standard measurement methods (e.g. emission chamber methods) are complex to implement and time consuming for the monitoring of the temporal evolution of VOCs emissions [33,34]. As an alternative, HS-SPME is the most widely used technique for sampling VOCs emitted by polymeric materials [5,31,35–37]. Its advantages are simplicity and time saving according to short extraction times. But this method involves material destruction by cutting it in small pieces for introduction in the headspace vial. Hence, this sampling procedure is not relevant to provide quantitative data related to surface emission. The sampling methodology used for this work and previously developed, is based on a home-made emission cell coupled with SPME [38,39]. This simple and non-destructive passive sampling method allows determining the VOCs concentration at the material/air interface which is related to the emission rate by the first Fick's law of diffusion under steady state conditions [39].

This study aims to assess the impact of VOCs emitted by hemp fibers reinforced PP on air quality and the influence of material ageing on theses emissions regarding hemp fibers rate and sampling temperature. A car interior environment was simulated by exposing laboratory-made materials under windshield glass for one year. Emitted VOCs were identified over the weathering and their concentrations at the material/air interface were determined. Results are discussed notably in terms of health impact. For this purpose, the European regulation classes of critical products according to their impact on human health and their concentrations were gathered as well as limit values already imposed, or at least advised, by VIAQ guidelines and national standards.

I.2. Materials and Methods

I.2.1 Materials

Polypropylene grade H733-07 with a melt flow rate of 7.5 g/10 min (230 °C, 2.16 kg) was purchased from Braskem (Sao Paulo, Brazil) and used as polymer matrix. Hemp fibers with size included in the 2-6 mm range were provided by AgroChanvre (Barenton, France). Their retting lasted 38 days and their cellulose, hemicelluloses, lignin and lipophilic extractives rates of 82, 8, 5 and 3 wt% respectively were determined by successive chemical extractions based on TAPPI T264, ASTM D1104 standards. Two hemp fibers loading 10 wt% (PP10) and

30 wt% (PP30) were tested (Table 1). Maleic anhydride grafted polypropylene (MA-g-PP) with a 1 wt% grafting rate, under the trademark Orevac CA100 and supplied by Arkema (France), was added at 3.1 wt% of PP as coupling agent.

Table 1 - Designation of materials

	Composition (wt%)		
	PP	**Hemp fibers**	**MA-g-PP**
PP	100	-	-
PP10	87.3	10	2.7
PP30	67.9	30	2.1

I.2.2 Process conditions

Prior to extrusion, hemp fibers and MA-g-PP have been dried for 15 h at 60 °C to remove residual water. Granules of PP and MA-g-PP were mixed with hemp fibers in a BC21 Clextral co-rotating twin-screw extruder (L/D = 36 with D = 25 mm) with the following temperature profile 190-190-190-180-175-175-175 °C from feed to die and a screw speed of 220 rpm. Then, pellets were dried in an air-circulating oven for 3 days at 60 °C. Finally, extruded pellets were injection molded into specimens in a Krauss Maffei KM50-T180CX at 210 °C with an injection speed of 30 $cm^3.s^{-1}$. Square samples of 100 × 100 × 2 mm^3 were obtained.

I.2.3 Weathering

Square samples were exposed in the South West of France (Pau) under flat windshield glass to simulate car interior environment according to ISO 877-2:2011 standard (Figure 1). The exposition panels were oriented towards South at 45° with the ground. Interior environment was naturally ventilated thanks to holes located at the top and bottom of the stainless steel boxes 2 hours per day. The exposure started in September 2015 and finished in September 2016 in order to study long-term ageing effects. Temperature T (°C) and relative humidity RH (%) were monitored (Figure 2). The maximum temperature and relative humidity values reached over the weathering were respectively 89 °C and 95 % whereas the minimum values were -5 °C and 3 %. Three samples of each material PP, PP10 and PP30 taken after 1, 2, 3, 6, 9 and 12 months of exposition were analyzed at the laboratory.

Figure 1 - Under windshield glass exposure racks

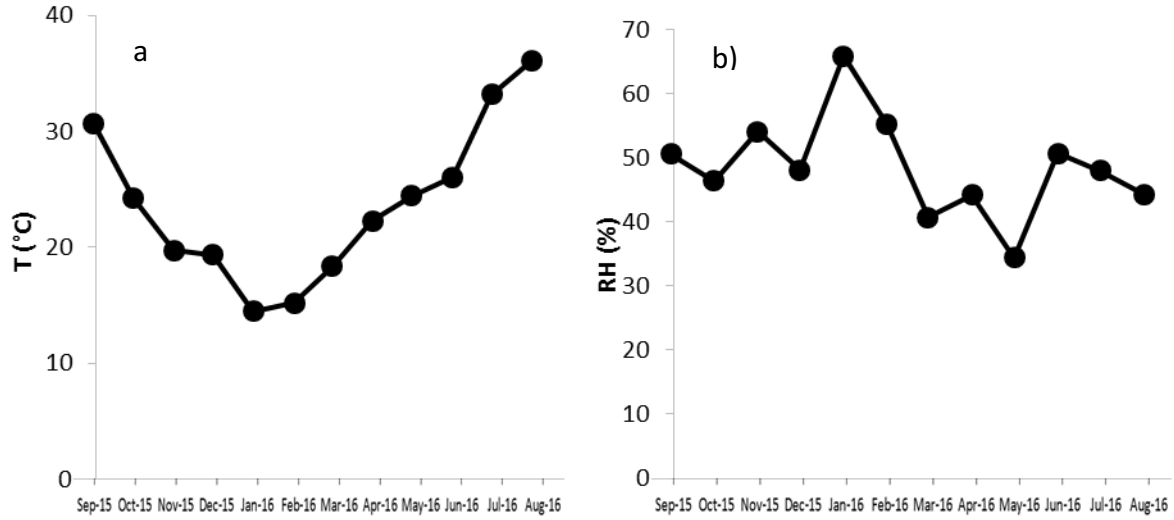

Figure 2 – Average monthly temperature (°C) (a) and relative humidity (%) (b) values in stainless steel boxes

I.2.4 Sampling and analytical methodology

VOCs were sampled according to a passive sampling method previously developed (Figure 3). It consists of two steps: firstly an emission 320-mL glass cell is deposited on the material in order to isolate its surface, the sampled area being 50 cm^2. Then, after 2 hours, time needed to reach material/air equilibrium [38], a Solid Phase MicroExtraction (SPME) fiber is introduced via a septum in the glass cell to extract emitted VOCs (Figure 3B). Then the fiber was thermally desorbed in a Varian CP-3800 gas chromatograph (GC) injector. A 1200Q quadrupole mass spectrometer (MS) was used for identification whereas a flame ionization detector (FID) (Varian, Les Ulis, France) was used for quantification. Separation was achieved

using a polydimethylsiloxane (PDMS) 5% phenyl capillary column of 60 m × 0.25 mm i.d. x 1 µm film thickness. The complete analytical procedure is detailed elsewhere [40].

Two different analyses were performed on non-weathered and weathered samples: VOCs screening to identify and quantify the widest range of emitted compounds, and specific analysis of formaldehyde and acetaldehyde which are classified as CMR [41]. For VOCs screening, a polydimethylsiloxane-divinylbenzene-carboxen fiber (PDMS/DVB/CAR, 50/30 µm) was selected. For formaldehyde and acetaldehyde, a polydimethylsiloxane-divinylbenzene (PDMS/DVB, 65 µm) fiber impregnated with *O*-(2,3,4,5,6-pentafluorobenzyl)hydroxylamine hydrochloride (PFBHA) (Fluka, Brucks, Switzerland) was used [40,42]. The two SPME fibers were purchased by Supelco (Bellefonte, USA). Two sampling temperatures, 23 °C and 80 °C, were tested to simulate ambient and extreme car interior conditions. For the two fibers, at 23 °C, an extraction time of 20 min was chosen from previous work [43]. At 80°C, an extraction time of 5 min was determined as a good compromise between sensitivity and short-time sampling. All samplings were conducted in triplicates to evaluate the measurement repeatability.

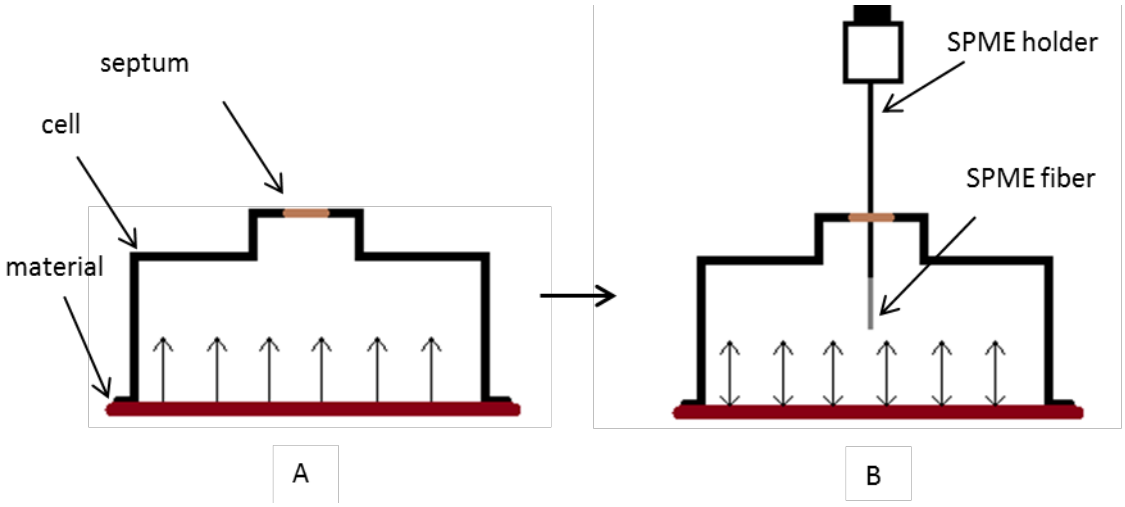

Figure 3- Schematic representation of the emission cell-SPME system (A: establishment of the material/air equilibrium, B: SPME sampling of VOCs)

I.2.5 Quantitative analysis

For the screening analysis using PDMS-DVB-CAR fiber, VOCs were quantified as toluene equivalent using FID response since it is proportional to the effective carbon atoms number in the molecule [20]. Standard gas of toluene was generated by a continuous syringe

injection system supplied by Calibrage (Saint Chamas, France) equipped with a syringe pump (PHD 2000, Harvard Apparatus, Les Ulis, France) [43]. Covered toluene concentrations ranged from 17 to 388 µg.m^{-3} for the 20 min-sampling and 67 to 1553 µg.m^{-3} for the 5 min-sampling. Furfural and 2-furanmethanol, compounds specific to hemp fibers and listed as CMR substances [41] were specifically quantified. Standard gases were also generated by a continuous syringe injection, as described above.

For the specific analysis of formaldehyde and acetaldehyde by PDMS/DVB fiber impregnated with PFBHA, standard gases were generated according to the permeation method [44]. The device used was supplied by Calibrage (Saint Chamas, France).

For the two SPME methods, the Limits of Detection (LOD) are in the µg.m^{-3} order level for the 20 min-sampling and are around 10 µg.m^{-3} for 5 min-sampling.

I.3. Results and Discussion

I.3.1 Chemical families evolution

I.3.1.1 Non-weathered state

The concentration of VOCs emitted by non-weathered PP, PP10 and PP30 and sampled by PDMS/DVB/CAR fiber was measured at two temperatures (23 and 80 °C). The last temperature was chosen to simulate thermal conditions that could be found in vehicles facing South in summer. No VOC was detected before weathering at ambient temperature. As expected, a higher temperature promoted the emission of volatile products. However, some VOCs were detected for all materials at 80 °C. Their levels are shown by chemical family in Figure 4. All VOCs surface concentration, which represents the concentration of all detected VOCs (PDMS-DVB-CAR fiber), increased with the hemp fibers loading from 7 ± 0.6 mg.m^{-3} for virgin PP to 10 ± 1 mg.m^{-3} for PP30 at non-weathered state. Thus, hemp fibers rate had an influence on VOCs concentration. These products were probably generated by the thermo-oxidative degradation during the extreme sampling temperature conditions during the extrusion and injection molding process. PP mainly emitted aliphatic hydrocarbons either caused by polymerization defects or thermal degradation of polymer chains during processing or sampling. A few oxygenated compounds were also identified due to the high process temperatures which induced oxidation of polymer chains. However, the

concentration of oxygenated products like alcohols, carboxylic acids, ketones and aldehydes increased with the fiber loading to the detriment of alkanes. Indeed, some oxygenated compounds specific to vegetal fibers were emitted at the mg.m^{-3} level, but also phenolic compounds and nitrogen containing products (azines) at about 400 µg.m^{-3} and 60 µg.m^{-3} in addition to aliphatic hydrocarbons and oxygenated VOCs emitted by the matrix.

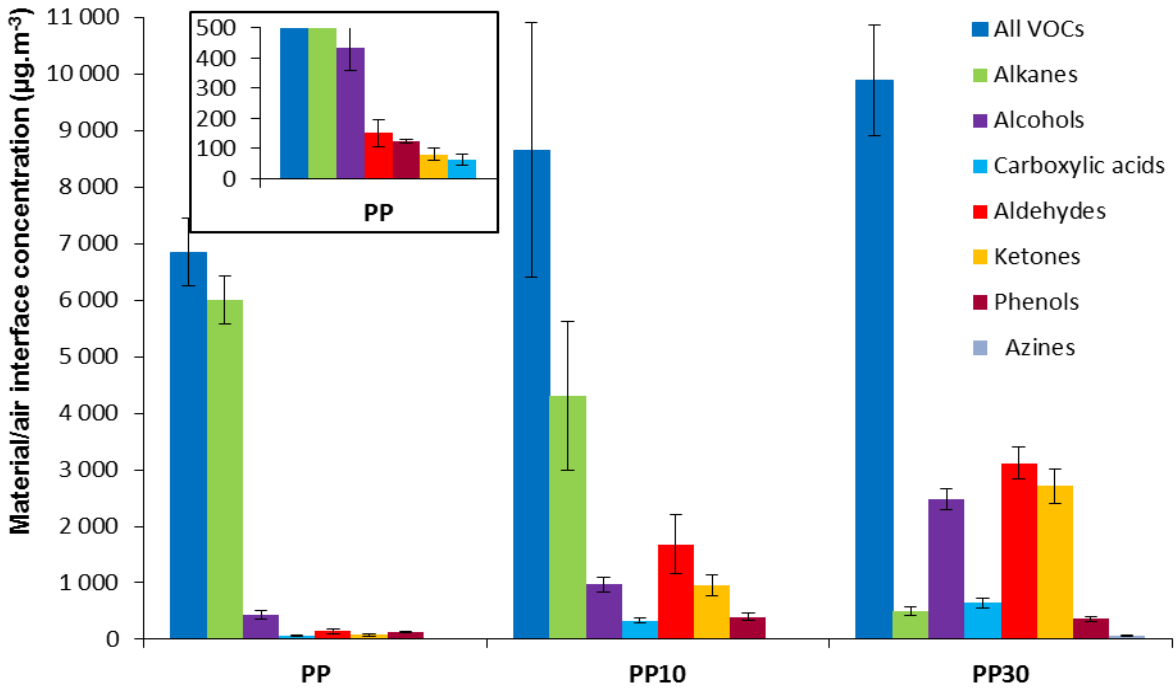

Figure 4 - VOCs chemical families at non weathered state (PDMS/DVB/CAR SPME fiber – sampling at 80 °C)

I.3.1.2 Weathered states

I.3.1.2.1 Sampling at ambient temperature (23 °C)

The material/air interface concentration evolution of VOCs emitted by all materials over under glass exposition and analysed by PDMS/DVB/CAR fiber at 23 °C is plotted in Figure 5. This concentration increased during the weathering suggesting that VOCs were issued from materials degradation during the weathering and caused by several parameters such as UV rays exposition, temperature and high humidity (Figure 2). Only ketones and carboxylic acids were detected. These oxygenated families come from the polymer chains and hemp fibers oxidation under high temperatures and UV rays, key factors favoring free-radical mechanisms involving reactions with oxygen from the atmosphere [45].

For these compounds, the surface concentration increase was more significant for the highest fiber loading whereas PP exhibited less significant variation. Indeed, oxygenated compounds level increased by 45 times for PP30 whereas it increased by 15 times for neat PP in 11 months. This means that weathering affected more hemp fibers stability than PP one, demonstrating that the under glass weathering had a bigger influence on degradation products emission from biocomposites. As concerns PP10, its emission level was similar to PP one during the first 9 months. For instance, the surface concentrations of oxygenated products emitted after 6 months of ageing were 22 ± 3 µg.m^{-3} and 29 ± 14 µg.m^{-3} for PP and PP10 respectively. Then, the concentration drastically rose from 65 to 638 µg.m^{-3} for PP10 from 9 to 12 months. Otherwise, standard deviations were high after weathering (until 168 µg.m^{-3} for one-year weathered PP30) because of a temperature inhomogeneity in stainless steel supports raised during the exposition.

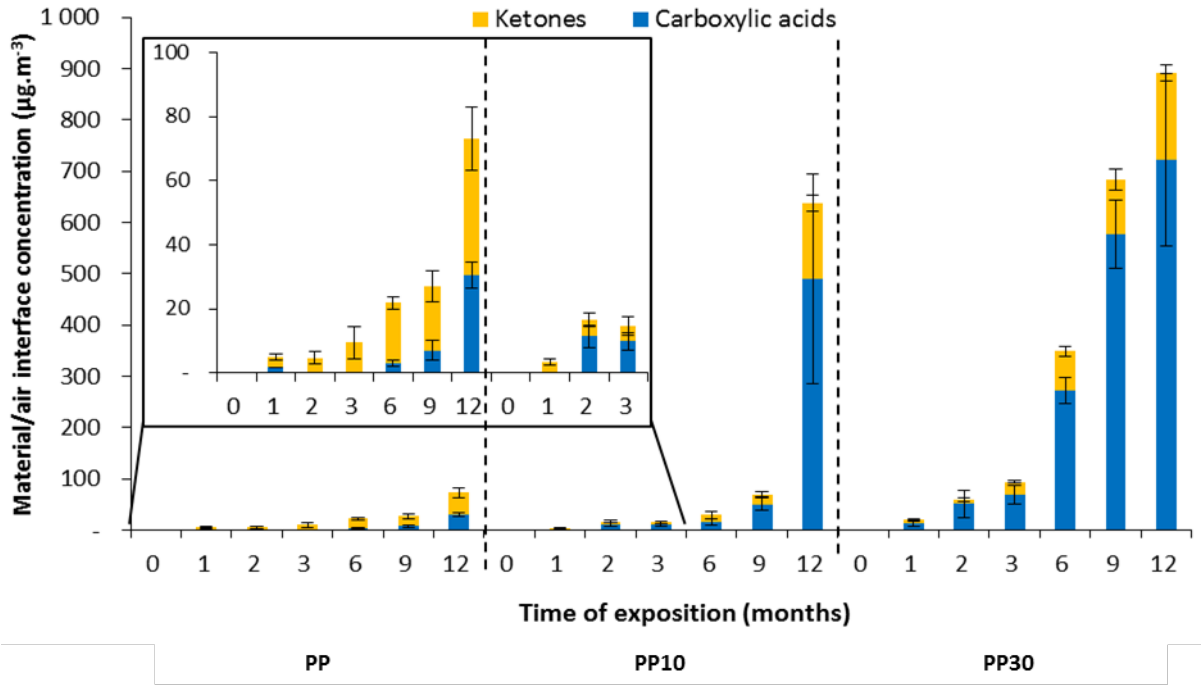

Figure 5 - Evolution of chemical VOCs over the weathering (PDMS/DVB/CAR SPME fiber – sampling at 23 °C)

I.3.1.2.2 Sampling at extreme temperature (80 °C)

The total concentration (sum of all chemical families concentrations) evolution during the weathering of VOCs emitted by PP, PP10 and PP30 and sampled at 80 °C is represented in Figure 6. During the first three-month stage of exposition, global concentrations largely exceeded values found under ambient conditions whatever the weathering time. Indeed,

after 3 months of exposition, all VOCs level increased from 94 ± 22 µg.m^{-3} at 23 °C to 22196 ± 2648 µg.m^{-3} at 80 °C for the highest fiber loading. The VOCs concentrations for PP and PP10 were quite similar and did not significantly vary whereas PP30 emitted VOCs at higher concentrations. After this short period, the concentration of VOCs emitted by biocomposites drastically increased by 10 and 5 times for PP10 and PP30 in 10 months whereas PP emitted VOCs at the same level. This global observation confirms that natural weathering of hemp fibers is responsible to the VOCs concentration variation demonstrating that biocomposites are more subjected to weather conditions.

The evolution of VOCs surface concentrations measured at each time of exposition is also illustrated by main chemical family. As regards PP, C_9-C_{15} alkanes were among the predominant VOC species sampled all along the weathering. However, ketones, aldehydes and carboxylic acids proportion increased and represented 28% of VOCs surface concentration after 1 year. In addition, the substituted phenols detected in virgin PP identified as 2,6-bis(1,1-dimethylethyl)phenol and 2,6-di-butyl-2,5-cyclohexadiene-1,4-dione were derived from the Irganox L140® and Irganox 1010® antioxidants respectively probably incorporated during manufacturing process to stabilize the polymer and prevent its thermo-oxidation [31].

Higher concentration variations were observed for biocomposites. Indeed, the overall surface concentration of oxygenated compounds emitted by PP30 rose from 10 ±1 mg.m^{-3} at non-weathered state to 53 ±9 mg.m^{-3} at the final weathering stage. Moreover, carboxylic acids and ketones concentrations mostly contributed to the final level. As previously observed, this drastic increase with weathering time was due to the oxidation of both polymer and vegetal fibers caused by high temperatures and UV rays effects during the exposition. As already seen for ambient temperature sampling, PP10 presented a same VOCs emission profile as PP30 after 1 year. This suggests that hemp fibers proportion on PP10 surface could increase with the weathering time to the detriment of polymer matrix. Moreover, studies reporting the surface topography evolution during an ageing showed a roughness increase on natural fillers composites surface caused by fillers proportion increase [23,30].

These higher variations observed for biocomposites can be explained by their lower chemical stability than polymer. Indeed, the presence of chromophoric structures in natural fillers enhances energy absorption in UV rays range so much so that their reactivity is favored [26,46].

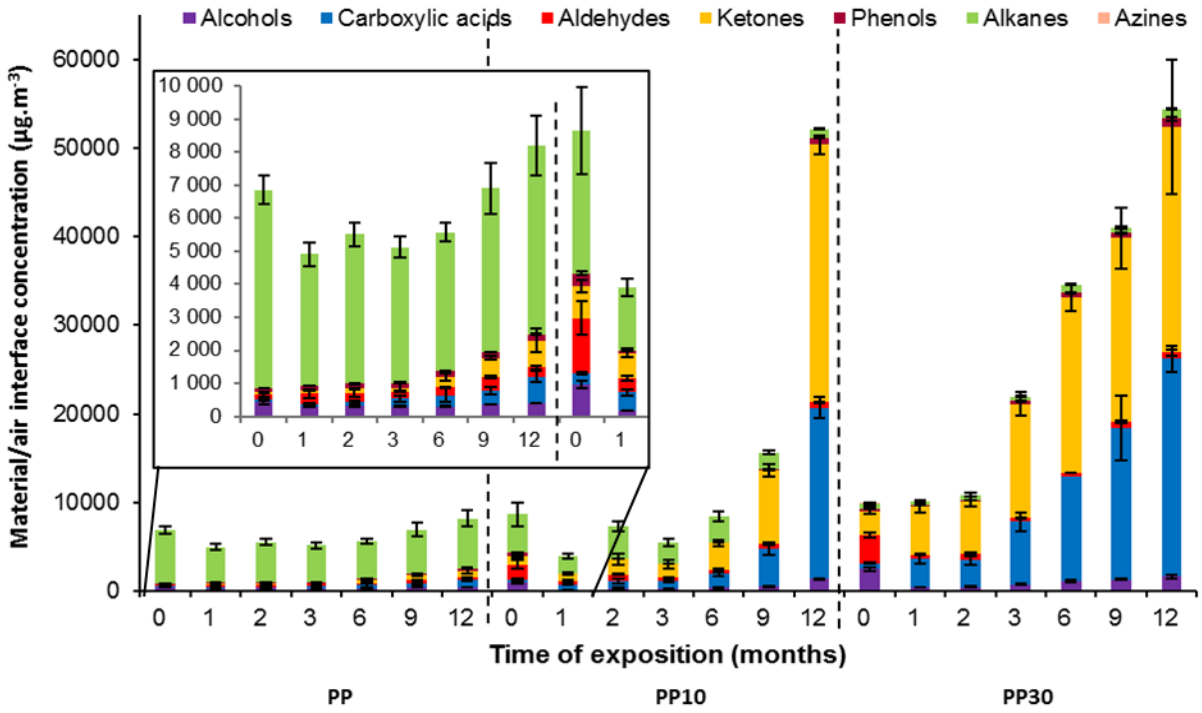

Figure 6 - Evolution of chemical families over the weathering (PDMS/DVB/CAR SPME fiber – sampling at 80°C)

I.3.2 Individual VOCs evolution

Surface concentrations of all VOCs identified before and after one-year weathering and evolved from virgin PP, PP10 and PP30 at 23 and 80 °C are resumed in Table 2. Branched and linear aliphatic hydrocarbons were gathered into groups having same carbon atoms number (9 to 15). At non-weathered state and 80 °C, 17 more volatile products were detected for PP30 than for PP.

For sampling at 23°C, acetone, acetic acid, propionic acid and 2,4-pentanedione were detected after weathering. These carbonyl products were emitted by weathered neat PP, PP10 and PP30, except propionic acid which was only emitted by biocomposites, suggesting that it was only issued from hemp fibers degradation. Also, acetic acid concentration largely exceeded the other products ones, especially for reinforced materials. Indeed, its surface concentration approximately reached 670 µg.m^{-3} after one-year exposition of PP30 that is 10

times higher than acetone. This result can be explained by an acidic catalysis favored by the presence of lignin in hemp fibers and resulting in a release of acetic acid as major product [47,48].

For sampling at 80°C, although the compounds nature differed, the number of detected VOCs did not significantly change for PP and PP30 before and after weathering. The most drastic change was observed for the group of ketones emitted by the biocomposites for which linear and cyclic molecules configurations were not similar between unweathered and weathered samples. Carboxylic acids, which also represented a considerable proportion of the overall concentration (37 % and 45 % of total concentration for one-year weathered PP10 and PP30 respectively), were mainly issued from main natural components decomposition but probably also from fatty acids constituting vegetal fillers too.

Table 2 - VOCs emitted by PP, PP10 and PP30 before and after one-year weathering (sampling at 23 and 80 °C) (NW: Non-weathered, W: weathered, SD: Standard deviation)

	Surface concentration ± SD (µg.m^{-3})								
	PP			PP30			PP10		
	W (23 °C)	NW (80 °C)	W (80 °C)	W (23 °C)	NW (80 °C)	W (80 °C)	W (23 °C)	NW (80 °C)	W (80°)
Aliphatic hydrocarbons									
C_9	-	65 ±5	179 ±8	-	-	-	-	-	-
C_{10}	-	786 ±14	1625 ±367	-	239 ±11	-	-	590 ±25	-
C_{11}	-	550 ±64	1061 ±92	-	104 ±2	-	-	291 ±52	-
C_{12}	-	820 ±27	692 ±116	-	114 ±8	-	-	575± 8	-
C_{13}	-	1768 ±50	1241 ±240	-	181 ±32	631 ±173	-	1230 ±136	833 ±39
C_{14}	-	339 ±117	140 ±16	-	59 ±5	260 ±8	-	238 ±20	139 ±3
C_{15}	-	1672 ±50	771 ±52	-	-	305 ±21	-	1388 ±26	-
Ketones									
Acetone	24 ±5	25 ±8	333 ±34	45 ±5	36 ±15	1108 ±406	35 ±7	15 ±1	1074 ±22
1-hydroxy-2-propanone	-	-	-	-	420 ±81	796 ±375	-	122 ±15	911 ±109
2,3-butanedione	-	-	-	-	84 ±7	-	-	31 ±5	-
2-pentanone	-	-	-	-	-	426 ±273	-	-	453 ±28
3-hydroxy-2-butanone	-	-	-	-	36 ±4	-	-	-	-
3-penten-2-one	-	-	-	-	-	927 ±52	-	-	619 ±71
2(5H)-furanone	-	-	-	-	355 ±38	-	-	157 ±10	-
Butyrolactone	-	-	-	-	230 ±10	324 ±125	-	123 ±9	295 ±5
Cyclopentene-1,3-dione	-	-	-	-	157 ±11	-	-	-	-
5-methyl-2(5H)-furanone	-	-	-	-	68 ±7	-	-	27 ±7	-
Cyclopentane-1,2-dione	-	-	-	-	89 ±7	-	-	42 ±1	-
5-methyl-2(3H)-furanone	-	-	-	-	40 ±14	-	-	53 ±16	-
Pentane-2,4-dione	19 ±5	-	441 ±106	124 ±10	27 ±1	7399 ±4216	-	-	7368 ±211
4-hydroxy-2-pentanone	-	-	-	-	-	255 ±161	-	-	275 ±21
1-(1H-pyrrol-2-yl)-ethanone	-	-	-	-	114 ±4	-	-	87 ±3	-
1-(2-furanyl)-ethanone	-	-	-	-	30 ±3	-	-	27 ±2	-
3-methyl-2,5-furandione	-	-	-	-	-	628 ±174	-	-	746 ±21
2,5-dihydro-3,5-dimethyl-2-furanone	-	-	-	-	-	267 ±149	-	-	218 ±8

3-methyl-1,2-cyclopentanedione	-	-	-	-	101 ±17	-	-	42 ±6	-
3-methyl-3-hexen-2-one	-	-	-	-	-	168 ±83	-	-	127 ±2
(1-(3,3-dimethyloxiranyl)-ethanone	-	-	-	-	-	663 ±27	-	-	872 ±5
3,4-epoxy-3-ethyl-2,3-butanone	-	-	-	-	-	361 ±53	-	-	313 ±6
2,5-hexanedione	-	-	-	-	-	868 ±107	-	-	521 ±40
1-acetyloxy-2-propanone	-	-	-	-	366 ±11	377 ±153	-	147 ±17	451 ±10
2-pentanone, 4-hydroxy-4-methyl	-	65 ±13	82 ±25	-	87 ±10	3125 ± 137	-	79 ±15	3592 ±82
6-methyl-5-hepten-2-one	-	-	49 ±1	-	-	-	-	-	-
4-methoxy-2-heptanone	-	-	-	-	-	162 ±64	-	-	189 ±6
Maltol	-	-	-	-	145 ±19	-	-	43 ±2	-
Levoglucosenone	-	-	-	-	97 ±4	-	-	68 ±9	-
3,4-dimethyl-2,5-furanedione	-	-	-	-	-	118 ±32	-	-	-
2,4,4-trimethylbut-2-enolide	-	-	-	-	-	1314 ±20	-	-	1990 ±146
3-ethyl-2-hydroxy-2-cyclopenten-1-one	-	-	-	-	72 ±9	-	-	-	-
5-hydroxy-4,5-dimethyl-2,5-(2H)-furanone	-	-	-	-	-	754 ±118	-	-	968 ±44
3,3-dimethyl-2,4-pentanedione	-	-	-	-	-	157 ±55	-	-	135 ±1
1-(2,4-dimethyl-furan-3-yl)-ethanone	-	-	-	-	-	1063 ±243	-	-	1807 ±149
3-acetonyl cyclopentanone	-	-	-	-	-	1899 ±70	-	-	2324 ±120
2,4-dihydro-5-hydroxy-3,3,5-trimethyl-2-furanone	-	-	-	-	-	303 ±48	-	-	330 ±18
4-acetonylcyclohexanone	-	-	-	-	-	277 ±63	-	-	333 ±5
4,6-dimethyl-2-heptanone	-	-	-	-	-	361 ±81	-	-	278 ±2
2-methyl-3-nonanone	-	-	-	-	-	110 ±9	-	-	85 ±11
3,6-dimethyloctan-2-one	-	-	-	-	-	265 ±56	-	-	344 ±4
6,10-dimethyl-5,9-undecadien-2-one	-	-	-	-	48 ±0	-	-	-	-
4,4,5,5-tetramethyl-2,7-octanedione	-	-	-	-	-	172 ±48	-	-	212 ±26
Carboxylic acids									
Acetic acid	30 ±4	26 ±1	542 ±61	667 ±152	397 ±62	18304 ±620	452 ±200	179 ±74	13008 ±874
Propionic acid	-	-	-	56 ±16	-	1403 ±3	39 ±4	-	839 ±75
Crotonic acid	-	-	-	-	-	3332 ±612	-	-	3682 ±175
Methacrylic acid	-	-	120 ±70	-	-	-	-	-	-
Hexanoic acid	-	24 ±8	81 ±25	-	130 ±8	213 ±48	-	69 ±15	199 ±17
Benzoic acid	-	-	-	-	45 ±6	-	-	44 ±13	-
Heptanoic acid	-	-	-	-	-	115 ±15	-	-	87 ±9
Octanoic acid	-	25 ±7	62 ±4	-	70 ±10	201 ±14		43 ±22	238 ±1
7-oxooctanoic acid	-	-	-	-	-	271 ±26	-	-	389 ±2
Nonanoic acid	-	-	-	-	-	266 ±27	-	-	304 ±2

Dehydroacetic acid	-	-	-	-	-	473 ±55	-	-	618 ±41
Aldehydes									
Methacrolein	-	-	-	-	-	291 ±44	-	-	107 ±76
Furfural	-	-	-	-	1611 ±20	-	-	703 ±15	-
Furfuryl formate	-	-	-	-	38 ±4	-	-	-	-
Furfuryl acetate	-	-	-	-	43 ±4	-	-	-	-
5-methylfurfural	-	-	-	-	660 ±30	-	-	245 ±14	-
Benzaldehyde	-	-	-		93 ±0	77 ±10	-	28 ±11	
Octanal	-	26 ±6	51 ±1	-	29 ±7	54 ±15	-	27 ±5	41 ±3
Nonanal	-	-	-	-	160 ±28	94 ±14		259 ±27	149 ±2
2,4-dimethyl-pentanal	-	-	-	-	-	64 ±1	-	-	89 ±9
2-nonenal	-			-	65 ±7	-	-	27 ±10	-
Decanal	-	89 ±28	135 ±1	-	119 ±30	121 ±16	-	128 ±12	146 ±1
1-(1,1-dimethylethyl)methyl-2-propenal	-	-	-	-	-	741 ±71	-	-	882 ±42
Dodecanal	-	40 ±9	57 ±30	-	63 ±3	-	-	53 ±8	-
1H-pyrrole-2-carboxaldehyde	-	-	-	-	121 ±22	-	-	79 ±6	-
Vanillin	-	-	-	-	159 ±27	-	-	-	-
Alcohols									
2-methyl-2-propen-1-ol	-	-	-		-	602 ±110	-	-	293 ±41
2-furanmethanol	-	-	-	-	2319 ±176	-	-	641 ±89	-
2-ethyl-1-hexanol	-	52 ±11	52 ±4	-	79 ±9	176 ±17	-	101 ±7	148 ±1
2-isopropyl-5-methyl-1-heptanol	-	206 ±9	214 ±1	-	44 ±1	-	-	166 ±15	-
4-methyl-1,6-heptadien-4-ol	-	-	-	-	-	832 ±46	-	-	889 ±23
2-ethyldecanol	-	-	62 ±1	-	-	-	-	-	-
Tridecanol	-	63 ±6	50 ±4	-	-	-	-	-	-
2-methyltridecanol	-	89 ±50	26 ±1	-	-	-	-	59 ±9	-
Phenols									
3,5-dimethylphenol	-	-	-	-	-	471 ±75	-	-	642 ±2
2-methoxy-4 vinylphenol	-	-	-	-	195 ±28	-	-	-	-
2,6-bis(1,1-dimethylethyl)phenol	-	124 ±7	195 ±22	-	163 ±16	120 ±11	-	392 ±60	158 ±7
Furans									
2,4-dimethylfuran/2,5-dimethylfuran	-	-	82 ±14	-	-	2462 ±143	-	-	990 ±82
Azines									
Methylpyrazine	-	-	-	-	25 ±2	-	-	-	-
N-acetyl-4(H)-pyridine	-	-	-	-	38 ±4	-	-	-	-
Non-quantified (N.Q.)							-		
C_{15} (1 VOC)	-	N.Q.	N.Q.	-	N.Q.	N.Q.	-	N.Q.	N.Q.
2,6-di-butyl-2,5-cyclohexadiene-1,4-dione	-	N.Q.	N.Q.	-	N.Q.	N.Q.	-	N.Q.	N.Q.

I.3.2.1 Polymer by-products

The evolution of polymer derivatives during the weathering is displayed on Figure 7 for PP and PP30. Concerning neat PP, long polymer chains between C_9 and C_{15} were detected. However, C_9, C_{10} and C_{11} alkane concentrations increased during the ageing to the detriment of C_{14} and C_{15} longer alkanes. Thus, this result suggests that the weathering induced polymer chain scissions which favored shorter chains formation. As regards C_{12} and C_{13}, their concentration decreased at the first stage of exposition then remained constant for 11 months.

As observed previously, PP30 emitted alkanes at lower concentrations. However, C_{13}, C_{14} and C_{15} levels increased during the exposition whereas C_9, C_{10} and C_{12} alkanes were no longer detected. This may be due to polymer derivatives emission hindrance at non-weathered state caused by the presence of physical entanglement of hemp fibers. Then, the degradation of vegetal fibers leads to fibers network overthrow inducing increase of long alkanes emission with weathering time.

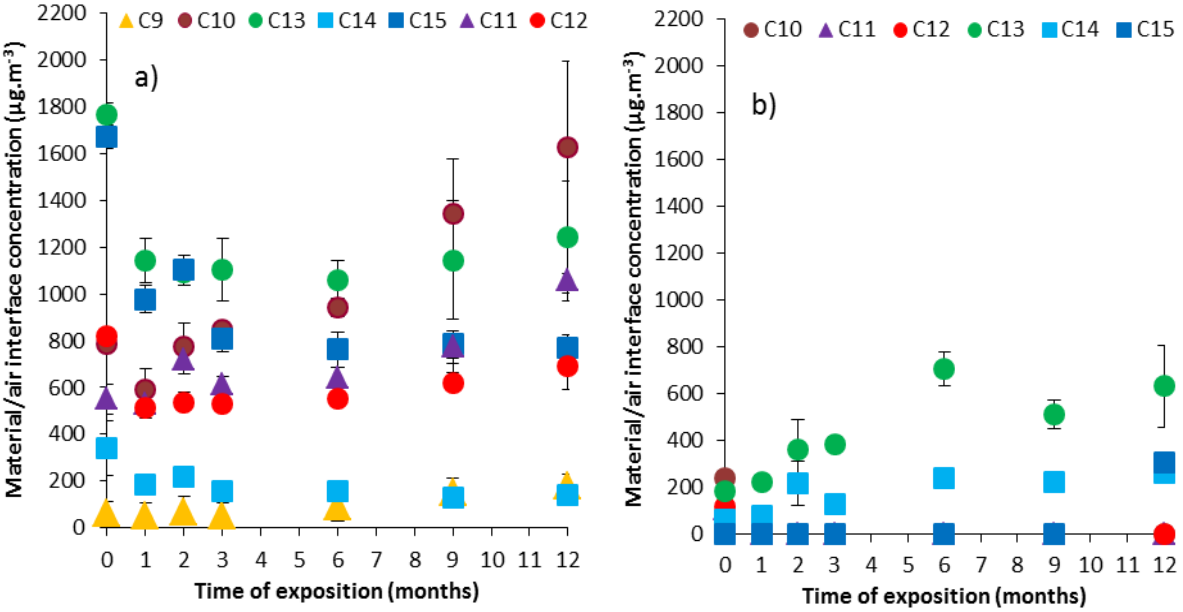

Figure 7 – Variations of alkanes emissions for PP (a) and PP30 (b) over the weathering (PDMS/DVB/CAR SPME fiber – sampling at 80°C)

I.3.2.2 Cellulose and hemicelluloses by-products

The evolution of VOCs issued from cellulose and hemicelluloses degradation was individually followed. Their surface concentrations variations measured for the highest fiber loading biocomposite are represented in Figure 8 for furan and cycloketone products.

Some products like furfural (1.6 ±0.0 $mg.m^{-3}$) and 2-furanmethanol (2.3 ±0.2 $mg.m^{-3}$), present for unaged samples, were no longer detected after the weathering of biocomposites. Other furans were emitted and, contrary to non-weathered state, mainly methyl substituted furanones appeared. After 6 months of weathering, their concentrations stagnated except for dimethylfuran, the lightest furan molecule, increasing all along the ageing. This last trend can be explained by a reaction equilibrium favored towards short carbonyl fragments formation, continually increasing, rather than furanone derivatives formation. Also, the higher temperatures observed during the second half-year exposition (Figure 2) could favor shorter products emissions due to long-term degradation favoring low molecular weight products emission. However, the rising release of dimethylfuran can be due to, contrary to other furan molecules, the contribution of polymer matrix to this product emission in addition to hemp fibers [49].

As regards cyclic alkane products, two acetonyl substituted cyclic ketone substances were formed during the ageing. Otherwise, 3-acetonylcyclopentanone was the main VOC released among all substances belonging to this group of compounds. This molecule present in great quantity (almost 2 $mg.m^{-3}$ after 1 year) is supposed to mainly originate from cellulose source rather than hemicelluloses [47,50]. Moreover, the lower thermal stability of hemicelluloses may mainly imply volatile products formation at the first stage of exposition.

I.3.2.3 Lignin by-products

Phenolic monomeric products emitted by PP30 were linked to the thermal breakdown of lignin, amorphous cross-linked phenolic polymer contained in vegetal fibers (Figure 8). Whatever the weathering duration, phenolic molecules concentrations are lower than carbohydrates derived VOCs. It may be explained by the lower proportion of lignin present in hemp fibers, which approximately accounts for less than 10 wt% whereas the holocellulose part almost represents 85 wt% [51,52]. Moreover, hemp fibers having undergone a long retting time to facilitate separation of the fiber from the stem, it could lead to a lower lignin

proportion since chromophores present in lignin are sensitive to retting parameters such as solar radiation [53–55].

Methoxy substituted phenol groups like 4-hydroxy-3-methoxybenzaldehyde (vanillin) and 2-methoxy-4-vinylphenol (4-vinylguaiacol) disappeared after weathering. These compounds were originated from a lignin primary decomposition [56]. 3,5-dimethylphenol, which is an alkyl substituted aromatic ring, replaced them after ageing as secondary decomposition product. The last one involves reactions in vapor phase or heterogeneous gas/solid reactions whereas primary reactions occur in solid phase. Indeed, bonds cleavage of preformed guaiacol structures can induce alkyl substituted phenols formation.

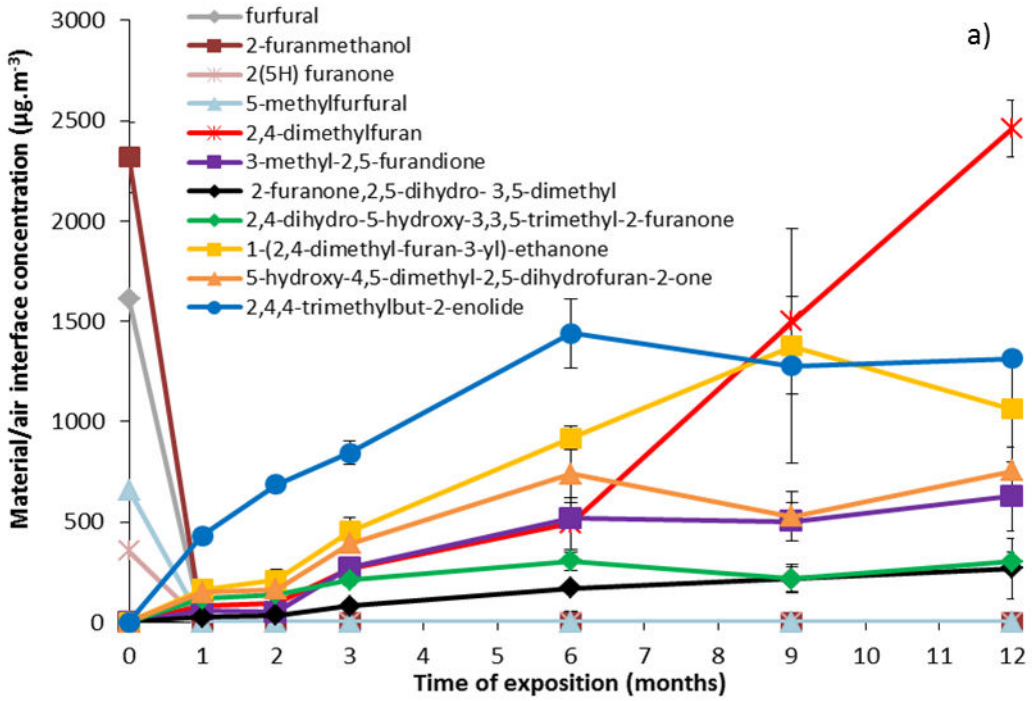
a)
furfural
2-furanmethanol
2(5H) furanone
5-methylfurfural
2,4-dimethylfuran
3-methyl-2,5-furandione
2-furanone,2,5-dihydro- 3,5-dimethyl
2,4-dihydro-5-hydroxy-3,3,5-trimethyl-2-furanone
1-(2,4-dimethyl-furan-3-yl)-ethanone
5-hydroxy-4,5-dimethyl-2,5-dihydrofuran-2-one
2,4,4-trimethylbut-2-enolide
Material/air interface concentration (µg.m-3)
Time of exposition (months)

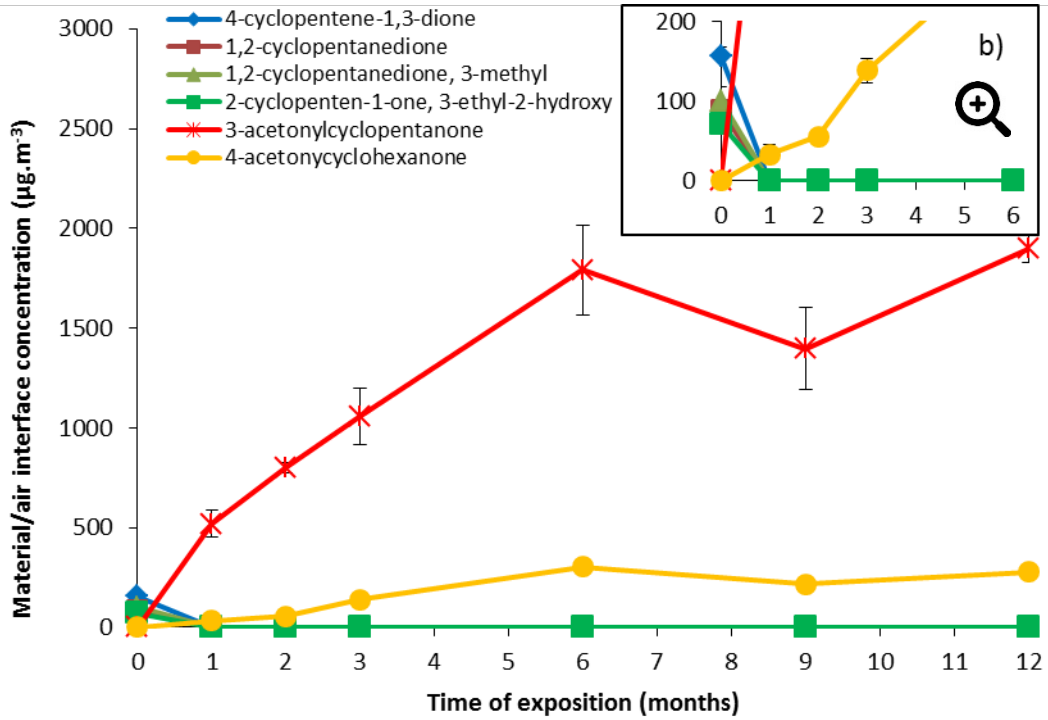
b)
4-cyclopentene-1,3-dione
1,2-cyclopentanedione
1,2-cyclopentanedione, 3-methyl
2-cyclopenten-1-one, 3-ethyl-2-hydroxy
3-acetonylcyclopentanone
4-acetonycyclohexanone
Material/air interface concentration (µg.m-3)
Time of exposition (months)

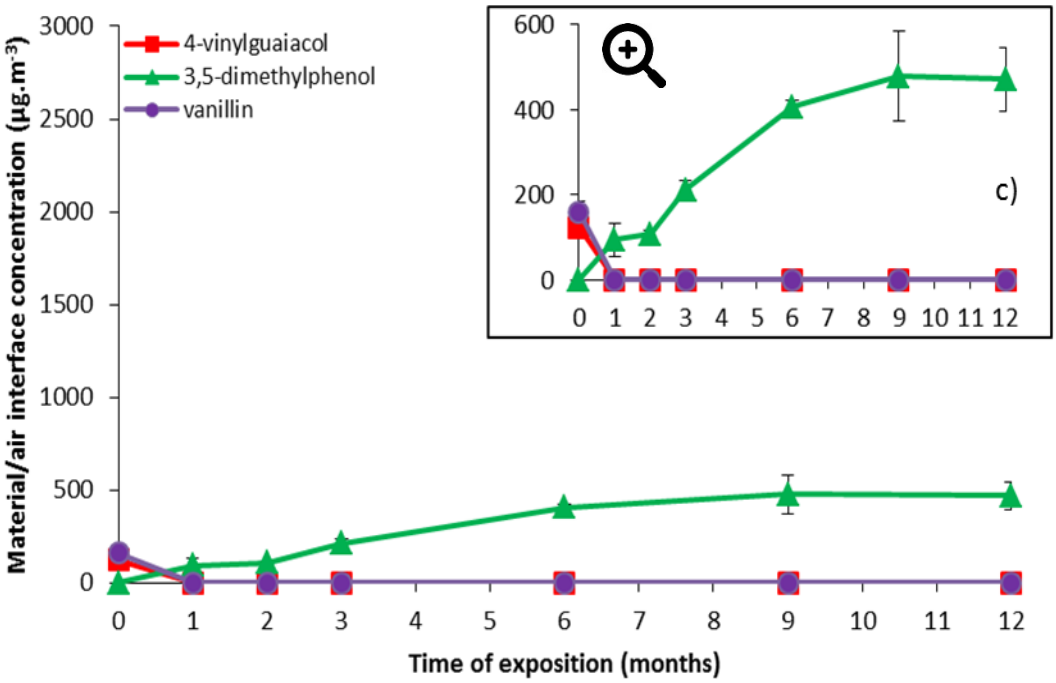

Figure 8 – Variations of major furan (a), cyclic ketones (b) and phenolic VOCs (c) released by PP30 over the exposition (PDMS/DVB/CAR SPME fiber – sampling at 80°C)

I.3.3 Impact on indoor air quality (IAQ)

According to their well-known toxicity [21,57], formaldehyde and acetaldehyde emissions were specifically monitored thanks to PDMS-DVB fiber impregnated with PFBHA. Indeed, formaldehyde is carcinogenic to humans whereas acetaldehyde is classified in C2 category in CLP regulation meaning that it is suspected of being carcinogenic [41] (Table 3). Concentrations were measured after 0, 6 and 12 months of weathering (Figure 9). At non-weathered state, aldehydes concentrations increased with the fiber loading. This suggests that they mainly originated from hemp fibers degradation due to high process temperatures. Otherwise, the concentration increased for all materials during the exposition, especially for PP30, reaching 20.3 ±0.9 µg.m^{-3} (formaldehyde) and 39.5 ±0.3 µg.m^{-3} (acetaldehyde) after one year.

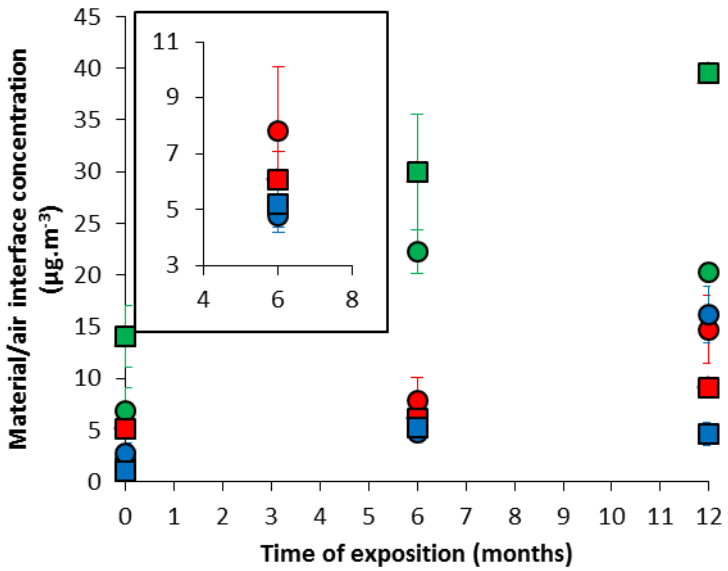

Figure 9 – Formaldehyde (spheres) and acetaldehyde (squares) surface concentrations over the weathering (blue: PP, red: PP10, green: PP30) (PDMS/DVB SPME fiber impregnated with PFBHA – sampling at 23°C)

Recently, the vehicle indoor air quality (VIAQ) has been getting extensive attention as a result of various hazardous substances detection. Hence, this part focuses on the possible toxicity or noxiousness of some identified products.

Furfural (2-furaldehyde) and 2-furanmethanol (furfuryl alcohol), emitted by biocomposites at high surface concentration in high-heat conditions (1.6 ±0.0 and 2.3 ±0.2 $mg.m^{-3}$ respectively for PP30), are classified in C2 category (Table 3). Nevertheless, the biocomposites weathering induced their disappearance and would thus no longer have negative effects. Other substituted furan compounds appeared and could be of concern since furan molecule is presented as a C1B M2. Also, alkanes released at high level by the polymer heated at 80°C are also classified in C1B category. Otherwise, phenols coming from lignin component are notified as impacting organic pollutants and are classified as of concern.

Table 3 - CLP regulation of harmful substances (C1B: carcinogenic, M2: suspected to be mutagenic, C2: suspected to be carcinogenic, M3: substance of concern in reason of possible mutagenic effects)

Substances	CMR classification
Formaldehyde	C1B M2
Acetaldehyde	C2
Furan	C1B M2
2-furaldehyde	C2
Furfuryl alcohol	C2
C_{12}-C_{26} branched and linear alkanes	C1B
Phenols	M3

Table 4 resumes formaldehyde, acetaldehyde and TVOCs surface concentrations determined in this study. Limit values of indoor concentrations given by existing VIAQ guidelines and standards were gathered in Table 5. Only formaldehyde and acetaldehyde are concerned. It should be noticed that the data from tables 4 and 5 cannot be directly compared. Indeed, the relationship between indoor air concentration and surface concentration of a pollutant is deduced from the first Fick's law of diffusion and is given by equation 1, considering that the studied indoor environment (e.g. the car cabin) behaves as a continuous stirred reactor operating in steady state conditions [38].

$$Q_{ij} = h_{ij} \frac{A_j}{V} (C_{sij} - C_i) \qquad \text{Eq. 1}$$

with h_{ij} the convective mass transfer coefficient of pollutant i through the boundary layer over the material j ($m.s^{-1}$), A_j the surface area of the material j (m^2), V the volume of the studied indoor environment (m^3), C_{sij} the concentration of the pollutant i at the material surface and C_i the average indoor air concentration of the pollutant i ($\mu g.m^{-3}$).

Table 4 shows that surface concentrations of aldehydes slightly increased over the weathering but they are always lower than their respective indoor concentration limits. Hence, the materials studied here can be considered as very low emissive regarding these compounds and they would comply with the current VIAQ regulations.

Currently, no VIAQ standard or guideline has been found preconizing TVOCs limit concentration. However, as reported in the introductory part, TVOCs indoor concentration is an indicator of health effects. Relationship between TVOCs levels found in indoor air and

discomfort felt by individuals has been investigated through epidemiological studies [58]. Four exposure ranges were proposed that are a comfort (< 20 µg.m^{-3}), a multifactorial exposure (20-300 µg.m^{-3}), a discomfort (300-25,000 µg.m^{-3}), and a toxic (> 25,000 µg.m^{-3}) ranges. Weathered PP10 and PP30 can imply possible irritation and discomfort if other exposures interact according to this dose-response model. However, all materials may potentially cause more severe effects when they are heated at 80 °C. This assumption should be moderated by the fact that biocomposites are generally implemented with other materials (for example, door panels). Thus, linings and coatings may act as barrier and reduce biocomposite emission in indoor air, as observed for other material assemblies [59,60].

Table 4 - Formaldehyde, acetaldehyde and TVOCs levels (ST: sampling temperature)

		Surface concentration (µg.m^{-3})					
	ST (°C)	Before weathering			After weathering		
		PP	PP10	PP30	PP	PP10	PP30
Formaldehyde	**23**	2.8	2.24	6.9	16.2	14.7	20.3
Acetaldehyde	**23**	-	5.1	14.1	4.6	9.1	39.5
TVOCs	**23**	-	-	-	19	112	124
	80	6342	8322	9267	7676	35284	30849

Table 5 - Guideline and recommended standard limit values

	VIAQ limit values (µg.m^{-3})		
	JAMA (Japan)	GB/T 27630 (China)	No 2007-539 (Korea)
Formaldehyde	100	100	250
Acetaldehyde	48	50	-
TVOCs	-	-	-

I.4. Conclusion

The weathering had a higher impact on the evolution of VOCs types and emitted concentrations of biocomposites than of neat PP. VOCs emission level was influenced by the sampling temperature for all materials. This demonstrates the importance of ventilation in

case of car interior end-use under hot climatic conditions. At non-weathered state, the greater the fiber loading was, the higher the VOCs surface concentration was. Moreover, the VOCs emission drastically increased for the highest loading (PP30) after 12 months of weathering. Oxygenated products mostly contributed to the weathered biocomposites emission concentration, demonstrating an oxidative degradation due to UV radiation and high temperatures.

All products toxicity was checked and a potential impact on VIAQ was noted because of the release of some products issued from both PP and vegetal fibers. Even if their concentrations satisfy with current VIAQ regulation, this emphasizes a drawback of these fibers reinforced polymers regarding their use in indoor environments because of the higher concentration of hazardous VOCs emitted by biocomposites than virgin PP. The TVOCs level, which considerably increased with weathering time, the temperature and the hemp fiber rate, indicated that health effects by exposition to heated aged biocomposites could become of greater concern. Nevertheless, biocomposites in vehicles are generally implemented in materials assemblies and possible barrier effects could reduce the impact on VIAQ.

Otherwise, VOCs emissions characterization can be a useful way for understanding degradation mechanisms explaining the formation of the identified products issued from the polymer matrix and the carbohydrates and lignin decomposition. This last topic will be treated in another paper.

I.5. Acknowledgements

This research did not receive any specific grant from funding agencies in the public, commercial, or not-for-profit sectors.

I.6. References

[1] Nova Institut, Feature Wind Energy, JEC Compos. Mag. (2015) 18–19.

[2] D. Müller, D. Klingelhöfer, S. Uibel, D. a Groneberg, Car indoor air pollution - analysis of potential sources., J. Occup. Med. Toxicol. 6 (2011) 33. doi:10.1186/1745-6673-6-33.

[3] X. Chen, G. Zhang, H. Chen, Controlling strategies and technologies of volatile organic compounds pollution in interior air of cars, Proc. - 2010 Int. Conf. Digit. Manuf. Autom. ICDMA 2010. 1 (2010) 450–453. doi:10.1109/ICDMA.2010.375.

[4] MCS-Aware, Sick Car Syndrome, (2015). http://www.mcs-aware.org/general-

articles/189-sick-car-syndrome.

[5] J.S. Félix, C. Domeño, C. Nerín, Characterization of wood plastic composites made from landfill-derived plastic and sawdust: volatile compounds and olfactometric analysis, Waste Manag. 33 (2013) 645–55. doi:10.1016/j.wasman.2012.11.005.

[6] K. Sakakibara, K. Kaitani, C. Hamada, S. Sato, M. Matsuo, Analysis of odor in car cabin, JSAE Rev. 20 (1999) 237–241. doi:10.1016/S0389-4304(98)00073-3.

[7] Underwriters Laboratories UL LLC, Vehicle Interior Air Quality: Addressing Chemical Exposure in Automobiles, (2015).

[8] H. Kim, B. Lee, S. Choi, Sustainable biocomposites for automotive interior parts, in: 18TH Int. Conf. Compos. Mater., n.d.

[9] Korean Automobile Testing & Research Institute, Proposal for Vehicle Indoor Air Quality (VIAQ), GRPE-69-28, n.d.

[10] Ministry of environmental protection, GB/T 27630-2011 Chinese national standard: Guideline for air quality assesment of passenger car, (2011).

[11] JAMA, Announces Voluntary Guidelines for Reducing Vehicle Cabin VOC Concentration Levels, 2005. http://www.jama-english.jp/.

[12] European Automobile Manufacturers Association, (n.d.). http://www.acea.be/.

[13] ISO 12219-1: Whole vehicle test chamber — Specification and method for the determination of volatile organic compounds in cabin interiors, (2012).

[14] ISO 12219-2: Screening method for the determination of the emissions of volatile organic compounds from vehicle interior parts and materials — Bag method, (2012).

[15] ISO 12219-3: Screening method for the determination of the emissions of volatile organic compounds from vehicle interior parts and materials — Micro-scale chamber method, (2012).

[16] K.-W. Kim, B.-H. Lee, S. Kim, H.-J. Kim, J.-H. Yun, S.-E. Yoo, J.R. Sohn, Reduction of VOC emission from natural flours filled biodegradable bio-composites for automobile interior, J. Hazard. Mater. 187 (2011) 37–43. doi:10.1016/j.jhazmat.2010.07.075.

[17] B. Xu, Y. Wu, Y. Gong, S. Wu, X. Wu, S. Zhu, T. Liu, Investigation of volatile organic compounds exposure inside vehicle cabins in China, Atmos. Pollut. Res. 7 (2015) 215–220. doi:10.1016/j.apr.2015.09.005.

[18] Y.C. Chien, Variations in amounts and potential sources of volatile organic chemicals in new cars, Sci. Total Environ. 382 (2007) 228–239. doi:10.1016/j.scitotenv.2007.04.022.

[19] T. Yoshida, I. Matsunaga, A case study on identification of airborne organic compounds and time courses of their concentrations in the cabin of a new car for private use, Environ. Int. 32 (2006) 58–79. doi:10.1016/j.envint.2005.04.009.

[20] M.J. Fedoruk, B.D. Kerger, Measurement of volatile organic compounds inside automobiles, J. Expo. Anal. Environ. Epidemiol. 13 (2003) 31–41. doi:10.1038/sj.jea.7500250.

[21] S. Kim, J.-A. Kim, H.-J. Kim, S. Do Kim, Determination of formaldehyde and TVOC emission factor from wood-based composites by small chamber method, Polym. Test. 25 (2006) 605–614. doi:10.1016/j.polymertesting.2006.04.008.

[22] S. Overton, J. Manura, Identification of volatile organic compounds in a new automobile, Sci. Instrum. Serv. (1999) 1–6.

[23] Y. Peng, R. Liu, J. Cao, Characterization of surface chemistry and crystallization behaviour of polypropylene composites reinforced with wood flour, cellulose, and lignin during accelerated weathering, Appl. Surf. Sci. (2015). doi:10.1016/j.apsusc.2015.01.147.

[24] J.S. Fabiyi, A.G. McDonald, M.P. Wolcott, P.R. Griffiths, Wood plastic composites weathering: Visual appearance and chemical changes, Polym. Degrad. Stab. 93 (2008) 1405–1414. doi:10.1016/j.polymdegradstab.2008.05.024.

[25] O. Gil-Castell, J.D. Badia, T. Kittikorn, E. Strömberg, A. Martínez-Felipe, M. Ek, S. Karlsson, A. Ribes-Greus, Hydrothermal ageing of polylactide/sisal biocomposites. Studies of water absorption behaviour and Physico-Chemical performance, Polym. Degrad. Stab. 108 (2014) 212–222. doi:10.1016/j.polymdegradstab.2014.06.010.

[26] M.Z. Ahmad Thirmizir, Z. a. Mohd Ishak, R. Mat Taib, S. Rahim, S. Mohamad Jani, Natural Weathering of Kenaf Bast Fibre-Filled Poly(Butylene Succinate) Composites: Effect of Fibre Loading and Compatibiliser Addition, J. Polym. Environ. 19 (2010) 263–273. doi:10.1007/s10924-010-0272-2.

[27] D. Chen, J. Li, J. Ren, Influence of fiber surface-treatment on interfacial property of poly(l-lactic acid)/ramie fabric biocomposites under UV-irradiation hydrothermal aging, Mater. Chem. Phys. 126 (2011) 524–531. doi:10.1016/j.matchemphys.2011.01.035.

[28] L. Soccalingame, D. Perrin, J.-C. Bénézet, S. Mani, F. Coiffier, E. Richaud, A. Bergeret, Reprocessing of artificial UV-weathered wood flour reinforced polypropylene composites, Polym. Degrad. Stab. 120 (2015) 313–327. doi:10.1016/j.polymdegradstab.2015.07.013.

[29] L. Soccalingame, D. Perrin, J.-C. Bénézet, A. Bergeret, Reprocessing of UV-weathered wood flour reinforced polypropylene composites: Study of a natural outdoor exposure, Polym. Degrad. Stab. 133 (2016) 389–398. doi:10.1016/j.polymdegradstab.2016.09.011.

[30] C. Badji, L. Soccalingame, H. Garay, A. Bergeret, J.-C. Bénézet, Influence of weathering on visual and surface aspect of wood plastic composites: Correlation approach with mechanical properties and microstructure, Polym. Degrad. Stab. (2017). doi:10.1016/j.polymdegradstab.2017.01.010.

[31] A. Espert, L. a. de las Heras, S. Karlsson, Emission of possible odourous low molecular weight compounds in recycled biofibre/polypropylene composites monitored by head-space SPME-GC–MS, Polym. Degrad. Stab. 90 (2005) 555–562. doi:10.1016/j.polymdegradstab.2005.03.009.

[32] H.-S. Kim, B.-H. Lee, H.-J. Kim, H.-S. Yang, Mechanical–Thermal Properties and VOC Emissions of Natural-Flour-Filled Biodegradable Polymer Hybrid Bio-Composites, J. Polym. Environ. 19 (2011) 628–636. doi:10.1007/s10924-011-0313-5.

[33] ISO 16000-9: Indoor air -- Part 9: Determination of the emission of volatile organic compounds from building products and furnishing -- Emission test chamber method, (2006).

[34] ISO 16000-6: Indoor air -- Part 6: Determination of volatile organic compounds in indoor and test chamber air by active sampling on Tenax TA sorbent, thermal desorption and gas chromatography using MS or MS-FID, (2011).

[35] Ó. Ezquerro, B. Pons, M.T. Tena, Development of a headspace solid-phase microextraction–gas chromatography–mass spectrometry method for the identification of odour-causing volatile compounds in packaging materials, J. Chromatogr. A. 963 (2002) 381–392. doi:10.1016/S0021-9673(02)00211-X.

[36] J. Salafranca, I. Clemente, F. Isella, C. Nerín, O. Bosetti, Influence of oxygen and long term storage on the profile of volatile compounds released from polymeric multilayer food contact materials sterilized by gamma irradiation, Anal. Chim. Acta. 878 (2015) 118–130. doi:10.1016/j.aca.2015.03.055.

[37] P. Kusch, G. Knupp, Headspace-SPME-GC-MS Identification of Volatile Organic Compounds Released from Expanded Polystyrene, 12 (2004) 83–87.

[38] D. Bourdin, P. Mocho, V. Desauziers, H. Plaisance, Formaldehyde emission behavior of building materials: on-site measurements and modeling approach to predict indoor air pollution., J. Hazard. Mater. 280 (2014) 164–73. doi:10.1016/j.jhazmat.2014.07.065.

[39] V. Desauziers, D. Bourdin, P. Mocho, H. Plaisance, Innovative tools and modeling methodology for impact prediction and assessment of the contribution of materials on indoor air quality, Herit. Sci. 3 (2015) 1. doi:10.1186/s40494-015-0057-y.

[40] D. Bourdin, V. Desauziers, Development of SPME on-fiber derivatization for the sampling of formaldehyde and other carbonyl compounds in indoor air, Anal. Bioanal. Chem. 406 (2014) 317–328. doi:10.1007/s00216-013-7460-6.

[41] Chemical Risk Prevention Unit, CNRS, European harmonised classification and labelling of carcinogenic, mutagenic and toxic for reproduction (CMR) substances according to the criteria of the CLP Regulation, (2015).

[42] J.A. Koziel, J. Noah, J. Pawliszyn, Field sampling and determination of formaldehyde in indoor air with solid-phase microextraction and on-fiber derivatization, Environ. Sci. Technol. 35 (2001) 1481–1486. doi:10.1021/es001653i.

[43] J. Nicolle, V. Desauziers, P. Mocho, Solid phase microextraction sampling for a rapid

and simple on-site evaluation of volatile organic compounds emitted from building materials, J. Chromatogr. A. 1208 (2008) 10–15. doi:10.1016/j.chroma.2008.08.061.

[44] V. Desauziers, Traceability of pollutant measurements for ambient air monitoring, Trends Anal. Chem. 23 (2004) 252–260. doi:10.1016/S0165-9936(04)00310-3.

[45] Y. Peng, R. Liu, J. Cao, Y. Chen, Effects of UV weathering on surface properties of polypropylene composites reinforced with wood flour, lignin, and cellulose, Appl. Surf. Sci. 317 (2014) 385–392. doi:10.1016/j.apsusc.2014.08.140.

[46] G. Bonifazi, L. Calienno, G. Capobianco, A. Lo, C. Pelosi, R. Picchio, S. Serranti, Modeling color and chemical changes on normal and red heart beech wood by re fl ectance spectrophotometry, Fourier Transform Infrared spectroscopy and hyperspectral imaging, Polym. Degrad. Stab. 113 (2015) 10–21. doi:10.1016/j.polymdegradstab.2015.01.001.

[47] Y. Peng, S. Wu, Fast pyrolysis characterisctics of sugarcane bagasse hemicellulose, 45 (2011) 605–612.

[48] G. Dorez, L. Ferry, R. Sonnier, A. Taguet, J.-M. Lopez-Cuesta, Effect of cellulose, hemicellulose and lignin contents on pyrolysis and combustion of natural fibers, J. Anal. Appl. Pyrolysis. 107 (2014) 323–331. doi:10.1016/j.jaap.2014.03.017.

[49] R. Bernstein, S.M. Thornberg, A.N. Irwin, J.M. Hochrein, D.K. Derzon, S.B. Klamo, R.L. Clough, Radiation-oxidation mechanisms: Volatile organic degradation products from polypropylene having selective C-13 labeling studied by GC/MS, Polym. Degrad. Stab. 93 (2008) 854–870. doi:10.1016/j.polymdegradstab.2008.01.020.

[50] M. Carrier, A. Loppinet-Serani, C. Absalon, C. Aymonier, M. Mench, Degradation pathways of holocellulose, lignin and alpha-cellulose from Pteris vittata fronds in sub- and super critical conditions, Biomass and Bioenergy. 43 (2012) 65–71. doi:10.1016/j.biombioe.2012.03.035.

[51] O. Faruk, A.K. Bledzki, H.-P. Fink, M. Sain, Biocomposites reinforced with natural fibers: 2000–2010, Prog. Polym. Sci. 37 (2012) 1552–1596. doi:10.1016/j.progpolymsci.2012.04.003.

[52] Z.L. Yan, H. Wang, K.T. Lau, S. Pather, J.C. Zhang, G. Lin, Y. Ding, Reinforcement of polypropylene with hemp fibres, Compos. Part B Eng. 46 (2013) 221–226. doi:10.1016/j.compositesb.2012.09.027.

[53] L. Sisti, G. Totaro, M. Vannini, P. Fabbri, S. Kalia, A. Zatta, A. Celli, Evaluation of the retting process as a pre-treatment of vegetable fibers for the preparation of high-performance polymer biocomposites, Ind. Crops Prod. 81 (2016) 56–65. doi:10.1016/j.indcrop.2015.11.045.

[54] P. Md. Tahir, A.B. Ahmed, S.O.A. SaifulAzry, Z. Ahmed, Retting process of some bast plant fibres and its effect on fibre quality: A review, BioResources. 6 (2011) 5260–5281. doi:10.15376/biores.6.4.5260-5281.

[55] O.F. Unit, C. Scouring, Influence of wet processing on physico-chemical properties of

okra bast fibre, 29 (2016) 412–414.

[56] R. Wittkowski, J. Ruther, H. Drinda, F. Rafiei-Taghanaki, Formation of smoke flavor compounds by thermal lignin degradation, ACS Symp. Ser. 490 (1992) 232–243.

[57] M. Baharoğlu, G. Nemli, B. Sarı, S. Bardak, N. Ayrılmış, The influence of moisture content of raw material on the physical and mechanical properties, surface roughness, wettability, and formaldehyde emission of particleboard composite, Compos. Part B Eng. 43 (2012) 2448–2451. doi:10.1016/j.compositesb.2011.10.020.

[58] L. Molhave, Volatile organic compounds, indoor air quality and health, Indoor Air. 1 (1991) 357–376. doi:10.1111/j.1600-0668.1991.00001.x.

[59] K.W. Kim, S. Kim, H.J. Kim, J.C. Park, Formaldehyde and TVOC emission behaviors according to finishing treatment with surface materials using 20L chamber and FLEC, J. Hazard. Mater. 177 (2010) 90–94. doi:10.1016/j.jhazmat.2009.09.060.

[60] G. Nemli, G. Çolakoğlu, The influence of lamination technique on the properties of particleboard, Build. Environ. 40 (2005) 83–87. doi:10.1016/j.buildenv.2004.05.007.

II. Under windshield glass weathering of hemp fibers reinforced polypropylene biocomposites: Reactions between Volatile Organic Compounds

Célia Badji[a], Jean-Marc Sotiropoulos[b], Joana Beigbeder[a], Hélène Garay[a], Anne Bergeret[a], Jean-Charles Bénézet[a] and Valérie Desauziers[a*]

[a]C2MA, Ecole des Mines d'Alès, 6 Avenue de Clavières, 30319 Alès Cedex, France

[b]IPREM, Université de Pau et des Pays de l'Adour, 2 Avenue du Président Pierre Angot, 64000 Pau, France

Abstract

The durability of hemp fibers reinforced polypropylene biocomposites was investigated after one-year under glass exposure. Volatile Organic Compounds (VOCs) emissions were assessed using a new passive sampling method. Degradation pathways were examined in order to understand the weathering mechanisms. The polymer matrix was decomposed into oxygenated products due to UV rays and high temperatures. As regards hemp fibers, different degradation steps of the carbohydrates were highlighted according to the nature of the detected furans. At non-weathered state, dehydrations preceded ring-opening mechanism, often catalysed by Maillard reactions. The further cyclisation induced the formation of 2- or 5-substituted furans emitted by non-weathered materials. Reactions between identified products after weathering were proposed. They often implied a keto-enol tautomerism but also dehydrations that induced the formation of 3- and 4-substituted furanones. These differences can be explained by a primary decomposition of carbohydrates favoured at non-weathered state and a secondary one occurring at weathered state.

Keywords: hemp fiber; polypropylene; oxidation; dehydration; VOCs

II.1. Introduction

Recently, bio-fillers have emerged as an attractive alternative to inorganic fillers in the reinforcement of thermoplastics in response to the environmental consciousness and increasing global waste problems. The main application areas of vegetal filler reinforced composites are automotive and building industries [1,2]. Otherwise, with the increasing

concerns about indoor air quality, Volatile Organic Compounds (VOCs) emissions behaviour of the interior materials used as automotive parts has become widely recognized as an important topic for indoor environment quality [3,4].

During the melt mixing process of biocomposites through extrusion and injection molding, the high manufacturing temperatures exceed the bio-fillers degradation temperature [5,6]. Also, during their use, climatic conditions weaken their chemical stability because of their high sensitivity [7,8]. Temperature variations induce a carbonization and odors emanating from the heated matter. Also, a press molding temperature increase induces biocomposites color turning from brown to close to black [9]. This was thought to be the result of vegetal fibers caramelization. Some solutions for reducing the odors and the amount of VOCs produced by biocomposites have been studied [10,11]. But molecules responsible for the worsening air quality, color changes and odors must be assessed.

VOCs emitted by plastics are generally due to the polymer degradation. Studies on thermal and photochemical oxidation of polypropylene (PP) showed that radical processes are responsible for chain scission leading to low molecular weight products migration from the polymeric matrix to the atmosphere [12,13]. This is widely accepted that Norrish type I and II photochemical reactions occur involving C-C cleavage, leading to oxygenated compounds formation [14,15]. Those generally result from the oxidation of tertiary carbon atoms of the polymer chains leading to methyl ketones, along with alcohols and aldehydes formation in addition to aliphatic hydrocarbons.

The pyrolysis of lignocellulosic biomass was widely studied and further identification of volatile compounds issued from the natural fibers thermal degradation was sometimes performed. Some products, originating from pyrolysis of cellulose (molecular formula: $(C_6H_{10}O_5)_n$), are identified as low molecular weight compounds. They are formed by ring-opening reactions, while pyrans and furans are obtained from dehydration reactions [16,17]. These molecules are generally stable aromatic compounds and hardly decompose into lower molecular weight compounds [18]. Their decomposition accounts for the major reactions occurring in the secondary reaction stage of cellulose. Hemicelluloses consist of saccharides such as glucose, mannose, xylose and arabinose [16,19]. Once pyrolyzed, the derivatives of these pentose sugars such as cyclopentanes and cyclopentenones are detected in large

quantity in addition to furan molecules [20,21]. Lignin component, a highly complex aromatic structure, breaks down into phenolic structures [22,23]. It mainly consists of three basic building blocks that are guaiacyl, syringyl and p-hydroxyphenyl units. However, non-cellulosic polysaccharides such as proteins are also found in lower proportion under amino acids forms [24]. Each component proportion present in the vegetal fibers depends on several parameters such as their nature, retting time and geographic origin.

Maillard reactions are mainly responsible for the formation of flavor compounds like the 2-furanones with similar structures than those of volatile substances issued from biofillers degradation. Besides the flavoring of food, the interest in Maillard mechanism has grown in fields like physico-chemical properties of proteins and polysaccharides [25,26]. This reaction implies the interaction between the amino group from an amino acid, a protein or an amine and the carbonyl functional group from the carbohydrate part (glucose, fructose) under heating conditions [27]. It gives unstable N-substituted glycosylamino compound. This first step is reversible but the generated glycosylamine is immediately converted into an Amadori compound [28]. Amadori intermediates compounds belonging to the 1-amino-1-deoxy-2-ketoses family are important precursors in the formation of flavor compounds from Maillard reactions [27,29]. Caramelized sugar aromas furanones, such as furfural and 5-methylfurfural, or pyranones such as maltol, evolving from holocellulose are generated through sugar-amine condensation. Then, the formed Amadori compound can react along multiple pathways to form Maillard reaction products at lower temperature than those found in pyrolysis studies of natural fibers since the presence of nitrogen containing compounds catalyses the reaction [28]. For instance, maltol, a well-known carbohydrate derivative, and 4-hydroxy-2,5-dimethyl-3(2H)-furanone, derives from a common intermediate arising by sugar-amine condensation and Amadori rearrangement. 2,3-enolization of the 1-amino-1-deoxy-2-ketose and elimination of the 1-amino group finally occur at the final step [29]. Then, dehydrations and cyclisation lead to furans generation [30] and ene-diol scissions and retroaldolisation to short products [31].

However, formations of the substances found in literature dealing with biomass and their controlled decomposition (pyrolysis) were not explained thanks to this mechanism. Indeed, the reactions involved require the presence of artificial catalysts (chromium, copper) facilitating the conversion [19,32]. Otherwise, when decomposition products are obtained

from pyrolysis process, this includes energetic conditions so favourable (temperature reaching 800 °C) that ring-opening, dehydrogenation and cracking can occur [17,20]. Moreover, formation of other methylfurans that could issue from thermal decomposition and reactions between volatile chemicals emitted by natural fibers were not reported.

A one-year natural under glass weathering of hemp fibers reinforced PP biocomposites was investigated to simulate car interior environment. VOCs emissions were assessed all along the ageing. The objective is to understand the components degradation way by firstly examining the well-known Maillard mechanism for the holocellulose part decomposition thanks to VOCs identification. Secondly, reactions between identified VOCs and their concentration evolution were proposed. Finally, the lignin degradation was also investigated.

II.2. Material and methods

II.2.1 Materials

Polypropylene (PP) grade H733-07 with a melt flow rate of 7.5 g/10 min (230 °C, 2.16 kg) (Braskem, Brazil) was used as polymer matrix. Hemp fibers were provided by AgroChanvre (France). Two hemp fibers loading, 10 wt% (PP10) and 30 wt% (PP30) were tested. Maleic anhydride grafted polypropylene (MA-g-PP) under the trademark Orevac CA100 (Arkema, France), was added at 3.1 wt% of PP as coupling agent.

II.2.2 Process conditions

Hemp fibers and MA-g-PP were dried for 15 h at 60 °C. Then, granules of PP and MA-g-PP were mixed with hemp fibers in a BC21 Clextral twin-screw extruder (L/D = 36 with D = 25 mm) (Clextral, France) with the temperature profile 190-190-190-180-175-175-175 °C and a screw speed of 220 rpm. Once dried for 3 days at 60 °C, extruded pellets were injection molded into specimens in a Krauss Maffei machine (Krauss Maffei, Germany) at 210 °C with an injection speed of 30 $cm^3.s^{-1}$. Square samples of 100 × 100 × 2 mm^3 were obtained.

II.2.3 Weathering conditions

Samples were exposed from September 2015 to September 2016 in the South West of France under windshield glass to simulate car interior environment according to ISO 877-2:2011 (Figure 1). The exposition panels were oriented towards South at 45° with the

ground. Interior environment was naturally ventilated thanks to holes located on stainless steel boxes 2 hours per day. Temperature T(°C) and relative humidity RH(%) were monitored and PP, PP10 and PP30 materials were sampled after 1, 2, 3, 6, 9 and 12 months. Temperature ranged from -5°C in February to 91°C in August and relative humidity fluctuated between 3% in September and 95% in November.

Figure 1 - Under windshield glass exposure racks

II.2.4 Sampling and analytical methodology

At each weathering step, 3 samples of each material were brought from the racks to the laboratory where VOCs emission analysis was carried out through a passive sampling method developed at the laboratory [33]. It consists of two steps: firstly, a glass cell is placed on the material in order to isolate a part of its surface, and the VOCs were let to diffuse from the material to the air enclosed in the cell. When the VOCs concentration stabilized, i.e. when material/air equilibrium is reached [33], a Solid Phase MicroExtraction (SPME) fiber was introduced in the glass cell through a septum to sample emitted VOCs. Then, the SPME fiber was desorbed in the injector of a gas chromatograph (GC) coupled with mass spectrometer (MS) and flame ionization detector (FID) (Varian, France) for identification and quantification of VOCs. The analytical procedure is detailed elsewhere [34]. Both VOCs screening and specific analysis of formaldehyde and acetaldehyde, which are classified as Carcinogen Mutagenic and Reprotoxic (CMR) substances, were performed [35]. A polydimethylsiloxane-divinylbenzene-Carboxen fiber (PDMS/DVB/CAR, 50/30 µm) was selected for VOCs screening whereas a polydimethylsiloxane-divinylbenzene (PDMS/DVB, 65

µm) fiber impregnated with *O*-(2,3,4,5,6-pentafluorobenzyl)hydroxylamine hydrochloride (PFBHA) (Fluka, Switzerland) was used for formaldehyde and acetaldehyde [34,36]. The SPME fibers were purchased from Supelco (United States). Sampling temperature of 80 °C was tested to simulate extreme car interior conditions. The extraction time was fixed at 5 min.

II.2.5 Quantitative analysis

The methodology described above allows determining the concentration (in $\mu g.m^{-3}$) of VOCs at the material/air interface. That concentration is related to the emission rate of the considered substance by the first Fick law of diffusion under steady state conditions [26]. For the screening analysis using PDMS-DVB-CAR fiber, VOCs were quantified as toluene equivalent using FID response since it is proportional to the effective carbon atoms number in the molecule [37]. Furfural and 2-furanmethanol, compounds specific to hemp fibers and listed as CMR substances [35], as well as formaldehyde and acetaldehyde, were specifically quantified. Standard gases of formaldehyde and acetaldehyde were generated by a permeation device [27]. For the other standard VOCs (toluene, furfural and 2-furanmethanol), a continuous syringe injection method was used, as described elsewhere [38,39]. The detection limit and quantification limit are around 8 $\mu g.m^{-3}$ and 23 $\mu g.m^{-3}$ respectively for all compounds and the repeatability (relative standard deviation) is about 3% for 3 replicates.

II.3. Results and discussion

II.3.1 Polypropylene oxidation

Some emitted VOCs were issued from the polymer degradation: long-chain aliphatic hydrocarbons and oxygenated products (linear ketones, aldehydes and carboxylic acids). Acetic acid, acetone and 2,4-pentanedione were the main compounds emitted by weathered PP. Some pathways are proposed in the literature to explain the formation of molecules containing carbonyl functional group. The scheme given by François-Heude et al. resumes their mechanistic formation [40]. Mainly radical reactions lead to intermediate tertiary alkoxy radicals and their β-scission induces the previous identified carbonyl products (Figure 2). 2,4-pentanedione can result from the oxidation of methylketone issued from polymer

chain reaction with unstable hydroperoxide. Moreover, 4-hydroxy-4-methyl-2-pentanone was also detected as high-level ketone (65 ± 13 and 82 ± 25 µg.m^{-3} for non-weathered and for one-year weathered PP respectively). It is proposed to originate from the same methyl ketone precursor. Indeed, the hydroxyl formation resulting from alkoxy radical reaction with hydrogen followed by scission could form 4-hydroxy-4-methyl-2-pentanone.

Formaldehyde and acetaldehyde were also released by the polymer and biocomposites. Their levels increased with the time of exposure. A polymer degradation way, similar to previous oxygenated chemicals pathway, could explain acetaldehyde generation with secondary alkoxy radical initiator responsible for this low molecular compound formation. Moreover, formaldehyde generation is reported according to the mechanism of Hoff and Jacobsson, which consists of the oxidation of primary alkyl radicals [41].

Alcohols, resulting from polymer degradation, could arise from intermediate alkoxy radicals. However, abstract of a hydrogen from another molecule yields an hydroxyl group in tertiary carbon rather than a carbonyl group [42].

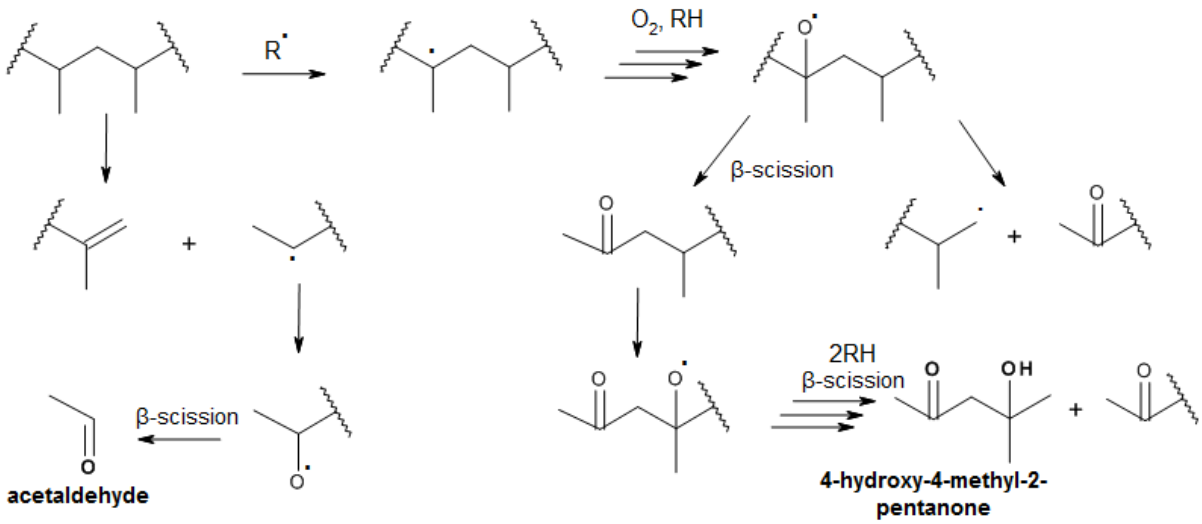

Figure 2 - PP degradation global scheme (from [42])

II.3.2 Cellulose and hemicelluloses degradation

II.3.2.1 Primary decomposition

Two specifically quantified furan derivatives, furfural and 2-furanmethanol were emitted at 1611 ±20 and 2319 ±176 µg.m^{-3} respectively by non-weathered PP30. Also, 5-methylfurfural (660 ±30 µg.m^{-3}), 5-methyl-2(3H)-furanone (40 ±14 µg.m^{-3}), furfuryl formate (38 ±4 µg.m^{-3}) and furfuryl acetate (43 ±4 µg.m^{-3}) evolved from biocomposites at the initial state. Apart from the two last compounds, these low molecular weight products were evidenced to be generated by holocellulose sequential degradation [19,43–45]. Figure 3 shows the formation pathways of degradation products identified in this study and issued from the carbohydrate part of hemp fibers. The nominated products were those identified as VOCs issued from biocomposites. The carbohydrates degradation under high temperature involves the depolymerization of polysaccharides by the glycosidic bonds cleavage between D-glucose units [30]. This process is followed by dehydrations, leading to D-glucopyranose and D-xylofuranose formation. The formation of 2- or 5-substituted furans is generally explained to occur via glucopyranose ring-opening pathway with acyclic forms such as hexoses and pentoses intermediates [17,19]. The further cyclisation of these oses leads to the furans formation. Primary subsequent dehydration steps produced specifically followed furfural and 2-furanmethanol emitted at high concentration by non-weathered biocomposites. In this mechanistic scheme, other cyclic molecules were derived from hydroxymethylfurfural which was not detected in the conditions of this study. Otherwise, the generation of levoglucosenone (97 ±4 µg.m^{-3}) derivative does not need the sugar ring-opening.

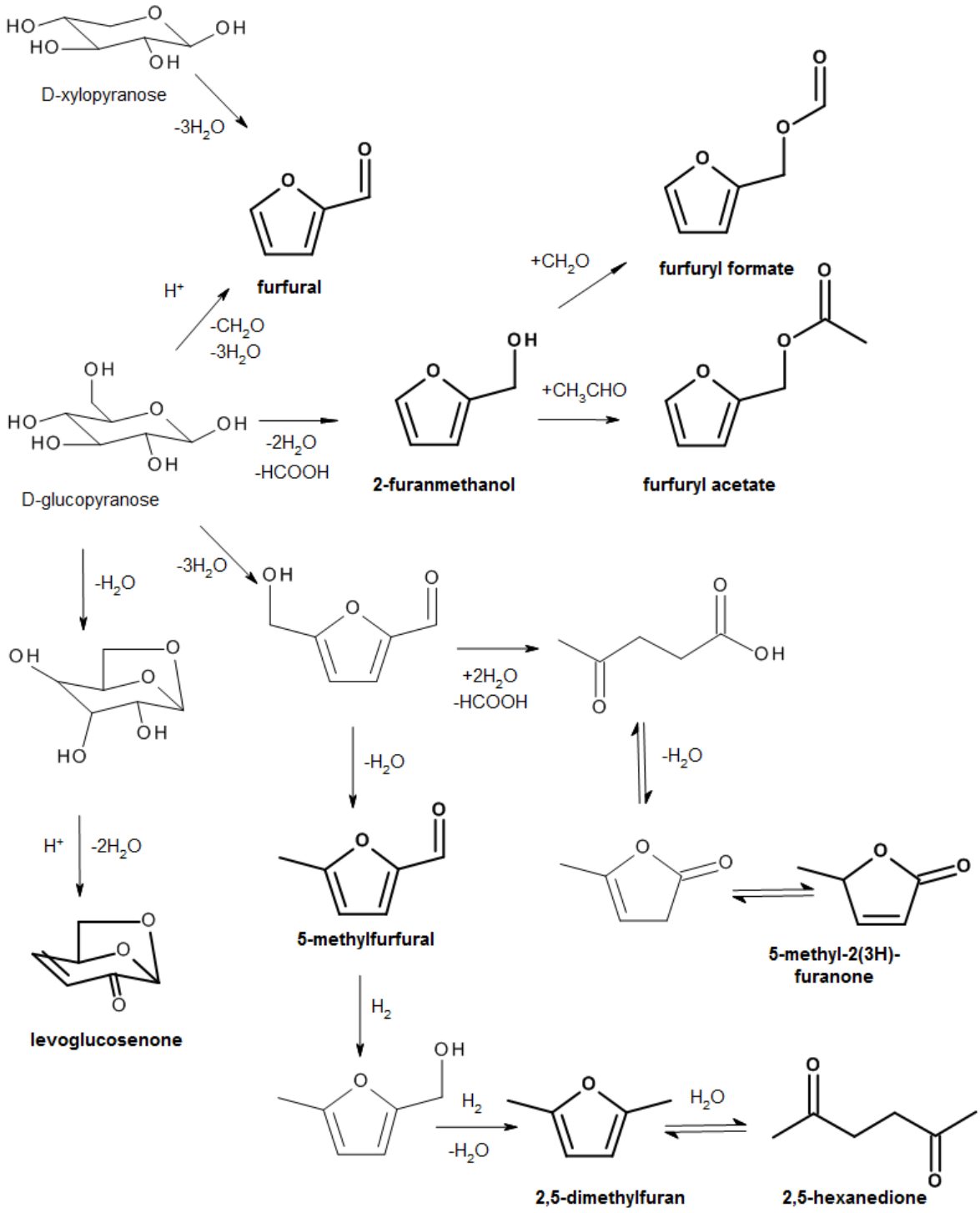

Figure 3 - Primary holocellulose decomposition products and their dehydrated derivatives through funneling pathways [19,43–45]

The products issued from the carbohydrate primary decomposition were mainly emitted by biocomposites at non-weathered state. It has been supposed that generation could also be favored by Maillard reactions for which non-elevated temperatures (almost 100°C) are required [28] (chosen sampling temperature and those found in exposure racks do not exceed 91°C) contrary to the pyrolysis method. Indeed, until now, Maillard reactions have

not supported degradation pathways of vegetal fibers. However, either 1,2- or 2,3-enolization of the Amadori compound, previously mentioned in the introductory part, rising from aldoses such as glucose could effectively lead to furfural and hydroxymethylfurfural. Indeed, these compounds were already explained to originate from sugar-containing food, such as lactose, through Maillard reactions [28]. But the same mechanism could justify the formation of products detected here. Also, further intermediate dicarbonyls (reductones) formed after intra-rearrangement (enolization) are responsible for the autocatalytic character of Maillard reaction (Figure 4). Moreover, as mentioned in the introductory part, proteins present in fibers could allow the glycosylamine precursor formation required for obtaining advanced Maillard reaction products. Otherwise, their presence is demonstrated by the detection of pyrazines emitted by biocomposites (methylpyrazine and N-acetyl-4(H)-pyridine at 25 ±2 and 38 ±4 $\mu g.m^{-3}$ respectively for PP30). These secondary products of Strecker degradation are due to aminoketones condensation.

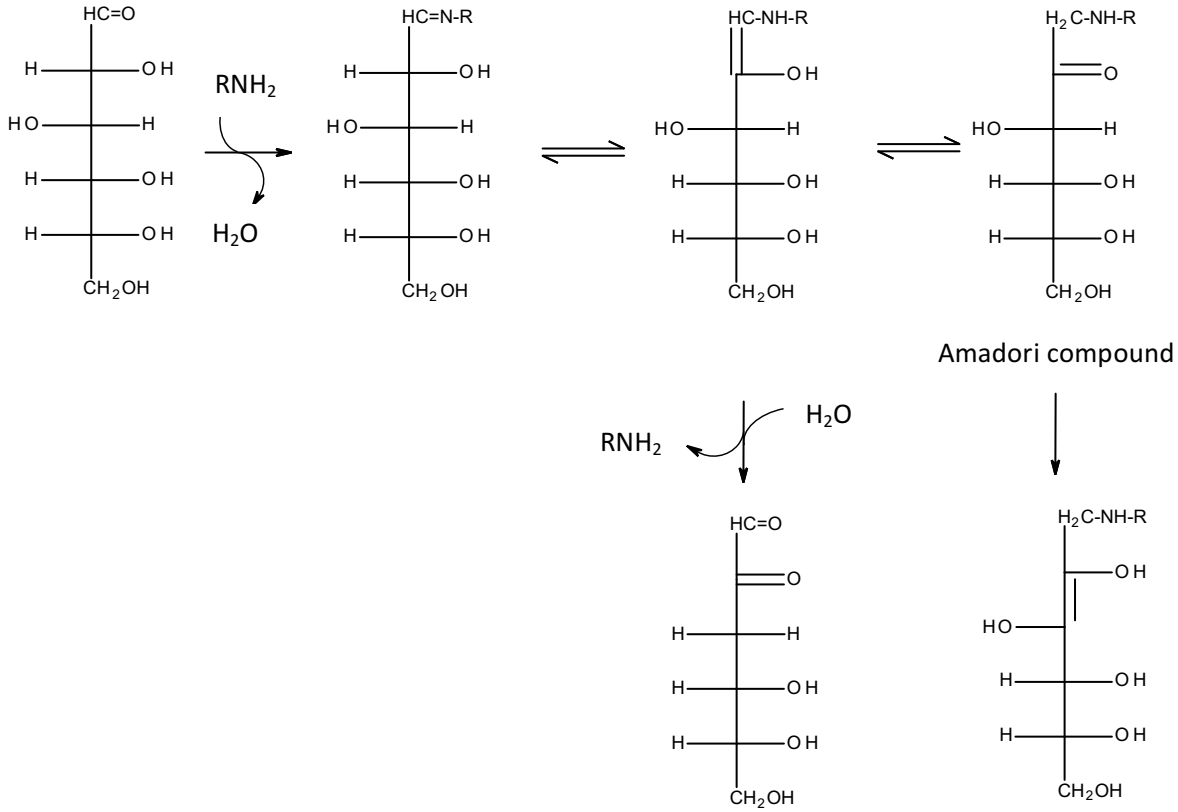

Figure 4 - Glucose and amino acid interaction (R = amino acid side group) (from [46])

Contrary to other compounds, the formation of furfuryl formate and furfuryl acetate (total concentration of 81 ±8 μg.m^{-3}) aroused from non-weathered PP30 composite is not reported in the literature. Here, it is suggested that they result from the interaction between the hydroxy functional groups of 2-furanmethanol and formaldehyde and acetaldehyde respectively (Figure 3). Formaldehyde and acetaldehyde could also evolve from the Strecker degradation [28,29] by β-scission. Indeed, for biocomposites, lots of aliphatic ketones and aldehydes such as 1-hydroxy-2-propanone, 1-acetyloxy-2-propanone and nonanal are emitted at the highest levels of their chemical family: 420 ± 81, 366 ± 11 and 160 ± 28 μg.m^{-3} respectively for unaged PP30. They were identified as hemp fibers by-products at non-weathered state. These by-products could be linked to reaction between amino acids and two-carbonyl compounds.

II.3.2.2 Secondary decomposition

After weathering, mainly methyl substituted furanones deriving from carbohydrates were formed. They represented 13% of the level of ketones released by PP30 after one year of weathering whereas they only accounted for 8% of ketones by-products emitted by non-weathered PP30. Moreover, contrary to non-weathered state, only furans compounds containing at least one substitution in 3 and 4 positions were identified after weathering. In addition, contrary to 2- and 5-substituted furanones presented in Figure 3, the explanation of 3- or 4-substituted furanones issued from vegetal fibers decomposition is not yet reported in the literature. The proposed reactions featured in Figure 5 involve the interaction between functional groups of identified volatile products. Substances that are designed by their names in Figure 5 correspond to substances detected in this work. The first reaction 1) implies a radical attack in α position of two same propionic acid by-products, whose levels increased from 39 ±4 to 839 ±75 μg.m^{-3} and 56 ±16 to 1403 ±3 μg.m^{-3} for PP10 and PP30 respectively, via photo-chemical way caused by ultraviolet (UV) rays. It is followed by the dehydration of the generated intermediate symmetrical molecule leading to an intramolecular cyclisation giving 3,4-dimethyl-2,5-furanedione (118 ±32 μg.m^{-3} for weathered PP30).

The reaction 2) occurs through the establishment of a keto-enolization equilibrium thermodynamically driven between the keto and enol forms of 4-hydroxy-4-methyl-2-

pentanone (Figure 5). Moreover, this ketone was detected at extremely high concentration after weathering (until almost 3000 $\mu g.m^{-3}$ for PP30 after 12 months), especially for biocomposites. Then, the attack of the enone form via C=C hydroformylation by carbon monoxide leads to an instable compound formation. Its further hydrolysis induces a cyclopropane ring-opening. Thus, these two previous steps lead to the functionalization of a formic acid group. Then, two successive dehydrations firstly induce a cyclisation into 2-furanone structure. After, the dehydroxylation in the 3-position induces a double bond formation to generate 2,4,4-trimethylbut-2-enolide. This volatile compound was emitted at the highest concentration of the 2-furanones group after one-year weathering. Indeed, since the group of 2-furanones products was emitted at 3285 ± 666 $\mu g.m^{-3}$ by PP30 weathered for one-year, 2,4,4-trimethylbut-2-enolide accounted for almost 40% (1314 ± 30 $\mu g.m^{-3}$) for PP30 weathered for one-year. This can be explained by the extremely high concentration of the 4-hydroxy-4-methyl-2-pentanone reactant previously mentioned giving way to the formation of 2,4,4-trimethylbut-2-enolide.

1-(2,4-dimethyl-furan-3-yl)-ethanone, whose generation (1063 ± 243 $\mu g.m^{-3}$ for PP30 and 1807 ± 149 $\mu g.m^{-3}$ for PP10) is explained in pathway 3) of Figure 5, implies the reaction between propionic acid and 2,4-pentanedione, two volatile compounds emitted in high quantity. Indeed, propionic acid was emitted at almost 800 and 1400 $\mu g.m^{-3}$ for PP10 and PP30 respectively and a concentration of almost 7300 $\mu g.m^{-3}$ of the 2,4-pentanedione was recorded for the two biocomposites after one year. The highly reactive C=C formed through keto-enolization tautomerism of propionic acid is opened by C3 of the diketone. Then, a further keto-enolization of the intermediate compound hydroxydiketone derivative is established and precedes dehydrations occurring in the final stage.

As regards reaction 4.1), the esterification of crotonic acid favored by the condensation of ethanol hydrate hydroxyl group, molecule easily generated from acetaldehyde hydration on crotonic acid, is followed by the removal of a water molecule. The C-C double bond initially present is opened after cyclisation. This brings to 4-hydroxy-4,5-dimethyl-2-furanone. However, the possible further dehydrogenation process being difficult to occur, the reaction 4.2) is an alternative to 4.1) that requires more energy than 4.2). This generates the previously explained structure (4-hydroxy-4,5-dimethyl-2-furanone) at the final stage. A

similar esterification way of the diketone intermediate product followed by a cyclisation and dehydration could explain its formation.

The same precursors as found in reaction 2) may be responsible to 5-hydroxy-3,3,5-trimethyl-2-furanone formation (pathway 5)). Indeed, the dehydration and hydroformylation of the methylpentanone due to its reactions with CO and O_2 lead to methyl substituted levulinic acid generation, well-known biomass derivative [44], that finally cyclizes after its keto-enolization.

Some of these reactions may require high energy conditions to occur. However, the biomass inorganic part contains metals which could catalyze these reactions [16].

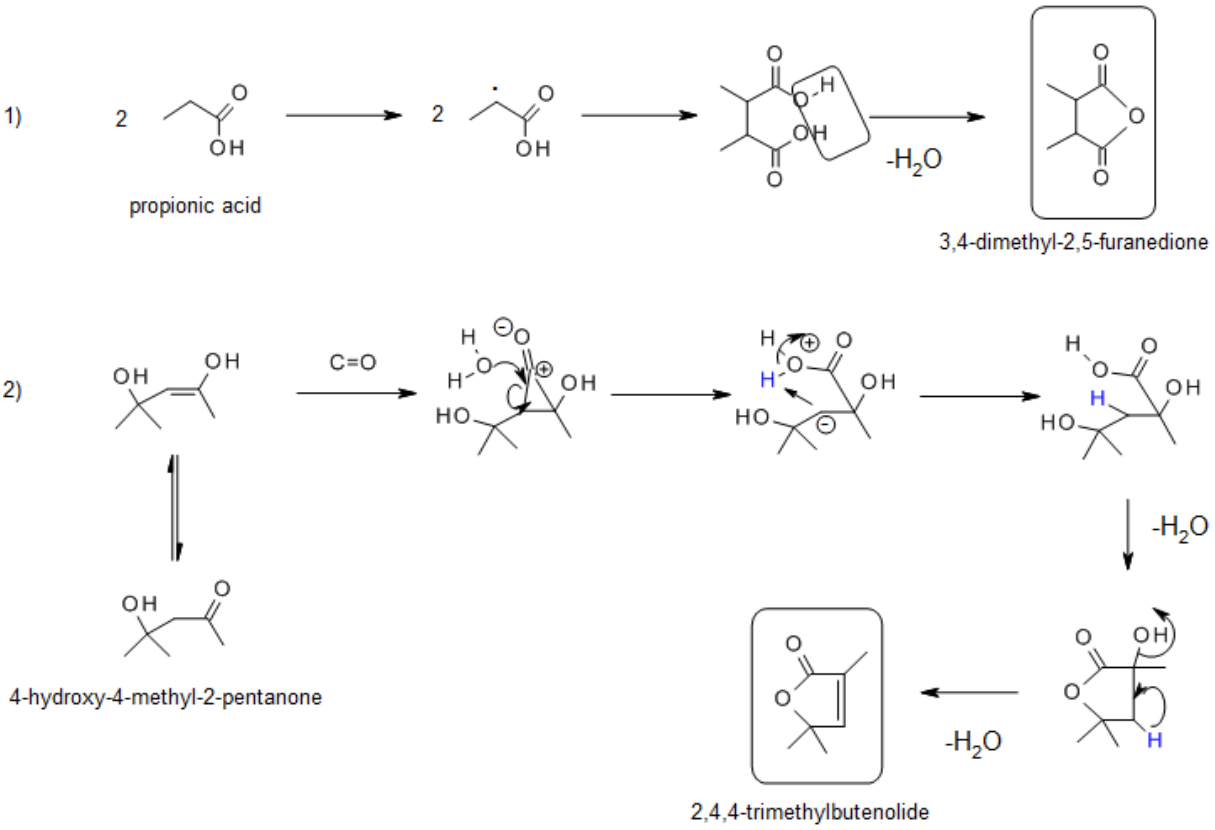

3)

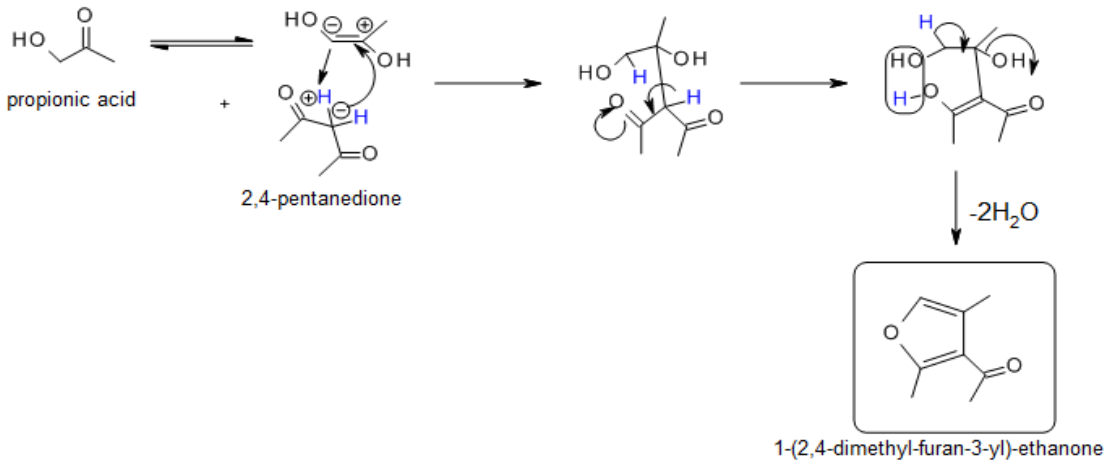
propionic acid
2,4-pentanedione
-2H2O
1-(2,4-dimethyl-furan-3-yl)-ethanone

4.1)

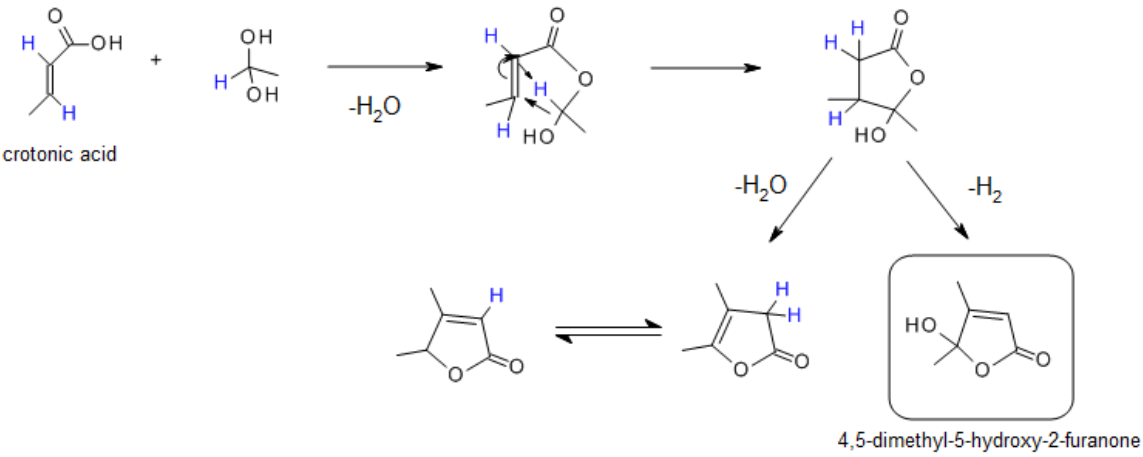
crotonic acid
-H2O
-H2O
-H2
4,5-dimethyl-5-hydroxy-2-furanone

4.2)

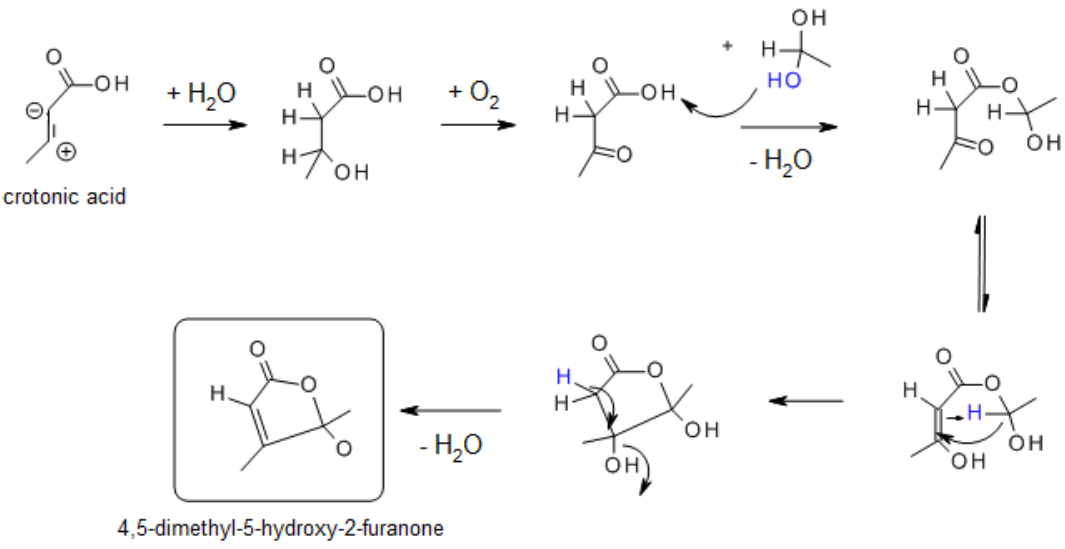
crotonic acid
+ H2O
+ O2
- H2O
- H2O
4,5-dimethyl-5-hydroxy-2-furanone

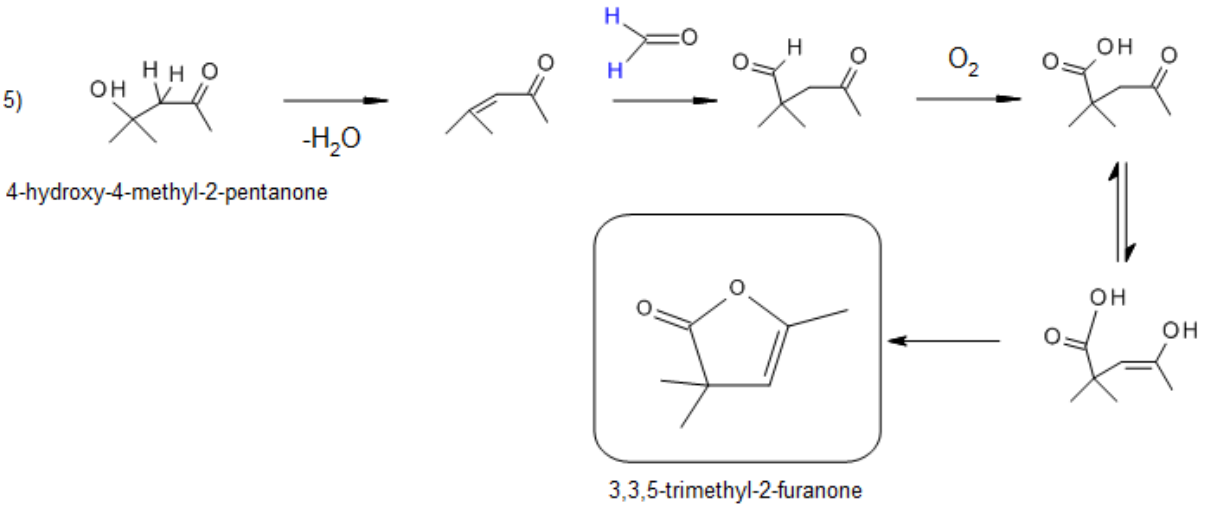

Figure 5 - Proposed reaction pathways of furan derivatives (VOCs identified in this work are designed by their names in this scheme)

II.3.3 Lignin degradation

II.3.3.1 Primary decomposition

Two methoxy-substituted phenols, vanillin and 4-vinylguaiacol, were emitted by non-weathered biocomposites. These two compounds are thought to originate from a primary decomposition of lignin favored in heating conditions of ferulic acid, a well-known by-product evolving from lignin degradation, but not identified in this study [47,48].

Firstly, decarboxylation of ferulic acid may cause the formation of vinylguaiacol through 1.1) pathway (Figure 6) [47]. Indeed, it is reported that temperatures ranging from 100 to 250 °C (including the process temperature) cause severe damage on natural fibers chemical structure through depolymerization, dehydration or decarboxylation [49]. Vanillin is explained to originate from the oxidation of 4-vinylguaiacol issued from lignin (1.2)). The literature also proposed vanillin arising through the hydrolysis of the ferulic acid by-product (2.1)) [48]. A further deacetylation could induce the formation of vanillin (2.2)). This pathway could occur more easily than the vinylguaiacol or eugenol oxidation. Indeed, even if the decarboxylation consists in a naturally occurring step, the oxidation of carbon-carbon double bond must be catalyzed. Moreover, it has been shown that 2) pathways preferentially occur for obtaining vanillin than 1) ones [48]. Otherwise, presence of metalloproteins containing iron, cupper and manganese might catalyze by-products formation [50].

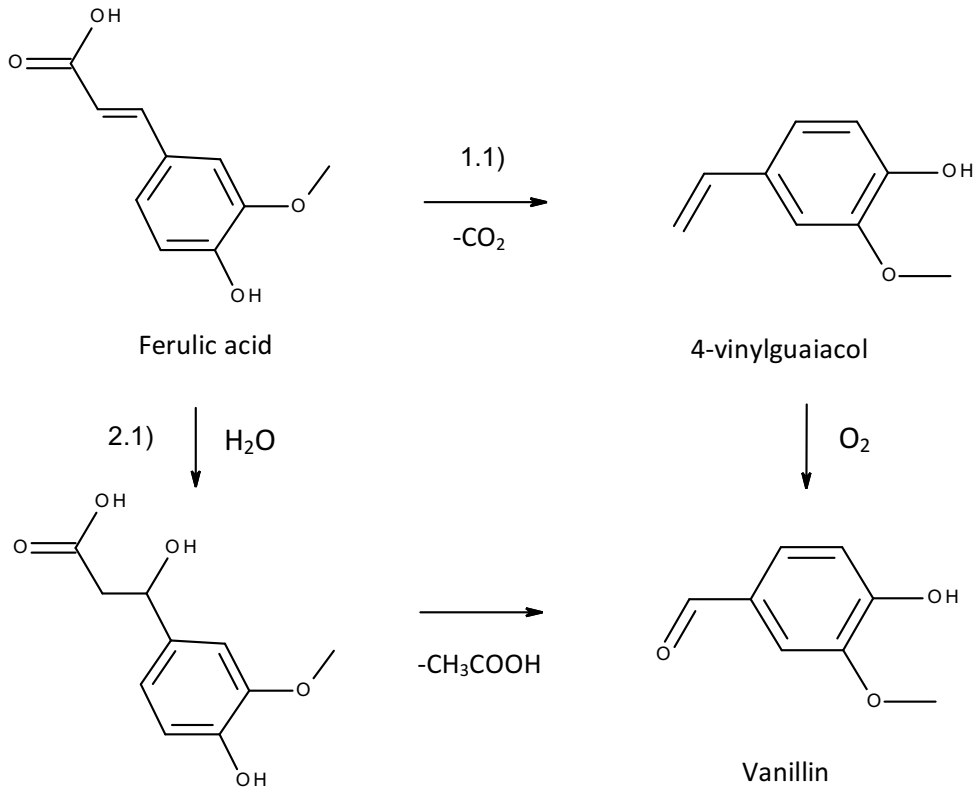

Figure 6 - Lignin primary by-products decomposition

II.3.3.2 Secondary decomposition

3,5-dimethylphenol (3,5-xylenol) was continuously emitted by biocomposites during the weathering. It rose from 94 ± 30 µg.m^{-3} after 1 month to 471 ± 75 µg.m^{-3} (PP30) after 12 months of exposition for PP30. At high temperatures, these alkylated phenols are formed by C-O radical cleavage of methoxy group and further coupling of phenolic radical with methyl radical group [23]. However, alkylphenols can easily appear only under pyrolysis conditions of lignin allowing alkylation. In our study, the temperature conditions are not enough favorable to trigger methylation. Nevertheless, as discussed previously, several factors could still contribute to alkylphenols sourcing. Indeed, brown and white-root fungi are recognized to be able to demethoxylize lignin [51]. Moreover, UV radiation leading to demethoxylation [52,53] may explain the formation of xylenol emitted only once biocomposites were exposed to climatic conditions. In this work, it has been assumed that this abstraction can give way to combination between methyl radical issued from demethylation of lignin allowed by O-demethylase enzymes active before hemp fibers process [54] and phenol radical. Moreover,

enzymes present in lignin and included in proteins could play the role of natural biocatalysts of these reactions before process of biocomposites [50]. In addition, the retting process could favor microorganisms formation accelerating by-products generation.

II.4. Conclusion

Since biocomposites are more and more integrated in vehicles, car indoor environment can be polluted by volatile substances released by cellulose-based materials. Moreover, the origins of the biocomposites odors caused by high manufacturing temperature have to be determined. The aim of this work was to understand the formation of VOCs and their structures issued from non-weathered and under glass weathered PP and hemp fibers reinforced biocomposites. Reactions schemes were proposed according to volatile products that were identified in this study.

Firstly, it was assumed that primary decomposition of holocellulose and lignin in hemp fibers occurred at non-weathered state whereas secondary decomposition was favored at weathered state. Mainly 2- and 5-substituted furans were emitted by non-weathered biocomposites. Since same precursors and same nitrogen-containing chemicals evolved from non-weathered vegetal fibers decomposition as food thermal degradation, Maillard mechanism could be extrapolated to this study. 3-, 4- and 5-substituted furanones were preferentially emitted after weathering. Some reactions between volatile products were proposed: they mainly involved keto-enolization, dehydration and cyclisation mechanisms. As regards lignin decomposition, methoxyphenols, detected at non-weathered state, were explained by hydration and oxidation whereas dimethylphenol, evolved from weathered biocomposites, could originate from radical reactions.

However, the reactions implying dehydrogenation to give 4,5-dimethyl-5-hydroxy-2-furanone (cellulose) and oxidation of vinyl specie to give vanillin (lignin) need highly favorable conditions to occur. Thus, activation energy calculation of the proposed reactions could be further modeled to check their occurrence feasibility. Also, the precise role of proteins and enzymes in carbohydrates and lignin degradation must be deeper investigated. Additives such as light stabilizers or antioxidants incorporated in the materials can be used

to limit dehydrations inducing sugars ring-opening and the impact of exposition to UV rays and high temperature.

II.5. Acknowledgements

This research did not receive any specific grant from funding agencies in the public, commercial, or not-for-profit sectors.

II.6. References

[1] Z.N. Azwa, B.F. Yousif, A.C. Manalo, W. Karunasena, A review on the degradability of polymeric composites based on natural fibres, Mater. Des. 47 (2013) 424–442. doi:10.1016/j.matdes.2012.11.025.

[2] M. John, S. Thomas, Biofibres and biocomposites, Carbohydr. Polym. 71 (2008) 343–364. doi:10.1016/j.carbpol.2007.05.040.

[3] Air quality sciences Inc., Indoor Air Quality hazards of new cars, (2006) 47–51.

[4] C. Yu, D. Crump, A review of the emission of VOCs from polymeric materials used in buildings, Build. Environ. 33 (1998) 357–374. doi:10.1016/S0360-1323(97)00055-3.

[5] A. Khazaeian, A. Ashori, M.Y. Dizaj, Suitability of sorghum stalk fibers for production of particleboard, Carbohydr. Polym. 120 (2015) 15–21. doi:10.1016/j.carbpol.2014.12.001.

[6] G. Dorez, A. Taguet, L. Ferry, J.M. Lopez-Cuesta, Thermal and fire behavior of natural fibers/PBS biocomposites, Polym. Degrad. Stab. 98 (2013) 87–95. doi:10.1016/j.polymdegradstab.2012.10.026.

[7] P. Zou, H. Xiong, S. Tang, Natural weathering of rape straw flour (RSF)/HDPE and nano-SiO2/RSF/HDPE composites, Carbohydr. Polym. 73 (2008) 378–383. doi:10.1016/j.carbpol.2007.12.002.

[8] C. Badji, L. Soccalingame, H. Garay, A. Bergeret, J.-C. Bénézet, Influence of weathering on visual and surface aspect of wood plastic composites: Correlation approach with mechanical properties and microstructure, Polym. Degrad. Stab. 137 (2017) 162–172. doi:10.1016/j.polymdegradstab.2017.01.010.

[9] S. Shibata, Natural Fiber Composites, in: R.D.S.G. Campilho (Ed.), Nat. Fiber Compos., 2016: pp. 157–173.

[10] H.-S. Kim, S. Kim, H.-J. Kim, H.-G. Kim, Physico-mechanical properties, odor and VOC emission of bio-flour-filled poly(propylene) bio-composites with different volcanic pozzolan contents, Macromol. Mater. Eng. 291 (2006) 1255–1264. doi:10.1002/mame.200600212.

[11] H.-S. Kim, B.-H. Lee, H.-J. Kim, H.-S. Yang, Mechanical–thermal properties and VOC

emissions of natural-flour-filled biodegradable polymer hybrid bio-composites, J. Polym. Environ. 19 (2011) 628–636. doi:10.1007/s10924-011-0313-5.

[12] C. Rouillon, P.O. Bussiere, E. Desnoux, S. Collin, C. Vial, S. Therias, J.L. Gardette, Is carbonyl index a quantitative probe to monitor polypropylene photodegradation?, Polym. Degrad. Stab. 128 (2016) 200–208. doi:10.1016/j.polymdegradstab.2015.12.011.

[13] A. François-Heude, E. Richaud, E. Desnoux, X. Colin, Influence of temperature, UV-light wavelength and intensity on polypropylene photothermal oxidation, Polym. Degrad. Stab. 100 (2014) 10–20. doi:10.1016/j.polymdegradstab.2013.12.038.

[14] J.F. Rabek, Photostabilization of Polymers: Principles and applications, Elsevier Applied Science, 1990. doi:10.1007/978-94-009-07-47-8.

[15] M. Muasher, M. Sain, The efficacy of photostabilizers on the color change of wood filled plastic composites, Polym. Degrad. Stab. 91 (2006) 1156–1165. doi:10.1016/j.polymdegradstab.2005.06.024.

[16] D.J. Nowakowski, J.M. Jones, Uncatalysed and potassium-catalysed pyrolysis of the cell-wall constituents of biomass and their model compounds, J. Anal. Appl. Pyrolysis. 83 (2008) 12–25. doi:10.1016/j.jaap.2008.05.007.

[17] E.B. Sanders, A.I. Goldsmith, J.I. Seeman, A model that distinguishes the pyrolysis of d-glucose, d-fructose, and sucrose from that of cellulose. Application to the understanding of cigarette smoke formation, J. Anal. Appl. Pyrolysis. 66 (2003) 29–50. doi:10.1016/S0165-2370(02)00104-3.

[18] K. Katō, H. Komorita, Pyrolysis of Cellulose, Agric. Biol. Chem. 32 (1968) 21–26. doi:10.1080/00021369.1968.10859016.

[19] J.B. Binder, J.J. Blank, A. V. Cefali, R.T. Raines, Synthesis of furfural from xylose and xylan, ChemSusChem. 3 (2010) 1268–1272. doi:10.1002/cssc.201000181.

[20] Y. Peng, S. Wu, Fast pyrolysis characterisctics of sugarcane bagasse hemicellulose, Cellul. Chem. Technol. 45 (2011) 605–612.

[21] M. Carrier, A. Loppinet-Serani, C. Absalon, C. Aymonier, M. Mench, Degradation pathways of holocellulose, lignin and alpha-cellulose from Pteris vittata fronds in sub- and super critical conditions, Biomass and Bioenergy. 43 (2012) 65–71. doi:10.1016/j.biombioe.2012.03.035.

[22] I. Brzonova, E. Kozliak, A. Kubátová, M. Chebeir, W. Qin, L. Christopher, Y. Ji, Kenaf biomass biodecomposition by basidiomycetes and actinobacteria in submerged fermentation for production of carbohydrates and phenolic compounds., Bioresour. Technol. 173 (2014) 352–60. doi:10.1016/j.biortech.2014.09.057.

[23] R. Wittkowski, J. Ruther, H. Drinda, F. Rafiei-Taghanaki, Formation of smoke flavor compounds by thermal lignin degradation, ACS Symp. Ser. 490 (1992) 232–243.

[24] Y.W. Sari, Biomass and its potential for protein and amino acids; valorizing agricultural

by-products, PhD thesis, Wageningen University, 2015.

[25] Mitsuo Namiki, Chemistry of Maillard reactions: Recent studies on the browning reaction mechanism and the development of antioxydants and mutagens, in: C.O. Chichester, B.S. Schweigert (Eds.), Adv. Food Res., Elsevier Inc, 1988: pp. 116–143.

[26] C. He, C.L. Chen, A. Giannis, Y. Yang, J.Y. Wang, Hydrothermal gasification of sewage sludge and model compounds for renewable hydrogen production: A review, Renew. Sustain. Energy Rev. 39 (2014) 1127–1142. doi:10.1016/j.rser.2014.07.141.

[27] Q. Zhang, J.M. Ames, R.D. Smith, J.W. Baynes, T.O. Metz, A perspective on the Maillard reaction and the analysis of protein glycation by mass spectrometry: probing the pathogenesis of chronic disease, J. Proteome Res. 8 (2008) 754–769. doi:10.1021/pr800858h.

[28] A.E. Newton, A.J. Fairbanks, M. Golding, P. Andrewes, J.A. Gerrard, The role of the Maillard reaction in the formation of flavour compounds in dairy products - Not only a deleterious reaction but also a rich source of flavour compounds, Food Funct. 3 (2012) 1231–1241. doi:10.1039/c2fo30089c.

[29] J.E. Hodge, F.D. Mills, B.E. Fisher, Compounds of browned flavor derived from sugar-amine reactions, Am. Assoc. Cereal Chem. 17 (1972) 34–40.

[30] S. Wang, X. Guo, T. Liang, Y. Zhou, Z. Luo, Mechanism research on cellulose pyrolysis by Py-GC/MS and subsequent density functional theory studies, Bioresour. Technol. 104 (2012) 722–728. doi:10.1016/j.biortech.2011.10.078.

[31] H.-D. Belitz, W. Grosch, P. Schieberle, Aroma compounds, in: M. Dekker (Ed.), Food Chem., CRC Press, 2004: pp. 340–402. doi:10.1007/978-3-662-07279-0.

[32] R.F. Perez, M.A. Fraga, Hemicellulose-derived chemicals: one-step production of furfuryl alcohol from xylose, Green Chem. 16 (2014) 3942. doi:10.1039/C4GC00398E.

[33] D. Bourdin, P. Mocho, V. Desauziers, H. Plaisance, Formaldehyde emission behavior of building materials: on-site measurements and modeling approach to predict indoor air pollution., J. Hazard. Mater. 280 (2014) 164–73. doi:10.1016/j.jhazmat.2014.07.065.

[34] D. Bourdin, V. Desauziers, Development of SPME on-fiber derivatization for the sampling of formaldehyde and other carbonyl compounds in indoor air, Anal. Bioanal. Chem. 406 (2014) 317–328. doi:10.1007/s00216-013-7460-6.

[35] Chemical Risk Prevention Unit, CNRS, European harmonised classification and labelling of carcinogenic, mutagenic and toxic for reproduction (CMR) substances according to the criteria of the CLP Regulation, (2015).

[36] J.A. Koziel, J. Noah, J. Pawliszyn, Field sampling and determination of formaldehyde in indoor air with solid-phase microextraction and on-fiber derivatization, Environ. Sci. Technol. 35 (2001) 1481–1486. doi:10.1021/es001653i.

[37] M.J. Fedoruk, B.D. Kerger, Measurement of volatile organic compounds inside automobiles, J. Expo. Anal. Environ. Epidemiol. 13 (2003) 31–41.

doi:10.1038/sj.jea.7500250.

[38] J. Nicolle, V. Desauziers, P. Mocho, Solid phase microextraction sampling for a rapid and simple on-site evaluation of volatile organic compounds emitted from building materials, J. Chromatogr. A. 1208 (2008) 10–15. doi:10.1016/j.chroma.2008.08.061.

[39] V. Desauziers, Traceability of pollutant measurements for ambient air monitoring, Trends Anal. Chem. 23 (2004) 252–260. doi:10.1016/S0165-9936(04)00310-3.

[40] A. François-Heude, E. Richaud, J. Leprovost, M. Heninger, H. Mestdagh, E. Desnoux, X. Colin, Real-time quantitative analysis of volatile products generated during solid-state polypropylene thermal oxidation, Polym. Test. 32 (2013) 907–917. doi:10.1016/j.polymertesting.2013.04.008.

[41] A. Hoff, S. Jacobsson, Thermal oxidation of polypropylene close to industrial processing conditions, J. Appl. Polym. Sci. 27 (1982) 2539–2551. doi:10.1002/app.1982.070270723.

[42] R. Bernstein, S.M. Thornberg, A.N. Irwin, J.M. Hochrein, D.K. Derzon, S.B. Klamo, R.L. Clough, Radiation-oxidation mechanisms: Volatile organic degradation products from polypropylene having selective C-13 labeling studied by GC/MS, Polym. Degrad. Stab. 93 (2008) 854–870. doi:10.1016/j.polymdegradstab.2008.01.020.

[43] D.K. Shen, S. Gu, The mechanism for thermal decomposition of cellulose and its main products, Bioresour. Technol. 100 (2009) 6496–6504. doi:10.1016/j.biortech.2009.06.095.

[44] M.G. Al-Shaal, W. Ciptonugroho, F.J. Holzhäuser, J.B. Mensah, P.J.C. Hausoul, R. Palkovits, Catalytic upgrading of α-angelica lactone to levulinic acid esters under mild conditions over heterogeneous catalysts, Catal. Sci. Technol. 5 (2015) 5168–5173. doi:10.1039/C5CY00446B.

[45] P. Mäki-Arvela, E. Salminen, T. Riittonen, P. Virtanen, N. Kumar, J.P. Mikkola, The challenge of efficient synthesis of biofuels from lignocellulose for future renewable transportation fuels, Int. J. Chem. Eng. 2012 (2012). doi:10.1155/2012/674761.

[46] O.R. Fennema, Food Chemistry, 3rd ed., CRC Press, 1996.

[47] S. Coghe, K. Benoot, F. Delvaux, B. Vanderhaegen, F.R. Delvaux, Ferulic acid release and 4-vinylguaiacol formation during brewing and fermentation: indications for feruloyl esterase activity in Saccharomyces cerevisiae., J. Agric. Food Chem. 52 (2004) 602–608. doi:10.1021/jf0346556.

[48] H. Peleg, M. Naim, U. Zehavi, R.L. Rouseff, S. Nagy, Pathways of 4-vinylguaiacol formation from ferulic acid in model solutions of orange juice, J. Agric. Food Chem. 40 (1992) 764–767. doi:10.1021/jf00017a011.

[49] J. Gassan, A.K. Bledzki, Thermal degradation of flax and jute fibers, J. Appl. Polym. Sci. 82 (2001) 1417–1422. doi:10.1002/app.1979.

[50] L. Pollegioni, F. Tonin, E. Rosini, Lignin-degrading enzymes, FEBS J. 282 (2015) 1190–

1213. doi:10.1111/febs.13224.

[51] M. Lopretti, D. Cabella, J. Morais, A. Rodrigues, Demethoxylation of lignin-model compounds with enzyme extracts from Gloeophilum trabeum, Process Biochem. 33 (1998) 657–661. doi:10.1016/S0032-9592(98)00028-4.

[52] K. Srinivas, K.K. Pandey, Photodegradation of thermally modified wood, J. Photochem. Photobiol. B Biol. 117 (2012) 140–145. doi:10.1016/j.jphotobiol.2012.09.013.

[53] D.N.-S. Hon, S.-T. Chang, Surface degradation of wood by ultraviolet light, J. Polym. Sci. Polym. Chem. Ed. 22 (1984) 2227–2241. doi:10.1002/pol.1984.170220923.

[54] X. Peng, E. Masai, H. Kitayama, K. Harada, Y. Katayama, M. Fukuda, Characterization of the 5-Carboxyvanillate Decarboxylase gene and its role in lignin-related biphenyl catabolism in Sphingomonas paucimobilis SYK-6, 68 (2002) 4407–4415. doi:10.1128/AEM.68.9.4407.

III. Under glass exposure test of hemp fibers reinforced polypropylene biocomposites to simulate interior car ageing: Relationships between VOCs emissions, visual aspect, mechanical properties, and microstructure

Célia Badji, Joana Beigbeder, Hélène Garay, Anne Bergeret, Jean-Charles Bénézet and Valérie Desauziers

C2MA, Ecole des mines d'Alès, 6 avenue de Clavières, 30319 Cedex France

Keywords: VOCs emission, correlation, hemp fibers, oxidation, yellowness, mechanical properties

Abstract

Natural one-year under windshield degrading test was designed in order to measure the synergic effect of vehicle interior conditions on hemp fibers reinforced polypropylene (PP) biocomposites properties. For this purpose, physical, mechanical and chemical properties were correlated with Volatile Organic Compounds (VOCs) emissions. Considering the high number of samples and properties, a Principal Component Analysis (PCA) was proposed to easily identify the more important properties that describe the dataset. Also, the correlations between properties were assessed through this analysis. Statistical clustering of samples highlighted the similarities/differences between them. Preliminary calculation was performed and provided overview on global variables causal relationships. This allowed classifying through an unsupervised method the quantitative variables (properties) by determining the contribution of each variable to the axes drawing. Chemical composition and VOCs emission contributed to the more informative component drawing and thus best discriminated the individuals. Separating materials according to their hemp fibers loading (0, 10, 30 wt%) permitted only discussing the influence of the weathering time on variables relationships. Results revealed that VOCs emission could indicate the mechanical performance loss. Finally, correlations, either positive or negative, were determined at each time of weathering. This showed that correlation between roughness and gloss aspect was verified whatever the time of weathering. Nonetheless, mechanical properties and VOCs emissions remained non-correlated whatever the exposition time, certainly because neat PP and biocomposites were all included in the statistical calculation.

III.1. Introduction

With the depletion of fossil resources and environmental issues come requirements for deployment of renewable resources. That is why attention has turned to biocomposites development as natural fibers are eco-friendly and low energy manufacture consuming and present specific mechanical properties close to traditional glass ones. They are generally associated to petroleum-based such as polypropylene (PP), polyethylene (PE) and polyvinyl chloride (PVC)) or to bio-based polymers such as polyhydroxyalcanoate (PHA) and polylactic acid (PLA). Otherwise, Original automotive Equipment Manufacturers (OEMs) tend to supply different car parts made of natural fibers composites [1,2]. The dashboards are besides more and more made of biocomposites in vehicles from automakers such as Mercedes-Benz or Alfa Romeo [3,4]. These pieces are hence directly exposed to UV radiation and the low stability of natural fibers towards temperature, UV rays and moisture lead to color changes, strength loss and degradation products emission [5]. Assigned to lignocellulosic components decomposition, this last consequence can induce unpleasant odor, important factor for confined-space uses such as car interiors [6,7]. Indeed, furfural and 5-methylfurfural as holocellulose by-products, are mainly responsible for the odor emitted by biocomposites [8]. Lignin is also implied in odorous substances release since this amorphous aromatic cross-linked polymer decomposes into vanillin. So all these products can accentuate “new car smell” [9] towards use of biocomposites destined to vehicles interior parts. However, the scent of new vehicle can transform into more problematic Sick Car Syndrome (SCS) depending on the indoor conditions (temperature, ventilation, …) and Volatile Organic Compounds (VOCs) levels and toxicity [10]. Hence, in addition to regulations established by number of countries regarding limiting chemicals levels in vehicles [11–13], OEMs and automotive manufacturers have implemented VOCs targets in passenger cars based on standards methods and analytical implementation [14,15].

Some reports are available on the measurement and reduction of VOCs emission and odor of biocomposites [5–7,9]. But fewer studies relate the impact of biocomposites ageing on indoor air quality allowing to understand the polymer and natural fibers degradation mechanisms. Among the existing studies, Espert et al conducted a thermal degradation of pulp and hemp fibers reinforced PP biocomposites. They assessed its influence on the

materials VOCs emission. The type of identified volatile products emitted by thermally degraded materials differed from unaged ones [16]. Mainly alcohols and carboxylic derivatives increased in terms of detected compounds number.

Headspace-solid phase microextraction (HS-SPME) coupled with gas chromatography-mass spectrometry (GC-MS) has been recognized as a suitable characterizing tool in rapid diagnostic analysis of chemicals evolving from polymeric materials [17–19]. Moreover, this method is sensitive and easy to implement thanks to possible automation of the overall analytical procedure. These qualities have prompted some researchers for favoring this analytical method to follow degradation state of polymers [16,20,21]. Natural components weathering was also investigated by means of this technique. For instance, carbohydrates and lignin relevant degradation compounds (furfural, 5-methylfurfural, vanillin and guaiacol) having evolved from paper ageing were verified as ageing markers [22]. However, HS-SPME technique sometimes requires samples cutting to introduce samples in the vials. The passive sampling method used in this work allows to measure VOCs emission without damaging the analyzed material. The emission rate being described by the first Fick's law of diffusion under steady-state conditions, the VOCs concentration at the surface of the material can be determined [23].

VOCs emissions were sometimes related to other properties. For instance, polymeric parts of museum pieces including cellulose acetate, cellulose nitrate, PVC and polyurethane (PU) were naturally and artificially weathered [24]. It was demonstrated that aldehydes and ketones emissions were related to visual appearance evolution (discoloration) of polymers and infrared spectra bands evolution. Carlsson et al. investigated the influence of weathering on PVC discoloration and VOCs release behavior in Ottawa [25–27]. Plastic underwent chalking directly linked to chlorinated VOCs. PE films exhibited low molecular weight compounds emission fitting polymer chain scission phenomenon [28]. Otherwise, the relative amount of VOCs belonging to the dicarboxylic acids family correlated well with molecular weight decrease. VOCs emission from virgin and recycled polyamide-6,6 were measured by HS-SPME/GC-MS during their ageing [29]. A correlation between degradation product pattern, in particular 1-pentyl-2,5-pyrrolidinedione, and mechanical properties deterioration has been issued. Indeed, whatever the polymer state (virgin or recycled), the

decrease of mechanical performance inversely coincided with the increase of the relative abundance of the heaviest emitted degradation product. A quantitative correlation of volatile products derived from degrading cellulose (paper) and lignin with acidity and different components content (lignin, ash, protein, rosin) has been also evaluated [30]. A particular interest was focused on the effects of different compounds on cellulosic paper stability. Also, carbonyl group content was positively correlated with lignin while rosin was negatively correlated with protein rate. These two observations gave information on composition. It was observed that not only cellulosic compounds were responsible for carbonyl rate increase but also rosin thanks to volatile chemicals analyses. As regards biocomposites, Courgneau et al. measured several properties including molecular weight, thermal stability and odor emission behavior of cellulose fibers reinforced PLA biocomposites for car interior [9]**.** The relation between odor generated by chemicals release and degradation after their compounding was also investigated by these authors. They showed that the effect of the process-induced degradation was a decrease in molecular weight of PLA and the formation of odorant VOCs.

Principal Component Analysis (PCA) allows simplifying interpretation of multidimensional-space data by projecting properties and samples on a plan. It has besides found some application for estimating major source contributions to ambient VOCs concentrations [31–34]. Also, PCA was sometimes conducted in works bringing polymers under degradation conditions and assessing volatile products emission. As an example, the influence of γ-irradiation on volatile products release by polymeric multilayer materials was determined [35]. Considering the high number of samples, PCA was performed on the overall data in order to put forward the main chemical families differencing samples that were non-irradiated and irradiated at different rates. The more discriminating chemical families were aromatics and cyclic compounds closely related to the principal components explaining the most of variance. Other oxygenated products families such as ketones, and other oxidation products were opposed to antioxidants and alkenes respectively, suggesting that oxygenated VOCs were formed at the expense of the latter. Also, the same method was used to classify historical papers through chemicals issued from lignocellulosic structures [30]. This showed how well-known carbohydrates and lignin volatile derivatives dominated the main principal components and distinguished papers of different nature (rag, bleached-pulp and

groundwood-containing papers). Also, different classifications of the samples were achieved by considering either VOCs or compounds content. However, to our best knowledge, statistical analysis including VOCs emission of polymers and other common properties for a better understanding of material degradation was not carried out.

The aim of this study is to determine if the volatile degradation product pattern of PP and hemp fibers reinforced biocomposites can bring some elements on mechanisms of degradation by means of statistical way. For this purpose, VOCs emission will be related to macroscopic signs of degradation and to the simultaneous changes in mechanical, visual appearance and microstructure properties during under glass weathering. Otherwise, this calculation method will permit to verify if VOCs emission can be considered as a useful and reliant indicator of biocomposites degradation. Finally, the most important features will be extracted by plotting the data.

III.2. Materials and methods

III.2.1 Raw materials

Polypropylene (PP, grade H733-07) with a melt flow rate of 7.5 g/10 min (230 °C, 2.16 kg) (Braskem, Brazil) in the form of pellets was used as homopolymer matrix. Hemp fibers provided by AgroChanvre (Barenton, France) were sifted to select fibers length range of 2 to 6-mm. Maleic anhydride grafted polypropylene (MA-g-PP, Orevac CA100) (Arkema, France) was added at 3.1 wt% of PP as coupling agent. The hemp fibers were added at 10 wt% (PP10) and 30 wt% (PP30) in the (PP+PP-g-MA) part.

III.2.2 Process conditions

Oven-dried PP and MA-g-PP granules were mixed with hemp fibers in a BC21 Clextral co-rotating twin-screw extruder (L/D = 36 with the diameter D = 25 mm and L= 900 mm) (Clextral, France) with the temperature ranging from 190 to 175 °C from hopper to die end and a screw speed of 220 rpm. Once dried for 3 days at 60 °C in an air-circulating oven, extruded pellets were injection molded in a Krauss Maffei KM50-T180CX (Krauss Maffei, Germany) at 210 °C with an injection speed of 30 $cm^3.s^{-1}$. ISO 1 dog-bone specimens and square specimens of 100 × 100 × 2 mm and were obtained for both mechanical performance and visual appearance characterizations respectively.

III.2.3 Weathering

One-year exposition in the south west of France was carried out from September, 2015 to September, 2016 to represent application of biocomposites in car interiors, according to ISO 877:2-2011 standard [36]. The samples were fixed on galvanized racks at an angle fixed at 45° with the ground,directed toward the South and covered by laminated windshield glasses (Figure 1). Hygrothermic data were monitored. Monthly average temperature ranged from 15 °C in January to 37 °C in August and monthly average relative humidity took values between 33% in May to 69% in January. Materials properties were measured after 1, 2, 3, 6, 9 and 12 months. Non-weathered materials were designed as PP-UW, PP10-UW and PP30-UW. PP-GWn, PP10-GWn and PP30-GWn were affected to weathered samples with n the number of months of exposition.

Figure 1 - Under glass exposure racks

III.2.4 Flexural tests

To characterize the samples strength, flexural test was operated at room temperature on dog-bone samples in accordance to the ISO 178:2010 standard. The mechanical behaviours were tested by Zwick TH 010 press machine with a 2.5 kN load cell. The three point bending system was used with crosshead speeds of 2 and 100 $mm.min^{-1}$ for the modulus E and flexural stress at the conventional deflection σ_{fc} measurements respectively.

III.2.5 Differential Scanning Calorimetry (DSC)

Thermograms were obtained from PYRIS Diamond calorimeter (Perkin Elmer, United States). Samples of approximately 10 mg were ramped from 30°C to 210°C at 10°C.min^{-1} then cooled down to 30°C with a cooling rate of 10°C.min^{-1}. The first heat was finally repeated once time. All mesaurements were performed under N_2 atmosphere. The degree of crystallinity of PP was calculated from the ratio of the melting enthalpy ΔHm (J.g^{-1}) of the sample to the the melting enthalpy of 100% crystalline PP (209 J.g^{-1}) and the PP mass fraction:

$$\chi c\ (\%) = \frac{\Delta Hm}{W \times \Delta Hm_{100}} \times 100 \qquad \text{Eq. 1}$$

The crystallinity rate χc was determined from 2nd heating cycle since the second run provides information on the ability of degraded chains of the polymer to crystallize [29,37–40]. Moreover, same evolution tendencies were observed during the 1st and 2nd heating cycles. The analysis of each material was repeated 2 times in order to ensure the reproducibility.

III.2.6 Fourier Transform Infrared spectroscopy (FTIR)

Fourier Transform Infrared spectra were recorded with a IFS66 spectrometer (Bruker, United States) in Attenuated Total Reflectance (ATR) mode. This technique allowed to determine the variations of rates of vinyl bonds and carbonyl bonds in lactones, aldehydes and esters, carboxylic acids and ketones molecules. FT-IR spectra of the samples recorded in the range 4000–400 cm^{-1} with a resolution of 1 cm^{-1} and 32 scans. They were normalized according to the band at 2925 cm^{-1} assigned to CH_2 methylene stretching, which is usually used as a reference band for cellulose and PP since this bond is non affected by weathering conditions [41,42].

III.2.7 Spectrocolorimetry

The surface color analysis was performed by spectrocolorimetry on a Chroma Sensor CS3 (DataColor, United States). The CIE 1976 *L*, a*, b** uniform system was used to represent the color and the lightness. An increase of L* (from 0 to 100) demonstrates a material lightening whereas a* and b* are the chromaticity positions on axes from -300 to +300 axes

from green (-a*) to red (+a*) and from blue (-b*) to yellow (+b*). A total of 12 areas by material were characterized.

III.2.8 Spectrogoniometry

Gloss measurements were carried out using a GON 360 goniometer (Intrument Service, Germany) associated with a MAS 40 spectrometer equipped with a halogen lamp. The principl of this is developed elsewhere [43]. The goniometer light source was set at 20° and reflected light was collected in the detector angles range 5°-(-60°) with a step smaller in the specular zone to detect the high variations of intensity in this zone. The representation of the intensity versus the detector angle allowed to characterize the gloss aspect [44]. The haze gloss G_1 was determined from the ratio of the maximum intensity obtained for the angle of detection of -20° I(Θ = -20°) to the intensity obtained for the angle of -22° I(Θ = -22°) both situated in the specular zone. The contrast gloss G_2 was obtained from the ratio of I(Θ = -20°) to the intensity collected for the angle of -35° I(Θ = 35°) of a diffusely reflected light was also calculated. Mean values and standard deviations were obtained from the analysis of four areas of three samples. The higher G value is, the glossier and smoother the surface seems.

III.2.9 Rugosimetry

The microtopography consisted on measuring the altitude of each surface point on the sample according to the ISO 25178 standard. For this purpose, a MICROMESURE STIL system equipped with a STIL CHR150 optical sensor (STIL, France) was used to determine the roughness parameter Sa (µm) (Eq. 2). More details are given in a previous paper [43,45]. The micrometric range of the optical pen was 285 µm. It permits a tridimensional analysis and the analyzed area X*Y was 5 mm * 5 mm with an analysis step of 10 µm in X and Y directions.

$$\mathrm{Sa} = \frac{1}{NM}\sum_{x=0}^{N-1}\sum_{y=0}^{M-1}|z(x,y)| \qquad \text{Eq. 2}$$

with M the number of points along the X axis, N the number of points along the Y axis, and $z_{x,y}$ the altitude in µm. Four locations of three samples were examined.

III.2.10 VOCs emission

III.2.10.1 Sampling and analytical methodology

Unlike the different works presented in introduction and based on HS-SPME analysis, this study involved a specific passive sampling method to only measure materials surface emission [23]. It consists in two steps: a cylindrical glass cell (50 mL) equiped with a septum in central position is firstly deposited on the material in order to isolate a part of its surface. During this step, emitted VOCs diffuse from the material to the air in the cell until reaching stable concentrations meaning that material/air equilibrium is achieved [23]. A polydimethylsiloxane-divinylbenzene-carboxen SPME fiber (PDMS/DVB/CAR, 50/30 µm) (Supelco, United States) is then introduced in the glass cell through the septum to extract emitted VOCs. Then, the SPME fiber is thermally desorbed in the injection port of a gas chromatograph (GC) coupled with mass spectrometer (MS) and flame ionization detector (FID) (Varian, France) for VOCs identification and quantification. More details of analytical procedure are given elsewhere [46]. Sampling temperature of 23 °C was tested to simulate ambient interior conditions. Three samples of each material PP, PP10 and PP30 were analysed at each time of weathering.

III.2.10.2Quantitative analysis

The sampling method described above allows determining material/air interface concentration (in $\mu g.m^{-3}$) of VOCs [23]. VOCs were quantified as toluene equivalent using FID response [47]. For calibration, toluene standard atmospheres were generated by a continuous syringe injection method [48,49]. The quantification limit is about 3 $\mu g.m^{-3}$.

III.2.11Statistical analysis

The PCA is carried out on Statistica 13 software (Dell, France). This multivariate statistical method is a multivariate technique that analyzes a data table in which observations are described by several inter-correlated quantitative variables. For this purpose, a set of orthogonal linear combinations called principal components is built. More details on the calculation method principle are given elsewhere [43,50]. In order to overcome the difference of units between all the properties (variables) for accurate interpretation, the

standardization of the dataset by centering-reduction was conducted for the correlation circle representation:

$$X_i' = \frac{X_i - \bar{X}}{\sigma_x} \quad \text{Eq. 3}$$

where X_i' is the centered-reduced variable, X_i is the variable and $\bar{X}$ and σ_x are the mean and standard deviation of the variable X respectively.

Table 1 - Designation of parameters

Designation	Parameter
E	Modulus of elasticity (MPa)
s	Stress at the conventional deflection (MPa)
Xc	Crystallinity rate (%)
A1	Absorbance C=O at 1711 cm^{-1} (carboxylic acids and ketones)
A2	Absorbance C=O at 1740 cm^{-1} (esters and aldehydes)
A3	Absorbance C=O at 1780 cm^{-1} (γ-lactones)
A4	Absorbance C=C at 1650 cm^{-1} (vinyls)
Sa	Roughness (µm)
G1	Haze gloss
G2	Contrast gloss
L*	Lightness (light-dark)
a*	Chromatic coordinate (red-green)
b*	Chromatic coordinate (yellow-blue)
Cvoc	All VOCs concentration ($\mu g.m^{-3}$)
Cca	Carboxylic acids concentration ($\mu g.m^{-3}$)
Ck	Ketones concentration ($\mu g.m^{-3}$)

III.3. Results and discussion

III.3.1 Global treatment

The relationships between mechanical, physical and chemical properties including VOCs emissions were assessed over under windshield glass weathering. For this aim, the correlation loadings are plotted in Figure 2. Firstly, the two first principal components PC1 and PC2 summarize almost 80% of the total information of inertia. Therefore, this is a reliable representation of projected variables. Otherwise, variables are generally well represented since they exhibit high radius. Only variables related to color and lightness are far away from the circle, especially a*, meaning that they were not well projected.

As for carbonyl absorbance values, VOCs concentrations variables Cvoc, Cca and Ck exhibit the highest coefficients of correlation among all the studied variables with the first main

component PC1 bringing more than 50% of inertia. Cvoc corresponds to the sum of the concentration of Cca and Ck since only ketones and carboxylic acids were detected all along the ageing. Otherwise, variables increase with decreasing PC1. This implies their negative correlation with PC1. In addition to previous ones, the roughness variable also dominates the first principal component. Thus, this principal component can be perceived as an axis describing chemical properties and topography. Also, the carboxylic acids (Cca), ketones (Ck) and all VOCs (Cvoc) concentrations are strongly correlated with A1, A2 and A3 since they overlap. This suggests that these 6 criteria vary together: if one increases, the others tend to do as well. This appears obvious since A1 and A2 represent intensity of vibration of carbonyl bonds in acids and ketones for A1 and esters and aldehydes for A2. The higher proportion of carboxylic acids than ketones accounted in all VOCs level (Cvoc) might explain the higher angle formed between Cvoc and Ck vectors. Otherwise, C=C absorption band (A4) and roughness parameter (Sa) vary together.

The elastic modulus E, the stress at the conventional deflection s and the crystallinity ratio Xc positively highly contribute to PC2. Nevertheless, variables-PC2 correlation is much more important for E and s. Thus, primarily mechanical performance makes sense to PC2.

Scatter plot of individuals (samples) is also displayed in Figure 2. Each dot represents PP, PP10 and PP30 samples exposed during different weathering time. PCA clearly led to the differentiation between PP, PP10 and PP30 individuals. All weathered neat PP are close to each other suggesting that they are alike and take similar values especially on PC2 whereas weathered biocomposites are vertically and horizontally distant. This means that PP10 and PP30 were particularly affected by the exposure.

Gaps between PP, PP10 and PP30 according to PC2 are much higher after 1, 2 and 3 months of weathering than those according to PC1. Thus, the mechanical properties and crystallinity rate are the variables that mostly characterize differences between materials with different hemp fiber loadings at the early stage of ageing. Otherwise, the coordinate according to PC2 axis increases with fiber loading. Indeed, the highest fiber rate reinforced biocomposite is stiffer and stronger. Then, VOCs release, absorbance attributing to C=O and C=C bonds (chemical composition) and roughness (surface aspect) mostly discriminate the three materials from 6 to 12 months with the highest absolute scores attributed to PP30. This

confirms the high sensitivity of fiber face to oxidative degradation leading to by-products release from biocomposite.

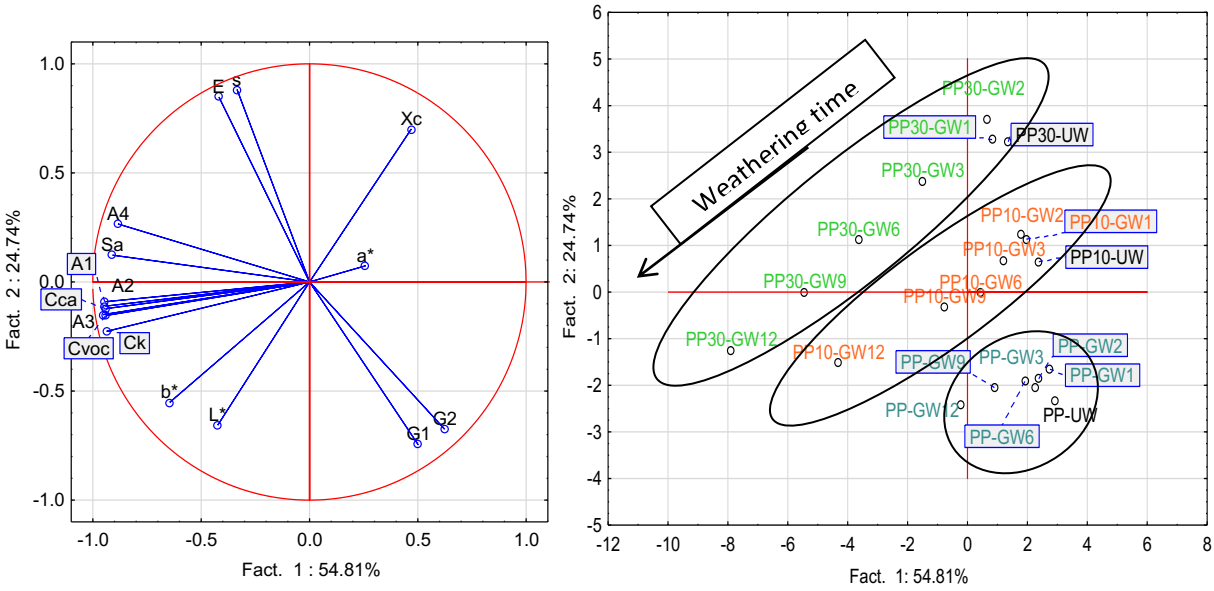

Figure 2 - Correlation circle and all individuals projection

III.3.2 Treatment by fiber loading

Correlation circle plots of PP, PP10 and PP30 separately are schematized in Figure 3. As regards neat PP, variables vectors are particularly exploded. Indeed, any particular correlation between variables is noted. On the contrary, a lot of information is captured from the data set of PP30 thanks to the first two principal components since they conserve almost 96 % of the inertia. Moreover, more variables, with radius close to $x^2 + y^2 = 1$ with x and y the variable coordinates on PC1 and PC2 respectively, are calculated for biocomposites. This indicates the highly satisfactory quality of representation.

In addition, the number of variables influencing the definition of PC1 increases with the fiber loading. For instance, by comparison to global analysis, E and s rotate so that they mostly devote to PC1. Otherwise, whereas mechanical properties were non-correlated with VOCs emissions for global treatment presented above, they are here anti-correlated with VOCs emission whatever the natural fiber rate. Indeed, the increasing emission of low molecular weight compounds from materials during its use might be the sign of degradation [16] and, in this case, of performance loss. This negative correlation was not previously verified maybe due to the fact that mechanical properties more explain fiber rate factor than weathering

time one. Similarly, Sa, Cvoc and Cca variables are opposed to Xc one according to the gravity center especially for biocomposites. It can be assumed that the polymer chain scissions might induce roughness [51] and favor release of volatile compounds. Moreover, as regards reinforced materials, degradation of polymer chains promoted emissions of chemicals linked to fibers decomposition due to matrix entanglement destruction. This last point could justify the spruce anti-correlation between Xc and Cvoc for PP10 and PP30 rather than for PP. Otherwise, Sa varies increasingly with the fiber loading in a same way as variables relating all chemicals emissions. Indeed, the correlation coefficient between these two parameters (Sa and Cvoc) reaches 0.98 for PP30. This can be interpreted by the increasing appearance of fibers at the surface inducing a rougher surface and release of aliphatic ketones, aldehydes and acids specifically evolving from natural fibers. All these causal relationships between hemp fibers degradation and mechanical and surface properties loss could translate the more informative components of biocomposites correlation circles.

Contrary to global treatment, color coordinates have been well projected. a* is well represented and close to PC2 for PP and PP10. But as already mentioned in a previous paper [43], any interpretation can be done for PP and PP10 since a* is assigned to the evolution of color of hemp fibers due to lignin degradation [52]. As regards PP30, b* is highly correlated with A2 and A3 suggesting that they increase in line. Actually, correlation coefficients equaling 0.99 and 0.98 respectively were noted. Thus, the yellowing observed all along the under glass exposition is assumed to originate from aldehydes and lactones formation issued from holocellulose and lignin depolymerisation. This is the reason why the relationship is only observed for biocomposites analyses. The small angle formed between A4 and L* vectors for biocomposites suggests a connection existing between C=C bonds level and lightness. Indeed, the evolution of the properties as a function of the time of weathering evidenced a plateau formed after 6 months (Figure 4). The stagnation of C=C level observed after long weathering time was assumed to originate from a conversion of C=C into C=O species. However, lignin highly contributes to C=C surface rate via carbon-carbon double bond in aromatic molecules [40,42]. On the basis of these facts, the growing appearance of lignin quinonic structures including C=C aromatic bonds at the surface might induce the bleaching of composites. Thus, in this study, lignin is also assumed to partially contribute and

be commonly responsible to bleaching and vinyl band increase and justify the close angle between A4 and L*.

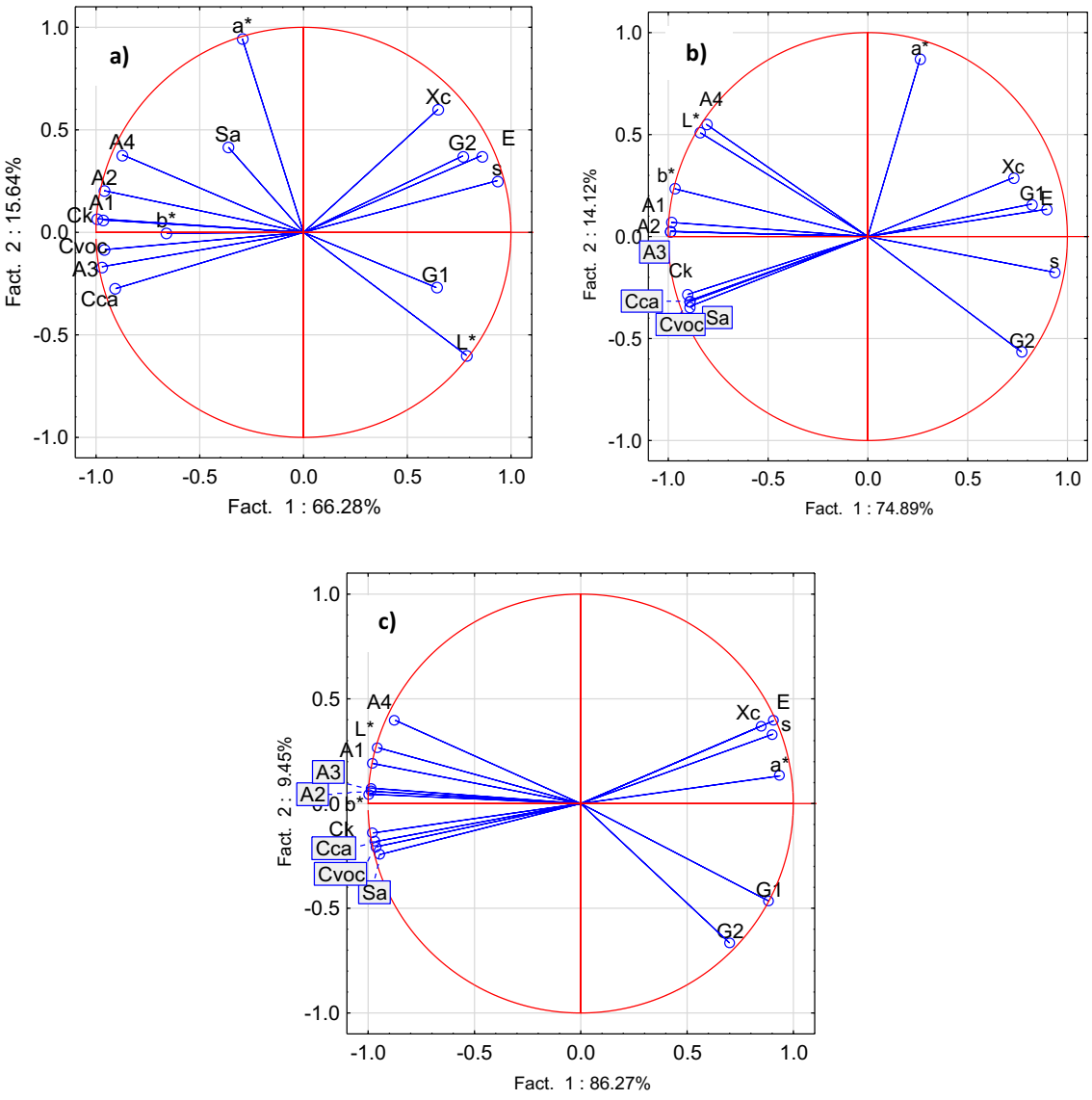

Figure 3 - Correlation circles of PP (a), PP10 (b) and PP30 (c)

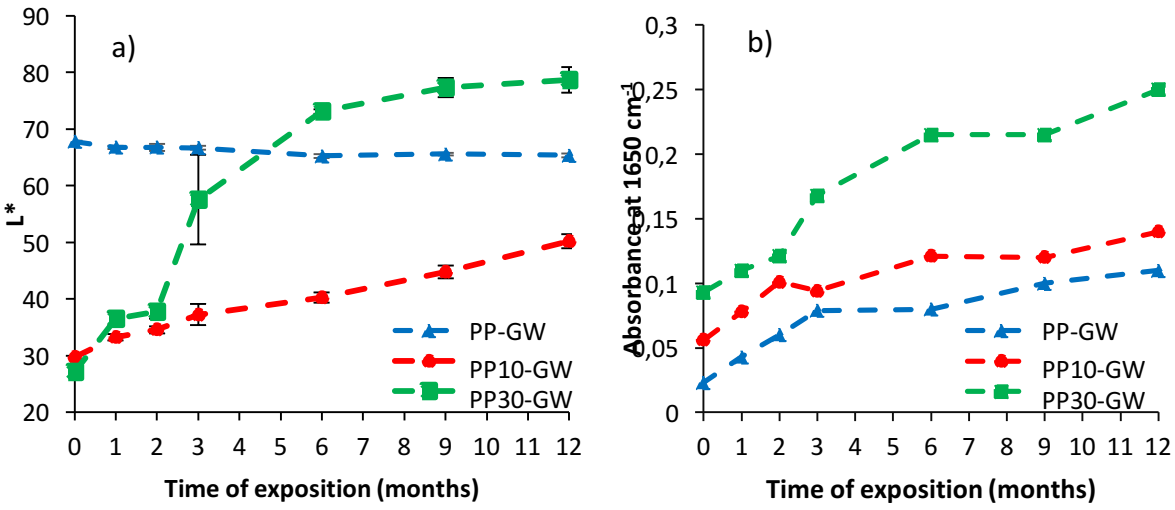

Figure 4 – Evolution of L* (a) and absorbance at 1650 cm^{-1} (b) over under glass weathering

Individuals exposed during different times of weathering are mainly spread according to PC1 (Figure 5). Indeed, they continuously take higher and higher values on variables demonstrating oxidation (VOCs emissions and C=O bonds from FTIR) and roughness. The differences according to PC2 are extremely low. Moreover, as mentioned before, a* cannot really explain vertical distances between samples for PP and PP10. However, it turns out that the coordinate on PC2 continuously increases from UW to GW6 for PP and PP10, then decreases. Therefore, the maximum on PC2 is attributed for PP-GW6, PP10-GW6 and PP30-GW6. This period effectively corresponds to the moment during which a* slightly decreased for PP and PP10 after its increase from 1 to 6 months. However, the decrease valued less than 1, and was hence considered non-significant [43].

As regards PP30 biocomposite, positions of individuals according to PC2 presented the same overall elbow-shaped profile that cannot be explained by redness coordinate since a* is mostly linked to PC1. However, chemicrystallization phenomenon due to chain scission induced increase of the crystallinity ratio and modulus during the first two months of weathering. This justifies the increase from UW to GW2 state according to PC2 that are partially characterized by E and Xc. Gloss partially negatively represented by PC2 is also responsible to this increase according to PC2. Otherwise, A4 and L* partially contribute to PC2 for biocomposites. Therefore, it can be assumed that the A4 and L* values increase of biocomposites until 6 months preceding their stability might be also related to the score increase of PP10 and PP30 on PC2 from UW to GW6. However, six-months weathering

corresponds to the stage when Xc of PP30 dropped below PP one justifying the further decrease on PC2. Thus, this stage corresponded to a critical period with variations trend changes.

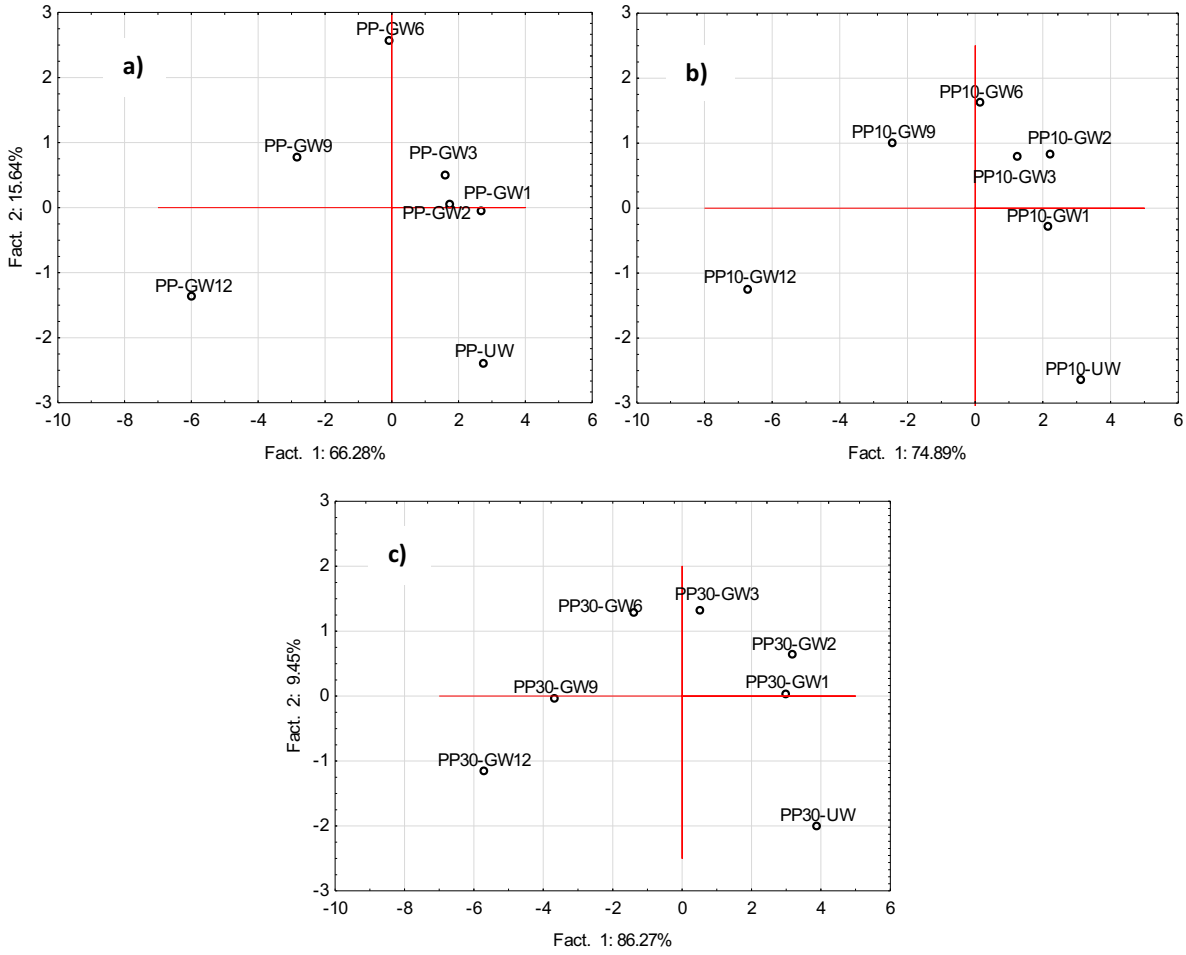

Figure 5 - Individuals projection of PP (a), PP10 (b) and PP30 (c)

III.3.3 Treatment by weathering time

The influence of the time of ageing on correlations between variables is determined after 1, 2, 3, 6, 9 and 12 months of under glass exposition (Figure 6). After 1 month, three main groups of variables (Sa, E, s, A4), (G1, G2, L*, b*) and (Cvoc, Cca, Ck) are distinguished. We notice that the two last ones describe visual appearance and VOCs emission respectively. This result indicates that the observed variables are grouped into the wide physical and emission properties categories. Also, most of the variables are mainly linked to PC1 except Cvoc, Cca and L* that equally contribute to PC1 and PC2. Otherwise, A2 attributed to

aliphatic aldehydes and esters absorption band is particularly close to PC1 since its vector is confused with PC1 axis.

During the exposition, the concentration of VOCs, ketones and carboxylic acids as well as their absorption bands maximum values A1 and A2 progressively tend to negatively correlate with PC1. However, even if PC1 always represents the highest variance, it is worthy to note that PC1 can be different since they are issued from different eigenvalues at each time. After one year, these parameters have given a great weight on PC1. Therefore, oxygenated products release more and more defines PC1 compared to other properties until Cvoc outright reaches PC1 axis. Also, Sa anti-correlates with G1 and G2 since they form an angle of almost 180°. Indeed, a rougher surface induces alteration of gloss aspect [53,44].

On another hand, E and s primarily strongly define PC1 and then characterize PC2. This justifies the increasing inertia rate carried by PC2. However, the crystallinity variable is not well projected at intermediate weathering time (6 months) whereas the other correlation circles exhibited high radius for this variable. By verifying raw data, this period corresponds to the critical stage when crystallinity ratio of PP30 gets definitively lower value than PP one whereas the contrary was observed before. Therefore, the nucleating agent role of hemp fibers that led to higher crystallization rate of polymer matrix in biocomposites than neat PP one was no longer kept. However, after this stage, it opposed carbonyl absorbance variables suggesting that the degradation led to polymer deterioration and crystalline phase oxidation. Otherwise, it is interesting to note that E and s are non-correlated with Cvoc for each weathering time whereas an anti-correlation was noted in analysis by fiber loading. As explained in the previous part (paragraph III.3.2), this can be due to the fact that, in this case, all materials (PP, PP10, PP30) are included in the statistical treatment leading to better differentiation of fiber rate by the modulus and stress. Finally, a* is close to the circle center whatever the weathering time. Thus, this color coordinate is not interpretable.

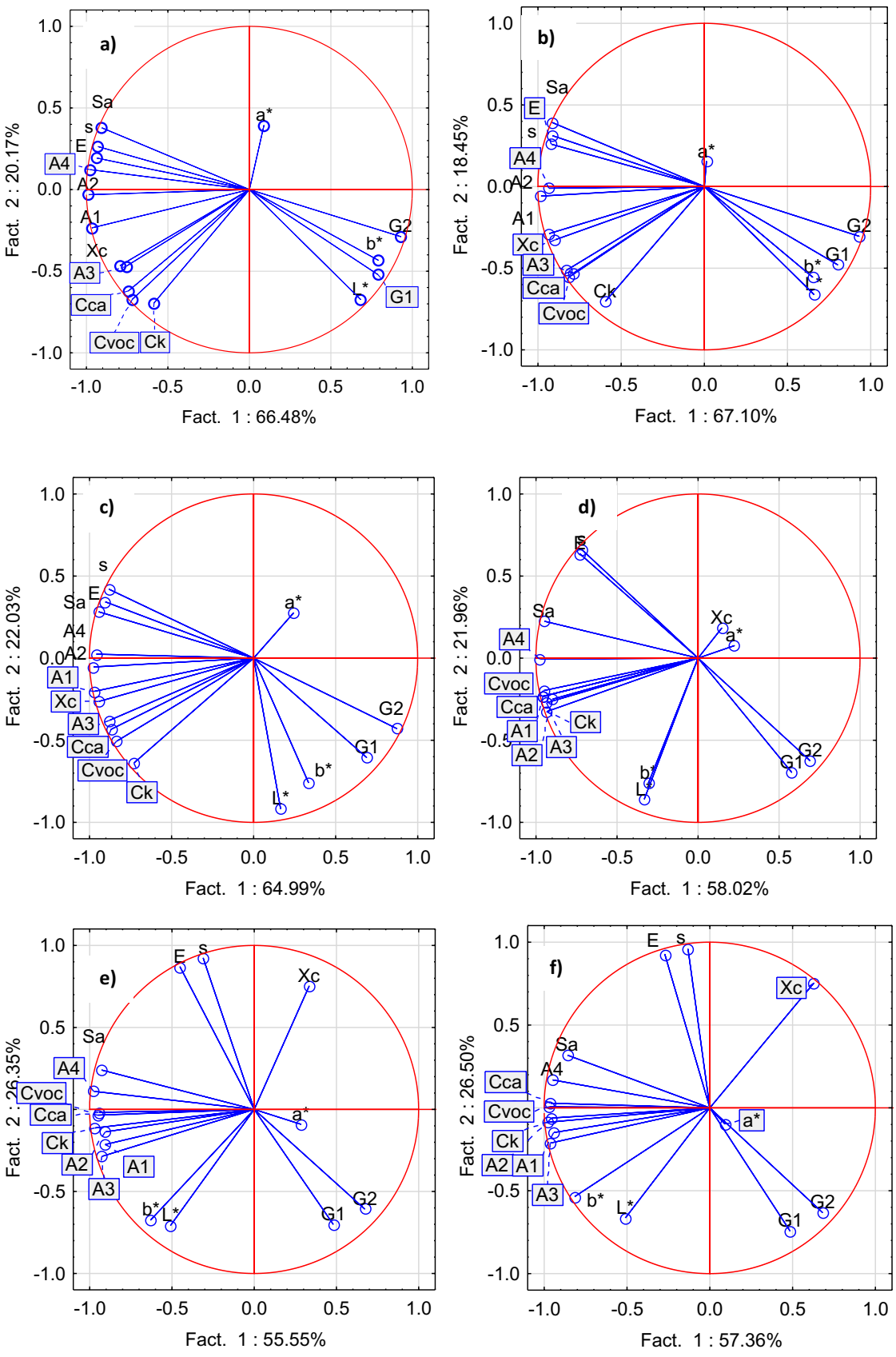

Figure 6 - Correlations circles after 1 (a), 2 (b), 3 (c), 6 (d), 9 (e) and 12 (f) months of weathering

The factorial plan can be divided in three parts corresponding to PP, PP10 and PP30 groups (Figure 7). For short-time weathering, most of the variables mainly differentiate the materials fiber rate since these three groups are discriminated through PC1 (Figure 6 and Figure 7). The one and two-month exposition certainly induced too low degradation to be consequently discriminated between their UW and GW state by the variables. However, VOCs emission also describes state of weathering (PC2) demonstrating emission profiles difference between UW and GW samples already at early exposition. Indeed, non-weathered samples were not emissive (concentration < quantification limit) whereas some carbonyls were detected once weathered. The score plots of individuals also considering non-weathered materials allows to highlight that mechanical parameters, here linked to PC2, more considerably explain the fiber loading at the non-weathered state than at weathered state.

After one year of exposition (Figure 7f)), PC1 mainly explains weathering state and hemp fiber loading through VOCs release and chemical structure whereas PP-UW, PP10-UW and PP30-UW are described by mechanical properties since they arrange according to PC2. The major difference of stiffness and strength between PP and biocomposites at UW state certainly cause these differences. Then, the degradation induced PP, PP10 and PP30 distinction through chemical composition caused by hemp fibers protrusion at the surface leading to their detection and VOCs emission specifically issued from vegetal fibers. Finally, whatever the time of exposition, volatile compounds emissions relate the state of weathering whereas mechanical properties translate the hemp fiber rate.

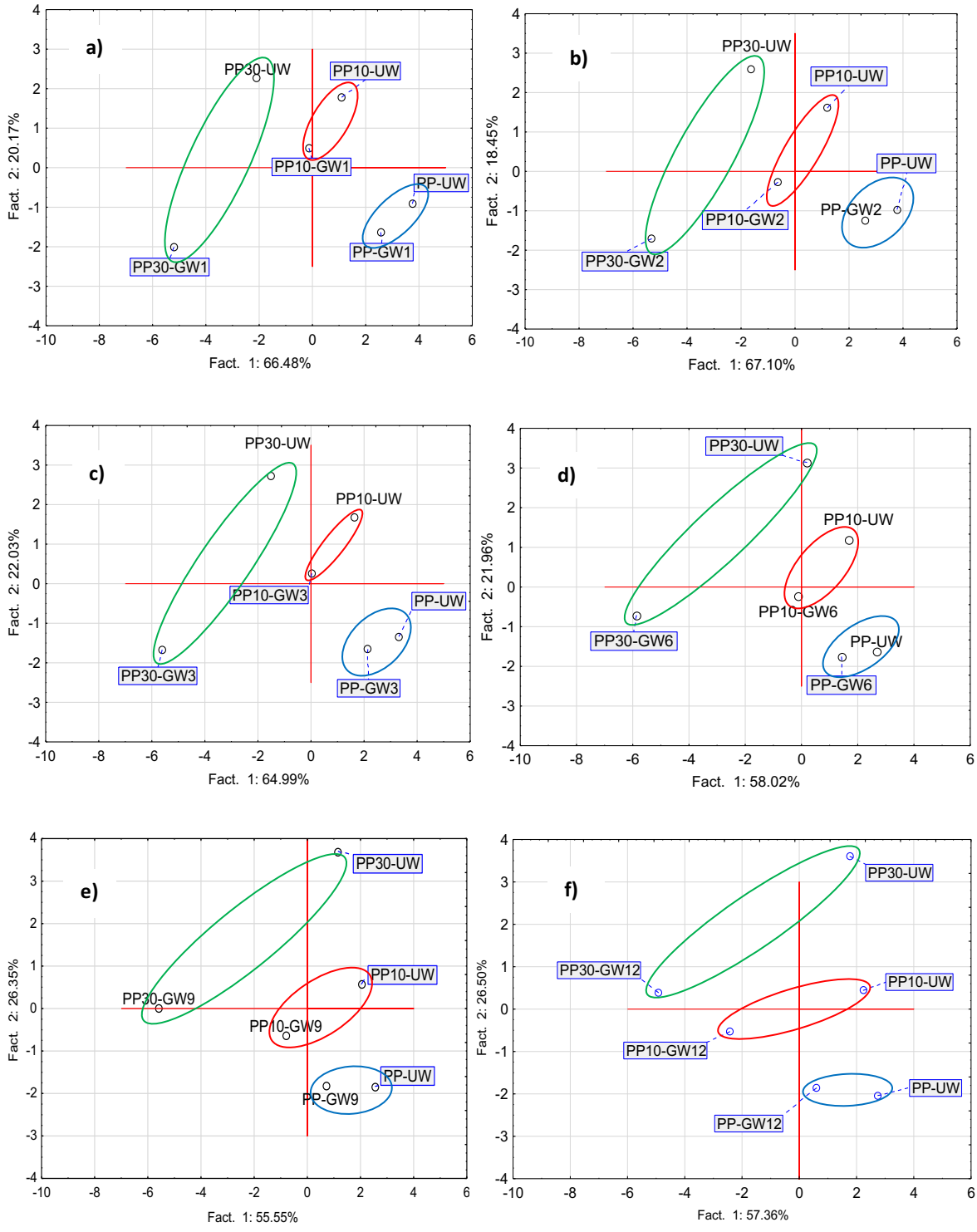

Figure 7 - Individuals projection after 1 (a), 2 (b), 3 (c), 6 (d), 9 (e) and 12 (f) months of weathering (green: PP30, red: PP10, blue: PP)

III.4. Conclusion

The aim of this work was to assess relationships between physico-chemical properties and similarities between PP and biocomposites samples over weathering representing a car interior environment.

Global treatment implying statistical calculation on all variables and individuals gave overview about information linked to correlations between variables including VOCs release. The variables discriminated either fiber rate or weathering time depending on exposition duration. Variables relating oxidative degradation mechanisms were non-correlated with mechanical properties variables. As regards individuals clusters size, weathered PP30 samples (30% hemp fiber loading) were more dispatched whereas neat PP exhibited small group. This indicates the high degradation kinetic and the impact of weathering time on biocomposites stability.

The analysis carried out by isolating the materials according to their different fiber loading level was more informative. Firstly, the highest fiber composite entailed the better projection of the dataset with the highest variance rate. This was assumed to be due to direct causal links existing between properties of hemp fibers. Also, this analysis showed that VOC emissions measurement can provide valuable information regarding degradation processes since it was anti-correlated with mechanical performance. Moreover, concerning biocomposites, roughness increase due to fibers loss and polymer matrix degradation was also linked to degradation product pattern. The crystallinity rate decrease was evidenced to be certainly due to crystalline phase oxidation. Also, thanks to this statistical method, the color changes (b* increase over the weathering) was linked to ketones and lactones formation whereas bleaching was explained by lignin chromophoric structures contribution.

Finally, the treatment by weathering time emphasized the impact of exposure duration on properties an their explanation of fiber rate and weathering state. After short-term exposure, volatile degradation products described weathering state and hemp fiber loading. Moreover, mechanical parameters always better differentiated fiber rate at non-weathered state rather than at weathering state. Indeed, bulk properties more differentiated non-weathered state PP and biocomposites samples than weathered ones. Thus, degradation

induced no longer significant stiffening and mechanical performance enhancement thanks to vegetal fibers after weathering. On the contrary, oxigenated bonds and volatile products opposed weathered PP and biocomposites due to the emergence of vegetal fibers at biocomposites surface and their higher sensitivity face to photothermal oxidative degradation of natural fibers components than PP one.

According to these statistical calculations, VOCs issued from matter degradation are linked to visual appearance evolution. Therefore, a sample visual aspect assessment could be monitored to foretell chemical structure degradation. Moreover, the degradation responsible for chemicals release must be limited and materials must be protected against oxidation to conserve their aesthetic appeal. Also, all along biocomposites uses, VOCs emission measured thanks to non-destructive method can be used as indicator for predicting mechanical properties changes without damaging the materials.

III.5. References

[1] D. Rusu, S.A.E. Boyer, M.F. Lacrampe, P. Krawczak, Bioplastics and Vegetal Fiber Reinforced Bioplastics for Automotive Applications, Handb. Bioplastics Biocomposites Eng. Appl. (2011) 397–449. doi:10.1002/9781118203699.ch15.

[2] O. Akampumuza, P.M. Wambua, A. Ahmed, W. Li, X. Qin, Review of the applications of biocomposites in the automotive industry, Polym. Compos. 16 (2016) 101–113. doi:10.1002/pc.23847.

[3] L. Mohammed, M.N.M. Ansari, G. Pua, M. Jawaid, M.S. Islam, A Review on Natural Fiber Reinforced Polymer Composite and Its Applications, Int. J. Polym. Sci. 2015 (2015). doi:10.1155/2015/243947.

[4] Feature, construction, solutions, medical, biocomposites, n°111, JEC Compos. Mag. (2017) 1–122.

[5] K.-W. Kim, B.-H. Lee, S. Kim, H.-J. Kim, J.-H. Yun, S.-E. Yoo, J.R. Sohn, Reduction of VOC emission from natural flours filled biodegradable bio-composites for automobile interior, J. Hazard. Mater. 187 (2011) 37–43. doi:10.1016/j.jhazmat.2010.07.075.

[6] H.-S. Kim, S. Kim, H.-J. Kim, H.-G. Kim, Physico-mechanical properties, odor and VOC emission of bio-flour-filled poly(propylene) bio-composites with different volcanic pozzolan contents, Macromol. Mater. Eng. 291 (2006) 1255–1264. doi:10.1002/mame.200600212.

[7] H.-S. Kim, B.-H. Lee, H.-J. Kim, H.-S. Yang, Mechanical–thermal properties and VOC emissions of natural-flour-filled biodegradable polymer hybrid bio-composites, J. Polym. Environ. 19 (2011) 628–636. doi:10.1007/s10924-011-0313-5.

[8] H.-S. Kim, B.-H. Lee, H.-J. Kim, H.-S. Yang, Mechanical–thermal properties and VOC emissions of natural-flour-filled biodegradable polymer hybrid bio-composites, J. Polym. Environ. 19 (2011) 628–636. doi:10.1007/s10924-011-0313-5.

[9] C. Courgneau, D. Rusu, C. Henneuse, V. Ducruet, M.F. Lacrampe, P. Krawczak, Characterisation of low-odour emissive polylactide/cellulose fibre biocomposites for car interior, Express Polym. Lett. 7 (2013) 787–804. doi:10.3144/expresspolymlett.2013.76.

[10] MCS-Aware, Sick Car Syndrome, (2015). http://www.mcs-aware.org/general-articles/189-sick-car-syndrome (accessed January 5, 2017).

[11] Ministry of environmental protection, GB/T 27630-2011 Chinese national standard: Guideline for air quality assesment of passenger car, (2011).

[12] JAMA, Announces Voluntary Guidelines for Reducing Vehicle Cabin VOC Concentration Levels, 2005. http://www.jama-english.jp/.

[13] Korean Automobile Testing & Research Institute, Ministry of Land Infrastructure and Transport, Proposal for a New GTR on Vehicle Indoor Air Quality (VIAQ), (n.d.) 25–28.

[14] Underwriters Laboratories UL LLC, Vehicle Interior Air Quality: Addressing chemical exposure in automobiles, (2015).

[15] C.S. Widdowson, Vehicle interior air quality - (S)VOC emission from materials: regulation, standard methods and analytical implementation, Top. C7 Transp. Cabin Environ. (2017).

[16] A. Espert, L.A. de las Heras, S. Karlsson, Emission of possible odourous low molecular weight compounds in recycled biofibre/polypropylene composites monitored by head-space SPME-GC–MS, Polym. Degrad. Stab. 90 (2005) 555–562. doi:10.1016/j.polymdegradstab.2005.03.009.

[17] Ó. Ezquerro, B. Pons, M.T. Tena, Direct quantitation of volatile organic compounds in packaging materials by headspace solid-phase microextraction-gas chromatography-mass spectrometry, J. Chromatogr. A. 985 (2003) 247–257. doi:10.1016/S0021-9673(02)01829-0.

[18] Ó. Ezquerro, B. Pons, M.T. Tena, Development of a headspace solid-phase microextraction–gas chromatography–mass spectrometry method for the identification of odour-causing volatile compounds in packaging materials, J. Chromatogr. A. 963 (2002) 381–392. doi:10.1016/S0021-9673(02)00211-X.

[19] M. Ghislain, J. Beigbeder, L. Dumazert, J.M. Lopez-Cuesta, M. Lounis, S. Leconte, V. Desauziers, Determination of the volatile fraction of phosphorus flame retardants in cushioning foam of upholstered furniture: towards respiratory exposure assessment, Environ. Monit. Assess. 188 (2016). doi:10.1007/s10661-016-5566-y.

[20] R. Bernstein, S.M. Thornberg, A.N. Irwin, J.M. Hochrein, D.K. Derzon, S.B. Klamo, R.L. Clough, Radiation-oxidation mechanisms: Volatile organic degradation products from polypropylene having selective C-13 labeling studied by GC/MS, Polym. Degrad. Stab.

93 (2008) 854–870. doi:10.1016/j.polymdegradstab.2008.01.020.

[21] C. Rouillon, P.-O. Bussiere, E. Desnoux, S. Collin, C. Vial, S. Therias, J.-L. Gardette, Is carbonyl index a quantitative probe to monitor polypropylene photodegradation?, Polym. Degrad. Stab. 128 (2016) 200–208. doi:10.1016/j.polymdegradstab.2015.12.011.

[22] A. Lattuati-Derieux, S. Bonnassies-Termes, B. Lavédrine, Characterisation of compounds emitted during natural and artificial ageing of a book. Use of headspace-solid-phase microextraction/gas chromatography/mass spectrometry, J. Cult. Herit. 7 (2006) 123–133. doi:10.1016/j.culher.2006.02.004.

[23] D. Bourdin, P. Mocho, V. Desauziers, H. Plaisance, Formaldehyde emission behavior of building materials: on-site measurements and modeling approach to predict indoor air pollution., J. Hazard. Mater. 280 (2014) 164–73. doi:10.1016/j.jhazmat.2014.07.065.

[24] K. Curran, M. Underhill, L. Gibson, A. Moore, M. Strlic, VOC analysis of degrading modern polymeric materials in museum collections, in: 9th Int. Conf. Modif. Degrad. Stab. Polym., 2016. Poland.

[25] D.J. Carlsson, M. Krzymien, J. Worsfold, Volatiles released during the weathering of PVC, J. Vinyl Addit. Technol. 3 (1997) 100–106.

[26] K. Curran, M. Strlic, Polymers and volatiles : Using VOC analysis for the conservation of plastic and rubber objects, Stud. Conserv. 0 (2014) 1–14. doi:10.1179/2047058413Y.0000000125.

[27] D.J. Carlsson, M.E. Krzymien, D.J. Pleizier, G., Worsfold, M. Day, Volatiles released from PVC during photochemical degradation. The fate of chlorine., in: Society of Plastics Engineers (Ed.), Conf. Soc. Plast. Eng., 1999.

[28] M. Hakkarainen, A.-C. Albertsson, Indicator products: A new tool for lifetime prediction of polymeric materials, Biomacromolecules. 6 (2005) 775–779. doi:10.1021/bm049483f.

[29] M. Groning, M. Hakkarainen, Headspace solid-phase microextraction with gas chromatography/mass spectrometry reveals a correlation between the degradation product pattern and changes in the mechanical properties during the thermooxidation of in-plant recycled polyamide 6,6, J. Appl. Polym. Sci. 86 (2002) 3396–3407. doi:10.1002/app.11345.

[30] M. Strlič, J. Thomas, T. Trafela, L. Cséfalvayová, I.K. Cigić, J. Kolar, M. Cassar, Material degradomics: On the smell of old books, Anal. Chem. 81 (2009) 8617–8622. doi:10.1021/ac9016049.

[31] M.A. Bari, W.B. Kindzierski, A.J. Wheeler, M.-È. Héroux, L.A. Wallace, Source apportionment of indoor and outdoor volatile organic compounds at homes in Edmonton, Canada, Build. Environ. 90 (2015) 114–124. doi:10.1016/j.buildenv.2015.03.023.

[32] J.G. Watson, J.C. Chow, E.M. Fujita, Review of volatile organic compound source

apportionment by chemical mass balance, Atmos. Environ. 35 (2001) 1567–1584. doi:10.1016/S1352-2310(00)00461-1.

[33] M.C. McCarthy, Y.-A. Aklilu, S.G. Brown, D.A. Lyder, Source apportionment of volatile organic compounds measured in Edmonton, Alberta, Atmos. Environ. 81 (2013) 504–516. doi:10.1016/j.atmosenv.2013.09.016.

[34] H. Guo, T. Wang, P.K.K. Louie, Source apportionment of ambient non-methane hydrocarbons in Hong Kong: Application of a principal component analysis/absolute principal component scores (PCA/APCS) receptor model, Environ. Pollut. 129 (2004) 489–498. doi:10.1016/j.envpol.2003.11.006.

[35] J. Salafranca, I. Clemente, F. Isella, C. Nerín, O. Bosetti, Influence of oxygen and long term storage on the profile of volatile compounds released from polymeric multilayer food contact materials sterilized by gamma irradiation, Anal. Chim. Acta. 878 (2015) 118–130. doi:10.1016/j.aca.2015.03.055.

[36] ISO 877-2: Plastics -- Methods of exposure to solar radiation -- Part 2: Direct weathering and exposure behind window glass, (2011).

[37] L. Sisti, G. Totaro, M. Vannini, P. Fabbri, S. Kalia, A. Zatta, A. Celli, Evaluation of the retting process as a pre-treatment of vegetable fibers for the preparation of high-performance polymer biocomposites, Ind. Crops Prod. 81 (2016) 56–65. doi:10.1016/j.indcrop.2015.11.045.

[38] K.B. Adhikary, S. Pang, M.P. Staiger, Accelerated Ultraviolet Weathering of Recycled Polypropylene--Sawdust Composites, J. Thermoplast. Compos. Mater. 22 (2009) 661–679. doi:10.1177/0892705709096550.

[39] C. Rouillon, P.O. Bussiere, E. Desnoux, S. Collin, C. Vial, S. Therias, J.L. Gardette, Is carbonyl index a quantitative probe to monitor polypropylene photodegradation?, Polym. Degrad. Stab. 128 (2016) 200–208. doi:10.1016/j.polymdegradstab.2015.12.011.

[40] S. Butylina, M. Hyvärinen, T. Kärki, A study of surface changes of wood-polypropylene composites as the result of exterior weathering, Polym. Degrad. Stab. 97 (2012) 337–345. doi:10.1016/j.polymdegradstab.2011.12.014.

[41] N. Le Moigne, M. Longerey, J.-M. Taulemesse, J.-C. Bénézet, A. Bergeret, Study of the interface in natural fibres reinforced poly(lactic acid) biocomposites modified by optimized organosilane treatments, Ind. Crops Prod. 52 (2014) 481–494. doi:10.1016/j.indcrop.2013.11.022.

[42] L. Soccalingame, D. Perrin, J.-C. Bénézet, S. Mani, F. Coiffier, E. Richaud, A. Bergeret, Reprocessing of artificial UV-weathered wood flour reinforced polypropylene composites, Polym. Degrad. Stab. 120 (2015) 313–327. doi:10.1016/j.polymdegradstab.2015.07.013.

[43] C. Badji, L. Soccalingame, H. Garay, A. Bergeret, J.-C. Bénézet, Influence of weathering on visual and surface aspect of wood plastic composites: Correlation approach with

mechanical properties and microstructure, Polym. Degrad. Stab. 137 (2017) 162–172. doi:10.1016/j.polymdegradstab.2017.01.010.

[44] R. Alexander-Katz, R.G. Barrera, Surface correlation effects on gloss, J. Polym. Sci. 36 (1997) 1321–1334.

[45] STIL, Presentation of optical principles 1: Confocal chromatic, (2016) 38–40.

[46] D. Bourdin, V. Desauziers, Development of SPME on-fiber derivatization for the sampling of formaldehyde and other carbonyl compounds in indoor air, Anal. Bioanal. Chem. 406 (2014) 317–328. doi:10.1007/s00216-013-7460-6.

[47] M.J. Fedoruk, B.D. Kerger, Measurement of volatile organic compounds inside automobiles, J. Expo. Anal. Environ. Epidemiol. 13 (2003) 31–41. doi:10.1038/sj.jea.7500250.

[48] J. Nicolle, V. Desauziers, P. Mocho, Solid phase microextraction sampling for a rapid and simple on-site evaluation of volatile organic compounds emitted from building materials, J. Chromatogr. A. 1208 (2008) 10–15. doi:10.1016/j.chroma.2008.08.061.

[49] V. Desauziers, Traceability of pollutant measurements for ambient air monitoring, Trends Anal. Chem. 23 (2004) 252–260. doi:10.1016/S0165-9936(04)00310-3.

[50] L.J. Williams, H. Abdi, Principal Component Analysis, Wiley Interdiscip. Rev. Comput. Stat. 2 (2010) 433–459. doi:10.1002/wics.101.

[51] J.S. Fabiyi, A.G. McDonald, M.P. Wolcott, P.R. Griffiths, Wood plastic composites weathering: Visual appearance and chemical changes, Polym. Degrad. Stab. 93 (2008) 1405–1414. doi:10.1016/j.polymdegradstab.2008.05.024.

[52] P. Filson, B.E. Dawson-Andoh, L. Matuana, Colorimetric and vibrational spectroscopic characterization of weathered surfaces of wood and rigid polyvinyl chloride–wood flour composite lumber, Wood Sci. Technol. 43 (2009) 669–678. doi:10.1007/s00226-009-0254-5.

[53] W.J. O'Brien, W.M. Johnston, F. Fanian, S. Lambert, The surface roughness and gloss of composites., J. Dent. Res. 63 (1984) 685–688. doi:10.1177/00220345840630051601.

CHAPITRE IV

VIEILLISSEMENT NATUREL EXTÉRIEUR ET VIEILLISSEMENT ACCÉLERÉ EN ENCEINTE DES BIOCOMPOSITES PP/CHANVRE :

UNE ÉTUDE COMPARATIVE

Chapitre IV

Vieillissement naturel en extérieur et vieillissement artificiel en enceinte des biocomposites PP/chanvre : une étude comparative

L'évaluation de la durabilité des matériaux implique une mesure de leur comportement face aux conditions climatiques dans lesquelles ils seront potentiellement utilisés durant leur cycle de vie. Les vieillissements artificiels en enceinte offrent la possibilité de réduire le temps de vieillissement naturel pour dégrader significativement les matériaux et estimer leur temps de vie. En quelques jours ou semaines, les enceintes de vieillissement artificiel reproduisent les dégradations observées après plusieurs mois ou plusieurs années de vieillissement naturel en l'extérieur.

Un vieillissement naturel extérieur et un vieillissement artificiel en enceinte climatique des biocomposites étudiés font donc l'objet de ce chapitre. Plusieurs prélèvements sont effectués au cours d'une année de vieillissement naturel en extérieur et au cours de 42 jours de vieillissement artificiel. Une analyse des propriétés mécaniques, de microstructure et d'aspect de surface des composites ayant subi les deux vieillissements est effectuée afin de comparer les deux types de vieillissement. Les résultats montrent une accélération de la dégradation des biocomposites et du PP en enceinte de vieillissement artificiel. En effet, pour une même durée d'exposition, un taux de dégradation plus élevé est constaté après vieillissement artificiel. L'étude comparative s'est basée sur le profil des corrélations (obtenu par analyse statistique en composantes principales ACP dont le principe est détaillé dans l'Anne II) entre les différents paramètres suivis. La représentativité, en enceinte climatique, des mécanismes de dégradation mis en jeu sous vieillissement naturel a été validée par ACP. De ce fait, il a été possible d'estimer des équivalences temporelles par type de matériau prenant en compte l'ensemble des propriétés mesurées. Ces résultats suggèrent que l'ACP peut être employée pour corréler les deux types d'exposition et prédire la durée de vie des biocomposites.

Ce chapitre fait l'objet d'une publication à soumettre au journal Polymer Degradation and Stability.

I. Correlation between artificial and natural weathering of hemp fibers reinforced polypropylene biocomposites

Célia Badji, Joana Beigbeder, Hélène Garay, Anne Bergeret, Jean-Charles Bénézet and Valérie Desauziers

C2MA, Ecole des mines d'Alès, 6 avenue de Clavières, 30319 Cedex France

Abstract

The degradation behavior of hemp fibers reinforced PP biocomposites under one-year outdoor and 1000-hour artificial laboratory weathering conditions were compared to establish a correlation. For this purpose, several measurements were performed throughout the expositions. Mechanical performance was tested by three-point bending test. Microstructure and chemical composition changes were also assessed. Otherwise, visual aspect (color, gloss) and topography which could be linked to chemical composition variations were determined. The artificial weathering effectively accelerated the degradation mechanisms. Oxidation pathways and thus surface aspect alteration of both polymer and biocomposites occurred faster. However, whereas biocomposites were mainly subjected to outdoor conditions due to high sensitivity of hemp fibers, virgin PP was globally mostly affected by laboratory chamber conditions. Its oxidation rate via lactones and aldehydes formation largely outstripped reinforced materials ones. Principal Component Analysis was used for verifying the differences of profiles of normalized variables correlations between artificial and exterior ageing dataset in order to compare the overall degradation mechanisms. Through the statistical analysis, some attempts were made to find equivalence between artificial and outdoor weathering times thanks to properties degradation rate similarities.

Keywords: accelerated ageing, natural ageing, statistical method, hemp fibers, temporal equivalence

I.1. Introduction

Environmental and production aspect benefits of natural fibers encourage research and industries to develop bio-based materials. Among them, hemp fibers have long been valued

for their high strength, and were besides extensively employed in the fabrication of ropes, sails and textiles [1]. Nowadays they are also used as a substitute for glass, carbon or metallic fibers for the reinforcement of thermoplastic matrix. Automotive, building and furniture industries constitute the main application of biocomposites.

Solar radiation, air, oxygen, rain, temperature and biotic factors constitute the main weather features of materials degradation. Some works reported results regarding biocomposites durability. Few trials performing natural weathering of natural fibers and flours reinforced biocomposites are reported in literature [2–4]. Synergic effect combining temperature, humidity and, ultraviolet (UV) radiation causes materials degradation. Even if exposition to real conditions is reliable to interpret the performance loss, it is difficult to understand the contribution of each factor to properties variations. Moreover, outdoor durability test is often laborious and includes irregular changes and slow degradation rate inducing long-term exposures needed to observe noticeable changes. Therefore, artificial weathering carried out in laboratory chambers can substitute them in order to accelerate the degradation phenomenon and predict outdoor weathering [5–7]. They intended to simulate exposure conditions that would potentially be experienced by materials employed in real world applications.

Most of estimations of correlations between artificial and exterior exposition assumed an intimate link of decomposition rate with only UV light since it is widely accepted that photo-chemical reactions are mainly responsible for properties variations of polymers. So UV lamps are supposed to closely simulate spectral power distribution of sunlight [8]. The reciprocity law is classically used to correlate two ageing [9–11]. This law implies that for a same cumulative UV energy under two types of ageing, the degradation degrees are similar even if light intensities differ. Laboratory ageing of polypropylene (PP) was compared to whole year outdoor weathering occurring in Shanghai reasoning only through UV radiation [12]. Intrinsic viscosity and tensile strength values obtained under outdoor exposure were compared to those measured under several lamps UV intensities. It was noticed that, at the same cumulative UV irradiation, the results of test carried out with lamps whose intensities are 82 and 163 $W.m^{-2}$ were more compatible with the outdoor weathering test, while test achieved under 325 $W.m^{-2}$ lamp induced higher loss of tensile strength. Moreover, it was

demonstrated by infrared spectroscopy that a different oxidative mechanism occurred under 325 $W.m^{-2}$ lamp. Thus, the reciprocity law is not verified in this case. Similarly, in another study, the increment of carbonyl absorbance (measured through infrared experiments) of PP against cumulative exposure energy highlighted outdoor exposure as more impactful than accelerated one for a same amount of UV exposure [13]. Yang et al attempted to correlate outdoor and artificial weathering (UV radiation followed by spray) of polyvinyl chloride (PVC) in terms of cumulative UV radiation energy Q [14]. When samples were subjected to a same Q value, desaturation and ultimate strength decrease were faster under accelerated ageing than under outdoor one. Therefore, as for previous works, both weathering conditions did not correlate according to the classic reciprocity law. However, results obtained from accelerated and natural weathering fitted by application of a power law generalization of the reciprocity law. Indeed, the power index added to the reciprocity formula and related to materials made consistent the aging levels of samples obtained at different radiation intensities when Q is constant.Nevertheless, even if samples behaviour is highly UV light dependent, it was shown that different weathering performances can occur even if the cumulative energy of UV irradiation is identical [15]. Indeed, depending on light intensity, different compounds having evolved from aged PP were detected. It was noted that different hydroperoxides decomposition pathways could occur generating either carboxylic acids and ketones or esters by varying UV intensity. Also, the lack of agreement between spectral radiation and solar spectrum on one side and the weather variability on the other side may jeopardize a good simulation. Moreover, other exterior factors such as humidity can catalyse photo-degradation [16–18].

Fabiyi et al conducted simultaneous natural and accelerated weathering of wood plastic composites (WPC). They compared PP matrix degradation of WPC after outdoor and xenon-arc ageing by considering all exterior factors [19]. Similarly, other comparisons were carried out without any calculation of degradation acceleration factor which corresponds to the ratio between time of natural weathering and time of accelerated weathering needed to obtain a same degradation degree [20,21]. However, quantitative correlation between artificial and exterior ageing was also performed to find a temporal equivalence by comparing the alteration degree of the analysed materials. Howard and Gilroy studied low-density polyethylene (LDPE) degradation after very long-term natural and Weather-Ometer

ageing [22]. On the basis of experimental data, they established an expression verifying the relationship between the two kinds of exposure. This equation indicated that during the early stage of exposure, changes were faster in the Weather-Ometer chamber than outdoor. Nevertheless, when exposition continued further, the efficacy of the accelerated device falls off at an ever increasing rate. Otherwise, the decisive element for use of wood in the harsh outside environment is its durability. Because of slowness of the natural weathering process of wood, the compressive strength values of wood samples recorded all along the artificial weathering were compared to the value obtained after one-year and two-year exterior weathering in Polish temperate climate [23]. The accelerated ageing included soaking (16h), high-temperature step at 70 °C (8h), and irradiation at 30 °C (6h). Equivalence was deduced from comparison between these artificial conditions and an exterior weathering by recording intersection of the two sets of data corresponding to a same rate of degradation. It revealed that the number of artificial cycles representing one-year ageing differed according the wood specie. It was found that short cyclical changes highly put samples under stress. Indeed, cyclic exposures tend to be more severe than steady-state exposures [24]. Otherwise, no particular factor was considered as major influential parameter. They suggested that interaction of many exterior factors induce their degradation. In addition, one single acceleration factor does not exist. Indeed, geographical and climatic conditions, materials composition, strongly contribute to the acceleration.

But correlations between natural and artificial ageing were also deduced from different kinds of properties. For instance, Lv et al determined microstructure, surface morphology and mechanical properties of isotactic polypropylene under several outdoor weathering stations situated in China. They were compared to properties measured under artificial weathering [25]. A modified Arrhenius equation extended to three parameters that are temperature, UV radiation and oxygen pressure, was proposed to correlate properties of outdoor weathered PP with those measured under accelerated ageing. It was demonstrated that a single acceleration factor based on the improved Arrhenius equation and meteorological data could satisfactorily predict outdoor durability. Tidjani et al estimated an acceleration factor from the carbonyl absorbance whose value was arbitrarily fixed at 0.1 [26]. The acceleration factor (ratio between artificial and natural ageing times needed to obtain absorbance of 0.1) equalled 29. Most of the time, this ratio was often punctually

calculated at just one precise time of weathering and fewer verified the ratio over continuous periods.

Artificial weathering should obviously duplicate changes resulting from exterior exposure. However, artificial ageing does not sometimes exactly correlate with natural exposure [27,28]. Indeed, Martin et al conducted artificial and outdoor weathering on polyvinyl chloride (PVC) [29]. Short-period exposure in chamber reproduced same color variations as outdoor whereas longer duration caused darkening that was not observed under natural ageing. Nevertheless, Yang et al showed that when exposition continues further, the surface color of PVC could gradually change from chalky (1000h) to dark (2000h) [14]. Thus, this darkening can also result from too long artificial exposition.

The main target of this work is to study outdoor and accelerated weathering of PP and hemp fibers reinforced polypropylene biocomposites. The investigation focuses on physical, chemical and mechanical properties changes all along the exposure. Then, in view of literature reports conclusions, one must verify whether degradation mechanisms are similar or not through Principal Component Analysis (PCA). Finally, relationships between the two types of ageing by finding temporal equivalence will be attempted.

I.2. Materials and Methods

I.2.1 Materials

Polypropylene grade H733-07 with a melt flow rate of 7.5 g/10 min (230 °C, 2.16 kg) purchased from Braskem Co. (Brazil) was used as thermoplastic matrix. Hemp fibers (2-6mm) were provided by AgroChanvre (France). After the retting process, their cellulose, hemicelluloses and lignin rates displayed in Table 1 were determined by successive chemical extractions based on TAPPI T264, ASTM D1104 standards [30,31]. Two hemp fibers loading 10 wt% (PP10) and 30 wt% (PP30) were chosen. Maleic anhydride grafted polypropylene (MA-g-PP) coupling agent with a 1 wt% grafting rate (Orevac CA100) and supplied by Arkema (France), was added at 3.1 wt% of PP in the biocomposites.

Table 1 - Hemp fibers chemical composition

	Cellulose	Hemicelluloses	Lignin	Liphophilic extractives	Ash
(wt%)	82.1	8.5	4.5	2.7	2.1

I.2.2 Material processing

Hemp fibers and MA-g-PP have been dried before process for 15 h at 60 °C in an oven to remove residual water. Granules of PP and MA-g-PP were mixed with hemp fibers in a BC21 Clextral co-rotating twin-screw extruder (L/D = 36 with the diameter D = 25 mm) with the temperature ranging from 190 to 175 °C from feed to die and a screw speed of 220 rpm. Once dried for 3 days at 60 °C, extruded pellets were injection molded in a Krauss Maffei KM50-T180CX at 210 °C with an injection speed of 30 $cm^3.s^{-1}$ to obtain square specimens of 100 × 100 × 2 mm and ISO 1 dog-bone specimens.

I.2.3 Weathering conditions

I.2.3.1 Natural weathering

Natural weathering was carried out in the South West of France from September 2015 to September 2016. The exterior exposition corresponded to a decking use. The weathering conditions were in adequacy with ISO 877-1:2011 standard [32]. The samples were fixed on galvanized racks at an angle of 45° with the ground and looked South. Dog-bone and square specimens were sampled after 1, 2, 3, 6, 9 and 12 months for laboratory characterizations. Average seasonal data were recorded from Pau-Uzein meteorological station [33] and are illustrated in Figure 1.

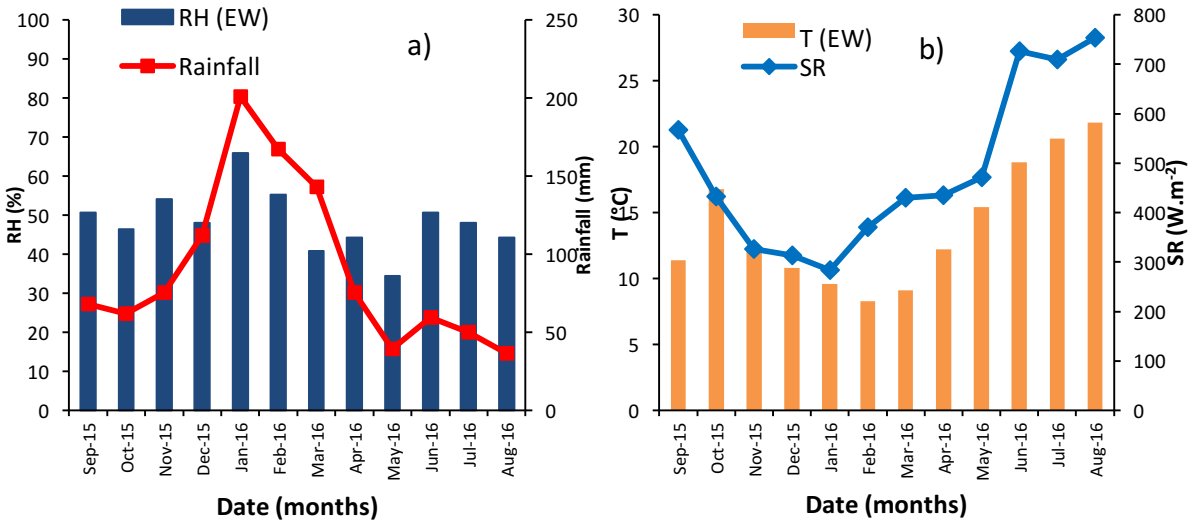

Figure 1 – Mean relative humidity RH (%) and rainfall (mm) (a) and mean temperature T (°C) and instantaneous solar radiation maximum SR ($W.m^{-2}$) (b)

I.2.3.2 Artificial weathering

Artificial weathering aimed to emulate exterior exposure. QUV-Spray apparatus from Q-Lab (Labomat Essor, France) using fluorescent UVA-340 lamps providing 365-295 nm UV solar spectrum part was used. The conditions followed the ISO 4892-3:2013 standard [34]. Each 12-hour weathering cycle consisted of 8h of dry UV exposure with an irradiance level of 0.76 $W.m^{-2}$ at λ = 340 nm at 50 °C, followed by 3.75h of condensation exposure at 50 °C without irradiation and 0.25h spray step. Specimens were collected for analysis after 100, 150, 250, 500, 750 and 1000h of exposure.

The designation of non-weathered and weathered materials is featured in Table 2.

Table 2- Designation of non-weathered and weathered materials (n: months number, m: hours number)

	Non-weathered materials	**Exterior weathered materials**	**Artificial weathered materials**
Designation	PP-UW, PP10-UW, PP30-UW	PP-EWn, PP10-EWn, PP30-EWn	PP-AWm, PP10-AWm, PP30-AWm

I.2.4 Mechanical characterization

Flexural properties characterization was conducted using Zwick TH 010 press apparatus with a 2.5 kN load cell. Test was carried out at 23 ± 2 °C and 50 ± 10% RH on ISO 1A dog-bone samples (ISO 178:2010) [35]. A three point bending system was utilized with cross-head speeds of 2 and 100 $mm.min^{-1}$ for the modulus and flexural stress at the conventional deflection measurements respectively. Flexural stress-strain behaviors of samples were analyzed in order to determine elastic modulus E_f calculated between 0.05 and 0.25% of strain and the stress at the conventional deflection σ_{fc} corresponding to the stress at a strain of 3.5 %. Eight replicates specimens of each material were tested.

I.2.5 Visual aspect characterization

I.2.5.1 Spectrocolorimetry

A Chroma Sensor 3 spectrocolorimeter (Datacolor, United States) was used to measure the surface color according to the CIE 1976 *L*, a*, b** uniform system. The configuration illuminant/observer was set at D65/10°. An increase of L* (from 0 to 100) witnesses a

material lightening whereas a* and b* are defined as the chromaticity positions on axes from -300 to +300 which are green (-a*) to red (+a*) and blue (-b*) to yellow (+b*) axes respectively. Color was measured on four areas of three specimens.

I.2.5.2 Spectrophotogoniometry

A GON 360 goniometer (Instrument Systems, Germany) coupled to a MAS 40 spectrometer with a halogen lamp was used to measure the gloss by collecting the radiometric power at different angles of detection. For this purpose, the source angle was fixed at 20° according to ISO 2813 standard [36] and detector angles varied from 5° to -60°. More details are given in a previous paper [20]. The haze gloss G_1 was determined from the ratio of the intensity obtained for the angle of detection to the intensity obtained for the angle of -22° both situated in the specular zone (Eq. 1). The contrast gloss G_2 was determined from the ratio between the intensity at -20°C and the intensity collected for the angle of -35° of a diffusely reflected light (Eq. 2). The higher the value of G_1 and G_2 are, the glossier the surface seems. The gloss was calculated for three replicates at four locations on each material.

$$G_1 = \frac{I(\Theta = -20°)}{I(\Theta = -22°)} \quad \text{Eq. 1}$$

$$G_2 = \frac{I(\Theta = -20°)}{I(\Theta = -35°)} \quad \text{Eq. 2}$$

I.2.6 Microstructure characterization

I.2.6.1 Differential scanning calorimetry (DSC)

The thermal properties were measured using a PYRIS Diamond calorimeter (Perkin Elmer, United States). The samples (10 mg) were heated from 30 to 210 °C with a heating ramp at 10 °C.min^{-1} under nitrogen atmosphere at a 20 mL.min^{-1} flow. Two heating steps with an intermediate cooling step were performed. Two replicate samples per material were analysed. The crystallinity was determined using Equations (3) and (4).

$$\chi_{c1}\,(\%) = \frac{\Delta H_{m1}}{W \times \Delta Hm_{100}} \times 100 \quad \text{Eq. 3}$$

$$\chi_{c2}\,(\%) = \frac{\Delta H_{m2}}{W \times \Delta Hm_{100}} \times 100 \quad \text{Eq. 4}$$

where W is the PP mass fraction, ΔHm ($J.g^{-1}$) is the first or second heating ramp melting enthalpy and ΔHm_{100} corresponds to the theoretical melting enthalpy of a fully crystalline PP (ΔHm_{100} = 209 $J.g^{-1}$ [37]).

I.2.7 Chemical composition characterization

I.2.7.1 Fourier Transform InfraRed spectroscopy (FTIR)

A IFS66 spectrometer (Bruker, United States) was used in Attenuated Total Reflectance (ATR) mode to follow the functional groups assigned to the samples degradation. The exposed surfaces were analysed and the spectra of materials were recorded between 400 and 4000 cm^{-1} with a resolution of 1 cm^{-1}. In order to normalize the spectra, the Min-Max normalization method of the spectra with the 2925 cm^{-1} reference band assigned to the CH_2 methylene groups was performed.

I.2.8 Surface characterization

I.2.8.1 Confocal rugosimetric measurement

A MICROMESURE STIL system equipped with a STIL CHR150 optical sensor (STIL, France) was used to evaluate the roughness by altitude measurement of each surface point on the sample without contact with the sample according to the ISO 25178 international standard. The analysis principle is detailed elsewhere [20]. The micrometric range of the optical pen was 285 µm. The analyzed area X*Y was 5 mm * 5 mm with an analysis step of 10 µm in X and Y directions. The roughness parameter Sa followed during the weathering corresponds to the arithmetic mean of the absolute of the height values (Eq. 5).

$$\mathrm{Sa} = \frac{1}{NM}\sum_{x=0}^{N-1}\sum_{y=0}^{M-1}|z(x,y)| \qquad \text{Eq. 5}$$

with M the number of points along the X axis, N the number of points along the Y axis, and zx,y the altitude in µm. Mean values and standard deviations were obtained from the analysis of four areas of three samples.

I.2.9 Principal Component Analysis (PCA)

Principal Component Analysis (PCA) gives a simple graphical overview on large set of observations of variables (properties) by data reduction. It also estimates the correlation structure of the variables and relatedness between populations. Statistica 13 (Dell, France) software was employed for the statistical calculation. Statistical analysis was used to compare dataset of exterior and accelerated ageing. This aimed to first verify if the relationships established between properties are similar for the two weathering. Then, the method was used to attempt correlating the two weathering by individuals (samples) analysis. Variables values were centered-reduced to scale them for overcoming domination of variables with the highest variance. The Table 3 resumes denominations of variables.

Table 3 - Designation of variables

Designation	Parameter
E	Modulus of elasticity (MPa)
s	Stress at the conventional deflection (MPa)
X_{c1}, X_{c2}	Crystallinity rate from 1st and 2nd heating steps (%)
A1	Absorbance C=O at 1711 cm^{-1} (carboxylic acids and ketones)
A2	Absorbance C=O at 1740 cm^{-1} (esters and aldehydes)
A3	Absorbance C=O at 1780 cm^{-1} (γ-lactones)
A4	Absorbance C=C at 1650 cm^{-1} (vinyls)
Sa	Roughness (µm)
G1	Haze gloss
G2	Contrast gloss
L*	Lightness (light-dark)
a*	Chromatic coordinate (red-green)
b*	Chromatic coordinate (yellow-blue)

I.3. Results and discussion

I.3.1 Mechanical performance

Flexural properties of PP and biocomposites were determined all along one-year outdoor (EW) and 1000-hour artificial (AW) weathering. Their changes are illustrated in Figure 2. The higher values of biocomposites mechanical properties recorded whatever the time and type of exposure are associated with the reinforcement and stiffening effect of vegetal fibers. However, elastic modulus (E_f) and conventional deflection stress (σ_{fc}) of all materials declined during the two weatherings due to polymer and hemp fibers degradation.

Otherwise, the longest-time accelerated ageing more affected more elastic modulus of PP and PP/hemp fibers composites than outdoor one due to high number of cyclical changes in moisture, temperature and UV radiation in short times [23]. Also, the performance loss rate over ageing increased from PP to PP30 after exterior ageing whereas it decreased after artificial one. Indeed, elastic modulus decreased by 20% and 8% for PP30-EW and neat PP-EW respectively after 12 months. On the contrary, it diminished by 30% and 41% for PP30-AW and PP-AW respectively after 1000 hours. This can be explained by either different degradation mechanisms during EW and AW leading to different performance loss speeds or too-long exposition corresponding to more than 1 year of natural exposure covered by the accelerated ageing. The properties presented later will allow further understanding of these variations and target the possible reasons of differences.

As regards trend of σ_{fc} changes, neat PP stress was more influenced than PP30 whatever the type of weathering after the total duration. Also, in the last six months, σ_{fc} of PP-EW fell by 21% whereas it remained almost constant before. After a 250-hour stable period, it linearly dropped by 36% for PP-AW. Thus, artificial ageing amplified the strength loss.

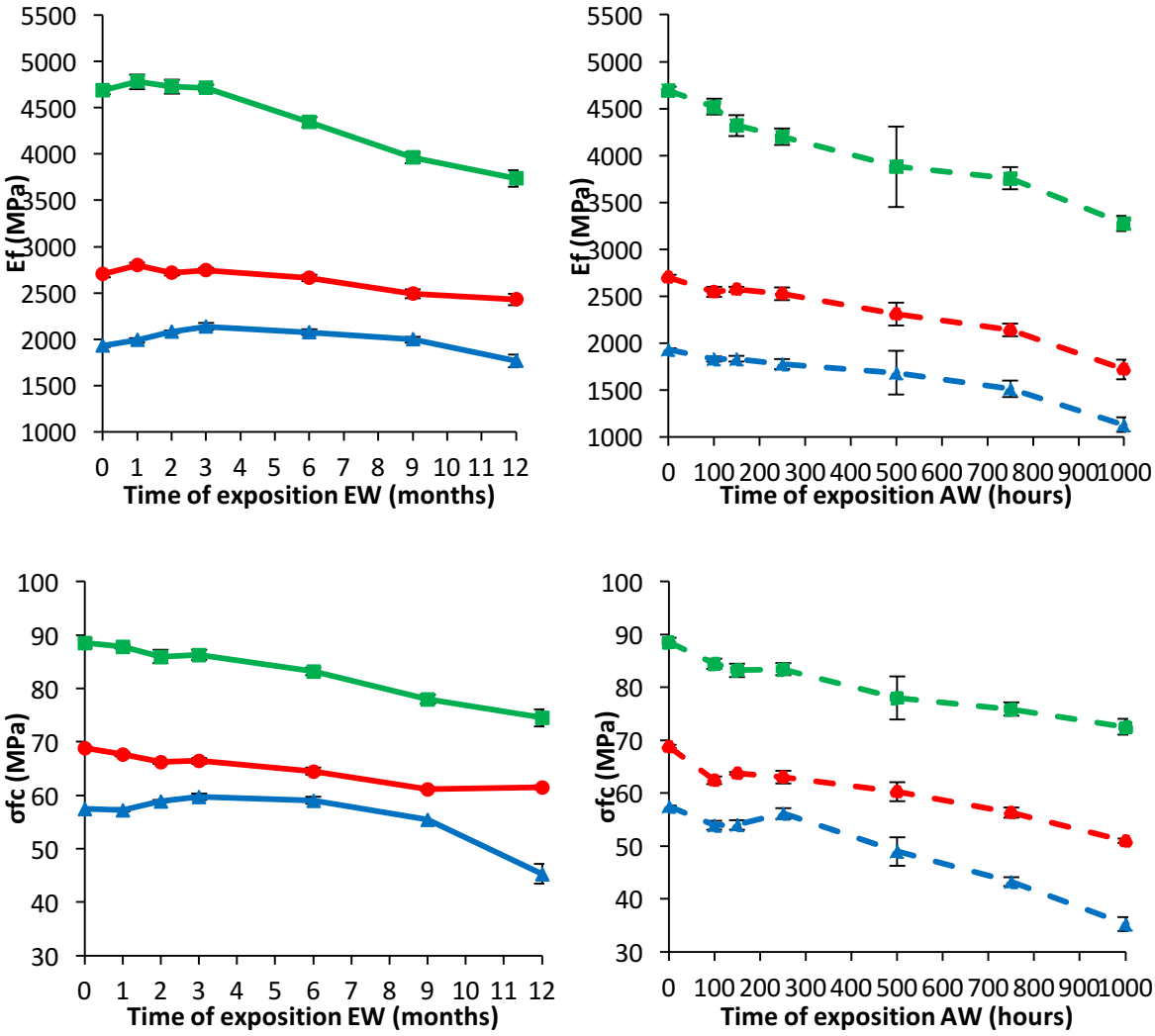

Figure 2 - Elastic modulus and conventional deflection stress of PP (blue), PP10 (red) and PP30 (green) over EW (full line) and AW (dashed line)

I.3.2 Microstructure

The crystallinity degree of polymer was influenced by the weathering (Figure 3). Indeed, even if the photodegradation is prevalent in the amorphous phase whose molecular chains can further crystallize, the global decrease of crystallinity rate suggests that crystalline phase was mostly affected [3,38]. Firstly, χ_{c1} was slightly less impacted by weatherings than χ_{c2}. Indeed, the main difference is noted for PP-AW decreasing from 46.1 ±0.2 % to 33.3 ±1.6 % and from 51.0 ±0.3 % to 25.0 ±2.8 % for χ_{c1} and χ_{c2} respectively at the end of the AW. Moreover, some differences were noted between AW and EW. Indeed, the high absolute curve slope of χ_{c2} evolution of artificially aged materials indicates a higher kinetic of crystallinity rate decrease under artificial weathering conditions. For instance, χ_{c2} of PP-AW

exhibited a drastic decrease of 50% in 1000 hours whereas PP-EW one lost only 7% of its crystallinity degree original value after 12 months. Otherwise, unlike for EW, neat PP was more subjected to QUV chamber conditions than PP10 and PP30. These observations match with results obtained from modulus measurements. It is noted that only χ_{c1} corresponds to materials microstructure when mechanically tested.

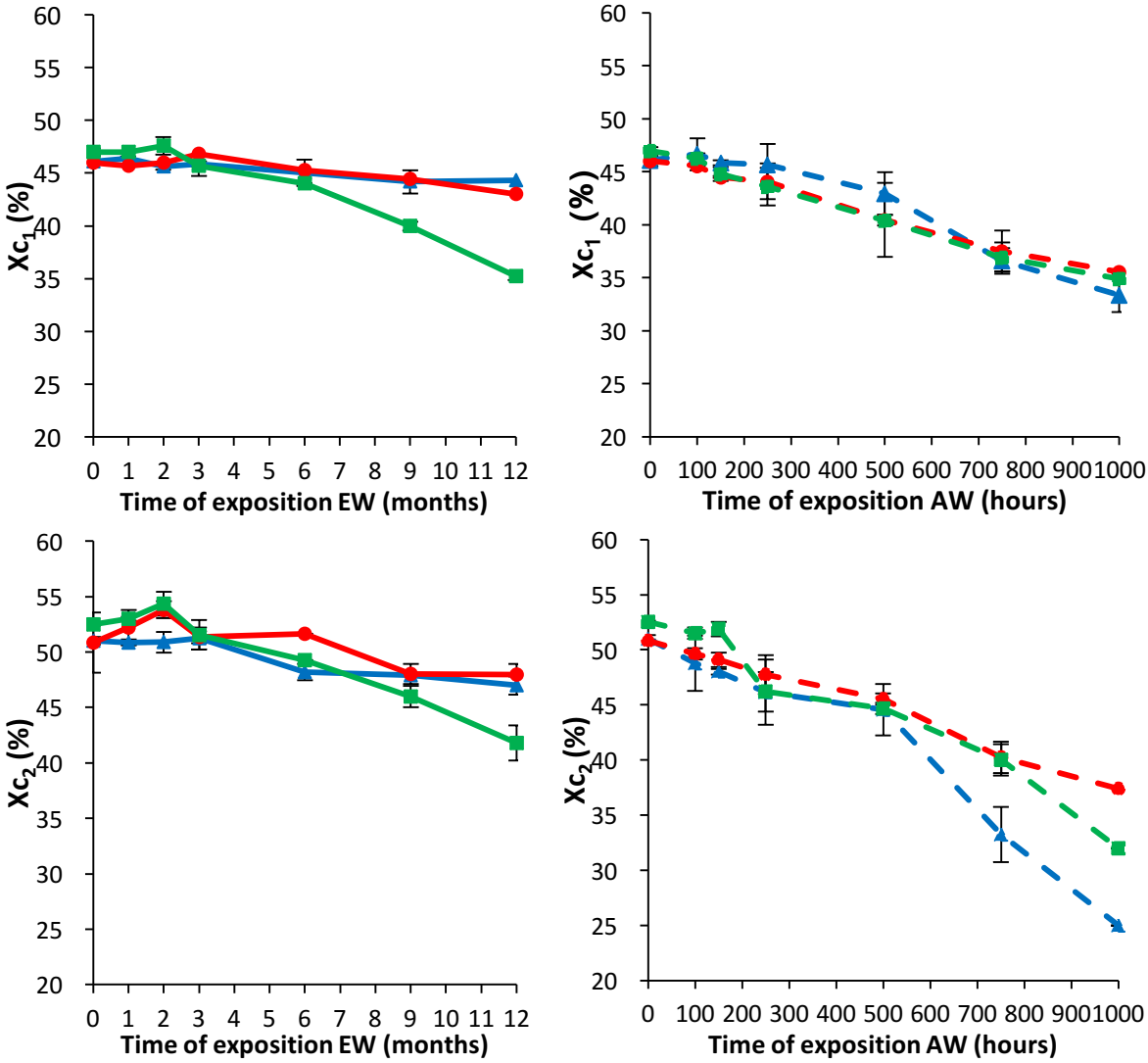

Figure 3 - Cristallinity rate of PP (blue), PP10 (red) and PP30 (green) over EW (full line) and AW (dashed line)

I.3.3 Chemical structure

It is common to monitor photooxidation products in the 1700-1800 cm^{-1} region of FTIR spectra of polymers throughout their ageing. Thus, carbonyls compounds including carboxylic acids in the dimer form and ketones, esters and aldehydes, and lactones peaking

at 1711, 1740 and 1780 cm^{-1} respectively were analysed [15]. Thermoplastic polymers can also undergo chain scission inducing vinyl species formation whose 1650 cm^{-1} infrared band attests its presence. The analysis is hence focused on absorption bands between 1490 and 1830 cm^{-1}. The infrared spectra of materials that were unweathered, artificially weathered for 1000h and exterior weathered for one year are featured in Figure 4.

Firstly, increase of all carbonyl and vinyl bands with the fiber loading comes from C=O and C=C bonds naturally present in cellulose, hemicelluloses and lignin. Also, their increase after exposition of all materials corroborates oxidative mechanism and scission of polymer chains. It can be noticed that lactones level of each material was not influenced by the kind of ageing after 1000 hours and one year of accelerated and exterior weathering respectively at the opposite of other carbonyl derived substances whatever the material. Indeed, oxidative degradation rate recorded after 1000 hours of AW corresponding to 41 days is higher than those after 1 year of EW. So artificial ageing was more impactful than exterior ageing for durations that were chosen in this work.

Similarly, C=C bond peak height was higher for PP-AW1000 than for PP-EW12 whereas no difference was observed for biocomposites. PP was, once again, mainly sensitive to laboratory chamber conditions that accelerated polymer chain scissions.

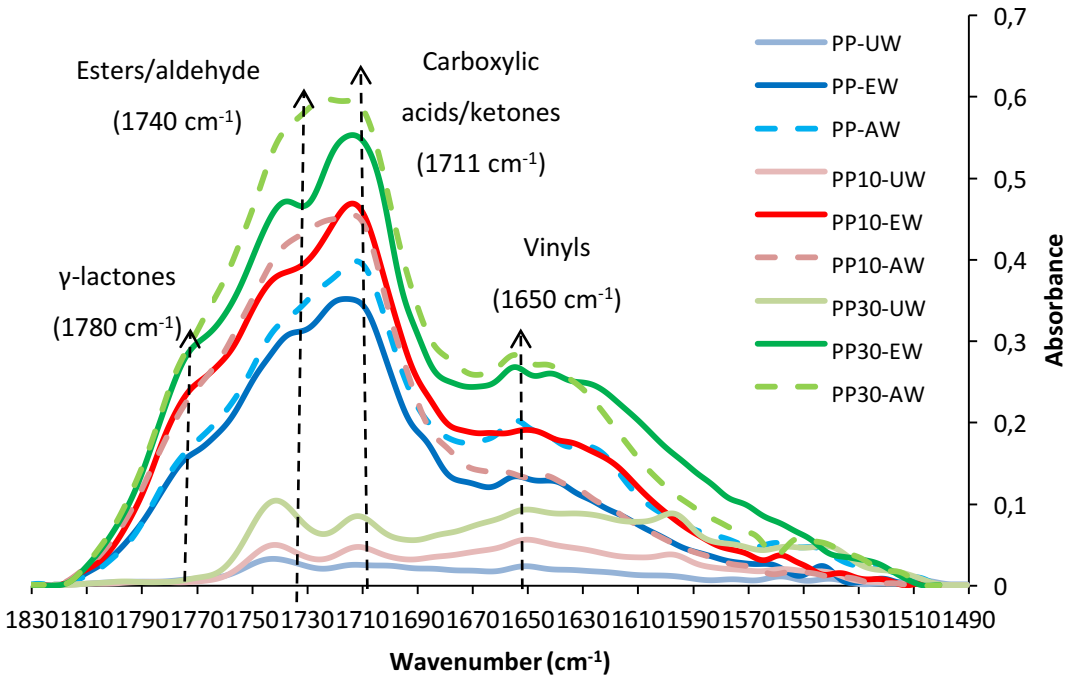

Figure 4 - Infrared spectra of UW, EW (1 year) and AW (1000h) materials: PP (blue based), PP10 (red based), PP30 (green based)

The maximum absorbance evolutions of C=O carboxylic acid and ketone bonds (1711 cm^{-1}), C=O ester and aldehyde bonds (1740 cm^{-1}), C=O γ-lactone bond (1780 cm^{-1}) and C=C vinyl bond (1650 cm^{-1}) with the ageing time and type (EW, AW) are showed on Figure 5. Oxygenated products aroused from hydroperoxide species formed under UV rays and high temperature of the two types of weathering that can decompose into alkoxy radicals which dissociate into lower molecular weight products [25,39]. However, the increase rate of oxygenated products was lower after natural ageing than after artificial ageing whatever the material. Otherwise, this trend was even more valid for virgin PP. So, artificially aged PP underwent stronger oxidative degradation.

As regards carbonyl bonds evolution profile, results show that esters and aldehydes (1740 cm^{-1}) on one hand and lactones (1780 cm^{-1}) on another hand evolving from PP degradation reached a constant absorbance value after 250h of 0.3 and 0.15 respectively whereas ketones and carboxylic acids (1711 cm^{-1}) were progressively detected for artificial weathering. This suggests that, at this weathering stage, ketones and acids were formed to the detriment of the previous ones. Same evolution was observed for biocomposites with a slightly slower increase of esters, aldehydes and lactones generation after 250h rather than a plateau. Therefore, ketones and acids groups could be favored in these conditions of

humidity, UV radiation and temperature. Concerning exterior weathering, continuous increase of these oxygenated compounds was recorded. However, the maximum shifted from 1740 to 1711 cm^{-1} from non-weathered to weathered state whatever the type of weathering. The hydrolysis of ester species leading to carboxylic acids could be responsible to the 1711 cm^{-1} band level increase.

γ-lactones generally originating from intramolecular reactions could evolve from back-bitting mechanism [25]. Otherwise, the evolution of lactones absorbance peak reveals an auto-accelerated shape meaning first induction stage followed by rapid increase and steady state period [40]. A short induction period, of about 100h, is observed for PP-AW whereas this stage lasted 6 months for PP-EW.

As regards vinyl bonds evolution profiles, biocomposites level stabilized after almost 6 months and 250h of natural and accelerated weathering respectively. Indeed, enolic groups can further rearrange into carbonyl species [41]. Also, even if they exhibit the same evolution profile, vinyl groups level less increased for AW biocomposites than for EW ones. It can be due to continuous high temperature in chamber (50 °C) inducing the higher decrease of vinyls to the profit of carbonyls [25]. However, a different tendency is observed for neat PP since, as for ketones evolution, it progressively increased. Moreover, the amount of C=C species after one year corresponds to 250h of accelerated ageing. Thus, this mechanism seems to correlate with an acceleration of degradation rate of PP under conditions of artificial exposure that were applied in this study.

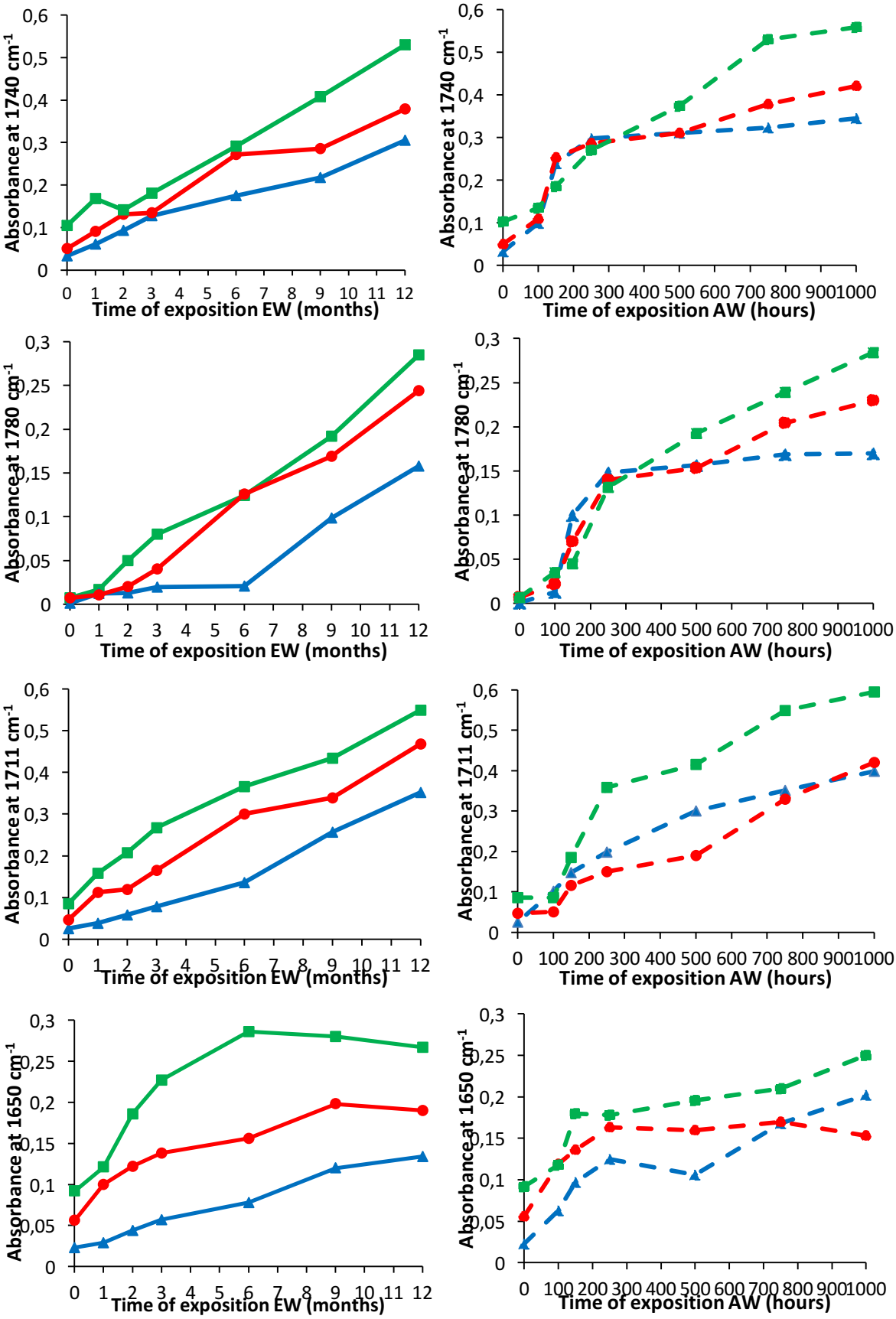

Figure 5 – Maximum absorbance values at 1711, 1740, 1780 and 1650 cm^{-1} of PP (blue), PP10 (red) and PP30 (green) infrared spectra over AW and EW

I.3.4 Visual appearance

I.3.4.1 Color

Figure 6 depicts lightness evolution versus exposure time. PP was not significantly influenced by the ageing. Nevertheless, results showed that lightness increased for biocomposites because of fibers photodegradation and structural changes. As reported in literature, oxido-reduction process of lignin leading to formation of hydroquinones due to chromophore structures formation in lignin may induce whitening [4]. The bleaching kinetics of PP10-AW and PP30-AW were more important than those of PP10-EW and PP30-EW respectively. Otherwise, PP30 bleaching saturated at almost 75 after 3 months of EW and 250h of AW. This can be explained by the increasing rate of holocellulose at the surface being uncovered after biocomposites exposition. Otherwise, they degraded in a similar manner. Thus, the type of weathering did not modify the evolution profile.

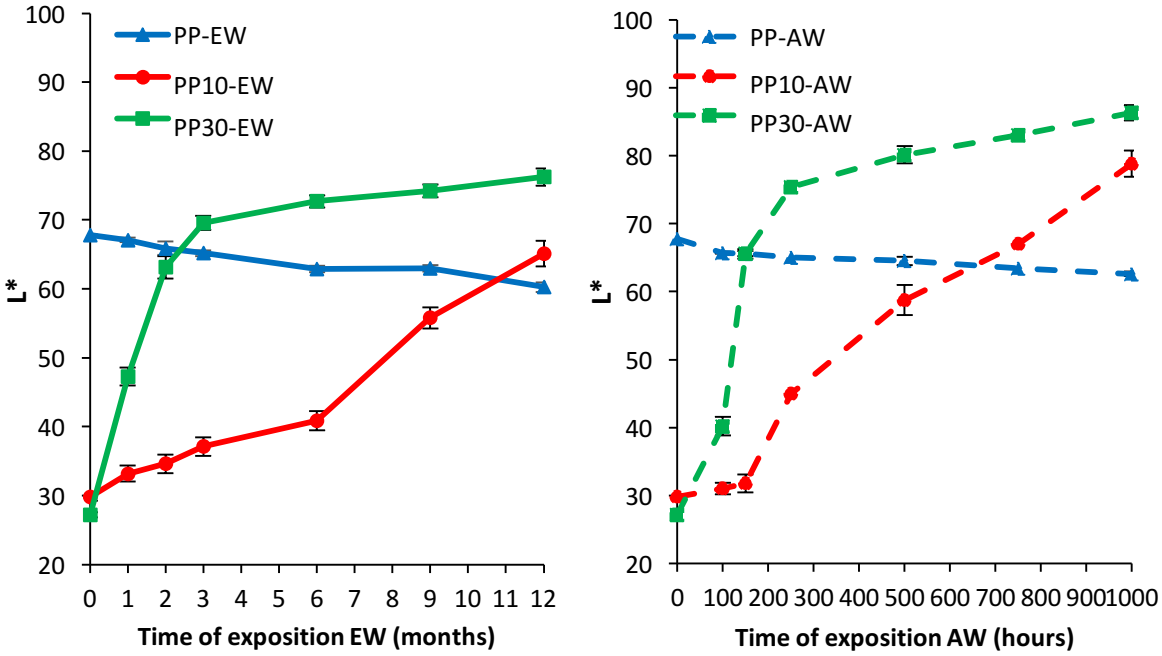

Figure 6 - Lightness evolution of PP (blue), PP10 (red), and PP30 (green) materials under EW and AW

Figure 7 shows a* and b* colorimetric coordinates in a two-dimension space.

Results show that PP colorimetric coordinates was not highly influenced by the two types of ageing.

As concerns a* coordinate values, results showed that non-weathered PP10 presented higher a* coordinate value (about 3) than non-weathered PP and PP30 (both about 1). This can be attributed to a greater extractives (whose color is reddish) migration at the surface during moulding process for low fiber rate than for higher fiber content because of steric hindrance due to holocellulose and lignin [42][43]. The higher extractives proportion at the surface of the lowest fiber rate biocomposite demonstrated by higher a* parameter value, was certainly due to extractives whereas steric hindrance due to holocellulose and lignin limits their migration at PP30 surface. Otherwise, the presence of vegetal fibers induced high chromatic variations of reinforced materials over the expositions. Indeed, a* value of biocomposites diminished whatever the type of weathering demonstrating a red color loss. This can be attributed to extractives and red chromophores degradation or removal due to radiation and rain for EW and spray for AW.

As regards b* coordinate changes, PP30 underwent yellowing during the first stage until 6 months (EW) and 500h (AW), then b* decreased. This evolution has already been observed by Peng et al demonstrating that yellow paraquinones and photooxidative products formation due to presence of chromophore comprised of carbonyl groups was firstly favoured. This preceded the further reduction of paraquinones part into hydroquinones. However, the quinones formation mechanism occurred slower during exterior ageing. Indeed, PP30-AW rose from 1.91 for non-aged sample to 2.45 after 500h then drastically dropped to 0.20 after 1000h whereas PP30-EW increased to 3.11 then decreased to 2.32 after 12 months. Similarly, b* value of PP10-AW decrease rate exceeded PP10-EW one. So, in our experimental conditions, chamber testing might be favourable for accelerating the degradation phenomenon.

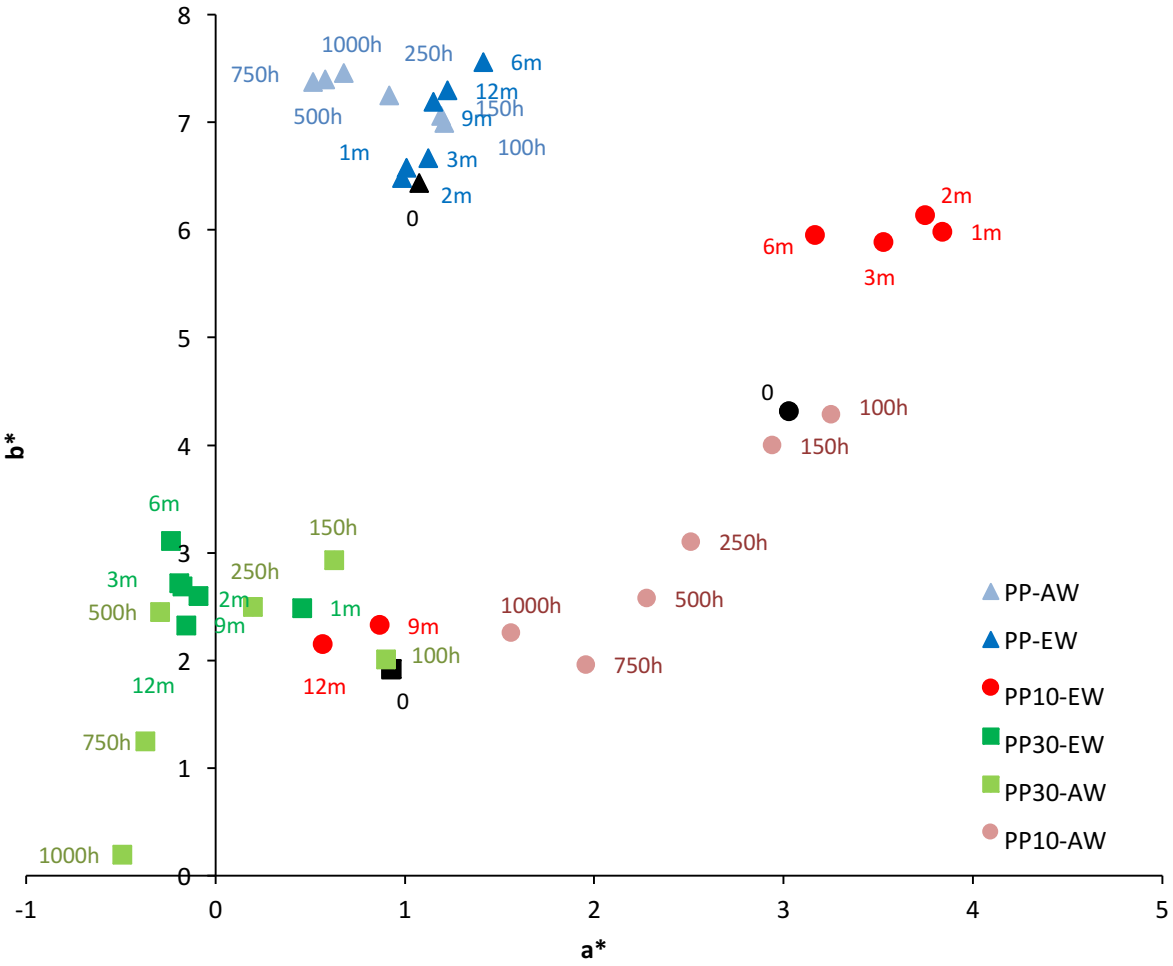

Figure 7 - Colorimetric coordinates of PP (triangles), PP10 (spheres) and PP30 (squares) over AW (lighter colors) and EW (darker colors) (h: hours, m: months)

I.3.4.2 Gloss

The light angular repartition profile of non-weathered and longest-weathered materials (1000h for AW and 1 year for EW) is shown in Figure 8.

For non-weathered sample, maximum intensity of the specular peak dropped with the vegetal fibers rate meaning that brightness decreased. Some irregularities brought by the presence of short hemp fibers at the sample surface were responsible for less smooth surfaces.

After ageing, gloss was reduced for all materials. Indeed, the peak was no longer prominent after weathering and specular zones were no longer well defined, especially for PP30 for which peak almost disappeared due to diffuse reflection enhancement. No significant difference between PP30-AW and PP30-EW curves was observed. Nevertheless, aged virgin

PP exhibited short and broad symmetric peak that was extremely less intense than PP-UW one, signifying that polymer was particularly affected. Indeed, the maximum radiometric power value went from 17,094 u.a. to 2,676 u.a. and 264 u.a. after EW and AW respectively. Thus, gloss and smoothness decreased faster in 1000h of artificial ageing than in one year of outdoor natural one. PP10 went through the same tendency.

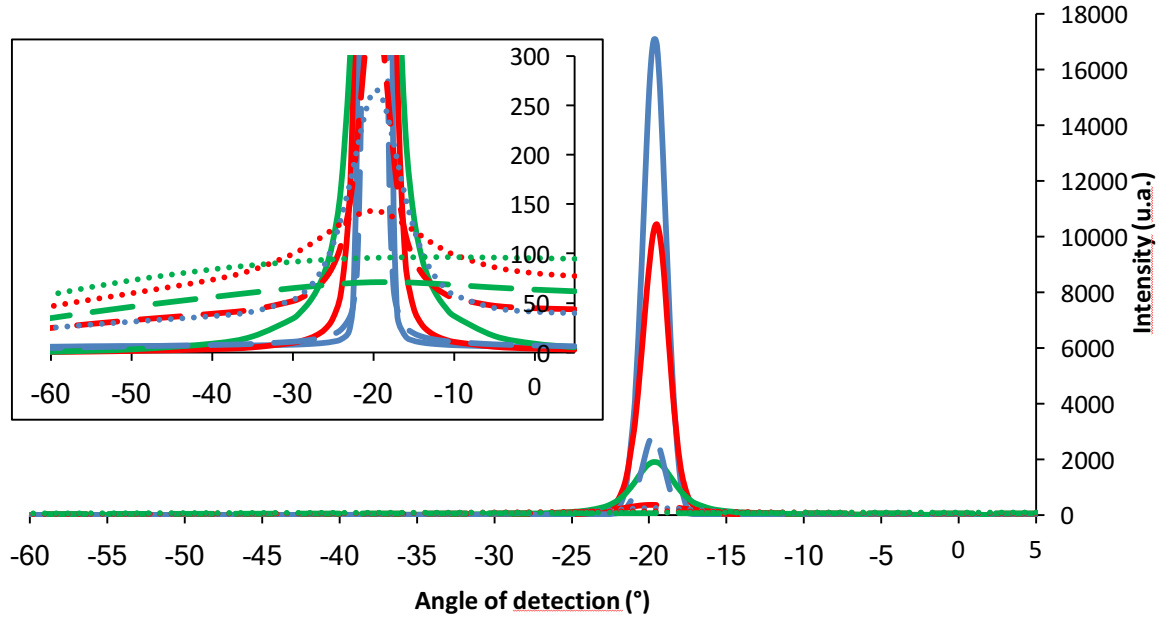

Figure 8 - Angular repartition of intensity of light reflected by PP (blue), PP10 (red) and PP30 (green) before (full line) and after 1000-hour artificial (dotted line) and one-year natural (dashed line) ageing

Evolutions of gloss parameters throughout weathering are presented in Figure 9.

G_1 and G_2 of PP-AW significantly decreased from 235 and 4275 to 1 and 5 respectively for the first 250h whereas G_1 and G_2 of PP-EW took one year to go down to 34 and 12 respectively. PP10-AW reached approximately 1 whatever the gloss ratio after longer time (500h) whereas PP10-EW reached 9 (G1) and 1 (G2) value ratio after 9 and 12 months respectively. Both PP30-AW and PP30-EW parameters rapidly tended to 1 suggesting that intensity level reached a same level whatever the detection angle. As previously seen, PP was mostly degraded. As regards gloss variations, this trend was confirmed for artificial and outdoor ageing. Moreover, the ratio cannot drop below 1, so the comparison between PP30 and PP decrease rates cannot directly be compared since non-weathered PP30 already exhibited low gloss parameters close to 1 and thus swiftly reached the lowest parameter.

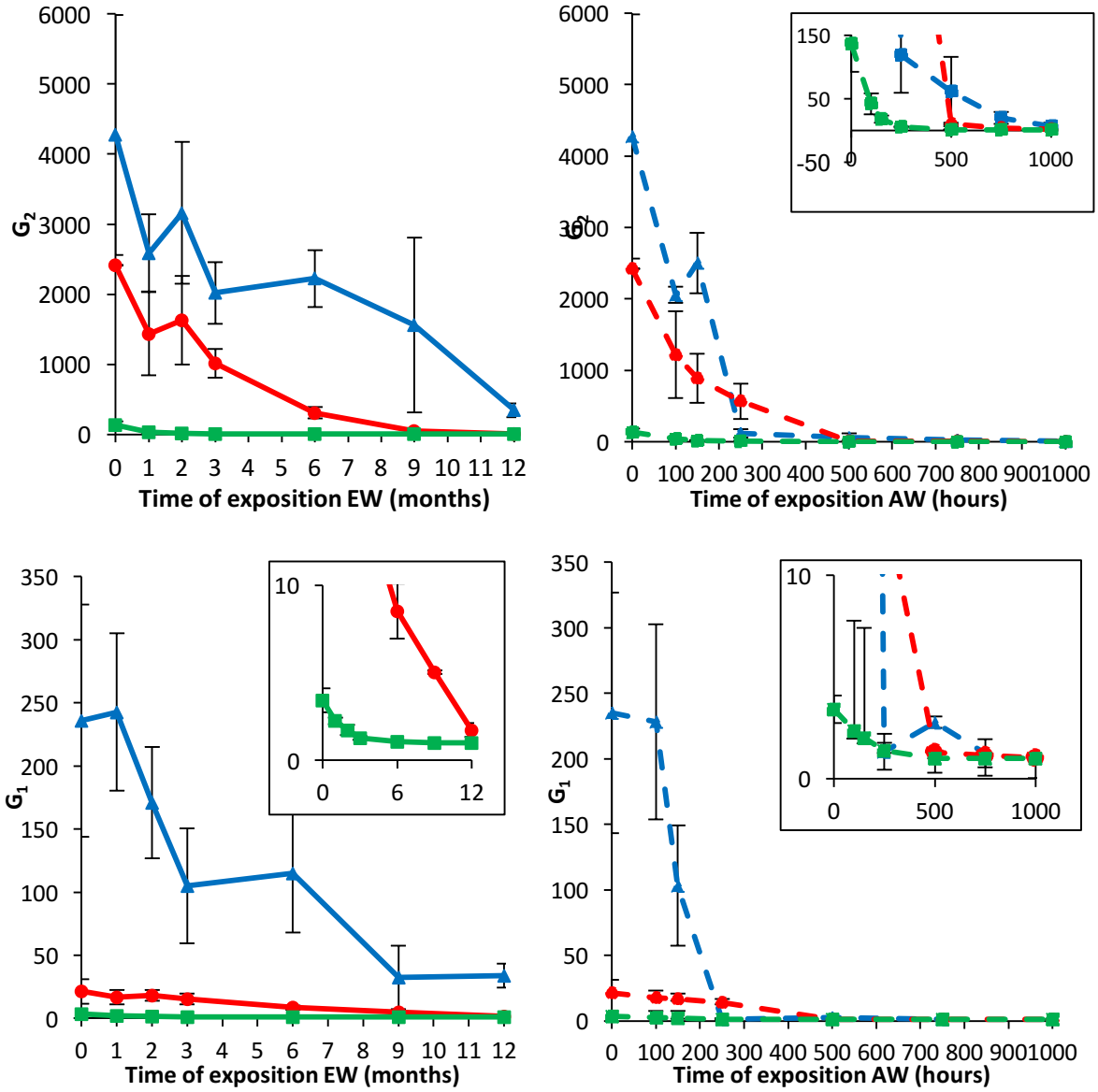

Figure 9 - Gloss parameters over EW (full line) and AW (dashed line) of PP (blue), PP10 (red), and PP30 (green)

I.3.5 Surface aspect

I.3.5.1 Roughness

Average roughness was estimated by altitude variations measurement at the samples surface. Figure 10 gathers non-aged and 1000-hour artificially and one-year naturally aged materials. Before ageing, materials surface was relatively smooth. Some surface crackles progressively appeared afterwards, deepened and propagated gradually with ageing time. It is observed that the surface pictures differed according to the kind of weathering and the

material and artificial weathering induced more surfaces deterioration. Finally, differences are noted according to the material as neat PP presented regular microcracks whose depth is higher after accelerated ageing. On the contrary, PP30 exhibited some dispersed hollows due to hemp fibers removal or protrusion caused by exterior parameters [8].

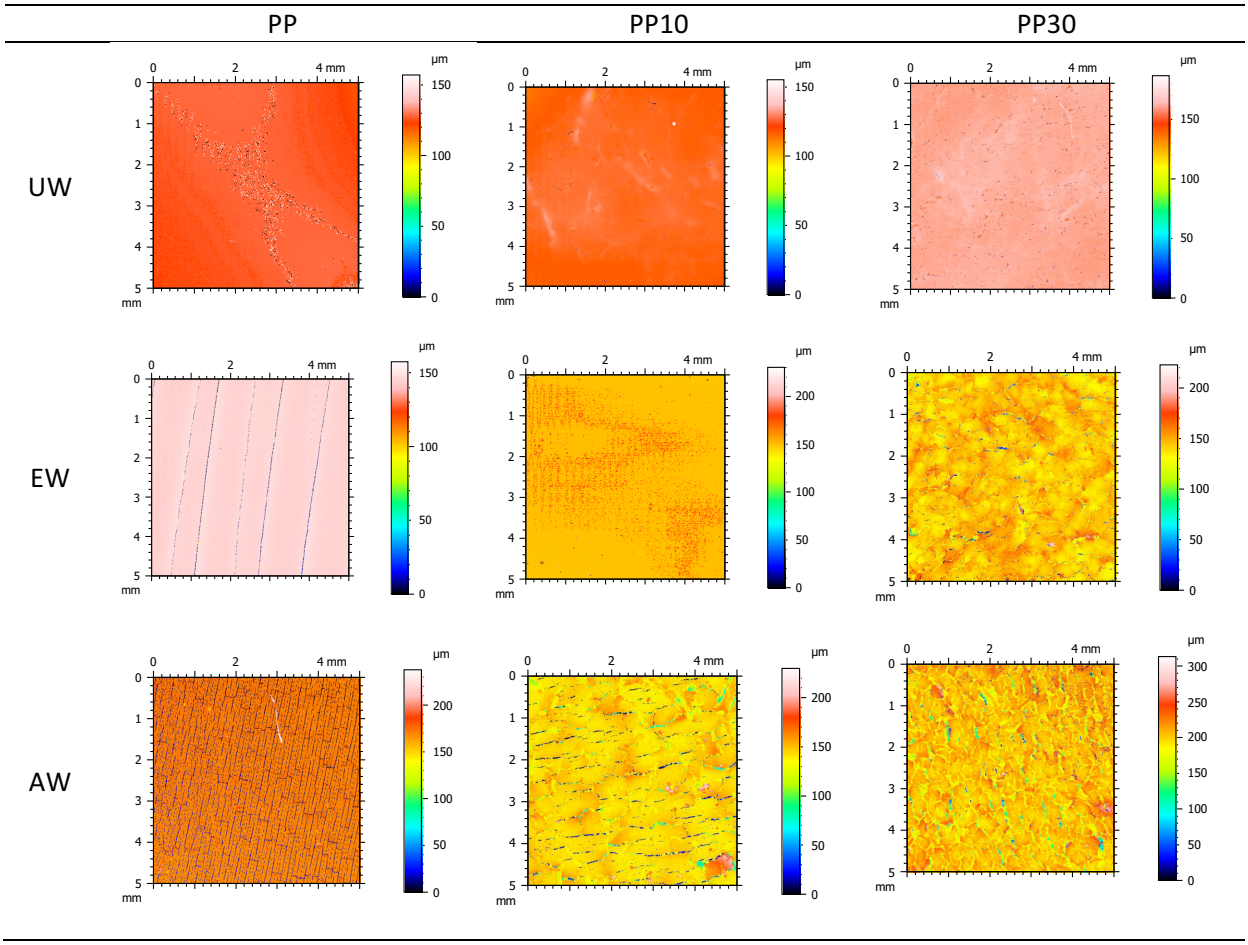

Figure 10 - Surface images of PP, PP10 and PP30 before (UW) and after artificial (AW) and exterior (EW) weathering

Figure 11 clearly emphasizes the roughness continuous increase of all materials. By comparing EW and AW graphs, the highest degradation kinetic measured through average roughness parameter during exterior weathering was attributed to biocomposites whereas neat PP roughness outstripped during artificial weathering.

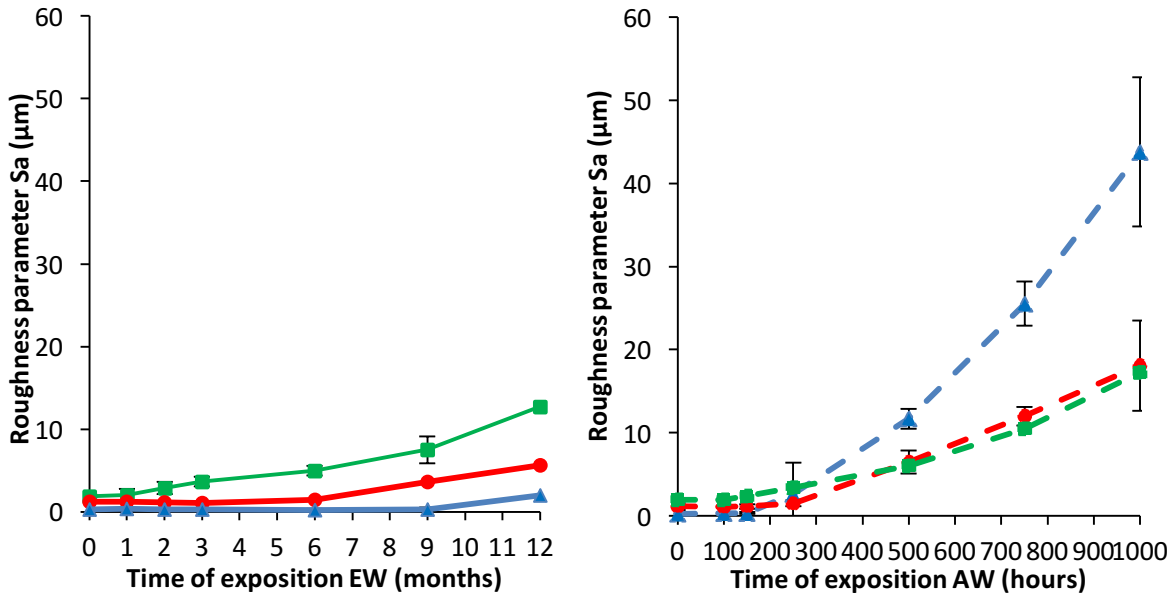

Figure 11 - Roughness parameter evolution of PP (blue), PP10 (red) and PP30 (green) over AW and EW

I.3.6 Statistical analysis

The previous observations do not corroborate the well-known higher sensitivity of biocomposites than conventional glass fibers composites face to UV radiation, temperature and humidity [1,45,46]. In view of properties changes, neat PP was globally particularly degraded due to artificial degradation. Therefore, parameters implemented in the laboratory chamber that strongly affected neat polymer stability may have been over-represented. PCA analysis will permit to understand and clarify these differences.

I.3.6.1 Global degradation mechanisms

All along the exposition, neat PP and biocomposites properties evolved at different rates. Moreover, depending on the property, the higher degradation kinetic was recorded either for PP or PP30 after artificial weathering whereas the contrary was noted after outdoor ageing. Thus, in order to verify the mechanisms and understand the observed differences, PCA is used to consider all studied properties.

The correlation circles allow representing the profile of correlations between variables and can bring elements on causal relationships (Figure 12). If the proximity between variables measured after EW differs from that measured after AW, we can assume that different mechanisms of degradation occurred. For this purpose, values were normalized to non-

weathered state values in order to only consider the influence of time of weathering on properties changes for accurate interpretation of global degradation mechanisms induced by exposure. It can be noticed that positions of variables projected on the two circles globally do not differ. Gloss parameters, microstructure and mechanical properties are effectively well defined and positively correlated with the first principal component PC1 (horizontal axis). On the contrary, lightness is positively represented by PC2 for both ageing. Since weathering times are mainly organized according to PC1 and fiber loading according to PC2 (Figure 13), normalized stiffness, conventional deflection stress and crystallinity ratio variables discriminate samples weathered at different ageing times. Finally, A1, A2 and A4 assigned to ketones and acids, to aldehydes and esters and to vinyls normalized absorption bands respectively equally contribute to PC1 and PC2. Otherwise, b* coordinate was far away from the two circles meaning that it was not well projected. Thus b* colorimetric parameter cannot be interpreted.

Variables representing roughness parameter Sa and lactone maximum absorbance A3 contribute at different rates to PC1 and PC2 principal components axes drawing. Indeed, A3 and Sa are close to PC1 carrying the highest rate of information of the cloud of data (almost 56%) for EW. But these variables get more contribution to PC2 for AW. By simultaneous interpretation of individuals scatterplots and correlation circles, it is deduced that these parameters mostly discriminate the weathering time according to PC1 than fiber rate according to PC2 for EW (Figure 12 and Figure 13). On the contrary, for AW, Sa and A3 mainly distinguish fiber loadings through PC2. Indeed, strong differences of evolution trend of roughness and lactone maximum absorbance between PP, PP10 and PP30 were observed (Figure 5 and Figure 11). Short-term induction times of 150h and 100h respectively before the increase of parameters were verified for PP-AW whereas they increased after 6 months and 1 month respectively for PP-EW. This fact maybe induced the main discrimination of fiber loadings for AW (Figure 13b). Thus, the difference of A3 and Sa positions between AW and EW is explained by the decomposition acceleration generated by the artificial ageing. Otherwise, they remain opposed according to PC1 axis whatever the kind of weathering.

Formation of cracks (Sa variations) were favored by UV rays and rain rather than high temperature [47]. Indeed, it was shown that temperature has not altered the crack growth

mechanism [48]. Moreover, it has been deduced from infrared spectroscopy that hydrolysis could be responsible for carboxylic acid and ketone functional groups continuously fast increase for AW. Therefore, spray step representing rainfall might accelerate polymer chains scissions. Moreover, water might enhance the diffusion of oxygen in the matter favoring chains oxidation. So, spray and UV radiation steps especially inducing surface aspect changes could be over-represented. Also, in this case, lignin component found in vegetal fibers certainly acted as antioxidant after extended-time artificial exposure since the increase of the roughness and oxygenated products of artificially aged PP30 kinetic was lower [5,49].

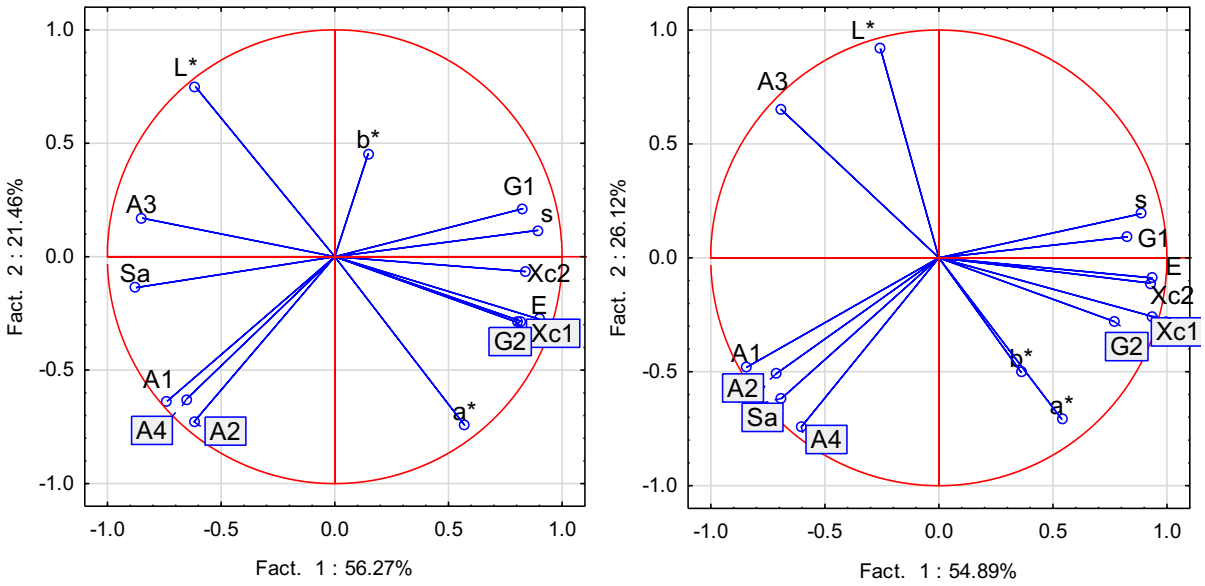

Figure 12 - Correlation circles of normalized variables under EW (a) and AW (b)

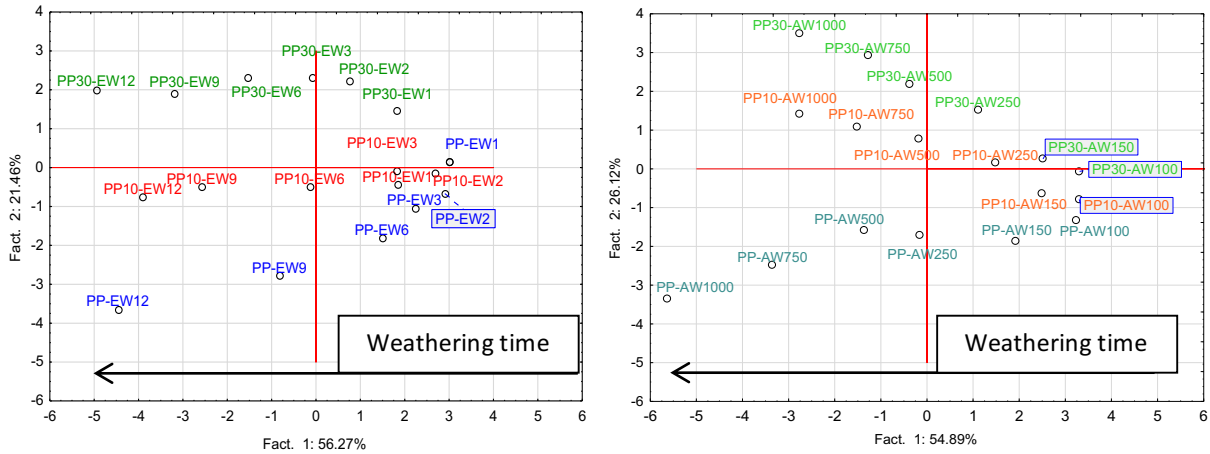

Figure 13 – Scatterplots of EW (a) and AW samples (b)

I.3.6.2 Temporal equivalence

The objective is to find similar behaviour between naturally exteriorly (EW) and artificially (AW) weathered samples. Hence, to assess eventual temporal equivalence, individuals living in a multidimensional space whose dimensions number corresponds to the number of variables, were projected on a plan to easily perceive the proximities (Figure 14). As previously, normalized variables were considered for only considering influence of exposition.

PP-AW100 and PP-EW3 present almost same coordinates according to PC1 axis to which all properties are mostly linked. Therefore, these materials are supposed to present same degradation rate according to the studied properties. Otherwise, they are also close to each other according to PC1 corresponding to the most important linear combination characterized by the most of variables and capturing the largest information (75%). PP-AW250 and PP-EW12 present almost same coordinates according to PC1 and PC2. Thus, acceleration factors were calculated by the ratio between time of natural weathering and that of artificial weathering. They were estimated at 22 and 35 at these precise periods. Indeed, it is evident that non-linear evolution induces different acceleration factors according to the weathering stage. However, ketone and acid groups absorbance represented by A1 only verified the first equivalence whereas most of other properties mainly confirmed the second one.

As regards biocomposite loaded at 10 wt% of hemp fibers, PP10-AW100 is related to PP10-EW2. Otherwise, 250h and 6 months also generated same amounts of damage. Thus, the acceleration factors equal almost 14 and 17.5. In addition, by comparison with neat PP, PP10 required two times higher of natural exposure duration than PP to reflect 250h of ageing in the QUV chamber.

Finally, as for previous materials, two temporal correspondences are given for PP30. Indeed, the two last natural weathering times 9 and 12 months coincide with 500 and 750h respectively. So acceleration factors are 13 and 12. The two acceleration factors are almost equivalent. This can be justified by the fact that the two sampling were very close in time as much outside (9 and 12 months) as in the chamber (500h and 750h). Also, plots of properties

such as carbonyl groups maximum absorbance, conventional deflection stress and elastic modulus as a function of weathering time present linear correlation coefficients superior to 0.90. This can justify the low difference between acceleration factors since for linear evolution, the ratio between the slope of EW and AW corresponds to acceleration factor.

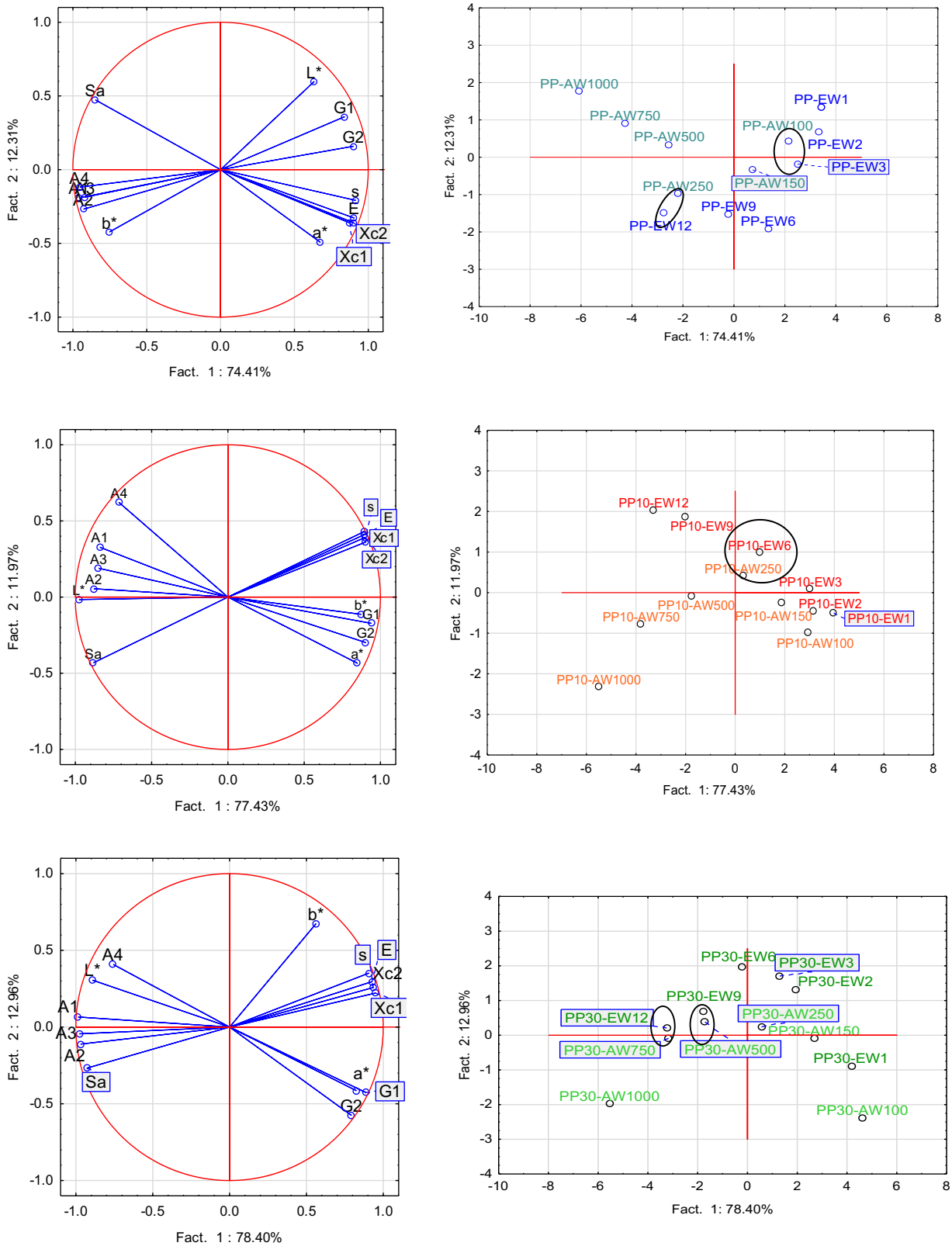

Figure 14 - Correlation circles and scatterplots of PP (a), PP10 (b) and PP30 (c)

I.4. Conclusion

This work aimed to perform natural and artificial ageing of neat PP and biocomposites and correlate the two weathering conditions. Results showed that conditions of irradiation, humidity, temperature and water spraying chosen in this work accelerated oxidation kinetics and enhanced mechanical performance decrease under artificial weathering compared to outdoor conditions. The natural fibers photo-oxidation mechanisms inducing surface color variations of biocomposites were accentuated in the QUV chamber. a* and b* colorimetric parameters decrease due to carbohydrates and lignin components decomposition was mostly intensified through artificial ageing. Smooth surface aspect of samples was also altered. Otherwise, the type of roughness differed according to the material with regular cracks for neat PP and some holes for the biocomposite with the highest fiber rate limiting the surface gloss.

Otherwise, results showed that modulus decrease of neat PP is more important than those of biocomposites after artificial ageing. Elsewhere it was observed that the degradation generally increased with the fiber rate after outdoor weathering whereas it decreased after artificial one. It also dug the cracks and holes formed after decomposition causing more deep cracks at virgin PP surface.

PCA allowed comparing artificial and exterior weathering. It was found that correlation circles were quite similar apart from variables whose profile exhibited induction stage. Thus, this statistical method has disclosed a relationship between outside and chamber weathering. It permitted to conclude that artificial ageing more accelerated neat PP degradation maybe due to overrepresentation of factors in cycles than those found out of doors and sensitivity of PP face to short cyclical changes.

Depending on the material, different acceleration factors were estimated from PCA. Indeed, one-year natural exposure of neat polymer was represented by 250h of accelerated ageing whereas 750h were required for the highest fiber loading composite. Contrary to studies found in literature that classically face together values of a same property obtained after accelerated and natural ageing, this statistical method used to estimate acceleration factors allowed to take into account all parameters at the same time. It could be interesting to

generalize this approach to other materials and other quantitative parameters representative of weathering.

I.5. References

[1] A. Shahzad, Hemp fiber and its composites - a review, J. Compos. Mater. 46 (2012) 973–986. doi:10.1177/0021998311413623.

[2] M.Z. Ahmad Thirmizir, Z.A. Mohd Ishak, R. Mat Taib, S. Rahim, S. Mohamad Jani, Natural Weathering of kenaf bast fibre-filled poly(butylene succinate) composites: Effect of fibre loading and compatibiliser addition, J. Polym. Environ. 19 (2010) 263–273. doi:10.1007/s10924-010-0272-2.

[3] C. Homkhiew, T. Ratanawilai, W. Thongruang, Effects of natural weathering on the properties of recycled polypropylene composites reinforced with rubberwood flour, Ind. Crops Prod. 56 (2014) 52–59. doi:10.1016/j.indcrop.2014.02.034.

[4] S. Butylina, M. Hyvärinen, T. Kärki, A study of surface changes of wood-polypropylene composites as the result of exterior weathering, Polym. Degrad. Stab. 97 (2012) 337–345. doi:10.1016/j.polymdegradstab.2011.12.014.

[5] I. Spiridon, K. Leluk, A.M. Resmerita, R.N. Darie, Evaluation of PLA–lignin bioplastics properties before and after accelerated weathering, Compos. Part B Eng. 69 (2015) 342–349. doi:10.1016/j.compositesb.2014.10.006.

[6] K.C.C.C. Benini, H.J.C. Voorwald, M.O.H. Cioffi, Mechanical properties of HIPS/sugarcane bagasse fiber composites after accelerated weathering, Procedia Eng. 10 (2011) 3246–3251. doi:10.1016/j.proeng.2011.04.536.

[7] N.M. Stark, L.M. Matuana, Ultraviolet weathering of photostabilized wood-flour-filled high-density polyethylene composites, J. Appl. Polym. Sci. 90 (2003) 2609–2617. doi:10.1002/app.12886.

[8] L. Soccalingame, D. Perrin, J.-C. Bénézet, S. Mani, F. Coiffier, E. Richaud, A. Bergeret, Reprocessing of artificial UV-weathered wood flour reinforced polypropylene composites, Polym. Degrad. Stab. 120 (2015) 313–327. doi:10.1016/j.polymdegradstab.2015.07.013.

[9] A. François-Heude, E. Richaud, E. Desnoux, X. Colin, Influence of temperature, UV-light wavelength and intensity on polypropylene photothermal oxidation, Polym. Degrad. Stab. 100 (2014) 10–20. doi:10.1016/j.polymdegradstab.2013.12.038.

[10] J.W. Martin, R.A. Ryntz, J. Chin, R.A. Dickie, Service life prediction of polymeric materials: Global perspectives, in: R.A. Ryntz, J. Chin, R.A. Dickie (Eds.), Springer Science & Business Media, 2008: p. 537. doi:10.1007/978-0-387-84876-1.

[11] X. Yang, X. Jiang, J. Hu, F. Wang, C. Hu, Relationship between physical and mechanical properties of accelerated weathering and outdoor weathering of PVC-coated membrane material under tensile stress, J. Ind. Text. (2016). doi:10.1177/1528083716639062.

[12] X. Yang, X. Ding, Prediction of outdoor weathering performance of polypropylene filaments by accelerated weathering tests, Geotext. Geomembranes. 24 (2006) 103–109. doi:10.1016/j.geotexmem.2005.11.002.

[13] Y. Azuma, H. Takeda, S. Watanabe, H. Nakatani, Outdoor and accelerated weathering tests for polypropylene and polypropylene/talc composites: A comparative study of their weathering behavior, Polym. Degrad. Stab. 94 (2009) 2267–2274. doi:10.1016/j.polymdegradstab.2009.08.008.

[14] X. Yang, X. Jiang, J. Hu, F. Wang, C. Hu, Relationship between physical and mechanical properties of accelerated weathering and outdoor weathering of PVC-coated membrane material under tensile stress, J. Ind. Text. (2016). doi:10.1177/1528083716639062.

[15] J.L. Philippart, C. Sinturel, R. Arnaud, J.L. Gardette, Influence of the exposure parameters on the mechanism of photooxidation of polypropylene, Polym. Degrad. Stab. 64 (1999) 213–225. doi:10.1016/S0141-3910(98)00191-8.

[16] M.D.H. Beg, K.L. Pickering, Accelerated weathering of unbleached and bleached Kraft wood fibre reinforced polypropylene composites, Polym. Degrad. Stab. 93 (2008) 1939–1946. doi:10.1016/j.polymdegradstab.2008.06.012.

[17] D.R. Bauer, Interpreting weathering acceleration factors for automotive coatings using exposure models, Polym. Degrad. Stab. 69 (2000) 307–316. doi:10.1016/S0141-3910(00)00074-4.

[18] G.R. Fedor, P.J. Brennan, Technical bulletin (Q-LAB): Comparison between natural weathering and fluorescent UV exposures : UVA-340 lamp tests results, 2011.

[19] J.S. Fabiyi, A.G. McDonald, Degradation of polypropylene in naturally and artificially weathered plastic matrix composites, Maderas. Cienc. Y Tecnol. 16 (2014) 0–0. doi:10.4067/S0718-221X2014005000021.

[20] C. Badji, L. Soccalingame, H. Garay, A. Bergeret, J.-C. Bénézet, Influence of weathering on visual and surface aspect of wood plastic composites: Correlation approach with mechanical properties and microstructure, Polym. Degrad. Stab. 137 (2017) 162–172. doi:10.1016/j.polymdegradstab.2017.01.010.

[21] L. Belec, T.H. Nguyen, D.L. Nguyen, J.F. Chailan, Comparative effects of humid tropical weathering and artificial ageing on a model composite properties from nano- to macro-scale, Compos. Part A Appl. Sci. Manuf. 68 (2015) 235–241. doi:10.1016/j.compositesa.2014.09.028.

[22] J.B. Howard, H.M. Gilroy, Natural and artificial weathering of polyethylene plastics, Polym. Eng. Sci. 9 (1969) 286–294. doi:10.1002/pen.760090409.

[23] A. Jankowska, P. Kozakiewicz, Comparison of Outdoor and Artificial weathering using compressive properties, Wood Res. 59 (2014) 245–252.

[24] M. Crewdson, Outdoor Weathering Must Verify Accelerated Testing, Antec 2011. 91 (2010) 260–266.

[25] Y. Lv, Y. Huang, J. Yang, M. Kong, H. Yang, J. Zhao, G. Li, Outdoor and accelerated laboratory weathering of polypropylene: A comparison and correlation study, Polym. Degrad. Stab. 112 (2015) 145–159. doi:10.1016/j.polymdegradstab.2014.12.023.

[26] A. Tidjani, R. Arnaud, A. Dasilva, Natural and accelerated photoaging of linear low-density polyethylene: Changes of the elongation at break, J. Appl. Polym. Sci. 47 (1993) 211–216. doi:10.1002/app.1993.070470203.

[27] Z.N. Azwa, B.F. Yousif, a. C. Manalo, W. Karunasena, A review on the degradability of

polymeric composites based on natural fibres, Mater. Des. 47 (2013) 424–442. doi:10.1016/j.matdes.2012.11.025.

[28] C.A. Taylor, A. Amiri, D.C. Webster, C.A. Ulven, Long-term behavior of bio-composites for structural applications, CAMX 2016 - Compos. Adv. Mater. Expo. (2016). doi:10.13140/RG.2.2.33964.87682.

[29] K.G. Martin, R.I. Tilley, Division of Building Research report 04-2-6, CSIRO Aust. (1970).

[30] J.S. Han, J.S. Rowell, Chemical Composition of Fibers, in: R.M. Rowell, R.A. Young, J.K. Rowell. (Eds.), Pap. Compos. from Agro-Based Resour., CRC/Lewis Publishers, 1996: pp. 84–134.

[31] J. Acera Fernández, N. Le Moigne, A.S. Caro-Bretelle, R. El Hage, A. Le Duc, M. Lozachmeur, P. Bono, A. Bergeret, Role of flax cell wall components on the microstructure and transverse mechanical behaviour of flax fabrics reinforced epoxy biocomposites, Ind. Crops Prod. 85 (2016) 93–108. doi:10.1016/j.indcrop.2016.02.047.

[32] ISO 877-1: Plastics -- Methods of exposure to solar radiation -- Part 1: General guidance, (2011).

[33] Pau-Uzein meteorological station, Real-time weather reports, (2016). http://www.infoclimat.fr/observations-meteo/temps-reel/pau-uzein/07610.html (accessed June 16, 2017).

[34] EN ISO 4892-3: Plastics - Methods of exposure to laboratory light sources - Part 3: Fluorescent lamps, (2013) 2–14.

[35] ISO 178:2010, Plastics – Determination of flexural properties, (2010).

[36] ISO 2813: Coatings: Determination of gloss value at 20°, 60° and 85°, (2014) 1–31.

[37] Sperling L.H., Introduction to physical polymer science, 4th ed., John Wiley & Sons, 2006. doi:10.1002/0471757128.ch9.

[38] N.M. Stark, L.M. Matuana, Influence of photostabilizers on wood flour-HDPE composites exposed to xenon-arc radiation with and without water spray, Polym. Degrad. Stab. 91 (2006) 3048–3056. doi:10.1016/j.polymdegradstab.2006.08.003.

[39] J.F. Rabek, Photostabilization of Polymers: Principles and applications, Elsevier Applied Science, 1990. doi:10.1007/978-94-009-07-47-8.

[40] S. Morlat, B. Mailhot, D. Gonzalez, J.L. Gardette, Photo-oxidation of Polypropylene/Montmorillonite Nanocomposites. 1. Influence of Nanoclay and Compatibilizing Agent, Chem. Mater. 16 (2004) 377–383. doi:10.1021/cm031079k.

[41] S.A. Jabarin, E.A. Lofgren, Photooxidative effects on properties and structure of high-density polyethylene, J. Appl. Polym. Sci. 53 (1994) 411–423. doi:10.1002/app.1994.070530404.

[42] D. Rosu, R. Bodîrlău, C.A. Teacă, L. Rosu, C.D. Varganici, Epoxy and succinic anhydride functionalized soybean oil for wood protection against UV light action, J. Clean. Prod. 112 (2016) 1175–1183. doi:10.1016/j.jclepro.2015.07.092.

[43] A.J. Vinha, A.G. Carvalho, M. Teixeira de Souza, C. Marangon Jardim, A. de Cassia Oliveira Carneiro, J. Luiz Colodette, Effect of extractives on wood color of heat treated Pinus radiata and Eucalyptus pellita, Maderas. Cienc. Y Tecnol. 17 (2015) 857–864. doi:10.4067/S0718-

221X2015005000074.

[44] L. Soccalingame, D. Perrin, J.-C. Bénézet, S. Mani, F. Coiffier, E. Richaud, A. Bergeret, Reprocessing of artificial UV-weathered wood flour reinforced polypropylene composites, Polym. Degrad. Stab. 120 (2015) 313–327. doi:10.1016/j.polymdegradstab.2015.07.013.

[45] G. Dorez, L. Ferry, R. Sonnier, A. Taguet, J.-M. Lopez-Cuesta, Effect of cellulose, hemicellulose and lignin contents on pyrolysis and combustion of natural fibers, J. Anal. Appl. Pyrolysis. 107 (2014) 323–331. doi:10.1016/j.jaap.2014.03.017.

[46] P. Wambua, J. Ivens, I. Verpoest, Natural fibres: Can they replace glass in fibre reinforced plastics?, Compos. Sci. Technol. 63 (2003) 1259–1264. doi:10.1016/S0266-3538(03)00096-4.

[47] H. Du, W. Wang, Q. Wang, S. Sui, Y. Song, Effects of ultraviolet absorbers on the ultraviolet degradation of rice-hull/high-density polyethylene composites, J. Appl. Polym. Sci. 126 (2012) 906–915. doi:10.1002/app.36558.

[48] M.M. Thwe, K. Liao, Durability of bamboo-glass fiber reinforced polymer matrix hybrid composites, Compos. Sci. Technol. 63 (2003) 375–387. doi:10.1016/S0266-3538(02)00225-7.

[49] Y. Peng, R. Liu, J. Cao, Y. Chen, Effects of UV weathering on surface properties of polypropylene composites reinforced with wood flour, lignin, and cellulose, Appl. Surf. Sci. 317 (2014) 385–392. doi:10.1016/j.apsusc.2014.08.140.

CONCLUSION GÉNÉRALE

Aujourd'hui, l'industrie est confrontée à deux enjeux environnementaux importants. Le premier enjeu vise à limiter les émissions de gaz à effet de serre grâce à l'efficacité énergétique et à réduire la contribution des activités humaines aux changements climatiques. Le deuxième enjeu concerne la réduction de la dépendance aux énergies fossiles qui tendent à s'épuiser. Le développement de matériaux issus de ressources renouvelables semble être une réponse prometteuse à ces enjeux. Par ailleurs, les laboratoires et centres de recherche et de développement réalisent des travaux visant à incorporer des matériaux de renforcement d'origine végétale aux plastiques dont l'origine est généralement fossile. Aujourd'hui, ces composites à base de fibres végétales sont retrouvés dans les lames de terrasse (« decking »), les meubles de jardin, les bardages et les pièces intérieures d'automobile (panneaux de porte et tableaux de bord). Cependant, bien que les propriétés mécaniques spécifiques (caractéristiques mécaniques ramenées à la densité) des fibres végétales confèrent aux biocomposites une tenue mécanique compétitive vis-à-vis des composites renforcés de fibres de verre, leur développement est limité par la forte dépendance de leurs propriétés aux conditions d'usage et d'environnement. L'objectif principal de cette thèse a été d'évaluer l'impact de deux types de vieillissement naturel et d'un vieillissement artificiel sur plusieurs caractéristiques des biocomposites à matrice polypropylène (PP) renforcée de fibres de chanvre (à des taux massiques de 10 et 30%). Ce travail a ainsi permis de mieux appréhender les mécanismes physico-chimiques de dégradation impliqués lors d'une exposition compromettant la durabilité des biocomposites.

La première partie du premier chapitre a concerné l'étude des mécanismes de dégradations des biocomposites lors d'un vieillissement en conditions d'usage au cours d'une année. Le premier type de vieillissement a consisté en une exposition directe aux intempéries (en lien avec l'exposition réelle de lames de terrasse) alors que le deuxième a reflété un environnement intérieur de véhicule (exposition sous vitre pare-brise). Les résultats ont montré que les propriétés des biocomposites et du PP ont été dégradées par les trois facteurs prépondérants qui sont la pluie, le rayonnement UV et la température ainsi que par leur effet synergique. Globalement, la présence de fibres végétales accentue le mécanisme de scissions de chaîne et d'oxydation des chaînes macromoléculaires. Bien que la différence

entre les deux conditions d'exposition ait peu influé sur la réponse mécanique des biocomposites, la microstructure et l'aspect de surface des biocomposite et du PP vierge ont été plus impactés lors de l'exposition extérieure sans vitrage. En effet, l'exposition extérieure a favorisé la formation d'irrégularités de surface suggérant que la pluie et les rayons UV sont principalement responsables de cette rugosité.

Afin de comprendre les différences observées entre les matériaux chargés et non chargé et les évolutions des propriétés différant selon le type d'exposition, les relations existant entre tous les paramètres suivis ont été déterminées. Pour cela, une Analyse en Composantes Principales (ACP) a été effectuée. Les différents traitements statistiques ont apporté plusieurs informations complémentaires. La distinction des données par type de vieillissement (extérieur et sous vitrage) a indiqué que les liens entre les différents paramètres n'ont pas été significativement affectés alors que la distinction des données par taux de fibres a permis de dégager un lien de causalité entre la formation de composés oxygénés (mesurés par spectroscopie infrarouge) et la réduction des performances mécaniques telles que le module d'élasticité et la contrainte à la flèche conventionnelle. De plus, l'évolution des corrélations émergeant au cours du vieillissement a démontré qu'après 9 mois d'exposition, la réduction du taux de cristallinité était notamment due à l'oxydation de la structure cristalline.

Les biocomposites de l'étude étant notamment destinés à être utilisés en environnement clos (véhicules), il est important de connaitre leur potentiel d'émission de Composés Organiques Volatils (COV). La méthode DOSEC-SPME précédemment développée au laboratoire a donc été appliquée à la mesure des émissions de COV par les matériaux biocomposites exposés sous vitre pare-brise. Il a été constaté que la présence de fibres végétales augmente la concentration et la quantité en COV émis. De plus, l'exposition favorise les émissions suggérant que les substances identifiées proviennent essentiellement de la décomposition des fibres. La formation des composés volatils émis par les biocomposites non vieillis a été expliquée par les réactions de Maillard dont les interactions mettent en jeu les protéines à faible teneur dans les fibres et les polysaccharides. A partir de l'étude qualitative et quantitative des COV détectés tout au long du vieillissement, de nouveaux chemins réactionnels ont été proposés. Ainsi, à l'état vieilli, une décomposition

secondaire de la matière végétale fait intervenir des réactions intermoléculaires dans la phase gazeuse.

Aussi, les concentrations de COV émis par les matériaux ont été étudiées conjointement aux autres caractéristiques tout au long de l'exposition pour évaluer les dépendances par l'approche statistique d'ACP. La tendance majeure dégagée est que la mesure des émissions de COV peut fournir des informations sur les processus de dégradation puisque la concentration globale en COV est anti-corrélée au module et à la résistance à la flèche conventionnelle de chaque type de matériau.

Dans cette étude, il nous a paru primordial de mener en parallèle un essai de vieillissement accéléré, qui est privilégié au niveau industriel pour un gain de temps de développement, et de nous assurer de la représentativité des conditions simulées en enceinte de type QUV en les comparant au vieillissement extérieur. Le vieillissement en enceinte QUV a inclus un cycle d'exposition aux rayonnements UV, à une pulvérisation d'eau et à une température élevée. Une accentuation du phénomène de dégradation a été observée dans le cas du vieillissement QUV à travers les propriétés mécaniques et l'aspect de surface a été significativement affecté. Contrairement au vieillissement naturel, le taux de dégradation en enceinte QUV du PP a été globalement plus élevé que celui des biocomposites suggérant que le PP est plus sensible aux cycles courts de rayonnement et pulvérisation que les biocomposites ou plus vulnérable à la surreprésentation des paramètres rayons UVs/pulvérisation.

Le même outil statistique d'ACP a été utilisé pour évaluer la corrélation entre les deux vieillissements. En se basant sur la proximité des matériaux à différents temps de vieillissement sur un même graphe de projection, il a été conclu qu'une année de vieillissement naturel du PP et du biocomposite PP/30% en masse de fibres correspondait à 250h et 750h de vieillissement accéléré respectivement.

Plusieurs perspectives issues de ce travail sont proposées. Il a été démontré dans la littérature que des charges poreuses (zéolithes, pouzzolane, argile, …) incorporées dans les plastiques pouvaient piéger les COV émis. Ainsi, ce même principe de piégeage pourrait être extrapolé à une étude sur les émissions de COV par les biocomposites et donc pourrait être une voie intéressante à développer pour réduire leur impact sur la qualité de l'air intérieur.

Aussi, les différentes réactions proposées dans ce travail de thèse pourraient être validées à travers une modélisation de l'énergie d'activation des réactions dans la phase gazeuse qui nécessitent des conditions favorables.

Il serait intéressant de continuer le vieillissement naturel après 12 mois d'exposition afin de tester la durabilité des biocomposites à plus long terme mais aussi vérifier si les résultats corroborent ceux observés après vieillissement artificiel, ce dernier ayant potentiellement représenté un état de vieillissement naturel plus avancé. Par ailleurs, une étude plus poussée visant à découpler les différents facteurs (rayonnement, pulvérisation, température) en enceinte apporterait des éléments de compréhension sur leurs contributions respectives à l'évolution des propriétés des matériaux. Ainsi le découplage des paramètres effectué au cours de la thèse de Vincent Berthé (C2MA, IMT Mines Alès) pour des matériaux à base de PLA pourrait être extrapolé à notre étude. Il serait d'ailleurs judicieux de procéder à un vieillissement artificiel thermique du PP pour notamment conforter nos hypothèses émises sur la surreprésentation des paramètres rayonnement/pluie en enceinte par rapport aux conditions naturelles. Aussi, le renforcement de thermoplastiques par les carbohydrates et la lignine séparément constituerait des résultats complémentaires à la compréhension de la contribution des composants lignocellulosiques à l'évolution de tous les aspects, notamment des émissions de COV par les biocomposites, abordés durant ce travail de thèse.

ANNEXES

ANNEXE I: L'aspect visuel

I.1. La couleur

La perception d'une couleur dépend de trois critères qui doivent être pris en compte pour sa caractérisation. Ces trois critères sont :

- L'objet qui réémet, absorbe ou transmet les longueurs d'ondes du rayon lumineux incident [1] selon la structure moléculaire de ses constituants. Par exemple, un objet sera rouge s'il absorbe les radiations vertes et bleues ou jaune s'il absorbe les radiations rouges et bleues [1].

- La source lumineuse (ou illuminant) définie par son spectre d'émission qui représente la distribution des intensités d'émission, en fonction de la longueur d'onde. Pour éviter des variations non maîtrisées des sources lumineuses, la Commission Internationale de l'Eclairage (CIE) a défini plusieurs illuminants standards qui permettent de simuler des éclairages réels. On peut citer l'éclairement naturel solaire (D65) ou l'éclairement sous lampe à tungstène (A) ou fluorescente (F2) [2]. La Figure 1 montre la distribution spectrale de ces éclairages.

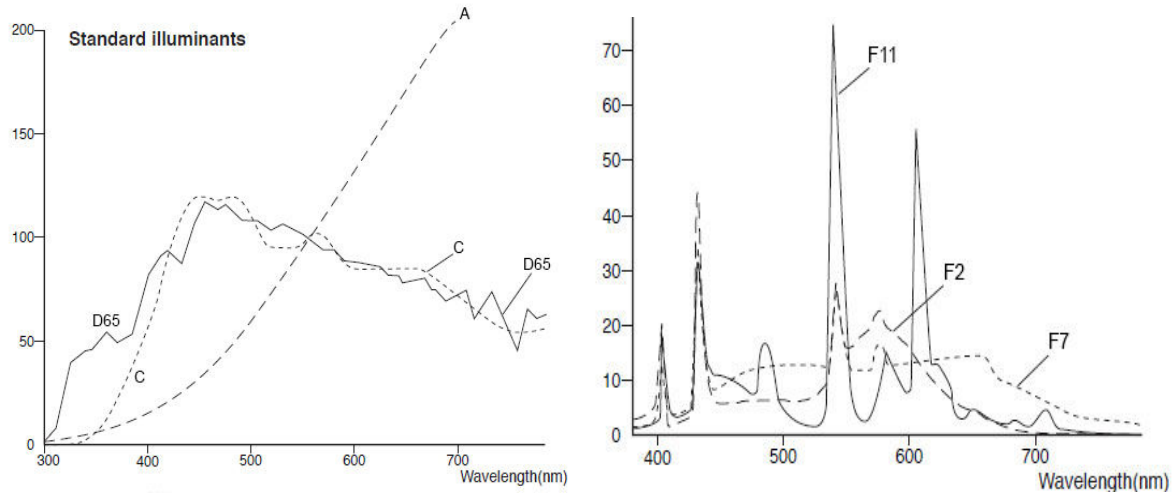

Figure 1 - Spectres d'émission de différents illuminants standards [193] [190] (éclairements naturel solaire (D65), (C), sous lampe à tungstène (A) fluorescente (F2), (F7), (F11))

- L'observateur/détecteur capte la part du signal renvoyé par l'objet et arrivant dans son champ de vision. La CIE propose également l'utilisation d'un observateur standard, dont la sensibilité visuelle correspond à la sensibilité moyenne observée sur une centaine de

personnes au cours d'expériences menées en 1931 [2]. Puisque la perception des couleurs varie en fonction du point de vue de l'observateur, l'observateur standard défini en 1931 a été fondé dont l'angle d'ouverture du champ visuel est fixé à 2° (zone de la rétine ou la vision atteint sa plus grande netteté). La CIE a défini un observateur standard supplémentaire basé sur un champ de 10° en 1964.

Selon le principe de la trivariance visuelle issu des travaux de Grassman (1853) et Abney (1913), la couleur d'un objet est déterminée suivant trois attributs que sont la teinte, la clarté ou luminosité et la saturation [1]. Compte tenu de la trivariance de la vision humaine, des systèmes de synthèse des couleurs tridimensionnels sont proposés en colorimétrie. Cependant, plusieurs espaces tridimensionnels existent. On peut citer les systèmes Luv, xyz ou Lab.

I.2. La brillance

Le brillant est une grandeur visuelle qui dérive de l'analyse de la distribution géométrique de la lumière réémise par la surface d'un matériau. En effet, la brillance d'un matériau est d'autant plus marquée que la lumière est réfléchie de manière dirigée. Ainsi, lorsque la lumière illumine la surface d'un objet, elle peut être :

- complètement réfléchie dans une seule direction. On parle alors de réflexion spéculaire suivant la loi de Snell-Descartes pour une surface parfaitement lisse (Figure 2). On entend par « lisse » une surface dont la rugosité est de dimension très inférieure à la longueur d'onde de la lumière.
- réfléchie dans toutes les directions, définie par une réflexion diffuse. Ce phénomène caractérisé par le modèle de Lambert pour un diffuseur parfait se manifeste notamment pour des surfaces rugueuses [3] et est dû à la multiple orientation des facettes constituant la surface du matériau et éclairées par le spot lumineux.
- réfléchie dans une direction donnée où le comportement mixte inclut la réflexion spéculaire et la réflexion diffuse.

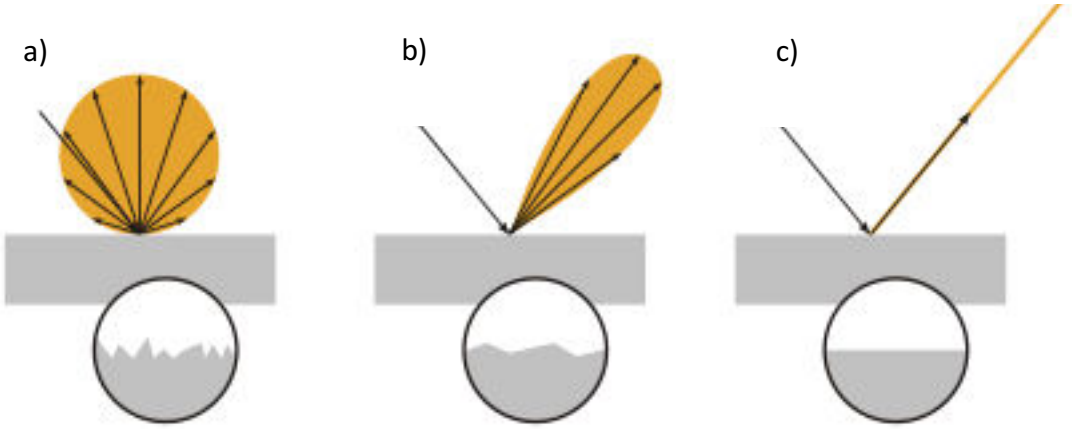

Figure 2 – Différentes modélisations de la réflexion d'un faisceau sur une surface (diffusion dans toutes les directions (a), diffusion dans une région donnée (b), réflexion spéculaire (c))

La grandeur pertinente dans la caractérisation de la brillance de la surface d'un objet est la fonction de distribution bidirectionnelle de réflectance (BRDF) définie par le quotient de la luminance de l'élément de surface mesurée dans une direction, par l'éclairement produit par un rayonnement ayant une incidence définie [3]. Ce concept physique met en œuvre des quantités infinitésimales puisque la BRDF correspond à des faisceaux lumineux incident et réfléchi compris dans des angles solides infinitésimaux [4]. La BRDF est une grandeur multidimensionnelle complexe souvent modélisée. En effet, l'acquisition de la BRDF de matériaux est un processus long qui produit une quantité de données considérable difficile à manipuler. Cependant, des paramètres alternatifs tels que le brillant de contraste et le brillant de haze, déterminés à partir de la répartition angulaire de la lumière réfléchie par le matériau, permettent d'évaluer le type de réflexion mis en jeu.

I.3. Références

[1] M. Sablier, M. Perraudeau, Lumière et couleur, Tech. l'Ingénieur. (2004).

[2] P. Callet, Couleur et apparence visuelle - Le transparent et l'opaque, Tech. L'ingénieur. (2004).

[3] V. Domurado, Étude et modélisation de la réflectance de la surface d'objets réels, Mémoire de fin d'études, 2001.

[4] L. Bousquet, Mesure et modélisation des propriétés optiques spectrales et directionnelles des feuilles, Thèse de doctorat, Université Paris 7 - Denis Diderot, 2007.

ANNEXE II : L'analyse en composantes principales (ACP)

L'analyse en composantes principales (ACP) est une méthode statistique multivariée qui s'avère utile lorsqu'un nombre important de variables quantitatives est étudié. Elle permet d'appréhender la structure d'un nuage de données et de déterminer les liaisons sur l'ensemble des variables considérées. Cette méthode de calcul repose sur la projection d'un ensemble de données quantitatives appartenant à un espace multidimensionnel sur un espace bidimensionnel. Ainsi, des relations non visualisables dans un espace dont le nombre de dimensions est supérieur à 2 sont mises en lumière sur le plan de projection. De même, elle permet de mieux distinguer les ressemblances entre les individus de cet espace.

Pour un ensemble de données quantitatives, si n variables sont observées sur N individus, le tableau suivant peut être représenté (Figure 1) :

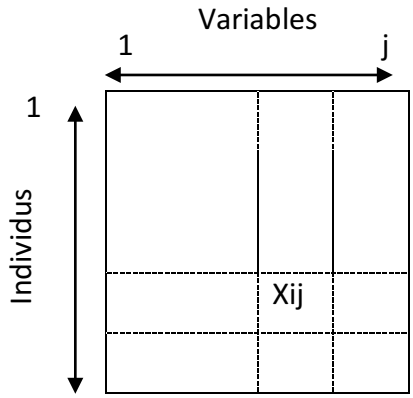

Figure 1 - Tableau des individus N dans l'espace R^n (lignes) aux variables n dans l'espace R^N (colonnes)

Xij correspond à la valeur de la ième observation pour la jième variable. Ce tableau des données brutes définit donc deux nuages de points [1] :

- Le nuage des variables (colonnes) : coordonnées des vecteurs variables tracés dans le repère dont les axes représentent les individus (espace de dimension N)
- Le nuage des individus (lignes) : coordonnées des vecteurs variables tracés dans le repère dont les axes représentent les individus (espace de dimension n).

II.1. Projection des individus

Afin de visualiser l'ensemble des données du tableau exposé précédemment et mettre en évidence les relations par une représentation graphique synthétique, un sous-espace F de

dimension j de R^N avec j=2 doit être déterminé [1]. Pour ce faire, j(=2) nouvelles variables correspondant aux combinaisons linéaires des n variables initiales déformant le moins possible le nuage initial sont définies. Cela équivaut à trouver la meilleure image projetée du nuage de points de dimensions n de sorte que la distance entre l'individu i appartenant à l'espace initial et sa projection H_i soit minimisée (Figure 2). D'après le théorème de Pythagore, si la distance entre l'individu et le centre de gravité du nuage de points initial $(Oi)^2$ est constante, $(OH_i)^2$ doit être maximisée pour que $(iH_i)^2$ soit la plus petite possible.

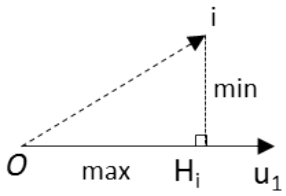

Figure 2 - Projection H_i de l'individu i

Donc, si tous les individus sont pris en compte, la somme des distances ΣOH_i^2 doit être maximisée pour refléter au mieux la dispersion du nuage d'individus initial. Ainsi, un premier axe Composant Principal 1 (CP1) correspondant à la première combinaison linéaire des variables initiales est tracé. Un second axe CP2 orthogonal à CP1 est généré pour représenter le plan de projection. Après CP1, cet axe représente le composant principal le plus proche du nuage brut synthétisant au mieux la dispersion des données appartenant à l'espace initial [2].

Si l'on considère A et B des individus appartenant à l'espace de dimensions n sur la Figure 3, A' et B' sont des images projetés sur l'axe CP1 et A'' et B'' sont les images projetées sur CP2.

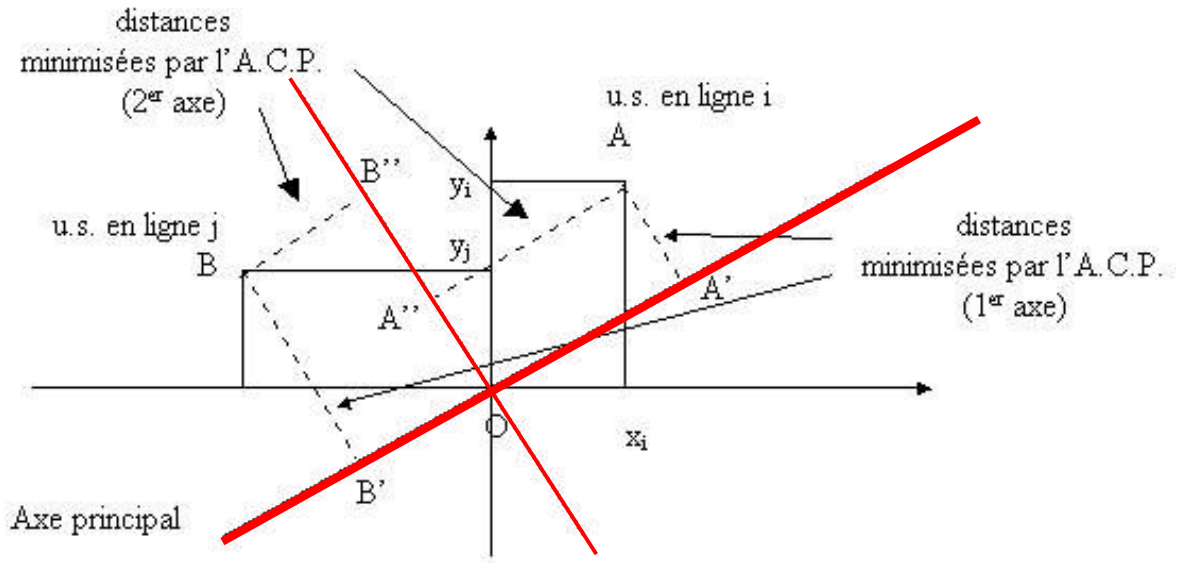

Figure 3 – Plan principal de projection des individus A et B (PC1 et PC2 représentés en rouge) [3]

Cette dispersion est traduite par le pourcentage d'inertie du nuage des individus, mesurant la qualité de la projection, expliqué par chaque axe de projection qui est déterminé comme suit [4]:

$$I = \frac{1}{N}\sum_{1}^{N} d^2\,(O, H_i) \qquad \text{Eq. 1}$$

avec d la distance entre le centre de gravité O et la projection H_i de l'individu i sur l'axe CP1. L'inertie du sous-espace factoriel est égale à la somme des pourcentages d'inertie portés par CP1 et CP2.

II.2. Projection des variables

De même que pour les individus, le nuage des variables à dimensions N est ajusté afin de projeter ces variables sur un plan en minimisant la perte d'information, c'est-à-dire en conservant la dispersion des variables. Ainsi, les sommes des corrélations entre le vecteur F_1 et chacune des variables k $\Sigma r(F_1,k)^2$ et entre le vecteur F_2 orthogonal à F_1 et chacune variables k $\Sigma r(F_2,k)$ sont maximisées. Ces deux facteurs permettant la visualisation du nuage des variables, sont de nouvelles variables qui synthétisent le plus fidèlement possible l'angle formé entre les vecteurs des variables et permettent donc l'interprétation correcte des corrélations entre les variables dégagées sur le plan. Ces corrélations peuvent être interprétées sur les graphiques des variables, nommés cercles des corrélations, obtenus en

calculant la corrélation entre les variables de l'espace non projeté et les axes principaux de vecteur directeur F (Figure 4).

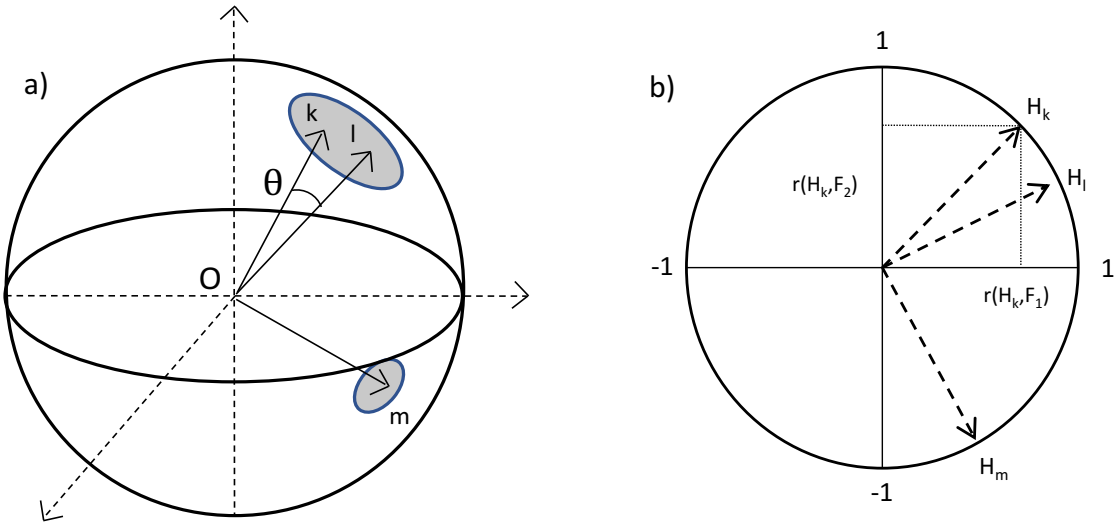

Figure 4 – Espace de dimension N contenant le nuage des variables U, V, W (a) et cercle des corrélations (U', V', W': variables projetées) (b)

De plus, lorsque les unités des variables sont différentes, les données sont normalisées par centrage-réduction. Une fois centrées-réduites, les angles entre les vecteurs des variables sur le cercle des corrélations peuvent être interprétés puisque le coefficient de corrélation entre la variable k et la variable l r(k,l) correspond au cosinus de l'angle formé entre les mêmes variables une fois projetées H_k et H_l:

$$r(k,l) = \cos(\theta_{k,l}) \approx \cos(\theta_{Hk,Hl}) \qquad \text{Eq. 2}$$

Ainsi, d'après cette relation, plus l'angle formé entre deux variables sera faible, plus ces deux variables seront liées.

II.3. Contribution des variables et des individus aux composantes principales

Une variable k contribuera d'autant plus à la confection d'un axe, que sa projection sur cet axe sera éloignée du centre de gravité du nuage. La contribution Ctr de la variable k à la construction de l'axe étant un des composantes principales P exprimée en % peut être déterminée à partir du coefficient de corrélation entre la variable k et le vecteur de l'axe p F_P :

$$Ctr(k)(\%) = \frac{r(F_P,k)^2}{\sum_1^n r(F_P,k)^2} \qquad \text{Eq. 3}$$

De même, la contribution d'un individu i peut être déterminée selon sa coordonnée F_i sur l'axe P [2]:

$$Ctr(i)(\%) = \frac{{X_{\mathrm{i(P)}}}^2}{\sum_1^N {X_{\mathrm{i(P)}}}^2} \qquad \text{Eq. 4}$$

avec X_{iP} la coordonnée de l'individu i sur l'axe P. Cela permet de mettre en évidence les individus particuliers contribuant principalement à la construction d'un axe CP.

II.4. Conclusion

Finalement, cet outil statistique permet, par un changement de référentiel, de simplifier la description d'un ensemble de données afin d'en extraire les informations les plus pertinentes. Par le calcul de combinaisons linéaires des anciennes variables, la structure est visualisée et analysée et les relations entre variables et similitudes entre individus sont déterminées. L'ACP a été utilisée dans le cadre de cette étude pour l'étude des relations entre les paramètres mesurés.

II.5. Références

[1] "Introduction à l'Analyse en Composantes Principales (ACP)," *WikiStat*, pp. 1–5.

[2] L. J. Williams and H. Abdi, "Principal Component Analysis," *Wiley Interdiscip. Rev. Comput. Stat.*, vol. 2, no. 4, pp. 433–459, 2010.

[3] T. Foucart, "Cours sur l'Analyse en Composantes Principales, Chap. 9." 2013.

[4] C. Duby and S. Robin, "Analyse en Composantes Principales," *Cours AgroParisTech*, pp. 1–54, 2009.